



LOMA LINDA UNIVERSITY

Loma Linda University  
TheScholarsRepository@LLU: Digital  
Archive of Research, Scholarship &  
Creative Works

---

Loma Linda University Electronic Theses, Dissertations & Projects

---

12-2022

## High-Intensity Interval Training and Biological Age

Trevor Lohman

Follow this and additional works at: <https://scholarsrepository.llu.edu/etd>



Part of the [Physical Therapy Commons](#)

---

### Recommended Citation

Lohman, Trevor, "High-Intensity Interval Training and Biological Age" (2022). *Loma Linda University Electronic Theses, Dissertations & Projects*. 1761.  
<https://scholarsrepository.llu.edu/etd/1761>

This Dissertation is brought to you for free and open access by TheScholarsRepository@LLU: Digital Archive of Research, Scholarship & Creative Works. It has been accepted for inclusion in Loma Linda University Electronic Theses, Dissertations & Projects by an authorized administrator of TheScholarsRepository@LLU: Digital Archive of Research, Scholarship & Creative Works. For more information, please contact [scholarsrepository@llu.edu](mailto:scholarsrepository@llu.edu).

LOMA LINDA UNIVERSITY  
School of Allied Health Professions  
In conjunction with the  
Faculty of Graduate Studies

---

High-Intensity Interval Training and Biological Age

by

Trevor Lohman

---

A Dissertation submitted in partial satisfaction of  
the requirements for the degree  
Doctor of Philosophy in Physical Therapy

December 2022

©2022

Trevor Lohman  
All Rights Reserved

Each person whose signature appears below certifies that this dissertation in his/her opinion is adequate, in scope and quality, as a dissertation for the degree Doctor of Philosophy.

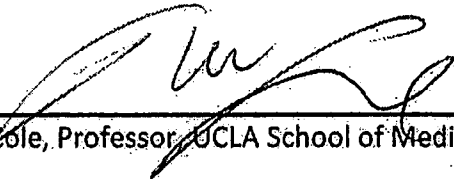


, Chairperson

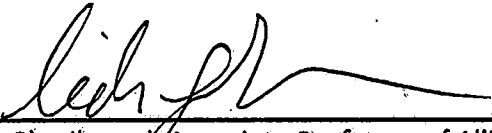
Gurinder Bains, Professor of Allied Health Studies



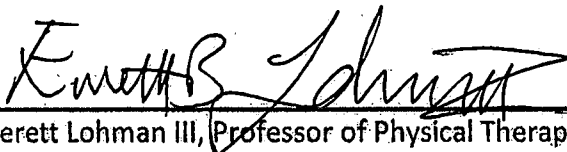
Lee Berk, Professor of Allied Health Studies, Associate Research Professor School of Medicine



Steve Cole, Professor, UCLA School of Medicine



Lida Gharibvand, Associate Professor of Allied Health Studies



Everett Lohman III, Professor of Physical Therapy, Assistant Dean for Graduate Academic Affairs

## ACKNOWLEDGEMENTS

I wish to express my sincere gratitude to my chair, Dr. Bains, who provided me with both the autonomy and guidance that I needed to succeed at this journey in scholarship. His patience, support, mentorship, and wisdom were invaluable.

To Dr. Cole, whose generosity of knowledge is unparalleled, I offer my wholly inadequate, but extremely heartfelt, appreciation. His breadth and depth of expertise, and more importantly, his willingness to share it is what made this endeavor possible.

To Drs. Berk and Gharibvand, I can only say very gratefully and very humbly, thank you.

To Dr. Lohman, I have a great deal to be grateful for. Most relevant to this dissertation, I am grateful for your recognition that I needed to begin a new chapter. Thank you for giving me the courage to take that first step, and for all your support along the way.

To my wife Olivia, thank you for your limitless understanding and generosity. You are truly the embodiment of what it means to be a partner. I could not have done this without you.

To my children, Harper, and Nash. Thank you for understanding my dedication to this work. I can only hope you find the investment worthwhile, and that you share the same joy for discovery that I've found so fulfilling. I love you; you are both precious to me, and I will work every day to make you proud.

## CONTENT

Acknowledgements.....	iv
Table of Contents.....	v
List of Figures.....	vii
List of Tables.....	viii
List of Abbreviations.....	ix
Abstract.....	xi
Chapter	
1. Introduction.....	1
References.....	8
2. Predictors of Biological Age: The Implications for Wellness and Aging Research.....	10
Abstract.....	10
Introduction.....	11
Article Search Strategy and Selection Criteria.....	15
Telomere Length.....	15
Composite Biomarkers/Allostatic Load Indices.....	17
DNA Methylation “Epigenetic Clocks”.....	20
Transcriptional Predictors of Biological Age.....	24
Functional Age Estimators.....	26
Discussion.....	29
Conclusion.....	31
References.....	33
3. High-Intensity Interval Training Reduces Transcriptomic Age: A Randomized Controlled Trial.....	42
Abstract.....	42
Introduction.....	44
Methods.....	47
Data Analysis.....	50
Results.....	51
Discussion.....	56

Significance.....	60
Conclusion.....	61
References.....	62
Supplementary File 1.....	See Appendix B
Supplementary File 2.....	See Appendix C
4. Discussion.....	66
Discussion.....	66
Conclusion and Future Directions.....	68

## Appendices

A. Loma Linda University Institutional Review Board Determination Form.....	70
B. Supplementary File 1: Genetic Expression Data.....	71
C. Supplementary File 2: Advaita Bioinformatics iPathway Guide Pathway Analyses.....	143
D. Informed Consent Document.....	182

## FIGURES

Figures	Page
1. CONSORT Chart Diagram.....	52

## TABLES

Table	Page
1. Telomere Length.....	16
2. Composite Biomarkers/Allostatic Load Indices.....	19
3. DNA Methylation Clocks.....	23
4. Transcriptomics.....	25
5. Functional Age Estimators.....	28
6. Selected Characteristics of Participants at Baseline.....	53
7. Effects of High Intensity Interval Training on Transcriptomic Age, PHQ-9, PSS-10, PSQI, Skeletal Muscle Mass, Body Fat Mass, and Visceral Fat Area. Between and Within Group Effects.....	54

## ABBREVIATIONS

HIIT	High-Intensity Interval Training
DNA	Deoxyribonucleic Acid
CpG	5' - Cytosine – Phosphate – Guanine – 3'
TRAP	Transcriptomic Age Prediction
HIE	High Intensity Exercise
SIT	Sprint Interval Training
DNAmAge	DNA Methylation Age
RNA	Ribonucleic Acid
MeSH	Medical Search Heading
BA	Biological Age
FP	Frailty Phenotype
FI	Frailty Index
TL	Telomere Length
PSS-10	10 Item Perceived Stress Scale
PHQ-9	9 Item Patient Health Questionnaire Depression Module
PSQI	Pittsburg Sleep Quality Index
BMI	Body Mass Index
mTOR	Mammalian Target of Rapamycin
AMPK	Adenosine Monophosphate-Activated Protein Kinase
PI3K	
TA	Transcriptomic Age

TAaccel	Transcriptomic Age Acceleration
IPAQ	International Physical Activity Questionnaire
DE	Differentially Expressed
DEG	Differentially Expressed Gene
mRNA	Messenger Ribonucleic Acid
mTORC1	Mammalian Target of Rapamycin Complex 1
CDC	Centers for Disease Control and Prevention

## ABSTRACT OF THE DISSERTATION

### High-Intensity Interval Training and Biological Age

By

Trevor Lohman

Doctor of Philosophy, Graduate Program in Physical Therapy  
Loma Linda University, December 2022  
Dr. Gurinder Bains, Chairperson

The emergence of valid predictors of biological age has enabled researchers to test the effects of various interventions on biological aging processes. The established virtues of exercise and its effects on health and longevity make it a suitable candidate for investigation.

This dissertation reviews the current state of biological age prediction models and presents a trial in which a specific exercise protocol's ability to modulate biological age is tested. The specific protocol used is a 10X1 high-intensity interval training (HIIT) protocol, 10X1 referring to the quantity and duration of high intensity exercise intervals in each exercise session. The specific biological age prediction model chosen as the trial's primary outcome measure relies on transcriptomic inputs to make biological age predictions.

A significant difference in biological age was observed between groups. Reduction in biological age was observed in the exercise group, while increased biological age was observed in the control group. Exploratory, hypothesis generation analyses of gene expression revealed potential modification of autophagy, neurotrophin, and cancer biological pathways.

This dissertation concludes that HIIT induces transcriptional changes which may in part account for the established beneficial effects of exercise on health and longevity.

## CHAPTER ONE

### INTRODUCTION

Age-related diseases are a persistent and increasingly prevalent burden on healthcare systems around the world. An analysis of the 2017 Global Burden of Disease identified 92 diseases that increase quadratically with age including: cardiovascular diseases, cancers, chronic respiratory diseases, digestive diseases, diabetes, kidney diseases, and others (Chang, Skirbekk, Tyrovolas, Kassebaum, & Dieleman, 2019). These age-related diseases were found to account for 51.3% of total global health burden, defined as the sum of disability-associated life-years (Chang et al., 2019). In addition to age-related disease prevalence, the cost is staggering as well. Heart disease and stroke alone accounted for 352 billion dollars per year in healthcare costs and lost productivity in 2018 (Benjamin et al., 2018). Another age-related disease, Cancer, is expected to account for 174 billion dollars in cost by 2020 (Mariotto, Yabroff, Shao, Feuer, & Brown, 2011), with an average of 1.7 million Americans being diagnosed each year. As of 2013, the cost attributable to Arthritis was 305 billion dollars (Murphy, Cisternas, Pasta, Helmick, & Yelin, 2018). Alzheimer's accounts for an additional 215 billion dollars in healthcare costs as of 2010 (Hurd, Martorell, Delavande, Mullen, & Langa, 2013). Unfortunately, these costs are predicted to continue to rise (Atella et al., 2019), and any affordable and accessible protocol capable of ameliorating these trends would be of significant value.

While experimental aging research has progressed a great deal in the past decades, an inherent challenge to progress is the inability to measure an intervention's effects on lifespan without a costly multi-decade longitudinal study. Recently, a new class of biomarkers has

emerged that could potentially address this challenge called biological age predictors. The term biological age has become more prevalent in aging research as a reference to the apparent fact that humans do not seem to age at a homogenous rate. This is intuitive, as anyone would suspect a group of people with the same chronological age to be in varying states of health and mortality risk. Until relatively recently however, there had not been validated markers designed to measure mortality-risk, time-to-death, time-to-cancer, biological age, or other markers of lifespan and healthspan from peripheral blood samples.

The term “predictors of biological age” widely encompasses many different tools designed to predict mortality risk and remaining lifespan. One category of biomarkers within this larger group that has received significant attention is called epigenetic “clocks”. The term epigenetic clock refers to tools that analyze DNA methylation levels within a set of Cytosine-Phosphate-Guanine (CpG) sites and are generally acknowledged as accurate measures of biological age (Bell et al., 2019; Jylhävä, Pedersen, & Hägg, 2017; Lohman, Bains, Berk, & Lohman, 2021; Lu et al., 2019). Like the broader category, epigenetic clocks are a group of tools rather than specific biomarkers, and therefore the nature and capability of each tool varies. One metric known as GrimAge for example, can significantly predict time-to-death, time-to-coronary artery disease, and time-to cancer (Lu et al., 2019). These capabilities provide a useful “proxy biomarker” mechanism to assess the effectiveness of interventions designed to increase lifespan.

While GrimAge is one of the most highly validated measures of mortality risk, it does not provide any information regarding the underlying changes to genetic expression associated with methylation (Li et al., 2020; Lu et al., 2019). Chapter 2 of this dissertation presents a

review of biological age prediction models that was published in the journal of Gerontology and Geriatric Medicine. Among the categories of models reviewed in the paper is transcriptomic age prediction. An example of such a model was published in a paper titled “The Transcriptional Landscape of Age in Human Peripheral Blood” written by Peters et al and it identified 1,497 genes that are differentially expressed with age (Peters et al., 2015). The data required for the model’s input is derived from peripheral whole blood samples and subsequent mRNA extraction (Peters et al., 2015). Using a statistical formula called the Transcriptomic Age Prediction Tool (TRAP), this genetic expression data can be used to estimate biological age (Peters et al., 2015). Gene expression data from Affymetrix Human Exon (1.0 ST) Arrays can be uploaded to a freely available online platform. The TRAP tool then provides an estimate of biological age measured in years for each sample. In doing so, this tool provides a means to analyze the effects of an intervention on biological age from a gene expression profile. We will utilize this tool in chapter 3 to quantify the effects of high-intensity interval training on biological age.

The availability and validity of these tools has provided a new mechanism to measure the effectiveness of biological age reversal interventions in clinical trials. Studies have now successfully used these metrics to demonstrate that epigenetic aging (biological age as measured by a DNA methylation “clock”) can be reversed in humans (Fahy et al., 2019; Fitzgerald et al., 2020). The study performed by Fahy et al in 2019 utilized a metformin and 1 yr. exogenous human growth hormone protocol, that demonstrated a 2.5 year mean reversal of epigenetic aging as well as a significant increase in thymic fat free fraction (Fahy et al., 2019). This was the first study to date to demonstrate a reduction of epigenetic aging and thymic

involution in humans. While these are very exciting results, exogenous human growth hormone administration is not risk free and it is also not accessible to the general population. This has led us to ask the question, “Can biological age be reversed through a safer, more affordable method such as lifestyle modification?”

Intuitively, the answer should be yes, however no controlled trial to date has quantified the effects of a lifestyle intervention on biological age using a transcriptomic age prediction model. Although there are many potential interventions like diet, sleep quality, and stress reduction strategies that could potentially reduce biological age, we have chosen to examine the effects of exercise on biological age due to its relevance to the field of physical therapy, known health benefits, general safety, and accessibility.

Given the volume of research regarding the benefits of exercise, it seems a likely candidate intervention to promote longevity. For example, an analysis of 16 recent systematic reviews found a dose-dependent relationship between exercise and improved health outcomes related to cardiovascular disease, all-cause mortality, all-cancer mortality, type 2 diabetes, hypertension, breast cancer, colon cancer, gestational diabetes, gallstone disease, ischemic heart disease, and ischemic stroke (Warburton & Bredin, 2017). There is also epidemiological data that supports exercise being associated with decreased biological age, as well as increased lifespan and healthspan (Gremeaux et al., 2012; Quach et al., 2017; Zhao et al., 2019).

Like the term biological age, exercise is a broad category rather than a specific intervention. Exercise protocols are highly variable and can fall into many different categories with many different physiological effects. There is also no consensus on which type of exercise best promotes longevity. In recent decades, high intensity exercise (HIE) has become an

increasingly popular subject of research interest. HIE can be defined in various ways, most often described as exercise above a certain heart rate percentage. When HIE is punctuated by rest breaks it is referred to as high-intensity interval training (HIIT), which can be further categorized as aerobic HIIT, or anaerobic HIIT (sprint interval training (SIT) (Ito, 2019). This type of exercise is further described in terms of activity and active rest period durations that occur at certain heart rate percentages, most often 85-95% of peak heart rate (Gibala, Little, Macdonald, & Hawley, 2012; Ito, 2019; Levinger et al., 2015). The most commonly researched SIT protocol being the Wingate test (Burgomaster, Hughes, Heigenhauser, Bradwell, & Gibala, 2005), and the most commonly researched HIIT exercise protocols being the 4X4 and 10X1 protocols (Ito, 2019). A 4X4 protocol consists of 4, 4-minute HIE sessions, while a 10X1 consists of 10, 1-minute HIE sessions. Rest break durations vary, with research studies supporting various ratios of work to rest.

The selection of our specific protocol was based in part on a meta-analysis performed by O'Donoghue et al. comparing six different exercise regimes' (vigorous-intensity aerobic, moderate-intensity aerobic, high-load resistance, moderate-load resistance, combined vigorous intensity, and combined moderate intensity) effects on cardiorespiratory fitness and anthropometry in obese individuals. The authors concluded that combined aerobic and resistance training at moderate or high intensity, and moderate aerobic intensity exercise had the most significant effects on body composition and physical fitness (O'Donoghue, Blake, Cunningham, Lennon, & Perrotta, 2021). Moderate aerobic exercise was defined according to the American College of Sports Medicine definition: 65%-75% of HR max 3-5 times per week for 30-60 minutes (O'Donoghue et al., 2021). Another study performed by Naylor et al. which was

relevant to the selection of our protocol examined the metabolic effects of six minutes of no-resistance cycle ergometry and 6 minutes of a ramped resistance high intensity cycle ergometry session (Nayor et al., 2020). Following this single, short bout of exercise the authors found statistically significant changes in over 500 circulating metabolites (Nayor et al., 2020). This study supports the notion that significant physiological changes can occur with even short duration acute exercise bouts. Possible mechanisms for exercise's role in increased longevity are the cardioprotective effects associated with exercise. These could include effects on endothelial function, autonomic tone, and inflammation among other potential cardioprotective mechanisms. A 2020 randomized controlled clinical trial by Stensvold et al. investigated the effects on mortality between three different exercise protocols in older women: high intensity interval training (HIIT) versus moderate intensity continuous training, versus standard exercise guidelines (Stensvold et al., 2020). Mortality in the HIIT group was 37% lower than in the control group, and 49% lower than in the moderate intensity continuous exercise group (Stensvold et al., 2020), although these differences did not reach statistical significance due to the overall low mortality rate, and involved wide confidence intervals. Despite the significant volume of exercise research, including the effects of exercise on aging processes and longevity, no studies to date have examined the specific effects of exercise on biological age and the underlying genes that are differentially expressed as we age. Until recently in fact, there had not been a single study investigating any non-pharmaceutical intervention's effect on biological age. That changed in July 2020 however, when a pilot study was published showing a greater than 3-year epigenetic age (using the Horvath DNAmAge clock) reversal through lifestyle modification, including exercise (Fitzgerald et al., 2020).

Unfortunately, multiple interventions were included in this study making it impossible to determine what portion of epigenetic age reversal is attributable to exercise. However, this study serves to validate the general hypothesis that lifestyle modification can reverse biological aging, but there is still a gap in the literature regarding the specific effects of exercise on biological aging and the mechanistic pathways underlying those effects.

The purpose of this graduate student research study is to determine the effect of a 4-week duration, 3-times per week, high-intensity interval exercise protocol on biological age as measured by blood cell RNA profiles (i.e., transcriptomic age). Although not directly studied, our overarching hope is that such effects might forecast longer-term benefits for healthspan and lifespan. Furthermore, we suggest specific transcriptomic mechanisms behind this exercise-induced reversal of biological age by examining the underlying genetic expression profiles of our participants at baseline and at the conclusion of our trial.

## References

- Atella, V., Piano Mortari, A., Kopinska, J., Belotti, F., Lapi, F., Cricelli, C., & Fontana, L. (2019). Trends in age-related disease burden and healthcare utilization. *Aging Cell*, *18*(1), e12861. doi:10.1111/accel.12861
- Bell, C. G., Lowe, R., Adams, P. D., Baccarelli, A. A., Beck, S., Bell, J. T., . . . Rakyan, V. K. (2019). DNA methylation aging clocks: challenges and recommendations. *Genome Biology*, *20*(1), 249. doi:10.1186/s13059-019-1824-y
- Benjamin, E. J., Virani, S. S., Callaway, C. W., Chamberlain, A. M., Chang, A. R., Cheng, S., . . . Muntner, P. (2018). Heart Disease and Stroke Statistics-2018 Update: A Report From the American Heart Association. *Circulation*, *137*(12), e67-e492. doi:10.1161/cir.0000000000000558
- Burgomaster, K. A., Hughes, S. C., Heigenhauser, G. J., Bradwell, S. N., & Gibala, M. J. (2005). Six sessions of sprint interval training increases muscle oxidative potential and cycle endurance capacity in humans. *J Appl Physiol* (1985), *98*(6), 1985-1990. doi:10.1152/jappphysiol.01095.2004
- Chang, A. Y., Skirbekk, V. F., Tyrovolas, S., Kassebaum, N. J., & Dieleman, J. L. (2019). Measuring population ageing: an analysis of the Global Burden of Disease Study 2017. *Lancet Public Health*, *4*(3), e159-e167. doi:10.1016/s2468-2667(19)30019-2
- Fahy, G. M., Brooke, R. T., Watson, J. P., Good, Z., Vasanaawala, S. S., Maecker, H., . . . Horvath, S. (2019). Reversal of epigenetic aging and immunosenescent trends in humans. *Aging Cell*, *18*(6), e13028. doi:10.1111/accel.13028
- Fitzgerald, K., Hodges, R., Hanes, D., Stack, E., Cheishvili, D., Szyf, M., . . . Bradley, R. (2020). Reversal of Epigenetic Age with Diet and Lifestyle in a Pilot Randomized Clinical Trial. *medRxiv*, 2020.2007.2007.20148098. doi:10.1101/2020.07.07.20148098
- Gibala, M. J., Little, J. P., Macdonald, M. J., & Hawley, J. A. (2012). Physiological adaptations to low-volume, high-intensity interval training in health and disease. *J Physiol*, *590*(5), 1077-1084. doi:10.1113/jphysiol.2011.224725
- Gremeaux, V., Gayda, M., Lepers, R., Sosner, P., Juneau, M., & Nigam, A. (2012). Exercise and longevity. *Maturitas*, *73*(4), 312-317. doi:<https://doi.org/10.1016/j.maturitas.2012.09.012>
- Hurd, M. D., Martorell, P., Delavande, A., Mullen, K. J., & Langa, K. M. (2013). Monetary costs of dementia in the United States. *N Engl J Med*, *368*(14), 1326-1334. doi:10.1056/NEJMsa1204629
- Ito, S. (2019). High-intensity interval training for health benefits and care of cardiac diseases - The key to an efficient exercise protocol. *World J Cardiol*, *11*(7), 171-188. doi:10.4330/wjc.v11.i7.171
- Jylhävä, J., Pedersen, N. L., & Hägg, S. (2017). Biological Age Predictors. *EBioMedicine*, *21*, 29-36. doi:<https://doi.org/10.1016/j.ebiom.2017.03.046>
- Levinger, I., Shaw, C. S., Stepto, N. K., Cassar, S., McAinch, A. J., Cheetham, C., & Maiorana, A. J. (2015). What Doesn't Kill You Makes You Fitter: A Systematic Review of High-Intensity Interval Exercise for Patients with Cardiovascular and Metabolic Diseases. *Clinical Medicine Insights. Cardiology*, *9*, 53-63. doi:10.4137/CMC.S26230
- Li, X., Ploner, A., Wang, Y., Magnusson, P. K. E., Reynolds, C., Finkel, D., . . . Hägg, S. (2020). Longitudinal trajectories, correlations and mortality associations of nine biological ages across 20-years follow-up. *Elife*, *9*, e51507. doi:10.7554/eLife.51507
- Lohman, T., Bains, G., Berk, L., & Lohman, E. (2021). Predictors of Biological Age: The Implications for Wellness and Aging Research. *Gerontol Geriatr Med*, *7*, 23337214211046419. doi:10.1177/23337214211046419
- Lu, A. T., Quach, A., Wilson, J. G., Reiner, A. P., Aviv, A., Raj, K., . . . Horvath, S. (2019). DNA methylation GrimAge strongly predicts lifespan and healthspan. *Aging*, *11*(2), 303-327. doi:10.18632/aging.101684

- Mariotto, A. B., Yabroff, K. R., Shao, Y., Feuer, E. J., & Brown, M. L. (2011). Projections of the cost of cancer care in the United States: 2010-2020. *Journal of the National Cancer Institute, 103*(2), 117-128. doi:10.1093/jnci/djq495
- Murphy, L. B., Cisternas, M. G., Pasta, D. J., Helmick, C. G., & Yelin, E. H. (2018). Medical Expenditures and Earnings Losses Among US Adults With Arthritis in 2013. *Arthritis Care Res (Hoboken), 70*(6), 869-876. doi:10.1002/acr.23425
- Nayor, M., Shah, R. V., Miller, P. E., Blodgett, J. B., Tanguay, M., Pico, A. R., . . . Lewis, G. D. (2020). Metabolic Architecture of Acute Exercise Response in Middle-Aged Adults in the Community. *Circulation, 142*(20), 1905-1924. doi:10.1161/circulationaha.120.050281
- O'Donoghue, G., Blake, C., Cunningham, C., Lennon, O., & Perrotta, C. (2021). What exercise prescription is optimal to improve body composition and cardiorespiratory fitness in adults living with obesity? A network meta-analysis. *Obesity reviews : an official journal of the International Association for the Study of Obesity, 22*(2), e13137-e13137. doi:10.1111/obr.13137
- Peters, M. J., Joehanes, R., Pilling, L. C., Schurmann, C., Conneely, K. N., Powell, J., . . . Consortium, N. U. (2015). The transcriptional landscape of age in human peripheral blood. *Nature Communications, 6*(1), 8570. doi:10.1038/ncomms9570
- Quach, A., Levine, M. E., Tanaka, T., Lu, A. T., Chen, B. H., Ferrucci, L., . . . Horvath, S. (2017). Epigenetic clock analysis of diet, exercise, education, and lifestyle factors. *Aging, 9*(2), 419-446. doi:10.18632/aging.101168
- Stensvold, D., Viken, H., Steinshamn, S. L., Dalen, H., Støylen, A., Loennechen, J. P., . . . Wisløff, U. (2020). Effect of exercise training for five years on all cause mortality in older adults-the Generation 100 study: randomised controlled trial. *Bmj, 371*, m3485. doi:10.1136/bmj.m3485
- Warburton, D. E. R., & Bredin, S. S. D. (2017). Health benefits of physical activity: a systematic review of current systematic reviews. *Curr Opin Cardiol, 32*(5), 541-556. doi:10.1097/hco.0000000000000437
- Zhao, W., Ammous, F., Ratliff, S., Liu, J., Yu, M., Mosley, T. H., . . . Smith, J. A. (2019). Education and Lifestyle Factors Are Associated with DNA Methylation Clocks in Older African Americans. *Int J Environ Res Public Health, 16*(17). doi:10.3390/ijerph16173141

## CHAPTER TWO

### Predictors of Biological Age: The Implications for Wellness and Aging Research

#### **Abstract**

As healthspan and lifespan research breakthroughs have become more commonplace, the need for valid, practical markers of biological age is becoming increasingly paramount. The accessibility and affordability of biological age predictors that can reveal information about mortality and morbidity risk, as well as remaining years of life, has profound clinical and research implications. In this review, we examine 5 groups of aging biomarkers capable of providing accurate biological age estimations. The unique capabilities of these biomarkers have far-reaching implications for the testing of both pharmaceutical and non-pharmaceutical interventions designed to slow or reverse biological aging. Additionally, the enhanced validity and availability of these tools may have increasingly relevant clinical value. The authors of this review explore those implications, with an emphasis on lifestyle modification research, and provide an overview of the current evidence regarding 5 biological age predictor categories: Telomere length, composite biomarkers, DNA methylation "epigenetic clocks," transcriptional predictors of biological age, and functional age predictors.

## Introduction

Age-related disease is a persistent and increasingly prevalent burden on healthcare systems around the world.(Atella et al., 2019; Benjamin et al., 2018; Chang et al., 2019; Hurd et al., 2013; Mariotto et al., 2011) Any affordable and accessible intervention capable of ameliorating this trend would therefore be of significant value. One class of interventions that seems well suited for this challenge is lifestyle modification. (Ruiz-Estigarribia et al., 2020; Wu et al., 2020; Y. B. Zhang et al., 2021) Although lifestyle-based interventions such as diet and exercise are generally known to increase lifespan, (Chudasama et al., 2020) experimental evidence is not as abundant as one might expect. Large volumes of research show positive effects from exercise on specific disease processes,(Campbell & Turner, 2018; Edwards et al., 2007; Larson & Bruce, 1987; Warburton & Bredin, 2017) and other studies have found association between lifestyle factors and longevity.(Quach et al., 2017; Sae-Lee et al., 2018; Zhao et al., 2019) However, fewer studies experimentally validate or quantify the causal effects of non-pharmaceutical lifestyle modification interventions on lifespan. This is likely due in part to the inherent time scale challenge that longevity research entails. Any future studies that examine lifestyle modification interventions would benefit from a practical tool that is capable of measuring change in expected lifespan.

One persistent challenge when studying the efficacy of interventions intended to increase lifespan is identifying an outcome measure that is both valid and feasible to use experimentally. From a validity perspective, change in total years of lifespan between experimental and control groups would be ideal, except for the fact that it would necessitate multi-decade longitudinal studies. Not only does this add significant cost and effort, but it also makes controlling for confounding variables exceedingly difficult. The apparent alternative to measuring actual lifespan would be to identify a biomarker or group of biomarkers capable of estimating remaining years of life. This would grant researchers the ability to test the efficacy of

interventions designed to increase lifespan without necessitating the use of long-term longitudinal studies.

Generally, metrics designed to predict remaining lifespan, mortality risk, and age-related morbidity risk have come to be known as predictors of biological age or biomarkers of aging. Consensus around these terms' definitions is lacking, as is the definition of aging more generally.(Butler et al., 2004) In his review of recent papers attempting to identify biomarkers of aging, Thomas Johnson cites one of the original clarifying statements by Baker and Sprott (Johnson, 2006):

“A Biomarker of Aging is a biological parameter of an organism that either alone or in some multivariate composite will, in the absence of disease, better predict functional capability at some late age, than will chronological age.”(Baker & Sprott, 1988)

Even though it was written in 1988, this statement went a long way towards establishing the current criteria for biomarkers of aging. A potential concern with this definition for a researcher interested in examining interventions capable of biological age reversal is that there is no mention of lifespan. This definition discusses functional capability only. Another potential point of disagreement among researchers may be the “in the absence of disease” criterion. It seems that a useful metric for aging research would include the effects of age-related disease on lifespan.

In the time since this statement was published there has been much development and discussion regarding the exact meaning of the term, “biomarker of aging”. An interdisciplinary workshop cosponsored by the International Longevity Center-USA, The Ellison Medical Foundation, Kronos Longevity Research Institute, the Institute for the Study of Aging, and Canyon Ranch Health Resort proposed the following three parameters for biomarkers of aging:

1. The biomarker should predict the outcome of a wide range of age-sensitive tests in multiple physiological and behavioral domains, in an age-coherent way, and do so better than chronological age.

2. It should predict remaining longevity at an age at which 90% of the population is still alive and do so for most of the specific illnesses that afflict the species under study.
3. Its measurement should not alter life expectancy or the outcome of subsequent tests of other age-sensitive tests.

The American Federation for Aging Research (AFAR) formulated the criteria for aging biomarkers as follows(Butler et al., 2004; Johnson, 2006; Jylhävä et al., 2017)

1. It must predict the rate of aging. In other words, it would tell exactly where a person is in their total life span. It must be a better predictor of life span than chronological age.
2. It must monitor a basic process that underlies the aging process, not the effects of disease.
3. It must be able to be tested repeatedly without harming the person. For example, a blood test or an imaging technique.
4. It must be something that works in humans and in laboratory animals, such as mice. This is so it can be tested in lab animals before being validated in humans.

Although both clear and thorough lists, the existence of a biomarker that meets all of the criteria above may be unlikely.(Johnson, 2006) Perhaps the most challenging criterion for researchers intending to measure the effects of interventions on lifespan and healthspan is the American Federation for Aging Research criterion 2 listed above. This statement outlines the need for an aging biomarker to separate the aging process from disease processes. This may not always be possible, and it is hard to differentiate the effects of the aging process from the effects of age-related disease. That said, this criterion does illustrate the need to create markers that are not influenced by acute illnesses or diseases that have no effect on lifespan. As mentioned earlier there is not consensus on what the definition of aging is within the aging research community, let alone agreement that there is a specific aging process or aging rate that is separate from disease processes.(Butler et al., 2004; Johnson, 2006) What is clear, even to a lay observer, is that if we examine a large group of 70-year-old people, we would find a phenotypically diverse sample, despite all members being the same chronological age. This is described clearly and concisely by Lowsky et al. in their paper's introductory sentence: "For a

surprisingly large segment of the older population, chronological age is not a relevant marker for understanding, measuring, or experiencing healthy aging.”(Lowsky, Olshansky, Bhattacharya, & Goldman, 2014) This may be the most concise way to illustrate the need for a valid and easy to obtain measure of biological age.

For the purposes of this scoping review, we will be focusing on biomarkers of aging that satisfy at least some of the American Federation of Aging Research biomarkers of aging criteria. Given the lack of consensus around terminology and definition, we will seek to view biomarkers in the context of their ability to predict two aspects of biological age: healthspan and lifespan. These criteria best facilitate the selection of a marker that measures the effectiveness of interventions on biological age reversal. Until recently, the possibility of biological age reversal was uncertain, but thanks to recent experimental trials utilizing biological age predictors we now know that biological age as measured by biomarkers of aging can be slowed or even reversed. (Fahy et al., 2019; Fitzgerald et al., 2020; Hachmo et al., 2020) With that in mind, our specific aim is to compile the available evidence related to various readily accessible biological age predictors. In doing so we hope to provide a basis for selection in future experimental studies that utilizes wellness and lifestyle interventions to slow or reverse biological aging. For example, investigators could choose to examine diet modification, sleep quality, exercise type or quantity, supplementation, implementation of a stress management program, or any number of other wellness interventions’ effects on biological age. This has far reaching implications for the wellness and successful aging research communities, as it provides a means to assess the effectiveness of an intervention on biological age in a comparatively short time frame.

This paper investigates and summarizes the following predictors of biological age: Telomere length, allostatic load index, DNA methylation clocks, functional age, and transcriptional predictors of biological age. The ability of these tools to estimate mortality risk and biological age, operationally defined as an estimate of remaining healthspan/lifespan, will be highlighted. Various capabilities and weaknesses of each will be examined as well, including

criteria such as: ease of use, accessibility, ability to glean underlying mechanisms influencing lifespan/healthspan, and other relevant features.

### **Search Strategy and Selection Criteria**

Using the PubMed database, Medical Subject Headings (MeSH) terms “Aging” and “Humans” and the specific terms for each of the biomarkers of aging categories: 1) Telomere Length, 2.) Frailty Index or Deficit Accumulation or Functional age, 3.) Epigenetic clock, 4.) Transcriptomic age or Transcriptional age, 5) Composite biomarker or Allostatic load index, were combined. Cited papers in the selected publications and papers that referenced the selected publications were also considered. The searches were performed between December 2020 and May 2021.

### **Telomere Length**

Telomeres are repeating sequences of nucleoprotein caps located at the ends of chromosomes.(Sanders & Newman, 2013) Each time a cell undergoes mitosis, a section of these nucleotides is cleaved, and the telomere shortens incrementally. This is an overly simplistic description given that oxidative stress is also associated with telomere shortening and multiple mechanisms exist for telomere lengthening as well.(Sanders & Newman, 2013) Even with this simple definition however, an inference can be drawn that telomere length serves in part as a cumulative measure of cellular division and by extension, age. This would be a well-founded inference and one that has received significant attention from the aging research community. As of March 13, 2021, the search phrase “Telomere Length” on the PubMed database yielded 10,245 results, making it the most investigated biomarker of aging discussed in this article. Multiple meta-analyses exist examining the relationship between telomere length and age.(Gardner et al., 2014; Lapham et al., 2015) Additionally, many studies have shown

relationships between telomere length and specific disease processes associated with increased chronological age. A 2014 meta-analysis (43,725 individuals) showed an inverse relationship between telomere length and coronary heart disease independent of traditional vascular risk factors.(Haycock et al., 2014) Similar results have been obtained when investigating Alzheimer’s disease and telomere length. Both observational and mendelian randomization studies (a method of analyzing single nucleotide polymorphisms to determine causation) have shown that patients diagnosed with Alzheimer’s disease have shorter telomere lengths.(Forero et al., 2016; Zhan & Hägg, 2018) Despite this prevalence of age-related telomere research, data pertaining to telomere length and mortality risk specifically has been less consistent. Perhaps the most compelling investigation is a meta-analysis performed by Wang et al. in 2018 that examined the relationship between telomere length and all-cause mortality. Twenty-five studies were determined to meet eligibility for inclusion (121,749 combined individuals), including 4 Swedish Twin Registry (STR) cohorts (12,083 individuals). Results from the Swedish twin registry studies showed one standard deviation reduction of leukocytic telomere length corresponded to 13% increased all-cause mortality risk (95% confidence interval 7%-19%).(Wang, Zhan, Pedersen, Fang, & Hägg, 2018) However, a study by Li et al that examined 9 different biomarkers of aging over a 20 year timeframe found that the only marker not associated with mortality risk was in fact, telomere length.(Li et al., 2020) Another Swedish study performed by Svensson et al. examined the relationship between telomere length and mortality in 2744 elderly men and also found no association.(Svensson et al., 2014) The evidence presented here indicates that telomere length is associated with various disease processes, but that the research pertaining to its use as a predictor of biological age may be contradictory.

Table 1:

Telomere Length				
Study Title	BA Predictor Used	Cohort name (if applicable)	n	Results
Telomere Length and All-Cause	Telomere Length	Multiple cohorts	121,749	one standard deviation reduction of leukocytic

Mortality: A Meta-analysis				telomere length corresponded to 13% increased all-cause mortality risk (95% confidence interval 7%-19%)(Wang et al., 2018)
Longitudinal trajectories, correlations, and mortality associations of nine biological ages across 20-years follow-up	Telomere Length, DNAm Age (4 types), Physiological Age, Cognitive Function, Functional Aging Index, and Frailty Index	Swedish Population Based Cohort	636	No evidence that telomere length associated with mortality risk.(Li et al., 2020)
Leukocyte telomere length is not associated with mortality in older men	Telomere Length	Prospective population-based MrOS-Sweden study	2744	Using Cox proportional hazards regression, tertile of LTL did not associate with all-cause mortality [tertile 1 (shortest) or 2 (middle) vs. tertile 3 (longest); hazard ratio (HR)=1.05, 95% confidence interval (CI) 0.85-1.28 and HR=0.97, 95% CI 0.79-1.19, respectively].(Svensson et al., 2014)

**Composite Biomarkers/Allostatic Load Indices**

In 1998 Bruce McEwen described allostasis as “adaptation in the face of potentially stressful challenges [that] involves activation of neural, neuroendocrine, and neuroendocrine-immune mechanisms.”(McEwen, 1998) The phrase “constancy through change” is often used as shorthand to describe allostasis, as it so concisely describes the constant changing physiological processes that maintain homeostasis. Fava et al. describes allostatic load as reflecting the cumulative effects of stressful experiences in daily life that may lead to disease over time(Fava

et al., 2019). Like telomere length, allostasis and allostatic load have been extensively researched. Most commonly, this research focuses on the relationship between allostatic load and various health outcomes such as cognition,(Juster, McEwen, & Lupien, 2010) chronic stress,(Juster et al., 2010) sleep quality,(McEwen & Karatsoreos, 2015) age-related disease,(Danese & McEwen, 2012) cardiovascular disease,(Logan & Barksdale, 2008) and addiction(Koob & Schulkin, 2019) among others. A smaller portion of allostasis research is dedicated to evaluating the performance of allostatic load as a predictor of biological age. The study that has perhaps best demonstrated the capability of an allostatic predictor of biological age is part of the MacArthur studies of successful aging series in 2005 that utilized 10 physiological parameters to generate allostatic load scores in 171 70–79-year-old adults.(Karlamañgla, Singer, & Seeman, 2006) An Allostatic load score or index falls under a broader category of biological age predictors called composite biomarkers of aging. This is due to the combination of multiple blood biomarkers and clinical measures used to make an estimation regarding mortality risk. Other predictors within this category include phenotypic age(Levine et al., 2018) and physiological age.(Li et al., 2020)

In the previously mentioned study published by Karlamañgla in 2005,(Karlamañgla et al., 2006) allostatic load scores were generated first in 1988 and again in 1991. The mortality status of these individuals was determined 4.5 years later in 1995. This study found that individuals with increased allostatic load in 1991 compared to 1988 had increased risk of all-cause mortality (15% versus 5% respectively  $p = .47$ ). Further analysis revealed that each incremental increase in allostatic load score was associated with a mortality odds ratio of 3.3 (95% confidence interval 1.1-9.8).(Karlamañgla et al., 2006)

A study by Castagne et al (2018), took another significant step towards establishing allostatic load as a predictor of biological age. This study examined the relationship between 14 biomarkers across 4 physiological systems and their relationship to mortality in a UK birth cohort study of 8,113 adults.(Castagné et al., 2018) The hazard ratio for participants with a high allostatic load score was found to be 3.56 (2.2 to 5.3) and was significantly higher than in

participants with a low allostatic load score.(Castagné et al., 2018) Their data suggests that those with a high allostatic load score at age 44 are approximately 3 times more likely to die by age 55.(Castagné et al., 2018) The authors also analyzed the relative contribution of each of the 14 biomarkers that comprised the allostatic load score. Interestingly, after adjusting for various risk factors and adverse childhood experiences, 5 of the 14 biomarkers stood out as being significantly related to mortality (C-Reactive Protein, fibrinogen, glycated hemoglobin, heart rate, and peak expiratory flow).(Castagné et al., 2018) This highlights one potential challenge and opportunity for the future use of allostatic load indices as BA prediction tools. The challenge is the general lack of consensus regarding the relative contribution of each marker or combination of markers, and the opportunity is the potential to develop even simpler yet more accurate composite age biomarkers. Future validation studies examining a variety of different indices will be helpful in making these determinations. As it stands, allostatic load appears to be significantly correlated with mortality-risk, and allostatic indices will serve as valuable tools for aging research.

Table 2:

Allostatic Load/Composite Biomarkers				
Study Title	BA Predictor Used	Cohort name (if applicable)	n	Results
Reduction in allostatic load in older adults is associated with lower all-cause mortality risk: MacArthur studies of successful aging.	Allostatic Load Index		171	Adjusted for age and baseline allostatic load, each unit increment in the allostatic load change score was associated with mortality odds ratio of 3.3 (95% confidence interval, 1.1-9.8).(Karlman et al., 2006)
Allostatic load and subsequent all-cause mortality: which	Allostatic Load Index	1958 British birth cohort	8113	Hazard ratios for participants with a mid ( $3 \leq AL < 5$ ) and high AL ( $\geq 5$ ) were 1.98 (1.25 to

biological markers drive the relationship? Findings from a UK birth cohort				3.13) and 3.56 (2.2 to 5.53), respectively and were found to be significantly greater than in participants with a low AL (< 3)(Castagné et al., 2018)
An epigenetic biomarker of aging for lifespan and healthspan	Phenotypic Age Estimator	Third and Fourth National Health and Nutrition Examination Survey	9926, 6209	a one-year increase in phenotypic age is associated with a 9% increase in the risk of all-cause mortality (HR=1.09, p=3.8E-49), a 9% increase in the risk of mortality from aging-related diseases (HR=1.09, p=4.5E-34), a 10% increase in the risk of CVD mortality (HR=1.10, p=5.1E-17), a 7% increase in the risk of cancer mortality (HR=1.07, p=7.9E-10), a 20% increase in the risk of diabetes mortality (HR=1.20, p=1.9E-11), and a 9% increase in the risk of chronic lower respiratory disease mortality (HR=1.09, p=6.3E-4)(Levine et al., 2018)

### DNA Methylation “Epigenetic Clocks”

The term epigenetic “clock” refers to tools that analyze DNA methylation levels within a set of Cytosine-Phosphate-Guanine (CpG) sites and are generally acknowledged as accurate measures of biological age.(Bell et al., 2019; Fransquet, Wrigglesworth, Woods, Ernst, & Ryan, 2019; Jylhävä et al., 2017; Lu et al., 2019; Perna et al., 2016) In fact, one study we examined made the claim that DNA methylation clocks are the current best predictors of

mortality.(Unnikrishnan et al., 2019) While this may be true, it is important to realize that the term DNA methylation age or epigenetic clock can refer to many different tools. While all of these “clocks” analyze methylation in specific CpG sites, they all do so in different ways. For example, two clocks that were among the first to generate widespread interest are the Horvath clock(Horvath, 2013) and Hannum clock.(Hannum et al., 2013) The Horvath clock is based on methylation levels of 353 CpG sites using the Illumina 27k or 450k array,(Horvath, 2013) while the Hannum clock uses 71 CpG sites, and utilizes data from the Illumina 450k array.(Hannum et al., 2013) Epigenetic clocks’ ability to predict biological and chronological age can also be tissue dependent. For example, the Horvath clock performs similarly among various tissue types(Horvath, 2013) (“whole blood, peripheral blood mononuclear cells, cerebellar samples, occipital cortex, buccal epithelium, colon, adipose, liver, lung, saliva, uterine cervix as well as in individual cell types such as CD4 T cells and CD14 monocytes, and immortalized B cells”), while the Hannum clock performs best using peripheral whole blood samples(Hannum et al., 2013; Jylhävä et al., 2017). These clocks also vary in terms of their ability to predict biological and chronological age (chronological age  $r^2$  values = 0.96 for Horvath and 0.91 for Hannum).(Jylhävä et al., 2017) Accessibility is also highly variable; as property of the specific inventor or institution that created the algorithm capable of converting array-based methylation data into other useful data (such as biological age estimation in years or mortality risk among others), some of these tools may be commercial. While other clocks, such as the Horvath clock or GrimAge marker created by Steve Horvath and Ake Lu are freely available online. The clocks mentioned so far are just a few examples of DNA methylation biomarkers of aging. This is to illustrate that the term “epigenetic clock” is broad and not a specific marker. With this in mind, we can say generally that one of the most interesting and unique features of epigenetic clocks is their ability to predict mortality risk, also referenced as time-to-death. A 2016 meta-analysis of 13 cohorts representing a combined sample size of 13,089 showed that epigenetic age acceleration (a measure of the difference between chronological age and epigenetic age) was predictive of mortality independent of chronological age ( $p \leq 8.2 \times 10^{-10}$ )

<sup>9</sup>).(Chen et al., 2016) This was still found to be true after adjusting for additional risk factors, but at a significance of  $p < 5.4 \times 10^{-4}$ .(Chen et al., 2016) When epigenetic age estimates incorporated additional information pertaining to blood cell composition, the resulting time-to-death predictions were highly significant ( $p = 7.5 \times 10^{-43}$ ).(Chen et al., 2016)

In the time since this 2016 meta-analysis, new DNA methylation clocks have emerged that are even more capable in terms of their ability to estimate mortality risk. For example, a 2017 study by Zhang et al. proposes a mortality risk score based on 10 CpG sites that is strongly associated with all-cause mortality.(Y. Zhang et al., 2017) Participants with scores of 1 display a hazard ratio (95% confidence intervals) of 2.16 (1.1-4.24), compared to those with scores of 2-5 showing a hazard ratio of 3.42 (1.81-6.46) compared to those with 5+ scores showing a hazard ratio of 7.36 (3.69-14.68).(Y. Zhang et al., 2017) Another marker called DNAm PhenoAge was calculated in a meta-analysis of five large samples ( $n = 2,016$ ,  $n = 2,191$ ,  $n = 2,553$ , and  $n = 657$ ). It was found that a 1-year increase in DNAm PhenoAge is associated with a highly significant 4.5% increase in all-cause mortality risk (meta  $p$ -value =  $7.9 \times 10^{-47}$ ).(Levine et al., 2018)

In addition to measuring mortality risk, some markers have the added capability of predicting the risk of developing specific disease processes. For example, a metric known as GrimAge can strongly predict time-to-death (Cox regression  $P = 2.0 \times 10^{-75}$ ), time-to-coronary heart disease (Cox regression  $P = 6.2 \times 10^{-24}$ ), and time-to-cancer ( $P = 1.3 \times 10^{-12}$ ).(Lu et al., 2019) The study authors used large scale validation data from the Framingham heart study to complete this analysis. By adding a calculation that quantifies the difference between GrimAge and chronological age (AgeAccelGrim) other relevant age-related associations are found to be present. For example, AgeAccelGrim is associated with comorbidity count ( $p = 3.45 \times 10^{-17}$ ), time to congestive heart failure ( $p = 4.9 \times 10^{-10}$ ), time-to-incident coronary heart disease ( $p = 6.2 \times 10^{-24}$ ), hypertension ( $p = 5.1 \times 10^{-13}$ ), and type 2 diabetes ( $p = 0.01$ ).(Lu et al., 2019) All associations were in the expected direction (increased AgeAccelGrim = increased likelihood of poor outcome) with varying odds ratios.(Lu et al., 2019)

Table 3:

DNA Methylation "Clocks"				
Study Title	BA Predictor Used	Cohort name (if applicable)	n	Results
DNA methylation GrimAge strongly predicts lifespan and healthspan	GrimAge	Framingham Heart Study Offspring Cohort	2356	predictive ability for time-to-death (Cox regression $P=2.0E-75$ ), time-to-coronary heart disease (Cox $P=6.2E-24$ ), time-to-cancer ( $P=1.3E-12$ )(Lu et al., 2019)
DNA methylation age of human tissues and cell types	DNAm Age "Horvath Clock"	82 publicly available datasets	7844	The multi-tissue age predictor performs remarkably well in most tissues and cell types. (Age correlation 0.97, error = 2.9 years)(Horvath, 2013)
Genome-wide Methylation Profiles Reveal Quantitative Views of Human Aging Rates	"Hannum Clock"		656	Correlation between age and predicted age of 96% and an error of 3.9 years(Hannum et al., 2013)
An epigenetic biomarker of aging for lifespan and healthspan	PhenoAge	Women's Health Initiative (WHI), the Framingham Heart Study (FHS), the Normative Aging Study (NAS), the Jackson Heart Study (JHS)	2016, 2191, 2553, 657, 1747	A one-year increase in DNAm PhenoAge is associated with a 4.5% increase in the risk of all-cause mortality (Meta(FE)=1.045, Meta $p=7.9E-47$ (Levine et al., 2018)
Longitudinal trajectories, correlations and mortality associations of nine biological ages across 20-years follow-up	Telomere Length, DNAm Age (4 types), Physiological Age, Cognitive Function, Functional Aging Index,	Swedish Population Based Cohort	845	Individually, all BAs except for telomere length were associated with mortality risk independently of CA. The largest effects were seen for methylation age estimators (GrimAge) and the frailty index (FI). (Li et al., 2020)

	and Frailty Index			
DNA methylation-based measures of biological age: meta-analysis predicting time to death	Horvath and Hannum	13 cohorts	13,089	All considered measures of epigenetic age acceleration were predictive of mortality ( $p \leq 8.2 \times 10^{-9}$ ) (Chen et al., 2016)
DNA methylation signatures in peripheral blood strongly predict all-cause mortality	Zhang 10 CpG clock		1900	demonstrated that a risk score based on DNAm of ten identified CpGs was a very strong predictor for all-cause, CVD and cancer mortality (Y. Zhang et al., 2017)

### Transcriptional Predictors of Biological Age

A transcriptional predictor of biological age analyzes genetic expression in genes associated with aging to make some prediction regarding the biological aging process. One example of this tool is the Transcriptomic Age Prediction Tool (TRAP) which is described in the paper titled “The transcriptional landscape of age in human peripheral blood” written by Peters et al. in 2015. This study performed a whole-blood gene expression meta-analysis in 14,983 individuals and identified 1,497 genes that are differentially expressed with chronological age. This provided the basis for calculating a “transcriptomic age” and associating it with various age-related phenotypes including: blood pressure, fasting glucose, and BMI. (Peters et al., 2015) This was the first large scale meta-analysis to examine age-related gene expression profiles and build a predictor of biological age from this data. The correlation between the transcriptomic age predictor and chronological age was significant ( $p < 2 \times 10^{-29}$ ), (Peters et al., 2015) and observed differences between the transcriptomic age predictor (TRAP) and chronological age are thought to reflect altered biological age. This is supported by consistent associations

between increased delta age (increased TRAP compared to chronological age) and higher blood pressure, total cholesterol, fasting glucose levels, and BMI(Peters et al., 2015). Peters et al. identified a subset of 1,396 individuals from two studies within their meta-analysis (KORA(Holle, Happich, Löwel, & Wichmann, 2005) and Rotterdam studies(Hofman et al., 2007)) that had both methylation and gene expression data available. The presence of these two datasets allowed the investigators to generate a transcriptomic predictor of biological age, in addition to Horvath(Horvath, 2013) and Hannum(Hannum et al., 2013) clock values. This gave investigators the opportunity to examine correlation between three different biomarkers of aging: TRAP, Horvath Clock, Hannum Clock. They found TRAP to correlate positively, albeit weakly, with both clocks ( $r^2=.1$  for Hannum and  $.33$  for Horvath).

Other transcriptional predictors of biological age exist, such as the healthy ageing gene score, (Sood et al., 2015) and RNAAgeCalc. (Ren & Kuan, 2020) Like the previously discussed epigenetic clocks, these measures' ability to predict disease process, mortality, and association with age-related phenotypes varies. At the time of this writing the literature seems to indicate that the transcriptome is an age-associated variable indicating its utility in creating biological age predictors, but existing transcriptomic clocks are pending broader validation.(Harries et al., 2011; Holly et al., 2013; Jylhävä et al., 2017)

Table 4:

Transcriptomics				
Study Title	BA Predictor Used	Cohort name (if applicable)	n	Results
The Transcriptional Landscape of Age in Human Peripheral Blood	Transcriptomic Age Prediction Tool	The Rotterdam Study	14926	The correlation between chronological age and transcriptomic age was significant in all cohorts ( $P<2E-29$ ) A positive delta age, interpreted as reflecting more rapid biological ageing, was consistently associated with higher

				systolic and diastolic blood pressure, total cholesterol, HDL cholesterol, fasting glucose levels and body mass index (BMI) Transcriptomic age and epigenetic age (both Hannum and Horvath) were positively correlated, with $r^2$ values varying between 0.10 and 0.33(Peters et al., 2015)
--	--	--	--	---

### Functional Age Estimators

Although not blood biomarkers, functional age estimators are included here due to their ease of use and relevance to aging research. The term functional age is now commonly found in literature, but these tools were initially intended to be a method for estimating frailty and the likelihood of care entry, not biological age. More recently, some functional age estimators have been shown to estimate mortality-risk(Burn et al., 2018; Church, Rogers, Rockwood, & Theou, 2020; Finkel, Sternäng, Jylhävä, Bai, & Pedersen, 2019; Kojima, Iliffe, & Walters, 2018; Li et al., 2020) and therefore present as highly practical measures for lifestyle modification research. The large volume of functional age estimators merits a standalone review, but some notable examples will be discussed here. Two of these are the frailty index (FI) and frailty phenotype (FP). Although they are sometimes discussed as being interchangeable, they are two different tools for different purposes. The term frailty index refers to a method of quantifying frailty in older individuals, with the underlying mechanism being a measurement of deficit accumulation (deficits identified/deficits measured). Rather than a specific tool or metric, it is a method in which various measures of frailty and functional capability can be assessed and from which a scoring system can be derived. Frailty Phenotype on the other hand is based on the presence or absence of 5 signs or symptoms (>10lbs unintentional weight loss in the past 12 mo., self-reported exhaustion, weak grip strength, slow walking speed, and low physical activity).(Cesari,

Gambassi, Abellan van Kan, & Vellas, 2014; Fried et al., 2001) Although both FP and FI are associated with mortality-risk,(Shi et al., 2019) we will focus our discussion on Frailty index. This is not necessarily a comment on either's ability to predict biological age, but rather how responsive each may be to lifestyle interventions. Given the relatively broad scope and ordinal nature of the 5-item Frailty phenotype, it may be less responsive to intervention and less suited as a research variable compared to the Frailty Index.(Cesari et al., 2014; Clegg, Young, Iliffe, Rikkert, & Rockwood, 2013) The Frailty Phenotype may be better implemented as a screening tool, inclusion/exclusion criterion, or stratification mechanism given that it does not require a full geriatric comprehensive assessment like the FI.(Clegg et al., 2013)

One of the originally described functional indices, called the Canadian Study of Healthy Aging (CSHA) Frailty Index is validated by the Canadian Study of Healthy Aging and examines the presence or absence of 70 clinical deficits in order to quantify fitness and frailty in the elderly.(Kenneth Rockwood et al., 2005) This list of deficits was not meant to be a fixed index however, in fact it has been reported that indices with as few as 50 clinical deficits can be highly useful, and some indices with as few as 20 items have been explored.(K. Rockwood & Mitnitski, 2012) Other tools related to the frailty index have been developed such as the Edmonton Frailty scale(Clegg et al., 2013; Rolfson, Majumdar, Tsuyuki, Tahir, & Rockwood, 2006) and Clinical Frailty Scale.(Kenneth Rockwood et al., 2005) The Clinical Frailty Scale is a 7-point scale that is highly correlated to the original 70-point index ( $r^2=.90$ ). (Kenneth Rockwood et al., 2005) More importantly given an aging research context, each 1 point increase in the scale was found to correspond with a 21.2% increased risk of death in the next 70 months.(Kenneth Rockwood et al., 2005) In a study of 1788 community-dwelling elders frailty as defined by the FI was associated with a 2.31 fold increased risk of all-cause death compared to those who scored robust on the index.(Shi et al., 2019) Another study of 5536 community-dwelling elderly found the relationship between FI and mortality to be significant ( $P < .0001$ ). Interestingly, a meta-analysis examining frailty index scores between men and women found what the authors described as a "male-female health-survival paradox".(Gordon et al., 2017) The paradox was

that at all ages females displayed higher FI scores, despite males having higher mortality rates at each level of the frailty index.(Gordon et al., 2017) Frailty sex differences extended to diet as well. A study examining older adults found that low meat consumption (less than 2x/wk.) was associated with increased frailty in men only. Increased frailty in women was associated with decreased fish, meat, vegetables, and potatoes.(Shibasaki, Kin, Yamada, Akishita, & Ogawa, 2019) Perhaps most relevant to the aim of this paper, one study comparing nine different biological age predictors, found Frailty Index (42-item Rockwood(Jiang et al., 2017)) to have one of the strongest associations with mortality risk among the nine markers examined, being exceeded only by GrimAge.(Li et al., 2020) Given these results, some frailty indices may serve lifestyle intervention research well alongside other biomarkers, or perhaps even as stand-alone outcome variables.

Table 5:

Functional Age Estimators				
Study Title	BA Predictor Used	Cohort name (if applicable)	n	Results
Frailty index as a predictor of all-cause and cause-specific mortality in a Swedish population-based cohort	42-item Rockwood	Swedish Adoption/Twin Study of Aging	1477	The categorized FI levels demonstrated a dose-response increase in mortality risk with increased frailty in both men and women.(Jiang et al., 2017)
Frailty phenotype, frailty index and risk of mortality in Chinese elderly population-Rugao longevity and ageing study	Frailty Index	Ageing arm of Rugao Longevity and Ageing Study	1788	Frailty defined by the frailty index was associated with a 2.31 fold (95% CI 1.16-4.6) risk of all-cause death compared with robust elderly.(Shi et al., 2019)

Frailty index as a predictor of mortality: a systematic review and meta-analysis	Frailty Index	18 cohorts		All meta-analyses suggested that higher FI was significantly associated with higher mortality risk.(Kojima et al., 2018)
--	---------------	------------	--	--

**Discussion**

No statement in this paper is intended to make a recommendation regarding the use of a specific biological age predictor; neither is this review an exhaustive list. In addition to less investigated biological age predictors like proteomics, and metabolomics, there are multitudes of individual markers associated with accelerated biological aging such as glycated hemoglobin, triglycerides, blood pressure, resting heart rate, waist-to-hip ratio, fibrinogen, albumin, crp, interleukin-6, and many others. (Jylhävä et al., 2017; Kane & Sinclair, 2019) Our aim is to compile relevant information pertaining to various promising predictors of biological age validated in large cohorts to assist future researchers interested in using them as outcome measures. There is also no implication that all biomarkers of aging are equally valid. A compelling comparison of nine biological age estimators that examined longitudinal trajectories, correlations, and mortality associations across 20 years was performed by Li et al. 2020.(Li et al., 2020) Their study examined data from a Swedish based cohort of 845 men and women aged 63.6 (8.6) at baseline and compared the validity of four different DNA methylation age estimators Horvath,(Horvath, 2013) Hannum,(Hannum et al., 2013) PhenoAge,(Levine et al., 2018) and GrimAge(Lu et al., 2019)), three different functional age estimators (functional aging index,(Finkel et al., 2019) frailty index,(Jiang et al., 2017) cognitive function(Reynolds et al., 2005)), telomere length,(Berglund et al., 2016) and a composite biomarker called physiological age that included various biomarkers and measures of body composition. All four DNA methylation age estimators, physiological age, and all three functional age estimators were

associated with mortality risk independent of chronological age, while telomere length was not. Of the nine biomarkers of aging examined, GrimAge and the Frailty index stood out as being most associated with mortality risk.

The information presented here sheds light on the large variety of biomarkers of aging available, each with its own specific capabilities. Even still, the markers discussed are just a small portion of the available biomarkers of aging in existence. Like any other biomarker, the predictor used in future experimental studies should be based on the specific aims and needs of those studies. A study that aims to assess the effects of a vegan diet on coronary heart disease risk may benefit from utilizing the GrimAge marker since it has been shown to predict time-to-coronary heart disease.(Lu et al., 2019) Investigators could obtain a baseline GrimAge value, implement an intervention protocol, and obtain a GrimAge value at the conclusion of the trial. When compared to a control group, the difference in GrimAge values could be analyzed to determine if biological age was slowed or reversed. An example of this methodology was implemented in the 2019 Fahy et al study, Reversal of Epigenetic Aging and Immunosenescent Trends in Humans, in which investigators reported a 2.5 year reversal in mean epigenetic age following a 1 yr. human growth hormone and metformin treatment protocol.(Fahy et al., 2019) A study that aims to determine the transcriptional basis for any observed changes in biological age resulting from lifestyle modification may find a transcriptomic predictor most appropriate due to the ability to obtain a biological age estimation and gene expression profile from a single blood sample. If an investigator is limited in terms of their capability to analyze gene expression profiles, DNA methylation of CpG sites, or blood biomarkers, perhaps a functional age estimator such as a frailty index could provide relevant data on biological aging changes in an intervention group. If feasibility allows it, the combination of various predictors of biological age could yield even more robust results. Various factors will dictate the most appropriate selection for future lifestyle modification research, not the least of which being accessibility, cost, applicability to multiple tissue types, and conversely, specificity to a study's specific tissue of interest. A possible limitation to this review may be that only papers written in English were included. Additionally, this is an emerging field with many potential biological age predictors to consider. We selected five of the most investigated biological age predictors with large-scale cohort

validation and therefore there may be promising new predictors that were not included in this review.

### **Conclusion:**

This paper highlights an inherent challenge in searching for the “best” biomarker(s) of aging. Any researcher seeking to utilize one of these biomarkers must first clearly define their aims. They must also seek to understand and explain how they are using the term biological age or biomarker(s) of aging. It may be preferable to instead use more descriptive terminology such as DNA methylation age/Epigenetic age (BA as measured by an epigenetic clock), transcriptomic age (BA as measured by a transcriptomic age predictor), or functional age (BA as measured by a deficit accumulation index such as a frailty index). These terms go further to explain the nature of the data, how it is obtained, and how it may be best interpreted. They also help to add some clarity given the array of emergent terminology used in biological age prediction research. Our aim at the outset of this paper was to view these markers in the context of their ability to predict healthspan and lifespan. Telomere length is certainly the most extensively studied biomarker of age-related disease. Consequentially, many conclusions have been made regarding the association between telomere length, age, disease, stress, and multiple other health outcomes. While no study that we know of has sought to produce an easy-to-use telomere length biological age prediction tool, TL has been used to predict mortality risk, albeit with mixed results. Epigenetic clocks appear to have the upper hand in terms of accessibility (many are freely accessed online), and they also appear to best predict time-to-death, time-to-cancer, and other age-related processes.(Li et al., 2020; Lu et al., 2019; McCrory et al., 2020) It also seems that they may have the greatest degree of large-scale cohort validation. Perhaps the only area where epigenetic clocks are not the apparent “leader” of the biological age prediction discussion is in their ability to identify the mechanism behind differences in chronological and biological aging, although discovery is taking place rapidly.(W. Zhang, Qu, Liu, & Belmonte, 2020) It is in this domain that transcriptional predictors of biological aging may add value as

they rely on gene expression data to estimate biological age. A researcher could potentially examine changes in both biological age and genetic expression to make an inference regarding the mechanism behind the observed biological age acceleration/deceleration from a single blood sample. A “best of both worlds” scenario may involve the inclusion of a more validated DNA methylation marker like GrimAge, alongside a genetic expression profile of relevant genetic pathways. This would allow an investigator to report an intervention’s effect on biological age, as well as an analysis of the specific changes in gene expression that may have contributed to that change.

Each of these tools has unique capabilities and limitations. For this reason, the most robust option for a future researcher is likely the inclusion of multiple biomarkers of aging based on those unique features.

A central goal of lifestyle modification is to reduce disease risk and promote healthy, successful aging. The ability of biological age predictors to assess an intervention’s contribution to mortality/morbidity risk makes them highly relevant measures for studies examining the effects of lifestyle modification on age-related disease. Future studies examining the effects of diet, supplementation, exercise, stress-reduction techniques, sleep quality/quantity, or any number of other lifestyle modification interventions could benefit greatly from the inclusion of a biological age predictor.

## References

- Amar, D., Lindholm, M. E., Norrbom, J., Wheeler, M. T., Rivas, M. A., & Ashley, E. A. (2021). Time trajectories in the transcriptomic response to exercise - a meta-analysis. *Nature Communications*, *12*(1), 3471. doi:10.1038/s41467-021-23579-x
- Atella, V., Piano Mortari, A., Kopinska, J., Belotti, F., Lapi, F., Cricelli, C., & Fontana, L. (2019). Trends in age-related disease burden and healthcare utilization. *Aging Cell*, *18*(1), e12861. doi:10.1111/acel.12861
- Aune, D., Schlesinger, S., Leitzmann, M. F., Tonstad, S., Norat, T., Riboli, E., & Vatten, L. J. (2021). Physical activity and the risk of heart failure: a systematic review and dose-response meta-analysis of prospective studies. *Eur J Epidemiol*, *36*(4), 367-381. doi:10.1007/s10654-020-00693-6
- Baker, G. T., 3rd, & Sprott, R. L. (1988). Biomarkers of aging. *Exp Gerontol*, *23*(4-5), 223-239. doi:10.1016/0531-5565(88)90025-3
- Barrès, R., Yan, J., Egan, B., Treebak, J. T., Rasmussen, M., Fritz, T., . . . Zierath, J. R. (2012). Acute exercise remodels promoter methylation in human skeletal muscle. *Cell Metab*, *15*(3), 405-411. doi:10.1016/j.cmet.2012.01.001
- Bell, C. G., Lowe, R., Adams, P. D., Baccarelli, A. A., Beck, S., Bell, J. T., . . . Rakyan, V. K. (2019). DNA methylation aging clocks: challenges and recommendations. *Genome Biology*, *20*(1), 249. doi:10.1186/s13059-019-1824-y
- Benjamin, E. J., Virani, S. S., Callaway, C. W., Chamberlain, A. M., Chang, A. R., Cheng, S., . . . Muntner, P. (2018). Heart Disease and Stroke Statistics-2018 Update: A Report From the American Heart Association. *Circulation*, *137*(12), e67-e492. doi:10.1161/cir.0000000000000558
- Berglund, K., Reynolds, C. A., Ploner, A., Gerritsen, L., Hovatta, I., Pedersen, N. L., & Hägg, S. (2016). Longitudinal decline of leukocyte telomere length in old age and the association with sex and genetic risk. *Aging*, *8*(7), 1398-1415. doi:10.18632/aging.100995
- Burgomaster, K. A., Hughes, S. C., Heigenhauser, G. J., Bradwell, S. N., & Gibala, M. J. (2005). Six sessions of sprint interval training increases muscle oxidative potential and cycle endurance capacity in humans. *J Appl Physiol* (1985), *98*(6), 1985-1990. doi:10.1152/jappphysiol.01095.2004
- Burn, R., Hubbard, R. E., Scrase, R. J., Abey-Nesbit, R. K., Peel, N. M., Schluter, P. J., & Jamieson, H. A. (2018). A frailty index derived from a standardized comprehensive geriatric assessment predicts mortality and aged residential care admission. *BMC Geriatr*, *18*(1), 319. doi:10.1186/s12877-018-1016-8
- Butler, R. N., Sprott, R., Warner, H., Bland, J., Feuers, R., Forster, M., . . . Wolf, N. (2004). Aging: The Reality: Biomarkers of Aging: From Primitive Organisms to Humans. *The Journals of Gerontology: Series A*, *59*(6), B560-B567. doi:10.1093/gerona/59.6.B560
- Camarda, S. R., Tebexreni, A. S., Páfaró, C. N., Sasai, F. B., Tambeiro, V. L., Juliano, Y., & Barros Neto, T. L. (2008). Comparison of maximal heart rate using the prediction equations proposed by Karvonen and Tanaka. *Arq Bras Cardiol*, *91*(5), 311-314. doi:10.1590/s0066-782x2008001700005
- Campbell, J. P., & Turner, J. E. (2018). Debunking the Myth of Exercise-Induced Immune Suppression: Redefining the Impact of Exercise on Immunological Health Across the Lifespan. *Frontiers in immunology*, *9*, 648-648. doi:10.3389/fimmu.2018.00648
- Castagné, R., Garès, V., Karimi, M., Chadeau-Hyam, M., Vineis, P., Delpierre, C., & Kelly-Irving, M. (2018). Allostatic load and subsequent all-cause mortality: which biological markers drive the relationship? Findings from a UK birth cohort. *Eur J Epidemiol*, *33*(5), 441-458. doi:10.1007/s10654-018-0364-1

- CDC. (2022). Adult Physical Activity Prevalence. Retrieved from <https://www.cdc.gov/physicalactivity/data/inactivity-prevalence-maps/index.html>
- Cesari, M., Gambassi, G., Abellan van Kan, G., & Vellas, B. (2014). The frailty phenotype and the frailty index: different instruments for different purposes. *Age and Ageing, 43*(1), 10-12. doi:10.1093/ageing/aft160
- Chang, A. Y., Skirbekk, V. F., Tyrovolas, S., Kassebaum, N. J., & Dieleman, J. L. (2019). Measuring population ageing: an analysis of the Global Burden of Disease Study 2017. *Lancet Public Health, 4*(3), e159-e167. doi:10.1016/s2468-2667(19)30019-2
- Chen, B. H., Marioni, R. E., Colicino, E., Peters, M. J., Ward-Caviness, C. K., Tsai, P. C., . . . Horvath, S. (2016). DNA methylation-based measures of biological age: meta-analysis predicting time to death. *Ageing, 8*(9), 1844-1865. doi:10.18632/aging.101020
- Chudasama, Y. V., Khunti, K., Gillies, C. L., Dhalwani, N. N., Davies, M. J., Yates, T., & Zaccardi, F. (2020). Healthy lifestyle and life expectancy in people with multimorbidity in the UK Biobank: A longitudinal cohort study. *PLoS Med, 17*(9), e1003332. doi:10.1371/journal.pmed.1003332
- Church, S., Rogers, E., Rockwood, K., & Theou, O. (2020). A scoping review of the Clinical Frailty Scale. *BMC Geriatr, 20*(1), 393. doi:10.1186/s12877-020-01801-7
- Clegg, A., Young, J., Iliffe, S., Rikkert, M. O., & Rockwood, K. (2013). Frailty in elderly people. *Lancet (London, England), 381*(9868), 752-762. doi:10.1016/S0140-6736(12)62167-9
- Cobbold, C. (2018). Battle of the sexes: Which is better for you, high- or low-intensity exercise? *J Sport Health Sci, 7*(4), 429-432. doi:10.1016/j.jshs.2018.05.004
- Cole, S. W. (2009). Social Regulation of Human Gene Expression. *Current Directions in Psychological Science, 18*(3), 132-137. doi:10.1111/j.1467-8721.2009.01623.x
- Cole, S. W., Levine, M. E., Arevalo, J. M., Ma, J., Weir, D. R., & Crimmins, E. M. (2015). Loneliness, eudaimonia, and the human conserved transcriptional response to adversity. *Psychoneuroendocrinology, 62*, 11-17. doi:10.1016/j.psyneuen.2015.07.001
- Committee, P. A. G. A. In. Physical Activity Guidelines Advisory Committee Report Washington, DC: U.S. Dept of Health and Human Services.
- Danese, A., & McEwen, B. S. (2012). Adverse childhood experiences, allostasis, allostatic load, and age-related disease. *Physiol Behav, 106*(1), 29-39. doi:10.1016/j.physbeh.2011.08.019
- Denham, J., O'Brien, B. J., Marques, F. Z., & Charchar, F. J. (2015). Changes in the leukocyte methylome and its effect on cardiovascular-related genes after exercise. *J Appl Physiol (1985), 118*(4), 475-488. doi:10.1152/jappphysiol.00878.2014
- Draghici, S., Khatri, P., Tarca, A. L., Amin, K., Done, A., Voichita, C., . . . Romero, R. (2007). A systems biology approach for pathway level analysis. *Genome Res, 17*(10), 1537-1545. doi:10.1101/gr.6202607
- Edwards, K. M., Burns, V. E., Allen, L. M., McPhee, J. S., Bosch, J. A., Carroll, D., . . . Ring, C. (2007). Eccentric exercise as an adjuvant to influenza vaccination in humans. *Brain, Behavior, and Immunity, 21*(2), 209-217. doi:<https://doi.org/10.1016/j.bbi.2006.04.158>
- Fahy, G. M., Brooke, R. T., Watson, J. P., Good, Z., Vasanaawala, S. S., Maecker, H., . . . Horvath, S. (2019). Reversal of epigenetic aging and immunosenescent trends in humans. *Ageing Cell, 18*(6), e13028. doi:10.1111/acel.13028
- Fava, G. A., McEwen, B. S., Guidi, J., Gostoli, S., Offidani, E., & Sonino, N. (2019). Clinical characterization of allostatic overload. *Psychoneuroendocrinology, 108*, 94-101. doi:<https://doi.org/10.1016/j.psyneuen.2019.05.028>
- Finkel, D., Sternäng, O., Jylhävä, J., Bai, G., & Pedersen, N. L. (2019). Functional Aging Index Complements Frailty in Prediction of Entry Into Care and Mortality. *J Gerontol A Biol Sci Med Sci, 74*(12), 1980-1986. doi:10.1093/gerona/glz155

- Fiorito, G., Caini, S., Palli, D., Bendinelli, B., Saieva, C., Ermini, I., . . . Masala, G. (2021). DNA methylation-based biomarkers of aging were slowed down in a two-year diet and physical activity intervention trial: the DAMA study. *Aging Cell*, *20*(10), e13439. doi:<https://doi.org/10.1111/ace1.13439>
- Fitzgerald, K., Hodges, R., Hanes, D., Stack, E., Cheishvili, D., Szyf, M., . . . Bradley, R. (2020). Reversal of Epigenetic Age with Diet and Lifestyle in a Pilot Randomized Clinical Trial. *medRxiv*, 2020.2007.2007.20148098. doi:10.1101/2020.07.07.20148098
- Forero, D. A., González-Giraldo, Y., López-Quintero, C., Castro-Vega, L. J., Barreto, G. E., & Perry, G. (2016). Meta-analysis of Telomere Length in Alzheimer's Disease. *The Journals of Gerontology: Series A*, *71*(8), 1069-1073. doi:10.1093/gerona/glw053
- Fransquet, P. D., Wrigglesworth, J., Woods, R. L., Ernst, M. E., & Ryan, J. (2019). The epigenetic clock as a predictor of disease and mortality risk: a systematic review and meta-analysis. *Clinical Epigenetics*, *11*(1), 62. doi:10.1186/s13148-019-0656-7
- Fried, L. P., Tangen, C. M., Walston, J., Newman, A. B., Hirsch, C., Gottdiener, J., . . . McBurnie, M. A. (2001). Frailty in older adults: evidence for a phenotype. *J Gerontol A Biol Sci Med Sci*, *56*(3), M146-156. doi:10.1093/gerona/56.3.m146
- Gardner, M., Bann, D., Wiley, L., Cooper, R., Hardy, R., Nitsch, D., . . . Ben-Shlomo, Y. (2014). Gender and telomere length: systematic review and meta-analysis. *Exp Gerontol*, *51*, 15-27. doi:10.1016/j.exger.2013.12.004
- Gibala, M. J., Little, J. P., Macdonald, M. J., & Hawley, J. A. (2012). Physiological adaptations to low-volume, high-intensity interval training in health and disease. *J Physiol*, *590*(5), 1077-1084. doi:10.1113/jphysiol.2011.224725
- Glei, D. A., Goldman, N., Risques, R. A., Rehkopf, D. H., Dow, W. H., Rosero-Bixby, L., & Weinstein, M. (2016). Predicting Survival from Telomere Length versus Conventional Predictors: A Multinational Population-Based Cohort Study. *PLOS ONE*, *11*(4), e0152486. doi:10.1371/journal.pone.0152486
- Gordon, E. H., Peel, N. M., Samanta, M., Theou, O., Howlett, S. E., & Hubbard, R. E. (2017). Sex differences in frailty: A systematic review and meta-analysis. *Exp Gerontol*, *89*, 30-40. doi:10.1016/j.exger.2016.12.021
- Gremeaux, V., Gayda, M., Lepers, R., Sosner, P., Juneau, M., & Nigam, A. (2012). Exercise and longevity. *Maturitas*, *73*(4), 312-317. doi:<https://doi.org/10.1016/j.maturitas.2012.09.012>
- Gu, T., Hao, P., Chen, P., & Wu, Y. (2022). A Systematic Review and Meta-Analysis of the Effectiveness of High-Intensity Interval Training in People with Cardiovascular Disease at Improving Depression and Anxiety. *Evid Based Complement Alternat Med*, *2022*, 8322484. doi:10.1155/2022/8322484
- Hachmo, Y., Hadanny, A., Abu Hamed, R., Daniel-Kotovskiy, M., Catalogna, M., Fishlev, G., . . . Efrati, S. (2020). Hyperbaric oxygen therapy increases telomere length and decreases immunosenescence in isolated blood cells: a prospective trial. *Aging*, *12*(22), 22445-22456. doi:10.18632/aging.202188
- Hagströmer, M., Oja, P., & Sjöström, M. (2006). The International Physical Activity Questionnaire (IPAQ): a study of concurrent and construct validity. *Public Health Nutr*, *9*(6), 755-762. doi:10.1079/phn2005898
- Han, M., Qie, R., Shi, X., Yang, Y., Lu, J., Hu, F., . . . Zhao, Y. (2022). Cardiorespiratory fitness and mortality from all causes, cardiovascular disease and cancer: dose-response meta-analysis of cohort studies. *British Journal of Sports Medicine*, *56*(13), 733. doi:10.1136/bjsports-2021-104876
- Hannan, A. L., Hing, W., Simas, V., Climstein, M., Coombes, J. S., Jayasinghe, R., . . . Furness, J. (2018). High-intensity interval training versus moderate-intensity continuous training within cardiac rehabilitation: a systematic review and meta-analysis. *Open Access J Sports Med*, *9*, 1-17. doi:10.2147/oajsm.s150596

- Hannum, G., Guinney, J., Zhao, L., Zhang, L., Hughes, G., Sada, S., . . . Zhang, K. (2013). Genome-wide methylation profiles reveal quantitative views of human aging rates. *Mol Cell*, *49*(2), 359-367. doi:10.1016/j.molcel.2012.10.016
- Harries, L. W., Hernandez, D., Henley, W., Wood, A. R., Holly, A. C., Bradley-Smith, R. M., . . . Melzer, D. (2011). Human aging is characterized by focused changes in gene expression and deregulation of alternative splicing. *Aging Cell*, *10*(5), 868-878. doi:<https://doi.org/10.1111/j.1474-9726.2011.00726.x>
- Haycock, P. C., Heydon, E. E., Kaptoge, S., Butterworth, A. S., Thompson, A., & Willeit, P. (2014). Leucocyte telomere length and risk of cardiovascular disease: systematic review and meta-analysis. *Bmj*, *349*, g4227. doi:10.1136/bmj.g4227
- Hofman, A., Breteler, M. M., van Duijn, C. M., Krestin, G. P., Pols, H. A., Stricker, B. H., . . . Witteman, J. C. (2007). The Rotterdam Study: objectives and design update. *Eur J Epidemiol*, *22*(11), 819-829. doi:10.1007/s10654-007-9199-x
- Holle, R., Happich, M., Löwel, H., & Wichmann, H. E. (2005). KORA--a research platform for population based health research. *Gesundheitswesen*, *67 Suppl 1*, S19-25. doi:10.1055/s-2005-858235
- Holly, A. C., Melzer, D., Pilling, L. C., Henley, W., Hernandez, D. G., Singleton, A. B., . . . Harries, L. W. (2013). Towards a gene expression biomarker set for human biological age. *Aging Cell*, *12*(2), 324-326. doi:<https://doi.org/10.1111/accel.12044>
- Horvath, S. (2013). DNA methylation age of human tissues and cell types. *Genome Biology*, *14*(10), 3156. doi:10.1186/gb-2013-14-10-r115
- Hurd, M. D., Martorell, P., Delavande, A., Mullen, K. J., & Langa, K. M. (2013). Monetary costs of dementia in the United States. *N Engl J Med*, *368*(14), 1326-1334. doi:10.1056/NEJMsa1204629
- Ito, S. (2019). High-intensity interval training for health benefits and care of cardiac diseases - The key to an efficient exercise protocol. *World J Cardiol*, *11*(7), 171-188. doi:10.4330/wjc.v11.i7.171
- Jiang, M., Foebel, A. D., Kuja-Halkola, R., Karlsson, I., Pedersen, N. L., Hägg, S., & Jylhävä, J. (2017). Frailty index as a predictor of all-cause and cause-specific mortality in a Swedish population-based cohort. *Aging*, *9*(12), 2629-2646. doi:10.18632/aging.101352
- Johnson, T. E. (2006). Recent results: biomarkers of aging. *Exp Gerontol*, *41*(12), 1243-1246. doi:10.1016/j.exger.2006.09.006
- Juster, R. P., McEwen, B. S., & Lupien, S. J. (2010). Allostatic load biomarkers of chronic stress and impact on health and cognition. *Neurosci Biobehav Rev*, *35*(1), 2-16. doi:10.1016/j.neubiorev.2009.10.002
- Jylhävä, J., Pedersen, N. L., & Hägg, S. (2017). Biological Age Predictors. *EBioMedicine*, *21*, 29-36. doi:<https://doi.org/10.1016/j.ebiom.2017.03.046>
- Kane, A. E., & Sinclair, D. A. (2019). Frailty biomarkers in humans and rodents: Current approaches and future advances. *Mech Ageing Dev*, *180*, 117-128. doi:10.1016/j.mad.2019.03.007
- Karlamangla, A. S., Singer, B. H., & Seeman, T. E. (2006). Reduction in allostatic load in older adults is associated with lower all-cause mortality risk: MacArthur studies of successful aging. *Psychosom Med*, *68*(3), 500-507. doi:10.1097/01.psy.0000221270.93985.82
- Kojima, G., Iliffe, S., & Walters, K. (2018). Frailty index as a predictor of mortality: a systematic review and meta-analysis. *Age Ageing*, *47*(2), 193-200. doi:10.1093/ageing/afx162
- Koob, G. F., & Schulkin, J. (2019). Addiction and stress: An allostatic view. *Neurosci Biobehav Rev*, *106*, 245-262. doi:10.1016/j.neubiorev.2018.09.008
- Kresovich, J. K., Garval, E. L., Martinez Lopez, A. M., Xu, Z., Niehoff, N. M., White, A. J., . . . Taylor, J. A. (2021). Associations of Body Composition and Physical Activity Level With Multiple Measures of Epigenetic Age Acceleration. *American Journal of Epidemiology*, *190*(6), 984-993. doi:10.1093/aje/kwaa251

- Kroenke, K., Spitzer, R. L., & Williams, J. B. (2001). The PHQ-9: validity of a brief depression severity measure. *Journal of general internal medicine*, *16*(9), 606-613. doi:10.1046/j.1525-1497.2001.016009606.x
- Lapham, K., Kvale, M. N., Lin, J., Connell, S., Croen, L. A., Dispensa, B. P., . . . Blackburn, E. H. (2015). Automated Assay of Telomere Length Measurement and Informatics for 100,000 Subjects in the Genetic Epidemiology Research on Adult Health and Aging (GERA) Cohort. *Genetics*, *200*(4), 1061-1072. doi:10.1534/genetics.115.178624
- Larson, E. B., & Bruce, R. A. (1987). Health Benefits of Exercise in an Aging Society. *Archives of Internal Medicine*, *147*(2), 353-356. doi:10.1001/archinte.1987.00370020171058
- Lee, E.-H. (2012). Review of the Psychometric Evidence of the Perceived Stress Scale. *Asian Nursing Research*, *6*(4), 121-127. doi:<https://doi.org/10.1016/j.anr.2012.08.004>
- Levine, M. E., Lu, A. T., Quach, A., Chen, B. H., Assimes, T. L., Bandinelli, S., . . . Horvath, S. (2018). An epigenetic biomarker of aging for lifespan and healthspan. *Aging*, *10*(4), 573-591. doi:10.18632/aging.101414
- Levinger, I., Shaw, C. S., Stepto, N. K., Cassar, S., McAinch, A. J., Cheetham, C., & Maiorana, A. J. (2015). What Doesn't Kill You Makes You Fitter: A Systematic Review of High-Intensity Interval Exercise for Patients with Cardiovascular and Metabolic Diseases. *Clinical Medicine Insights. Cardiology*, *9*, 53-63. doi:10.4137/CMC.S26230
- Levis, B., Sun, Y., He, C., Wu, Y., Krishnan, A., Bhandari, P. M., . . . Zhang, Y. (2020). Accuracy of the PHQ-2 Alone and in Combination With the PHQ-9 for Screening to Detect Major Depression: Systematic Review and Meta-analysis. *Jama*, *323*(22), 2290-2300. doi:10.1001/jama.2020.6504
- Li, X., Ploner, A., Wang, Y., Magnusson, P. K. E., Reynolds, C., Finkel, D., . . . Hägg, S. (2020). Longitudinal trajectories, correlations and mortality associations of nine biological ages across 20-years follow-up. *Elife*, *9*, e51507. doi:10.7554/eLife.51507
- Little, J. P., Safdar, A., Wilkin, G. P., Tarnopolsky, M. A., & Gibala, M. J. (2010). A practical model of low-volume high-intensity interval training induces mitochondrial biogenesis in human skeletal muscle: potential mechanisms. *J Physiol*, *588*(Pt 6), 1011-1022. doi:10.1113/jphysiol.2009.181743
- Logan, J. G., & Barksdale, D. J. (2008). Allostasis and allostatic load: expanding the discourse on stress and cardiovascular disease. *J Clin Nurs*, *17*(7b), 201-208. doi:10.1111/j.1365-2702.2008.02347.x
- Lohman, T., Bains, G., Berk, L., & Lohman, E. (2021). Predictors of Biological Age: The Implications for Wellness and Aging Research. *Gerontol Geriatr Med*, *7*, 23337214211046419. doi:10.1177/23337214211046419
- López-Valenciano, A., Mayo, X., Liguori, G., Copeland, R. J., Lamb, M., & Jimenez, A. (2020). Changes in sedentary behaviour in European Union adults between 2002 and 2017. *BMC Public Health*, *20*(1), 1206. doi:10.1186/s12889-020-09293-1
- Lowsky, D. J., Olshansky, S. J., Bhattacharya, J., & Goldman, D. P. (2014). Heterogeneity in Healthy Aging. *The Journals of Gerontology: Series A*, *69*(6), 640-649. doi:10.1093/gerona/glt162
- Lu, A. T., Quach, A., Wilson, J. G., Reiner, A. P., Aviv, A., Raj, K., . . . Horvath, S. (2019). DNA methylation GrimAge strongly predicts lifespan and healthspan. *Aging*, *11*(2), 303-327. doi:10.18632/aging.101684
- Mariotto, A. B., Yabroff, K. R., Shao, Y., Feuer, E. J., & Brown, M. L. (2011). Projections of the cost of cancer care in the United States: 2010-2020. *Journal of the National Cancer Institute*, *103*(2), 117-128. doi:10.1093/jnci/djq495
- McCrary, C., Fiorito, G., Hernandez, B., Polidoro, S., O'Halloran, A. M., Hever, A., . . . Kenny, R. A. (2020). GrimAge Outperforms Other Epigenetic Clocks in the Prediction of Age-Related Clinical Phenotypes and All-Cause Mortality. *The Journals of Gerontology: Series A*. doi:10.1093/gerona/glaa286

- McEwen, B. S. (1998). Stress, adaptation, and disease. Allostasis and allostatic load. *Ann N Y Acad Sci*, 840, 33-44. doi:10.1111/j.1749-6632.1998.tb09546.x
- McEwen, B. S., & Karatsoreos, I. N. (2015). Sleep Deprivation and Circadian Disruption: Stress, Allostasis, and Allostatic Load. *Sleep Med Clin*, 10(1), 1-10. doi:10.1016/j.jsmc.2014.11.007
- Merrett, F. (2006). Reflections on the Hawthorne Effect. *Educational Psychology*, 26(1), 143-146. doi:10.1080/01443410500341080
- Meyer, D. H., & Schumacher, B. (2021). BiT age: A transcriptome-based aging clock near the theoretical limit of accuracy. *Aging Cell*, 20(3), e13320. doi:10.1111/accel.13320
- Min, L., Wang, D., You, Y., Fu, Y., & Ma, X. (2021). Effects of High-Intensity Interval Training on Sleep: A Systematic Review and Meta-Analysis. *Int J Environ Res Public Health*, 18(20). doi:10.3390/ijerph182010973
- Murphy, L. B., Cisternas, M. G., Pasta, D. J., Helmick, C. G., & Yelin, E. H. (2018). Medical Expenditures and Earnings Losses Among US Adults With Arthritis in 2013. *Arthritis Care Res (Hoboken)*, 70(6), 869-876. doi:10.1002/acr.23425
- Myers, J., Prakash, M., Froelicher, V., Do, D., Partington, S., & Atwood, J. E. (2002). Exercise Capacity and Mortality among Men Referred for Exercise Testing. *New England Journal of Medicine*, 346(11), 793-801. doi:10.1056/NEJMoa011858
- Nakajima, K., Takeoka, M., Mori, M., Hashimoto, S., Sakurai, A., Nose, H., . . . Taniguchi, S. (2010). Exercise effects on methylation of ASC gene. *Int J Sports Med*, 31(9), 671-675. doi:10.1055/s-0029-1246140
- Nayor, M., Shah, R. V., Miller, P. E., Blodgett, J. B., Tanguay, M., Pico, A. R., . . . Lewis, G. D. (2020). Metabolic Architecture of Acute Exercise Response in Middle-Aged Adults in the Community. *Circulation*, 142(20), 1905-1924. doi:10.1161/circulationaha.120.050281
- Northey, J. M., Cherbuin, N., Pampa, K. L., Smees, D. J., & Rattray, B. (2018). Exercise interventions for cognitive function in adults older than 50: a systematic review with meta-analysis. *British Journal of Sports Medicine*, 52(3), 154. doi:10.1136/bjsports-2016-096587
- O'Brien, M. A., Costin, B. N., & Miles, M. F. (2012). Using genome-wide expression profiling to define gene networks relevant to the study of complex traits: from RNA integrity to network topology. *Int Rev Neurobiol*, 104, 91-133. doi:10.1016/b978-0-12-398323-7.00005-7
- O'Donoghue, G., Blake, C., Cunningham, C., Lennon, O., & Perrotta, C. (2021). What exercise prescription is optimal to improve body composition and cardiorespiratory fitness in adults living with obesity? A network meta-analysis. *Obesity reviews : an official journal of the International Association for the Study of Obesity*, 22(2), e13137-e13137. doi:10.1111/obr.13137
- Ouerghi, N., Fradj, M. K. B., Bezrati, I., Khammassi, M., Feki, M., Kaabachi, N., & Bouassida, A. (2017). Effects of high-intensity interval training on body composition, aerobic and anaerobic performance and plasma lipids in overweight/obese and normal-weight young men. *Biology of sport*, 34(4), 385-392. doi:10.5114/biolSport.2017.69827
- Papadopoli, D., Boulay, K., Kazak, L., Pollak, M., Mallette, F., Topisirovic, I., & Hulea, L. (2019). mTOR as a central regulator of lifespan and aging. *F1000Research*, 8, F1000 Faculty Rev-1998. doi:10.12688/f1000research.17196.1
- Park, J. H., Moon, J. H., Kim, H. J., Kong, M. H., & Oh, Y. H. (2020). Sedentary Lifestyle: Overview of Updated Evidence of Potential Health Risks. *Korean J Fam Med*, 41(6), 365-373. doi:10.4082/kjfm.20.0165
- Perna, L., Zhang, Y., Mons, U., Holleczer, B., Saum, K.-U., & Brenner, H. (2016). Epigenetic age acceleration predicts cancer, cardiovascular, and all-cause mortality in a German case cohort. *Clinical Epigenetics*, 8, 64-64. doi:10.1186/s13148-016-0228-z

- Peters, M. J., Joehanes, R., Pilling, L. C., Schurmann, C., Conneely, K. N., Powell, J., . . . Consortium, N. U. (2015). The transcriptional landscape of age in human peripheral blood. *Nature Communications*, *6*(1), 8570. doi:10.1038/ncomms9570
- Quach, A., Levine, M. E., Tanaka, T., Lu, A. T., Chen, B. H., Ferrucci, L., . . . Horvath, S. (2017). Epigenetic clock analysis of diet, exercise, education, and lifestyle factors. *Aging*, *9*(2), 419-446. doi:10.18632/aging.101168
- Ren, X., & Kuan, P. F. (2020). RNAAgeCalc: A multi-tissue transcriptional age calculator. *PLOS ONE*, *15*(8), e0237006. doi:10.1371/journal.pone.0237006
- Reynolds, C. A., Finkel, D., McArdle, J. J., Gatz, M., Berg, S., & Pedersen, N. L. (2005). Quantitative genetic analysis of latent growth curve models of cognitive abilities in adulthood. *Dev Psychol*, *41*(1), 3-16. doi:10.1037/0012-1649.41.1.3
- Riebe, D., Ehrman, J. K., Liguori, G., & Magal, M. Chapter 6 General Principles of Exercise Prescription. In: ACSM's Guidelines for Exercise Testing and Prescription. 10th Ed. In (pp. 143-179). In: ACSM's Guidelines for Exercise Testing and Prescription.: Wolters Kluwer/Lippincott Williams & Wilkins.
- Rockwood, K., & Mitnitski, A. (2012). How Might Deficit Accumulation Give Rise to Frailty? *J Frailty Aging*, *1*(1), 8-12. doi:10.14283/jfa.2012.2
- Rockwood, K., Song, X., MacKnight, C., Bergman, H., Hogan, D. B., McDowell, I., & Mitnitski, A. (2005). A global clinical measure of fitness and frailty in elderly people. *CMAJ : Canadian Medical Association journal = journal de l'Association medicale canadienne*, *173*(5), 489-495. doi:10.1503/cmaj.050051
- Rolfson, D. B., Majumdar, S. R., Tsuyuki, R. T., Tahir, A., & Rockwood, K. (2006). Validity and reliability of the Edmonton Frail Scale. *Age and Ageing*, *35*(5), 526-529. doi:10.1093/ageing/af1041
- Rozenek, R., Salassi, J. W., 3rd, Pinto, N. M., & Fleming, J. D. (2016). Acute Cardiopulmonary and Metabolic Responses to High-Intensity Interval Training Protocols Using 60 s of Work and 60 s Recovery. *J Strength Cond Res*, *30*(11), 3014-3023. doi:10.1519/jsc.0000000000001414
- Ruiz-Estigarribia, L., Martínez-González, M., Díaz-Gutiérrez, J., Gea, A., Rico-Campà, A., & Bes-Rastrollo, M. (2020). Lifestyle-Related Factors and Total Mortality in a Mediterranean Prospective Cohort. *Am J Prev Med*, *59*(2), e59-e67. doi:10.1016/j.amepre.2020.01.032
- Sae-Lee, C., Corsi, S., Barrow, T. M., Kuhnle, G. G. C., Bollati, V., Mathers, J. C., & Byun, H. M. (2018). Dietary Intervention Modifies DNA Methylation Age Assessed by the Epigenetic Clock. *Mol Nutr Food Res*, *62*(23), e1800092. doi:10.1002/mnfr.201800092
- Sanders, J. L., & Newman, A. B. (2013). Telomere length in epidemiology: a biomarker of aging, age-related disease, both, or neither? *Epidemiol Rev*, *35*(1), 112-131. doi:10.1093/epirev/mxs008
- Scott, S. N., Shepherd, S. O., Hopkins, N., Dawson, E. A., Strauss, J. A., Wright, D. J., . . . Cocks, M. (2019). Home-hit improves muscle capillarisation and eNOS/NAD(P)H oxidase protein ratio in obese individuals with elevated cardiovascular disease risk. *The Journal of Physiology*, *597*(16), 4203-4225. doi:<https://doi.org/10.1113/JP278062>
- Sellami, M., Bragazzi, N., Prince, M. S., Denham, J., & Elrayess, M. (2021). Regular, Intense Exercise Training as a Healthy Aging Lifestyle Strategy: Preventing DNA Damage, Telomere Shortening and Adverse DNA Methylation Changes Over a Lifetime. *Front Genet*, *12*, 652497. doi:10.3389/fgene.2021.652497
- Shi, G. P., Ma, T., Zhu, Y. S., Wang, Z. D., Chu, X. F., Wang, Y., . . . Jiang, X. Y. (2019). Frailty phenotype, frailty index and risk of mortality in Chinese elderly population- Rugao longevity and ageing study. *Arch Gerontol Geriatr*, *80*, 115-119. doi:10.1016/j.archger.2018.11.001
- Shibasaki, K., Kin, S. K., Yamada, S., Akishita, M., & Ogawa, S. (2019). Sex-related differences in the association between frailty and dietary consumption in Japanese older people: a cross-sectional study. *BMC Geriatr*, *19*(1), 211. doi:10.1186/s12877-019-1229-5

- Sood, S., Gallagher, I. J., Lunnon, K., Rullman, E., Keohane, A., Crossland, H., . . . Timmons, J. A. (2015). A novel multi-tissue RNA diagnostic of healthy ageing relates to cognitive health status. *Genome Biology*, *16*(1), 185-185. doi:10.1186/s13059-015-0750-x
- Stensvold, D., Viken, H., Steinshamn, S. L., Dalen, H., Støylen, A., Loennechen, J. P., . . . Wisløff, U. (2020). Effect of exercise training for five years on all cause mortality in older adults-the Generation 100 study: randomised controlled trial. *Bmj*, *371*, m3485. doi:10.1136/bmj.m3485
- Su, L., Fu, J., Sun, S., Zhao, G., Cheng, W., Dou, C., & Quan, M. (2019). Effects of HIIT and MICT on cardiovascular risk factors in adults with overweight and/or obesity: A meta-analysis. *PLOS ONE*, *14*(1), e0210644. doi:10.1371/journal.pone.0210644
- Svensson, J., Karlsson, M. K., Ljunggren, Ö., Tivesten, Å., Mellström, D., & Movérare-Skrtic, S. (2014). Leukocyte telomere length is not associated with mortality in older men. *Exp Gerontol*, *57*, 6-12. doi:10.1016/j.exger.2014.04.013
- Tarca, A. L., Draghici, S., Khatri, P., Hassan, S. S., Mittal, P., Kim, J. S., . . . Romero, R. (2009). A novel signaling pathway impact analysis. *Bioinformatics*, *25*(1), 75-82. doi:10.1093/bioinformatics/btn577
- Unnikrishnan, A., Freeman, W. M., Jackson, J., Wren, J. D., Porter, H., & Richardson, A. (2019). The role of DNA methylation in epigenetics of aging. *Pharmacol Ther*, *195*, 172-185. doi:10.1016/j.pharmthera.2018.11.001
- Vaiserman, A., & Krasnienkov, D. (2020). Telomere Length as a Marker of Biological Age: State-of-the-Art, Open Issues, and Future Perspectives. *Front Genet*, *11*, 630186. doi:10.3389/fgene.2020.630186
- Wang, Q., Zhan, Y., Pedersen, N. L., Fang, F., & Hägg, S. (2018). Telomere Length and All-Cause Mortality: A Meta-analysis. *Ageing Res Rev*, *48*, 11-20. doi:10.1016/j.arr.2018.09.002
- Warburton, D. E. R., & Bredin, S. S. D. (2017). Health benefits of physical activity: a systematic review of current systematic reviews. *Curr Opin Cardiol*, *32*(5), 541-556. doi:10.1097/hco.0000000000000437
- Weichhart, T. (2018). mTOR as Regulator of Lifespan, Aging, and Cellular Senescence: A Mini-Review. *Gerontology*, *64*(2), 127-134. doi:10.1159/000484629
- Wewege, M., van den Berg, R., Ward, R. E., & Keech, A. (2017). The effects of high-intensity interval training vs. moderate-intensity continuous training on body composition in overweight and obese adults: a systematic review and meta-analysis. *Obesity reviews : an official journal of the International Association for the Study of Obesity*, *18*(6), 635-646. doi:10.1111/obr.12532
- Wewege, M. A., Ahn, D., Yu, J., Liou, K., & Keech, A. (2018). High-Intensity Interval Training for Patients With Cardiovascular Disease—Is It Safe? A Systematic Review. *Journal of the American Heart Association*, *7*(21), e009305. doi:10.1161/JAHA.118.009305
- Wu, M. Y., Wang, J. B., Zhu, Y., Lu, J. M., Li, D., Yu, Z. B., . . . Chen, K. (2020). Impact of Individual and Combined Lifestyle Factors on Mortality in China: A Cohort Study. *Am J Prev Med*, *59*(3), 461-468. doi:10.1016/j.amepre.2020.01.029
- Zhan, Y., & Hägg, S. (2018). Telomere Length Shortening in Alzheimer's Disease: Procedures for a Causal Investigation Using Single Nucleotide Polymorphisms in a Mendelian Randomization Study. *Methods Mol Biol*, *1750*, 293-306. doi:10.1007/978-1-4939-7704-8\_20
- Zhang, C., Zhang, H., Zhao, M., Li, Z., Cook, C. E., Buysse, D. J., . . . Yao, Y. (2020). Reliability, Validity, and Factor Structure of Pittsburgh Sleep Quality Index in Community-Based Centenarians. *Front Psychiatry*, *11*, 573530. doi:10.3389/fpsy.2020.573530
- Zhang, W., Qu, J., Liu, G. H., & Belmonte, J. C. I. (2020). The ageing epigenome and its rejuvenation. *Nat Rev Mol Cell Biol*, *21*(3), 137-150. doi:10.1038/s41580-019-0204-5

- Zhang, Y., Wilson, R., Heiss, J., Breitling, L. P., Saum, K. U., Schöttker, B., . . . Brenner, H. (2017). DNA methylation signatures in peripheral blood strongly predict all-cause mortality. *Nat Commun*, *8*, 14617. doi:10.1038/ncomms14617
- Zhang, Y. B., Pan, X. F., Chen, J., Cao, A., Xia, L., Zhang, Y., . . . Pan, A. (2021). Combined lifestyle factors, all-cause mortality and cardiovascular disease: a systematic review and meta-analysis of prospective cohort studies. *J Epidemiol Community Health*, *75*(1), 92-99. doi:10.1136/jech-2020-214050
- Zhao, W., Ammous, F., Ratliff, S., Liu, J., Yu, M., Mosley, T. H., . . . Smith, J. A. (2019). Education and Lifestyle Factors Are Associated with DNA Methylation Clocks in Older African Americans. *Int J Environ Res Public Health*, *16*(17). doi:10.3390/ijerph16173141

## CHAPTER 3

### High-Intensity Interval Training Reduces Transcriptomic Age: A Randomized Controlled Trial

#### **Abstract**

**Background:** While the relationship between exercise and lifespan is well documented, little is known about the effects of specific exercise protocols on modern measures of biological age. Transcriptomic age predictors provide an opportunity to test the effects of high intensity interval training (HIIT) on biological age utilizing whole-genome expression data.

**Methods:** A single-site, single-blinded, randomized controlled clinical trial design was utilized. Thirty sedentary participants (aged 40 to 65) were assigned to either a HIIT group or a no-exercise control group. After collecting baseline measures, HIIT participants performed three 10X1 HIIT sessions per week for 4 weeks. Each session lasted 23 minutes, and total exercise duration was 276 minutes over the course of the 1-month exercise protocol. Transcriptomic age, PSS-10 score, PSQI score, PHQ-9 score, and various measures of body composition were all measured at baseline and again following the conclusion of exercise/control protocols.

**Results:** Transcriptomic age reduction of 3.59 years was observed in the exercise group while a 3.28-year increase was observed in the control group. PHQ-9, PSQI, BMI, body fat mass, and visceral fat measures were all improved in the exercise group. A hypothesis-generation gene expression analysis suggested exercise may modify autophagy, mTOR, AMPK, IP3K, neurotrophin signaling, insulin signaling, and other age-related pathways.

**Conclusion:** A low dose of HIIT can reduce an RNA-based measure of biological age in sedentary males and females between the ages of 40 and 65. Other changes to gene expression

were relatively modest, which may indicate a focal effect of exercise on age-related biological processes.

**Acknowledgements:** We are grateful for the work carried out by our laboratory team: Chih-Chieh Chia, Fulden Cakir, Simran Jaisinghani, Kezia Marceline, Owee Mulay, and Maxine Shih. We also thank this paper's reviewers, who improved the manuscript in meaningful ways.

**Conflict of Interest Statement:** The authors declare no competing interests.

**Funding Statement:** Research funded by School of Allied Health Professions, Loma Linda University.

**Authors' Contributions:** T.L. conceived and designed the study, performed transcriptomic age and associated enrichment analyses, G.B. coordinated the project and together with T.L. and E.L. designed the study. S.C. performed all RNA extraction, quality control, and associated transcriptomic analyses. L.G. performed associated statistical analyses. All authors contributed to and approved of the manuscript.

**Data Availability Statement:** The data that support the findings of this study are available from the corresponding author, [T.L.], upon reasonable request.

## Introduction

The beneficial effects of exercise on healthspan and lifespan are among the most well documented scientific findings in health science research (Aune et al., 2021; Han et al., 2022; Myers et al., 2002; Northey, Cherbuin, Pumpa, Smee, & Rattray, 2018). Despite this, there are relatively few trials investigating the effects of exercise on gene regulatory mechanisms of healthspan and lifespan. Of those that have been performed, most examine the effects of a single bout of exercise on gene expression, rather than repeated bouts (Amar et al., 2021).

Given that many beneficial effects of exercise require repeated bouts over time to manifest, this represents an opportunity for discovery. Consider for example the inappropriate conclusions that could be drawn when studying the effects of a single bout of exercise on muscle hypertrophy, strength, or inflammation. The beneficial effects of exercise on biological aging is likely most apparent when studied over time.

The central theme of molecular biology holds that a cell's function and status are dictated by the specific sets of genes undergoing transcription at any given time, and to what degree these processes are occurring (O'Brien, Costin, & Miles, 2012). Genome-wide expression analyses allow us to take a snapshot of those processes, capturing a gene expression profile at the time of blood draw. A comparison of gene expression profiles before and after an intervention provides the means to identify patterns of differentially expressed genes.

As high throughput RNA sequencing becomes more commonplace, gene expression-based predictive models have emerged. Some of these models are designed to predict

biological age (Meyer & Schumacher, 2021; Peters et al., 2015; Ren & Kuan, 2020), or more specifically, transcriptomic age (TA). These models are easily accessible and comprehensive molecular surveys of biological processes that collectively contribute to healthspan and lifespan. It is this type of biological age predictor, a “transcriptomic clock” that is used in the trial described here.

The biological age prediction field is diverse and rapidly evolving, with models composed of various inputs (Cesari et al., 2014; Jylhävä et al., 2017; Levine et al., 2018; Lohman et al., 2021; Lu et al., 2019) and predictive capabilities (Li et al., 2020; McCrory et al., 2020). The discrepancy between a participant’s actual age and their predicted age is often of particular interest (Fahy et al., 2019; Fiorito et al., 2021). This measure, called age acceleration (biological age minus chronological age), can take a positive or negative value. Positive values are considered hazardous and indicative of an increased aging rate, while negative values are considered beneficial and evidence of a slowed aging rate. Any intervention that reverses age acceleration could therefore be considered beneficial and potentially health protective.

The effect of exercise on various biological age predictors is inconsistent. Most experimental studies that examine the relationship between exercise and biological age use telomere length as their primary biomarker of aging. These results are mixed, with positive relationships, U-shaped relationships, and no relationship all being reported (Sellami, Bragazzi, Prince, Denham, & Elrayess, 2021). This could be due to any number of factors, from differences in sample characteristics to the open question of whether telomere length even has

utility as a measure of biological age (Glei et al., 2016; Li et al., 2020; Svensson et al., 2014; Vaiserman & Krasnienkov, 2020; Wang et al., 2018).

Fewer studies have been performed using epigenetic alteration, such as DNA methylation or histone methylation/acetylation as an outcome measure. Of those that have been performed, various types of exercise have been shown to induce widespread changes to the methylome and associated gene expression (Barrès et al., 2012; Denham, O'Brien, Marques, & Charchar, 2015; Nakajima et al., 2010), but the number of studies performed is few.

To the authors' knowledge only two lifestyle modification trials have utilized a next generation predictor of biological age in humans, such as an epigenetic clock (Fiorito et al., 2021; Fitzgerald et al., 2020), and no prior study has used a transcriptomic predictor of biological age.

The trial described here aims to address this by utilizing high throughput RNA sequencing to explore the effects of twelve high intensity interval training (HIIT) sessions on biological age as measured by a blood mRNA-based "transcriptomic clock" (Peters et al., 2015).

To confirm previously observed effects of HIIT on various physiological parameters (Gu, Hao, Chen, & Wu, 2022; Min, Wang, You, Fu, & Ma, 2021; Ouerghi et al., 2017; Su et al., 2019; M. Wewege, van den Berg, Ward, & Keech, 2017) we also measured changes to body mass index (BMI), body fat mass (BFM) and visceral fat area, as well as measures of psychological stress, depression, and sleep quality.

## Methods

A randomized controlled trial design was used to investigate the effects of HIIT on the following dependent variables: 10-item Perceived Stress Scale (PSS-10) (Lee, 2012), Pittsburgh Sleep Quality Index (PSQI) (C. Zhang et al., 2020), Patient Health Questionnaire 9-item depression module (PHQ-9) (Kroenke, Spitzer, & Williams, 2001; Levis et al., 2020), body mass index (BMI), body fat mass, visceral fat area, skeletal muscle mass, waist-to-hip ratio, blood pressure, resting heart rate, and whole-genome RNA expression. The transcriptomic age prediction (TRAP) tool (Peters et al., 2015) was used to assess transcriptomic age and transcriptomic age acceleration (TAaccel = TA – chronological age) using the RNA AGE Calc Shiny App (Ren & Kuan, 2020). The TRAP biological age prediction model was trained to predict chronological age in a meta-analysis of 14,983 individuals and is based on 11,908 input gene expression levels (Peters et al., 2015).

Trial participants were recruited from local communities surrounding the Loma Linda University campus via flyers, approved social media, and word of mouth. The Loma Linda University Institutional Review Board approved the study on 11/18/2021 (IRB# 5210437, clinicaltrials.gov trial registration ID: NCT05156918). Males and females between the ages of 40 and 65 who self-identified as non-exercisers, were categorized as low activity using the International Physical Activity Questionnaire (IPAQ) (Hagströmer, Oja, & Sjöström, 2006), had no significant change to activity levels within the past 30 days, were not pregnant, had no prior or current history of any condition that would make exercise unsafe, and were not currently

taking antibiotics, glucocorticoids, anticoagulants, narcotics, antiepileptics, antipsychotics, or hypoglycemic agents were eligible for participation.

Study participants were instructed to avoid modifying their usual physical activity level or diet for the duration of the four-week study protocols, except for the additional HIIT assigned to exercise group. All participants maintained a compliance log, comprised of two questions weekly. For the control group: Have you performed more than your usual amount of physical activity this week? Secondly, have you made any significant changes to your diet this week? For the exercise group: Excluding the exercise assigned to you in this study, have you performed more than your usual amount of physical activity this week? Secondly, have you made any significant changes to your diet this week?

All participants arrived at the laboratory between the hours of 8am and 11am, and baseline measures were obtained. Body composition measurements were obtained using the InBody 770 body composition and body water analyzer (InBody USA, USA), surveys were completed in a private room, and a single vial of blood was collected by a certified phlebotomist from the antecubital vein into a PAXgene® Blood RNA Tube, PLH 16X100 2.5 PLBLCE CLR (Becton Dickinson, USA)

Following the completion of Day-1 data collection, exercise group participants returned the following day to begin the HIIT protocol which took place at the Loma Linda University Physical Fitness Laboratory. The authors chose a routinely studied 10X1 HIIT protocol that has been determined as safe and effective in various groups, including sedentary individuals (Ito, 2019; Little, Safdar, Wilkin, Tarnopolsky, & Gibala, 2010; Rozenek, Salassi, Pinto, & Fleming,

2016; M. A. Wewege, Ahn, Yu, Liou, & Keech, 2018). The protocol consists of a 2-minute warm up and cool down, with 10, 1-minute high intensity exercise intervals at 77-93% of the participants predicted maximum heart rate (Committee; Riebe, Ehrman, Liguori, & Magal) determined using Karvonen's formula (Camarda et al., 2008), followed by 1-minute self-selected intensity rest periods. The total exercise session lasted 23 minutes, of which 10 minutes was high intensity exercise and 13 minutes was warm-up/rest/cool down periods.

Participants rotated between three exercise machines (randomly assigned rotation order at outset): A Concept2 rowing ergometer, Concept2 bicycle ergometer, and a Noraxon PhysTread Pressure treadmill. Participants used a different machine each day so that they used each of the three exercise machines once per week.

Following the conclusion of the 4-week control and exercise protocols, all participants returned for results collection. Exercise group data was collected approximately 48 hours after their last HIIT session. Blood samples were stored at -79 degrees Celsius until RNA extraction (Qiagen RNeasy), quality assurance assays, mRNA sequencing, and related statistical analyses of differential gene expression and interpretive bioinformatics were performed by the UCLA Social Genomics Core Laboratory. Transcriptional profiling utilized a high-efficiency mRNA targeted reverse transcription and cDNA library synthesis system (QuantSeq 3' FWD; Lexogen Inc.) with cDNA libraries sequenced on in Illumina NovaSeq system by Lexogen Services GmbH. Assays targeted 5 million sequencing reads per sample (achieved median = 7.1 million), each of which was mapped to the GRCh38 reference human transcriptome using the STAR aligner (median 99.7% mapping rate) and quantified as gene transcripts per million total mapped reads, with values floored at 1 transcript per million to suppress spurious low-range variability, and log2-

transformed to stabilize variance. One follow-up sample yielded insufficient sequencing reads for valid analysis (< 1 million reads), and that sample and its paired pre-intervention baseline sample were excluded from all subsequent analyses. These data served as input into the RNA AGE Calc Shiny App for computation of the TRAP RNA age score. RNA AGE Calc Shiny App inputs were as follows: Tissue type: Blood, type of gene expression data: Count, samples used when building the calculator: All samples, gene ID type: Ensembl ID, signature: Peters.

A secondary analysis of differentially expressed genes (DEGs) was performed using two sets of cut off criteria. First, genes which displayed a group x time interaction expression fold change greater than 1.5 or less than .5 were selected for analysis. Also, an exploratory/hypothesis-generation analysis was performed using more liberal fold change values, greater than 1.2 or less than .8. Functional enrichment and pathway analyses were performed using Advaita Bio's iPathway Guide (Supplementary File 2).

### **Data Analysis**

Mean  $\pm$  SD was computed for quantitative variables and frequency (percentage) for categorical variables. Normality of quantitative variables was assessed using Shapiro-Wilk test and box plots. Independent t-test was used for all continuous and independent variables in both groups at baseline. The Mann-Whitney U test was used to compare the same variables due to small sample and lack of normality on some variables. The dependent paired t test was used to compare pre- and post-variables in both groups. Also, Wilcoxon Signed Rank test was used to compare the pre- and post-variables due to small sample and lack of normality on some variables.

Data were analyzed using SPSS Statistics Software version 28.0 (SPSS Inc, Chicago, IL, USA). All analyses were performed at an alpha level of .05.

### **Results**

Of the 35 participants screened, 30 subjects satisfied the eligibility criteria, agreed to participate, were randomly assigned to the experimental group (n=15) and the control group (n=15) using computer-generated block randomization, and completed all subsequent analyses

(Figure 1).

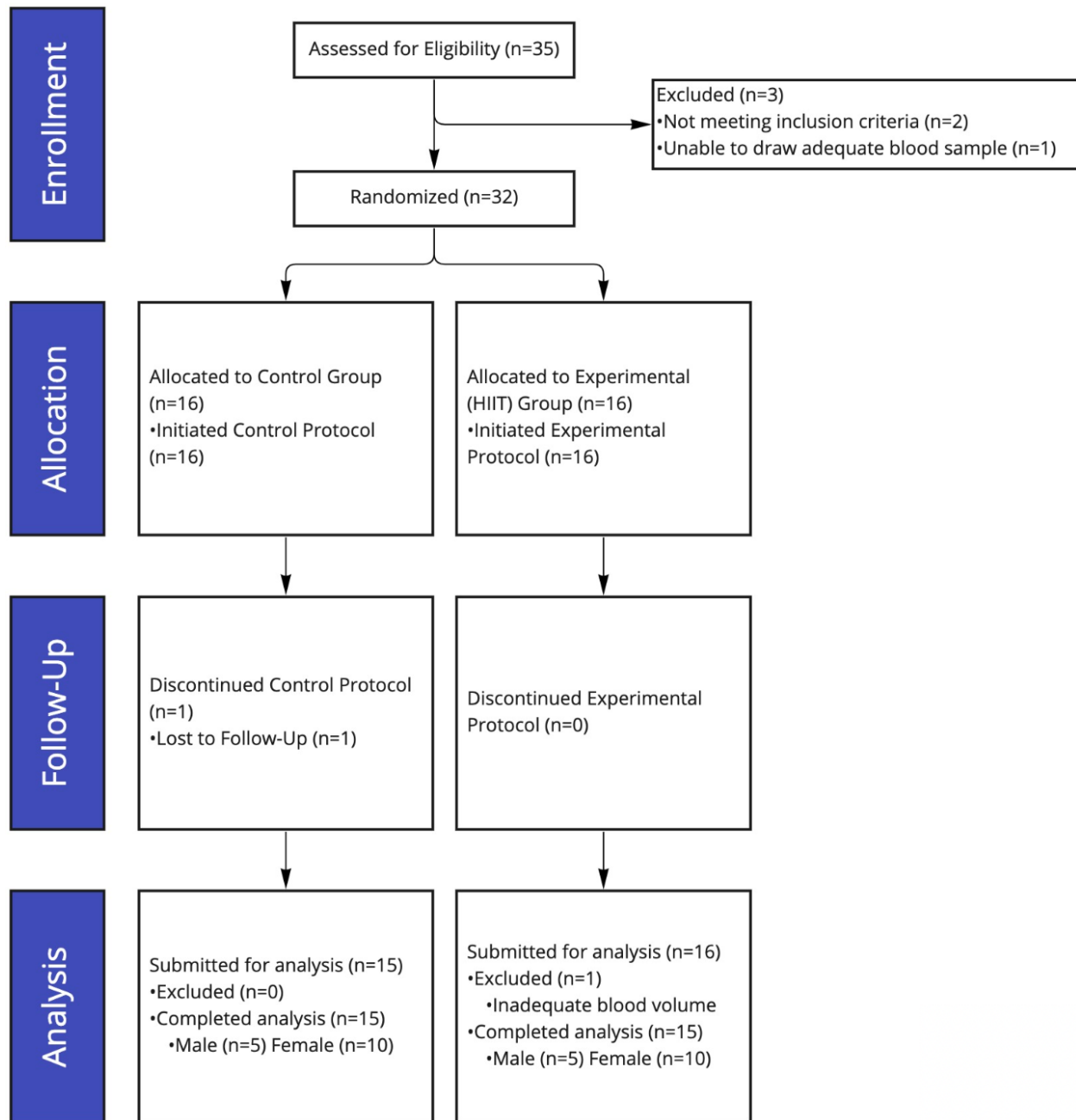


Figure 1: CONSORT chart diagram. 35 participants recruited, 2 excluded due to high activity level, 1 excluded due to an inability to draw blood sample. 1 control participant lost to follow up, 1 exercise participant excluded from analysis due to low blood volume in post exercise blood sample detected during RNA quality control tests. In total, 15 control participants and 15 experimental participants completed all aspects of the trial and subsequent analysis.

Baseline characteristics of participants are shown in Table 1. None of the demographic variables were significant for randomized design.

**Table 1. Selected Characteristics of Participants at Baseline.**

Variables	Experimental Frequency (%) (n=15)	Control Frequency (%) (n=15)
Age (years)	51.00±7.9 <sup>δ</sup>	47.93±7.6 <sup>δ</sup>
BMI (kg/m <sup>2</sup> )	31.08±4.9 <sup>δ</sup>	29.59±5.4 <sup>δ</sup>
Race/Ethnicity		
White	7 (46.7)	5 (33.3)
Black	2 (13.3)	1 (6.7)
Hispanic	4 (26.7)	4 (26.7)
Asian	1 (6.7)	5 (33.3)
Other	1 (6.7)	0 (0)
Sex		
Female	10 (66.7)	10 (66.7)
Male	5 (33.3)	5 (33.3)
Diabetic		
No	13 (86.7)	14 (93.3)
Yes	0(0)	0 (0)
Pre-Diabetic	2 (13.3)	1 (6.7)

<sup>δ</sup> Values are presented as mean ± SD

### Intervention Validation

There was a significant decrease in body fat mass, BMI, and visceral fat area (p= .031, .048, and .015 respectively) (Table 2), over time for the experimental group, a non-significant increase in BFM in the control group (p=.244), and a non-significant decrease in BMI and Visceral Fat Area in the control group (p=.598 and p=.062 respectively) (Table 2). No changes in body composition displayed group x time statistical significance.

### Primary Analysis: Transcriptomic Age

A significant group x time difference in TA ( $p=.026$ ) was observed. A significant decrease in TA was observed in the experimental group ( $p=.043$ ) and a significant increase in TA was observed in the control group ( $p=.018$ ) (Table 2). Changes to TAaccel were also significant between groups ( $p=.025$ ), with similar magnitude and direction of change as TA (Table 2).

**Table 2. Effects of High Intensity Interval Training on Transcriptomic Age, PHQ-9, PSS-10, PSQI, Skeletal Muscle Mass, Body Fat Mass, and Visceral Fat Area. Between and Within Group Effects**

Variables	Experimental (n=15)			Control (n=15)			P**
	Pre	Post	Mean difference (P*)	pre	post	Mean difference (P*)	
TA (years)	73.4±8.2	69.8±7.7	-3.59±7.72 (.043)	67.8±9.3	71.1±9.2	3.28±8.26 (.018)	.026
TAaccel (years)	21.8±7.6	17.9±9.2	-3.84±7.98 (.078)	19.2±7.9	22.4±6.8	3.21±8.26 (.156)	.025
PHQ-9	5.3±3.9	2.3±1.9	-3.07± 3.10 (.002 <sup>b</sup> )	6.9±6.9	7.0±5.9	.07± 6.15 (.964 <sup>b</sup> )	.063 <sup>a</sup>
PSS-10	20.1±5.3	19.8±4.0	-.33±5.89 (.53 <sup>b</sup> )	21.2±3.4	19.7±5.2	1.47±4.09 (.054 <sup>b</sup> )	.739 <sup>a</sup>
PSQI	7.0±3.9	5.5±3.5	-1.53± 2.42 (.042 <sup>b</sup> )	7.6±4.7	7.7±4.4	.07± 2.55 (.670 <sup>b</sup> )	.158 <sup>a</sup>
SMM (lbs)	69.5±11.7	69.6±11.5	.15± 1.39 (.676)	63.1±14.0	63.5±14.0	.39± 1.99 (.456)	.705
BFM (lbs)	74.6±22.1	73.1±22.2	-1.47± 2.29 (.031 <sup>b</sup> )	66.9±22.1	67.0±22.7	.17± 4.5 (.244 <sup>b</sup> )	.263 <sup>a</sup>
BMI (kg/m <sup>2</sup> )	31.1±4.9	30.9±5.0	-.23±.40 (.048)	29.6±5.4	29.5±5.1	-0.08±.57 (.598)	.513
Visceral Fat Area cm <sup>2</sup>	162.3±46.2	158.1±46.1	-4.25± 5.95 (.015)	157.0±58.3	154.3±58.3	-2.66± 5.08 (.062)	.426

Values are presented as mean ± SD

\* p- values for the null hypothesis that there is no difference between pre and post.

\*\* p- values for the null hypothesis that there is no difference between groups.

a: Mann-Whitney U test

b: Wilcoxon Signed Rank test

Abbreviations. TA: transcriptomic age, TAaccel: Transcriptomic Age Acceleration (transcriptomic age minus chronological age), PHQ-9: Patient Health Questionnaire 9 item depression module, PSS-10: 10 item Perceived Stress Scale, PSQI: Pittsburgh Sleep Quality Index, SMM: Skeletal Muscle Mass (lbs.), BFM: Body Fat mass (lbs.), BMI: Body Mass Index.

### Secondary Analyses: Gene Expression Analyses, Depression, Sleep, and Stress Ratings

There was a significant decrease in mean PHQ-9 (depression) and PSQI (sleep) ( $p=.002$  and  $p=.042$ ), over time for the experimental group but no significant change for control group ( $p=.063$  and  $p=.158$  respectively) (Table2). Lastly, there was no significant change in mean PSS-10 and SMM ( $p=.53$  and  $p=.676$  respectively) for the experimental group and similarly for the control group ( $p=.054$  and  $p=.456$ ). However, no changes in stress, sleep, or depression ratings displayed group x time statistical significance.

The group x time interaction gene expression analysis identified 98 genes that were differentially expressed using routinely accepted fold change cutoff values (86 up-regulated genes  $>1.5$ -fold change, and 12 down regulated genes  $<.5$ -fold change in the exercise group compared to control group). This number is insufficient for secondary enrichment analyses. Using more liberal fold change values of  $>1.2$  and  $<.8$  for this exploratory analysis, 2,653 DEGs were identified (1075 up-regulated genes  $>1.2$ -fold change, and 1778 down-regulated genes  $<.8$ -fold change) (Supplementary File 1). In addition, 1,365 Gene Ontology (GO) terms, 477 gene upstream regulators, 231 chemical upstream regulators and 259 diseases were found to be significantly enriched before correction for multiple comparisons (Supplementary File 2).

Pathway analysis was performed using Advaita Bio's iPathwayGuide, which scores pathways using the Impact Analysis method (Draghici et al., 2007; Tarca et al., 2009). Impact analysis uses two types of evidence: i) the over-representation of differentially expressed (DE) genes in a pathway and ii) the perturbation of that pathway computed by propagating the measured expression changes across the pathway topology. The top five pathways identified by this analysis and their associated p-values are as follows: Human T-cell leukemia virus 1

infection (p-value= 2.033e-7, p-value (FDR)= 3.888e-5, p-value (Bonferroni)= 6.851e-5), pathways in cancer (p-value= 2.308e-7, p-value (FDR)= 3.888e-5, p-value (Bonferroni)= 7.776e-5), neurotrophin signaling pathway (p-value= 4.670e-7, p-value (FDR)= 5.246e-5, p-value (Bonferroni)= 1.574e-4), RNA degradation (p-value= 1.140e-6, p-value (FDR)= 5.939e-5, p-value (Bonferroni)= 3.842e-4), and autophagy (p-value= 1.190e-6, p-value (FDR)= 5.939e-5, p-value (Bonferroni)= 4.009e-4). A detailed description of these results, including pathway diagrams, is shown in Supplementary File 2.

## Discussion

In this randomized controlled trial examining the effects of HIIT on an RNA-based measure of biological age, participants in the HIIT group showed greater reductions in TA and TAaccel than did those in the no-exercise control group. This improvement in biological age coincided with improvements in body composition, ratings of sleep quality, and ratings of depression within the exercise group. These results suggest that exercise exerts a causal effect on age-related patterns of gene expression, and that such effects could potentially contribute to the positive health and longevity effects associated with exercise.

### Transcriptomic Age and Transcriptomic Age Acceleration

Both groups began the trial with positive transcriptomic age acceleration. In other words, mean transcriptomic age (as computed by the TRAP algorithm) was significantly higher than mean chronological age in both groups. This baseline age bias most likely stems from methodological issues discussed below, and affected both groups similarly (i.e., exercise and

control groups did not differ in their baseline biological age measures). In the exercise group, TA and TAaccel decreased following the HIIT protocol, while both measures increased in the control group over the same timeframe. A 3.59-year reduction in TA was observed in the exercise group, which can be interpreted as the average gene expression pattern among exercise participants changing to reflect that of a person 3.59 years younger than their mean baseline TA. The 6.87-year difference in TA change, and 7.04-year difference in TAaccel change between exercise and control groups was statistically significant.

The only significant change observed in the control group was increased TA, and the authors propose two potential mechanisms for this. Control participants were asked to avoid altering their typical physical activity levels during the duration of the four-week control protocol. It is possible that once under observation, participants inadvertently lowered their activity levels. In essence, a Hawthorne effect (Merrett, 2006). Secondly, it is important to note the impact that loneliness, social exclusion, and isolation can have on gene expression (Steve W. Cole, 2009; S. W. Cole et al., 2015). Many control participants expressed disappointment at not being included in the exercise group. It is at least conceivable that this adversely affected their transcriptomic age.

Of note was that the TRAP model consistently overestimated participant age in all blood samples. The authors believe this is due to differences in data type between the TRAP training dataset and our sample. The TRAP model was developed and trained using microarray data (Peters et al., 2015), while our transcript counts were derived from RNAseq data. However, since this discrepancy applies equally to all blood samples regardless of group assignment or

time of collection, there is no reason to believe that this introduced any bias into the observed magnitude and direction of TA change.

### Gene Expression

The use of a gene expression-based measure of biological age has the added advantage of facilitating additional transcriptomic analyses which could shed light on the mechanisms underlying exercise's effect on aging processes. However, in an untargeted genome-wide expression analysis, 12 HIIT sessions had only modest effects on gene expression.

Although there were transcriptomic effects associated with HIIT, less than 100 genes displayed a fold change greater than 1.5 or less than .5, the values typically used to identify DEGs. This DEG count is less than the amount required for subsequent higher order bioinformatic analyses such as a functional enrichment analysis.

While these modest findings may seem surprising given the systemic physiological changes induced by exercise, it is important to remember that this trial examined the effects of a 1-month HIIT protocol on steady state (baseline) gene expression levels. The follow-up blood draw occurred approximately 48 hours after the final exercise session, meaning that whole genome expression was assessed while the participants were not experiencing the acute physiological aftereffects of exercise. Given the small dose and duration of our exercise protocol and the small sample size, this modest between group effect may not be surprising

An exploratory genome-wide discovery analysis using more liberal fold change cutoff values (greater than 1.2 or less than .8) revealed 1075 upregulated transcripts and 1778 downregulated transcripts potentially associated with HIIT (Supplementary File 1). The

subsequent bioinformatic analyses associated with these DEGs were performed using Advaita Bio's iPathwayGuide. This analysis suggests that autophagy processes, cancer pathways, neurotrophin signaling pathways, mRNA degradation processes, and other pathways were modified by HIIT (Supplementary File 2). These modifications are particularly interesting in the context of aging, especially autophagy. Various age-related signaling pathways were modified including mTOR signaling, AMPK signaling, PI3K signaling, and insulin signaling pathways. Inhibition of 3 out of 5 mTORC1 complex component genes (Raptor, Deptor, and mTOR) was noteworthy, since mTORC1 inhibition is associated with increased lifespan in every species studied so far, including humans (Papadopoli et al., 2019; Weichhart, 2018). Given the exploratory nature of these enrichment analyses, and the relatively liberal threshold for DEG detection however, these results should be treated as descriptive hypotheses to be tested in future research using more rigorous methods.

#### Body Composition and Self-Reported Measures of Sleep Quality and Depression

Previous work suggests that the effects of exercise on biological age are mediated by changes in body composition (Kresovich et al., 2021). This seems to support our findings, as improvements in BMI, body fat mass, and visceral fat area were observed in the exercise group over time.

Improvements in PHQ-9 and PSQI score were also seen in the exercise group over time.

Observed changes to body composition were consistent with previous studies' findings, indicating that this study's specific implementation of HIIT imparted the expected effects demonstrated in prior investigations. This serves as a positive control, or paradigm validation of the trial's specific HIIT intervention. However, it is important to note that none of these

biometric changes differed significantly across groups, likely due to the limited statistical power available from this relatively small sample.

### **Significance**

Starting and adhering to a new exercise program is difficult, a fact perhaps best illustrated by the current sedentary behavior rate in the United States. A recent Center for Disease Control and Prevention (CDC) telephone survey estimates that more than 25% of Americans participate in no physical activity outside of work (CDC, 2022) and contrary to popular opinion, this is not a uniquely American problem. A large European Union study found that 53.1% of the adult EU population participated in >4.5 hours of sedentary behavior per day (López-Valenciano et al., 2020). Inadequate physical activity is no longer just a western problem either, with the World Health Organization estimating that one third of the global population aged 15 years or older engages in insufficient physical activity, with some countries, such as Korea, engaging in >8 hours per day of sedentary behavior on average (Park, Moon, Kim, Kong, & Oh, 2020).

HIIT is a potential tool to help combat this trend given the decreased time commitment (Cobbald, 2018; Ito, 2019) and similar (or improved) health benefits to those bestowed by other forms of exercise (Hannan et al., 2018; Scott et al., 2019), but with increased adherence and compliance rates (Ito, 2019).

Despite the modest gene expression findings generally, the pre-specified hypothesis regarding HIIT-induced transcriptomic age reversal was proven out by the analysis. Considering that each exercise participant completed a combined 276 minutes of exercise over 1 month,

only 2 hours of which was high intensity exercise, the effect of HIIT on biological age appears promising.

This study further supports the notion that adding even a small amount of exercise can be beneficial, given that just 12 HIIT sessions were shown to significantly improve TA and TAaccel. To the authors' knowledge, this is the first trial to demonstrate the effects of a specific exercise protocol on a next generation measure of biological age. The results suggest that exercise exerts a causal effect on age-related patterns of gene expression, and that such effects could potentially contribute to the positive health and longevity effects associated with exercise.

### **Conclusion**

A low dose of HIIT over 4 weeks is sufficient to reduce transcriptomic age in sedentary middle-aged males and females. Other changes to gene expression were relatively modest in comparison to the transcriptomic age reduction effect size. These findings, along with modification to autophagic pathways, may indicate a particular HIIT specificity for age-related biological pathway modulation. The key observations presented here, namely reduced transcriptomic age, indicate that exercise may potentially improve health and longevity by altering age-related transcriptional processes.

## References

- Amar, D., Lindholm, M. E., Norrbom, J., Wheeler, M. T., Rivas, M. A., & Ashley, E. A. (2021). Time trajectories in the transcriptomic response to exercise - a meta-analysis. *Nature Communications*, *12*(1), 3471. doi:10.1038/s41467-021-23579-x
- Aune, D., Schlesinger, S., Leitzmann, M. F., Tonstad, S., Norat, T., Riboli, E., & Vatten, L. J. (2021). Physical activity and the risk of heart failure: a systematic review and dose-response meta-analysis of prospective studies. *Eur J Epidemiol*, *36*(4), 367-381. doi:10.1007/s10654-020-00693-6
- Barrès, R., Yan, J., Egan, B., Treebak, J. T., Rasmussen, M., Fritz, T., . . . Zierath, J. R. (2012). Acute exercise remodels promoter methylation in human skeletal muscle. *Cell Metab*, *15*(3), 405-411. doi:10.1016/j.cmet.2012.01.001
- Camarda, S. R., Tebexreni, A. S., Páfaró, C. N., Sasai, F. B., Tambeiro, V. L., Juliano, Y., & Barros Neto, T. L. (2008). Comparison of maximal heart rate using the prediction equations proposed by Karvonen and Tanaka. *Arq Bras Cardiol*, *91*(5), 311-314. doi:10.1590/s0066-782x2008001700005
- CDC. (2022). Adult Physical Activity Prevalence. Retrieved from <https://www.cdc.gov/physicalactivity/data/inactivity-prevalence-maps/index.html>
- Cesari, M., Gambassi, G., Abellan van Kan, G., & Vellas, B. (2014). The frailty phenotype and the frailty index: different instruments for different purposes. *Age and Ageing*, *43*(1), 10-12. doi:10.1093/ageing/aft160
- Cobbold, C. (2018). Battle of the sexes: Which is better for you, high- or low-intensity exercise? *J Sport Health Sci*, *7*(4), 429-432. doi:10.1016/j.jshs.2018.05.004
- Cole, S. W. (2009). Social Regulation of Human Gene Expression. *Current Directions in Psychological Science*, *18*(3), 132-137. doi:10.1111/j.1467-8721.2009.01623.x
- Cole, S. W., Levine, M. E., Arevalo, J. M., Ma, J., Weir, D. R., & Crimmins, E. M. (2015). Loneliness, eudaimonia, and the human conserved transcriptional response to adversity. *Psychoneuroendocrinology*, *62*, 11-17. doi:10.1016/j.psyneuen.2015.07.001
- Committee, P. A. G. A. In. Physical Activity Guidelines Advisory Committee Report Washington, DC: U.S. Dept of Health and Human Services.
- Denham, J., O'Brien, B. J., Marques, F. Z., & Charchar, F. J. (2015). Changes in the leukocyte methylome and its effect on cardiovascular-related genes after exercise. *J Appl Physiol* (1985), *118*(4), 475-488. doi:10.1152/jappphysiol.00878.2014
- Draghici, S., Khatrı, P., Tarca, A. L., Amin, K., Done, A., Voichita, C., . . . Romero, R. (2007). A systems biology approach for pathway level analysis. *Genome Res*, *17*(10), 1537-1545. doi:10.1101/gr.6202607
- Fahy, G. M., Brooke, R. T., Watson, J. P., Good, Z., Vasanaawala, S. S., Maecker, H., . . . Horvath, S. (2019). Reversal of epigenetic aging and immunosenescent trends in humans. *Aging Cell*, *18*(6), e13028. doi:10.1111/accel.13028
- Fiorito, G., Caini, S., Palli, D., Bendinelli, B., Saieva, C., Ermini, I., . . . Masala, G. (2021). DNA methylation-based biomarkers of aging were slowed down in a two-year diet and physical activity intervention trial: the DAMA study. *Aging Cell*, *20*(10), e13439. doi:<https://doi.org/10.1111/accel.13439>
- Fitzgerald, K., Hodges, R., Hanes, D., Stack, E., Cheishvili, D., Szyf, M., . . . Bradley, R. (2020). Reversal of Epigenetic Age with Diet and Lifestyle in a Pilot Randomized Clinical Trial. *medRxiv*, 2020.2007.2007.20148098. doi:10.1101/2020.07.07.20148098
- Glei, D. A., Goldman, N., Risques, R. A., Rehkopf, D. H., Dow, W. H., Rosero-Bixby, L., & Weinstein, M. (2016). Predicting Survival from Telomere Length versus Conventional Predictors: A Multinational Population-Based Cohort Study. *PLOS ONE*, *11*(4), e0152486. doi:10.1371/journal.pone.0152486

- Gu, T., Hao, P., Chen, P., & Wu, Y. (2022). A Systematic Review and Meta-Analysis of the Effectiveness of High-Intensity Interval Training in People with Cardiovascular Disease at Improving Depression and Anxiety. *Evid Based Complement Alternat Med*, 2022, 8322484. doi:10.1155/2022/8322484
- Hagströmer, M., Oja, P., & Sjöström, M. (2006). The International Physical Activity Questionnaire (IPAQ): a study of concurrent and construct validity. *Public Health Nutr*, 9(6), 755-762. doi:10.1079/phn2005898
- Han, M., Qie, R., Shi, X., Yang, Y., Lu, J., Hu, F., . . . Zhao, Y. (2022). Cardiorespiratory fitness and mortality from all causes, cardiovascular disease and cancer: dose–response meta-analysis of cohort studies. *British Journal of Sports Medicine*, 56(13), 733. doi:10.1136/bjsports-2021-104876
- Hannan, A. L., Hing, W., Simas, V., Climstein, M., Coombes, J. S., Jayasinghe, R., . . . Furness, J. (2018). High-intensity interval training versus moderate-intensity continuous training within cardiac rehabilitation: a systematic review and meta-analysis. *Open Access J Sports Med*, 9, 1-17. doi:10.2147/oajsm.s150596
- Ito, S. (2019). High-intensity interval training for health benefits and care of cardiac diseases - The key to an efficient exercise protocol. *World J Cardiol*, 11(7), 171-188. doi:10.4330/wjc.v11.i7.171
- Jylhävä, J., Pedersen, N. L., & Hägg, S. (2017). Biological Age Predictors. *EBioMedicine*, 21, 29-36. doi:<https://doi.org/10.1016/j.ebiom.2017.03.046>
- Kresovich, J. K., Garval, E. L., Martinez Lopez, A. M., Xu, Z., Niehoff, N. M., White, A. J., . . . Taylor, J. A. (2021). Associations of Body Composition and Physical Activity Level With Multiple Measures of Epigenetic Age Acceleration. *American Journal of Epidemiology*, 190(6), 984-993. doi:10.1093/aje/kwaa251
- Kroenke, K., Spitzer, R. L., & Williams, J. B. (2001). The PHQ-9: validity of a brief depression severity measure. *Journal of general internal medicine*, 16(9), 606-613. doi:10.1046/j.1525-1497.2001.016009606.x
- Lee, E.-H. (2012). Review of the Psychometric Evidence of the Perceived Stress Scale. *Asian Nursing Research*, 6(4), 121-127. doi:<https://doi.org/10.1016/j.anr.2012.08.004>
- Levine, M. E., Lu, A. T., Quach, A., Chen, B. H., Assimes, T. L., Bandinelli, S., . . . Horvath, S. (2018). An epigenetic biomarker of aging for lifespan and healthspan. *Aging*, 10(4), 573-591. doi:10.18632/aging.101414
- Levis, B., Sun, Y., He, C., Wu, Y., Krishnan, A., Bhandari, P. M., . . . Zhang, Y. (2020). Accuracy of the PHQ-2 Alone and in Combination With the PHQ-9 for Screening to Detect Major Depression: Systematic Review and Meta-analysis. *Jama*, 323(22), 2290-2300. doi:10.1001/jama.2020.6504
- Li, X., Ploner, A., Wang, Y., Magnusson, P. K. E., Reynolds, C., Finkel, D., . . . Hägg, S. (2020). Longitudinal trajectories, correlations and mortality associations of nine biological ages across 20-years follow-up. *Elife*, 9, e51507. doi:10.7554/eLife.51507
- Little, J. P., Safdar, A., Wilkin, G. P., Tarnopolsky, M. A., & Gibala, M. J. (2010). A practical model of low-volume high-intensity interval training induces mitochondrial biogenesis in human skeletal muscle: potential mechanisms. *J Physiol*, 588(Pt 6), 1011-1022. doi:10.1113/jphysiol.2009.181743
- Lohman, T., Bains, G., Berk, L., & Lohman, E. (2021). Predictors of Biological Age: The Implications for Wellness and Aging Research. *Gerontol Geriatr Med*, 7, 23337214211046419. doi:10.1177/23337214211046419
- López-Valenciano, A., Mayo, X., Liguori, G., Copeland, R. J., Lamb, M., & Jimenez, A. (2020). Changes in sedentary behaviour in European Union adults between 2002 and 2017. *BMC Public Health*, 20(1), 1206. doi:10.1186/s12889-020-09293-1
- Lu, A. T., Quach, A., Wilson, J. G., Reiner, A. P., Aviv, A., Raj, K., . . . Horvath, S. (2019). DNA methylation GrimAge strongly predicts lifespan and healthspan. *Aging*, 11(2), 303-327. doi:10.18632/aging.101684

- McCrary, C., Fiorito, G., Hernandez, B., Polidoro, S., O'Halloran, A. M., Hever, A., . . . Kenny, R. A. (2020). GrimAge Outperforms Other Epigenetic Clocks in the Prediction of Age-Related Clinical Phenotypes and All-Cause Mortality. *The Journals of Gerontology: Series A*. doi:10.1093/gerona/glaa286
- Merrett, F. (2006). Reflections on the Hawthorne Effect. *Educational Psychology, 26*(1), 143-146. doi:10.1080/01443410500341080
- Meyer, D. H., & Schumacher, B. (2021). BiT age: A transcriptome-based aging clock near the theoretical limit of accuracy. *Aging Cell, 20*(3), e13320. doi:10.1111/accel.13320
- Min, L., Wang, D., You, Y., Fu, Y., & Ma, X. (2021). Effects of High-Intensity Interval Training on Sleep: A Systematic Review and Meta-Analysis. *Int J Environ Res Public Health, 18*(20). doi:10.3390/ijerph182010973
- Myers, J., Prakash, M., Froelicher, V., Do, D., Partington, S., & Atwood, J. E. (2002). Exercise Capacity and Mortality among Men Referred for Exercise Testing. *New England Journal of Medicine, 346*(11), 793-801. doi:10.1056/NEJMoa011858
- Nakajima, K., Takeoka, M., Mori, M., Hashimoto, S., Sakurai, A., Nose, H., . . . Taniguchi, S. (2010). Exercise effects on methylation of ASC gene. *Int J Sports Med, 31*(9), 671-675. doi:10.1055/s-0029-1246140
- Northey, J. M., Cherbuin, N., Pumpa, K. L., Smee, D. J., & Rattray, B. (2018). Exercise interventions for cognitive function in adults older than 50: a systematic review with meta-analysis. *British Journal of Sports Medicine, 52*(3), 154. doi:10.1136/bjsports-2016-096587
- O'Brien, M. A., Costin, B. N., & Miles, M. F. (2012). Using genome-wide expression profiling to define gene networks relevant to the study of complex traits: from RNA integrity to network topology. *Int Rev Neurobiol, 104*, 91-133. doi:10.1016/b978-0-12-398323-7.00005-7
- Ouerghi, N., Fradj, M. K. B., Bezrati, I., Khammassi, M., Feki, M., Kaabachi, N., & Bouassida, A. (2017). Effects of high-intensity interval training on body composition, aerobic and anaerobic performance and plasma lipids in overweight/obese and normal-weight young men. *Biology of sport, 34*(4), 385-392. doi:10.5114/biolsport.2017.69827
- Papadopoli, D., Boulay, K., Kazak, L., Pollak, M., Mallette, F., Topisirovic, I., & Hulea, L. (2019). mTOR as a central regulator of lifespan and aging. *F1000Research, 8*, F1000 Faculty Rev-1998. doi:10.12688/f1000research.17196.1
- Park, J. H., Moon, J. H., Kim, H. J., Kong, M. H., & Oh, Y. H. (2020). Sedentary Lifestyle: Overview of Updated Evidence of Potential Health Risks. *Korean J Fam Med, 41*(6), 365-373. doi:10.4082/kjfm.20.0165
- Peters, M. J., Joehanes, R., Pilling, L. C., Schurmann, C., Conneely, K. N., Powell, J., . . . Consortium, N. U. (2015). The transcriptional landscape of age in human peripheral blood. *Nature Communications, 6*(1), 8570. doi:10.1038/ncomms9570
- Ren, X., & Kuan, P. F. (2020). RNAAgeCalc: A multi-tissue transcriptional age calculator. *PLOS ONE, 15*(8), e0237006. doi:10.1371/journal.pone.0237006
- Riebe, D., Ehrman, J. K., Liguori, G., & Magal, M. Chapter 6 General Principles of Exercise Prescription. In: ACSM's Guidelines for Exercise Testing and Prescription. 10th Ed. In (pp. 143-179). In: ACSM's Guidelines for Exercise Testing and Prescription.: Wolters Kluwer/Lippincott Williams & Wilkins.
- Rozenek, R., Salassi, J. W., 3rd, Pinto, N. M., & Fleming, J. D. (2016). Acute Cardiopulmonary and Metabolic Responses to High-Intensity Interval Training Protocols Using 60 s of Work and 60 s Recovery. *J Strength Cond Res, 30*(11), 3014-3023. doi:10.1519/jsc.0000000000001414
- Scott, S. N., Shepherd, S. O., Hopkins, N., Dawson, E. A., Strauss, J. A., Wright, D. J., . . . Cocks, M. (2019). Home-hit improves muscle capillarisation and eNOS/NAD(P)H oxidase protein ratio in obese individuals with elevated cardiovascular disease risk. *The Journal of Physiology, 597*(16), 4203-4225. doi:<https://doi.org/10.1113/JP278062>

- Sellami, M., Bragazzi, N., Prince, M. S., Denham, J., & Elrayess, M. (2021). Regular, Intense Exercise Training as a Healthy Aging Lifestyle Strategy: Preventing DNA Damage, Telomere Shortening and Adverse DNA Methylation Changes Over a Lifetime. *Front Genet, 12*, 652497. doi:10.3389/fgene.2021.652497
- Su, L., Fu, J., Sun, S., Zhao, G., Cheng, W., Dou, C., & Quan, M. (2019). Effects of HIIT and MICT on cardiovascular risk factors in adults with overweight and/or obesity: A meta-analysis. *PLOS ONE, 14*(1), e0210644. doi:10.1371/journal.pone.0210644
- Svensson, J., Karlsson, M. K., Ljunggren, Ö., Tivesten, Å., Mellström, D., & Movérare-Skrtic, S. (2014). Leukocyte telomere length is not associated with mortality in older men. *Exp Gerontol, 57*, 6-12. doi:10.1016/j.exger.2014.04.013
- Tarca, A. L., Draghici, S., Khatri, P., Hassan, S. S., Mittal, P., Kim, J. S., . . . Romero, R. (2009). A novel signaling pathway impact analysis. *Bioinformatics, 25*(1), 75-82. doi:10.1093/bioinformatics/btn577
- Vaiserman, A., & Krasnienkov, D. (2020). Telomere Length as a Marker of Biological Age: State-of-the-Art, Open Issues, and Future Perspectives. *Front Genet, 11*, 630186. doi:10.3389/fgene.2020.630186
- Wang, Q., Zhan, Y., Pedersen, N. L., Fang, F., & Hägg, S. (2018). Telomere Length and All-Cause Mortality: A Meta-analysis. *Ageing Res Rev, 48*, 11-20. doi:10.1016/j.arr.2018.09.002
- Weichhart, T. (2018). mTOR as Regulator of Lifespan, Aging, and Cellular Senescence: A Mini-Review. *Gerontology, 64*(2), 127-134. doi:10.1159/000484629
- Wewege, M., van den Berg, R., Ward, R. E., & Keech, A. (2017). The effects of high-intensity interval training vs. moderate-intensity continuous training on body composition in overweight and obese adults: a systematic review and meta-analysis. *Obesity reviews : an official journal of the International Association for the Study of Obesity, 18*(6), 635-646. doi:10.1111/obr.12532
- Wewege, M. A., Ahn, D., Yu, J., Liou, K., & Keech, A. (2018). High-Intensity Interval Training for Patients With Cardiovascular Disease—Is It Safe? A Systematic Review. *Journal of the American Heart Association, 7*(21), e009305. doi:10.1161/JAHA.118.009305
- Zhang, C., Zhang, H., Zhao, M., Li, Z., Cook, C. E., Buysse, D. J., . . . Yao, Y. (2020). Reliability, Validity, and Factor Structure of Pittsburgh Sleep Quality Index in Community-Based Centenarians. *Front Psychiatry, 11*, 573530. doi:10.3389/fpsy.2020.573530

## CHAPTER FOUR

### DISCUSSION

There is a quote attributed to Galileo which reads “measure what is measurable and make measurable what is not so”. It is an aphorism which lies at the heart of good research methodology, and its relevance to biological aging is particularly significant.

In the context of aging research, chronological age is readily measurable. The measurement of biological aging processes, however, is much more elusive. It is easy to imagine two individuals with different age-related disease risk profiles, different life expectancies, and different comorbidities, who are the same chronological age. The field of biological age prediction is as an attempt to measure the dissociation between chronological age and these age-related health outcomes. Not only are these capabilities informative, but they are also pragmatic.

Biological age is hard to measure and even harder to change, but new advances in molecular biology and the well-established virtues of exercise raise an exciting possibility that we now attempt to seize in this dissertation. Can exercise reduce biological age?

Prior to the creation of valid predictors of biological age, a researcher wishing to assess the effects of an intervention on aging processes, life expectancy, and age-related disease would need to design a multi-decade longitudinal trial. Alternatively, they could look for correlations in retrospective epidemiological data. In either case, a logistically challenging and expensive research endeavor needed to be undertaken. One that was potentially rife with confounding and unintentional bias. Biological age prediction models offer an intermediate step, where the effects of an intervention on biological aging can be assessed over

comparatively shorter time frames. These studies could provide a basis for selecting interventions for additional investigation and investment. Therefore, these models would not take the place of longitudinal validation, but they could catalyze the pace and efficiency of aging research discovery.

With biological age prediction models, researchers now possess the means to evaluate the effects of interventions on aging processes within practical time frames. Chapter Two of this text reviewed a sampling of these models and described the current state of biological age prediction methodology. The models described there serve as accessible measures of biological aging, providing a framework for the investigation of biological age modulating interventions. In numerous cases they are determined to be externally and longitudinally valid predictors of life expectancy and time-to-disease.

One category of biological age prediction model, transcriptomic age prediction, relies on gene expression inputs to assess biological age. The underlying transcriptomic data associated with these models also provides the basis for interesting secondary bioinformatic analyses. These analyses have the potential to help elucidate the mechanistic interplay between an intervention and biological age modulation.

It is this type of model, a transcriptomic age predictor, that served as the primary outcome measure for the experimental trial described in Chapter Three. This trial assessed the effects of High-intensity interval training on gene expression and transcriptomic age. Reduction in transcriptomic age was observed in the exercise group compared to the control group.

Exercise is a generally accepted modulator of health outcomes and life expectancy. However, it has not been previously demonstrated to modulate aging processes via

transcriptional means. In this way, the trial is significant, and to the authors' knowledge the first trial to assess the effects of a specific intervention on a modern measure of biological age. A secondary hypothesis generation analysis was performed, and multiple age-related pathways were amongst the most heavily enriched biological processes. Some of these processes included cancer pathways, neurotrophin signaling, and autophagy signaling. All are age-related, but of particular interest was the potential exercise-induced up-regulation of autophagic processes. Future trials with larger samples and larger exercise doses should investigate this further. Future research is also needed to assess the durability of these effects – i.e., are the “biological age reductions” observed here persistent over months or years of follow-up, or do they dissipate over time? Are such effects maintained if participants continue exercising following study cessation? And perhaps most importantly, do these “biological age” reductions observed here with exercise accurately forecast increases in health and longevity? These are all important topics for future research, and this dissertation's identification of HIIT as a viable strategy for reducing transcriptomic age in sedentary middle-aged adults provides a highly feasible paradigm for those future investigations.

### **Conclusions and Future Directions**

The authors conclude that a low dose HIIT intervention is sufficient to reduce transcriptomic age in sedentary middle-aged males and females. Other changes to gene expression were relatively modest in comparison to the transcriptomic age reversal effect size. These changes included potential modification to autophagic signaling, neurotrophin signaling, and cancer-related pathways. This may indicate a particular HIIT specificity for age-related

biological pathway modulation. The key trial observations, namely reduced transcriptomic age, indicate that exercise may potentially improve health and longevity via age-related transcriptional mechanisms.

Future studies should seek to quantify the biological age modulation capability of other exercise protocols, with the goal to identify forms of exercise which have the greatest affinity for biological age modification. Additionally, dose response curves should be established, and sex specific differences should be quantified.

Appendix A



LOMA LINDA UNIVERSITY  
HEALTH

**INSTITUTIONAL REVIEW BOARD**  
**HUMAN RESEARCH & COMPLIANCE**  
24887 Taylor Street • Suite 201 • Loma Linda, CA 92350  
(909) 558-4531 (voice) • (909) 558-0131 (fax)

---

**Initial Approval Notice - Expedited**

**IRB# 5210437**

To: **Gurinder Bains**  
Department: **SAHP: Allied Health Sciences**  
Protocol: **The Effects of High-Intensity Exercise on Biological Age**

This study was reviewed and approved administratively on behalf of the IRB. This decision includes the following determinations:

Risk to research subjects: **Minimal Risk**  
Approval begins: **18-Nov-2021**  
Stipulations of approval:  
See attached list of items (if applicable).  
See Appendix A for Conditions of Approval.

Adverse events and unanticipated problems must be reported in accord with the attached Adverse Event Reporting Matrix A.

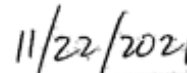
All investigators are responsible for assuring that studies are conducted according to the approved protocol. Principal investigators are responsible for the actions of sub-investigators and staff with regard to this approval.

Please note the PI's name and the assigned IRB number, as indicated above, on any future communications with the IRB.

Direct all communications to the IRB c/o Human Research and Compliance.

Thank you for your cooperation in LLUH's shared responsibility for the ethical use of human subject in research.

  
\_\_\_\_\_  
IRB Chair/Designee

  
\_\_\_\_\_  
Date

Appendix B

Gene	Intercept	Intervention	Between Group Fold Change
ZDHHC4	-0.64318	1.10685792	2.15376064
MYBBP1A	-0.7140497	1.07325568	2.10417643
PREB	-0.5967144	1.01629142	2.0227127
MROH1	-0.8331493	0.96407741	1.9508156
LCN2	-0.6619749	0.95137977	1.93372115
HMG1N1P8	-0.2241092	0.90334621	1.87039919
VPS39	-0.4116895	0.90099762	1.86735681
AP003108.4	-0.7705609	0.89689913	1.86205944
EPB41L2	-0.6040875	0.86804415	1.82518684
B4GALT7	-0.3555211	0.85998163	1.8150152
WSB2	-0.3373061	0.82855551	1.77590636
LRP8	-0.1076038	0.79815986	1.73888179
PILRB	-0.5574056	0.78197963	1.71948869
UMAD1	-0.5534117	0.77002794	1.7053028
RSAD1	-0.4137279	0.75449579	1.68704188
OXER1	-0.5325214	0.75321724	1.68554744
TAF13	-0.3187047	0.73840708	1.66833276
ZNF213	-0.4543647	0.73500036	1.66439789
ZBED4	-0.3624368	0.73056263	1.65928607
MT-TT	-0.7968331	0.72466956	1.65252209
WLS	-0.3127526	0.71846703	1.64543272
FAM234A	-0.2748992	0.71572082	1.64230356
CHCHD5	-0.4153742	0.70857759	1.63419211
PTGS1	-0.4770252	0.70455667	1.62964381
PGBD4	-0.3579984	0.70408233	1.62910809
PWAR6	-0.3889218	0.69805886	1.62232049
INAFM1	-0.0578553	0.69300494	1.61664727
CC2D1A	-0.4118007	0.68719569	1.61015067
HS1BP3	-0.3823085	0.68577978	1.60857118
XRRA1	-0.374259	0.67874249	1.60074387
MEPCE	-0.2877406	0.67652697	1.59828753
PLXNA3	-0.4264685	0.67628948	1.59802445
ALPL	-0.3432847	0.67585005	1.59753778
AC004448.1	-0.6120066	0.67423682	1.5957524
NIT1	-0.3100206	0.672585	1.59392639
HDC	-0.1141744	0.67202723	1.59331026
CTSF	-0.4429797	0.67141132	1.59263019

LINC01410	-0.5440711	0.67117044	1.5923643
VPS18	-0.1744318	0.67105478	1.59223665
RELB	-0.2268861	0.66384517	1.58429959
TTC7A	-0.2945996	0.66109695	1.5812845
NEDD4L	-0.0902757	0.6598819	1.57995329
ZMYM3	-0.3767391	0.65962037	1.57966689
NT5DC1	-0.2980943	0.65829361	1.57821484
AC099489.1	-0.3388034	0.65382112	1.5733298
CMAS	-0.3050014	0.6514107	1.57070331
APOBR	-0.1895204	0.64210889	1.56060874
CLUHP3	-0.2542009	0.63568555	1.55367586
RRP12	-0.4857814	0.63459408	1.55250088
ZCCHC14	-0.4657457	0.63344361	1.55126334
SCCPDH	-0.2193439	0.62658131	1.54390214
PLCD1	-0.217631	0.6239616	1.5411012
RNASEH1	-0.2105514	0.62384601	1.54097773
ORC4	-0.2485718	0.6228535	1.53991797
TMTC1	-0.2063448	0.62125078	1.53820819
CAPN5	-0.194019	0.62010772	1.53698994
SLC35C1	-0.4708322	0.61965238	1.53650491
GPAM	0.08477275	0.61851179	1.53529063
PLB1	-0.1548765	0.61734945	1.5340542
BX322557.1	-0.4050067	0.61554667	1.53213845
ZFY	-0.1898008	0.61479749	1.53134302
WDR4	-0.1598787	0.61473618	1.53127795
TRIM35	-0.4301148	0.61400216	1.53049906
ZCCHC24	-0.6062427	0.6133715	1.52983016
ZSCAN16-AS1	-0.3764581	0.61238904	1.52878872
LINC00243	-0.4671886	0.61237287	1.52877159
SAYSD1	-0.2396999	0.60771439	1.52384312
ATG2A	-0.3127145	0.60638105	1.52243544
RPS18P9	-0.3239201	0.60535822	1.52135646
NCALD	-0.2110895	0.60421595	1.52015238
PGAP2	-0.6060393	0.60067149	1.51642221
TTC21A	-0.1784798	0.59969287	1.51539392
NFKB2	-0.2431417	0.59675255	1.51230859
CYB561D2	-0.3030504	0.59513086	1.5106096
NTMT1	-0.2585302	0.59462974	1.51008498
PBX1	-0.441581	0.59452011	1.50997023
ZBTB16	0.05446244	0.59442258	1.50986816

ZBTB48	-0.1832489	0.59276524	1.50813464
B3GALNT2	-0.1574718	0.59197858	1.50731253
NUTM2A-AS1	-0.2719236	0.59024932	1.5055069
SLC6A8	-0.3737017	0.58890297	1.50410258
AC026356.2	-0.4109483	0.58866921	1.50385889
BICD1	-0.2914786	0.58865075	1.50383966
DHX33	-0.1698499	0.58785255	1.50300785
PRPSAP1	-0.4375926	0.58637201	1.50146622
FADD	-0.3283961	0.58563744	1.50070191
PARVB	-0.2322521	0.58429014	1.4993011
TMEM91	-0.2385151	0.58316557	1.49813286
LRIG2	-0.229744	0.58270335	1.49765295
CTTN	-0.477424	0.58179135	1.49670651
PAFAH2	-0.338788	0.58178623	1.4967012
MCUR1	-0.2730608	0.58091198	1.49579449
CCDC77	-0.4224037	0.58055334	1.4954227
SUPT7L	-0.4378561	0.57878557	1.49359144
SCYL1	-0.4654756	0.57781109	1.49258293
PDCD5	-0.2164347	0.57711012	1.49185789
IRF5	-0.3378033	0.57691036	1.49165134
BLOC1S1	-0.3794059	0.57521352	1.48989796
ANO9	-0.2263428	0.57498788	1.48966495
LRFN1	-0.2233739	0.57400263	1.48864797
ZNF296	-0.0663251	0.57380409	1.48844312
ZDHHC16	-0.299086	0.57360436	1.48823707
NMRAL1	-0.382243	0.57203658	1.48662068
AC103769.1	-0.1149116	0.57033869	1.48487212
FAR2	-0.1629727	0.56920888	1.48370974
AVIL	-0.1416968	0.5681596	1.48263102
AL157392.3	0.03026011	0.56800704	1.48247424
TXNDC17	0.07644287	0.5677581	1.48221846
ERCC6L2	-0.0293469	0.56734231	1.48179135
MAN2C1	-0.2122632	0.56498011	1.47936711
GNB1L	-0.2694688	0.56166851	1.47597523
AC025171.1	-0.3266479	0.56148698	1.47578953
ING5	-0.5000257	0.56103858	1.47533091
CAMTA1	-0.5893283	0.56033197	1.47460849
PRR14	-0.3086059	0.55756662	1.47178468
SH2B2	-0.3682654	0.55755397	1.47177177
COX14	-0.4744719	0.55727741	1.47148967

CMSS1	-0.4683867	0.5567968	1.47099954
SLC25A42	0.01731021	0.55550518	1.46968317
AL162424.1	-0.4308048	0.55404753	1.468199
SGSH	-0.1923809	0.55362578	1.46776986
AC092910.3	-0.4228364	0.55324294	1.46738042
TCEAL3	-0.2008306	0.55135532	1.46546176
MYO1E	-0.0943561	0.55029462	1.46438472
FADS1	-0.3146488	0.54883177	1.46290063
CAPN12	-0.2091913	0.54865567	1.46272206
ANKRD55	-0.3267835	0.54647673	1.46051455
ADCY9	-0.3803629	0.54544845	1.45947394
SLC10A3	-0.4019852	0.54531199	1.4593359
SLC31A1	-0.3788484	0.54459417	1.45860998
DHX37	-0.343388	0.54412095	1.45813161
N4BP2L2-IT2	-0.2740561	0.5434652	1.457469
IRF4	-0.3966495	0.54267559	1.45667153
TIAM2	-0.3410379	0.54012674	1.45410025
SLPI	-0.3060881	0.53919743	1.4531639
TTYH2	-0.2812814	0.53796171	1.45191975
HECW2	-0.1782137	0.53761011	1.45156594
ACO1	-0.1246852	0.53760916	1.45156498
C10orf105	-0.3119298	0.53717649	1.45112972
IRGQ	0.01525324	0.53650631	1.45045578
TREML1	-0.1793618	0.53617304	1.45012075
GDPD3	-0.2266769	0.53614628	1.45009385
TNFRSF8	-0.1850418	0.53605068	1.44999777
OSER1-AS1	-0.3044191	0.53514767	1.44909048
PYCARD-AS1	-0.1215818	0.53479418	1.44873546
AL356356.1	-0.2662193	0.53212895	1.44606154
NDRG2	-0.2905454	0.53185784	1.44578982
AC137932.2	-0.1464642	0.52999583	1.44392503
CEP128	-0.4676243	0.52955724	1.44348612
SAP130	-0.1807555	0.5287879	1.44271656
WDR19	-0.332162	0.52683678	1.44076674
MTHFD1	-0.3483787	0.52647422	1.4404047
STK3	-0.218426	0.5256965	1.43962844
ODF2	-0.0570127	0.5245195	1.43845441
TARBP2	-0.2514549	0.52446051	1.43839559
STAM2	-0.2903559	0.52410085	1.43803705
ELMOD3	-0.0737076	0.52328111	1.43722019

BAG3	-0.2615884	0.52292194	1.43686243
TCTN1	-0.3051124	0.5228695	1.43681021
ZHX1	-0.1342493	0.52275595	1.43669712
MYL9	-0.0159531	0.52262378	1.4365655
DDX20	-0.4430085	0.52155221	1.43549889
PET100	-0.4362205	0.52147926	1.4354263
AC079174.1	-0.2036104	0.52119332	1.43514182
VSTM1	-0.5758656	0.52050224	1.43445453
AASDH	-0.7317649	0.52047212	1.43442458
AKAP1	-0.2185469	0.51946709	1.43342567
TRIM65	-0.4379087	0.51849793	1.43246306
AFF3	-0.1661235	0.51710788	1.43108352
COLQ	-0.5466495	0.51697961	1.43095629
WDR74	-0.1498772	0.51667768	1.43065685
COX15	0.06084605	0.51665073	1.43063013
RNU6-60P	-0.1634298	0.51617827	1.4301617
CFAP20	-0.1866775	0.5156232	1.42961155
SART1	-0.3042603	0.51532803	1.42931909
CDCA7L	-0.0639965	0.51500376	1.42899786
ZFPL1	-0.4549406	0.51460269	1.42860066
TMCC3	-0.2861175	0.51291232	1.42692778
AC008764.7	-0.2632673	0.5127003	1.4267181
UNC13D	-0.2286469	0.5126595	1.42667775
DHRS12	-0.2589359	0.51167822	1.42570769
RHBDD2	-0.2020571	0.51121368	1.42524869
PLPPR2	-0.2957056	0.51119506	1.4252303
CBX1	-0.1882025	0.51055178	1.42459495
TMEM218	-0.3000107	0.51013318	1.42418166
TBC1D13	-0.1503596	0.50940128	1.42345933
ENSG00000274961	-0.1259208	0.5087276	1.42279479
RNU4-40P	-0.4465834	0.5087088	1.42277625
OSGEP	-0.3183966	0.50828067	1.4223541
HS3ST3B1	-0.1774161	0.50574946	1.41986076
EXD3	-0.2220811	0.50432839	1.41846288
FAM214A	-0.2856373	0.50393682	1.41807793
POLL	-0.3200469	0.50352752	1.41767567
NKX3-1	-0.2436954	0.50233225	1.41650162
YIF1B	-0.3984205	0.50216046	1.41633296
AC100835.2	-0.3656302	0.50215371	1.41632633
AL627309.7	-0.2979935	0.50031727	1.4145246

TOE1	-0.1681936	0.49996678	1.41418099
QTRT2	-0.3482938	0.49968486	1.41390468
LRCH1	0.08718628	0.49967179	1.41389187
APEX2	-0.4903039	0.49959658	1.41381816
CACNA2D3	-0.1699026	0.49955912	1.41378146
ARHGEF19	-0.3029106	0.49794048	1.41219614
OGDH	-0.3240059	0.49768512	1.4119462
ENGASE	-0.4373334	0.49751757	1.41178223
TRERF1	-0.2807537	0.49732753	1.41159627
ZDHHC24	-0.1078827	0.49728092	1.41155067
AL135818.1	-0.2339124	0.49604442	1.41034139
NDUFS4	-0.0698791	0.49510358	1.40942195
TMEM80	-0.1715758	0.49503705	1.40935695
GLT8D1	0.08966936	0.49501254	1.409333
FBXO31	-0.0828242	0.49461207	1.40894185
THOC5	-0.1389121	0.49372199	1.40807286
DOT1L	-0.4702729	0.49233873	1.40672345
AC007969.1	-0.2587203	0.49129732	1.40570837
ADARB1	-0.3067947	0.49080789	1.40523156
CCDC124	-0.1858478	0.48893116	1.40340476
FOLR3	-0.286569	0.48882891	1.4033053
FHL1	-0.3186283	0.488471	1.4029572
AC079922.2	-0.0833325	0.4884342	1.40292142
PRKRIP1	-0.2357345	0.48819643	1.40269022
IGHG4	-0.1369804	0.48808	1.40257702
GUCY1A3	-0.3265557	0.48772985	1.40223666
AC022167.3	-0.5337414	0.48678243	1.4013161
BRAP	-0.1550853	0.48677338	1.40130731
PDCD2L	-0.2535678	0.48632986	1.40087658
TSC22D2	-0.1033341	0.48517714	1.39975772
AP003170.4	-0.198984	0.48415201	1.39876346
MFSD3	-0.1529965	0.48350666	1.3981379
TBCE	-0.2358556	0.48346291	1.3980955
AHDC1	-0.2315792	0.48264627	1.39730433
FLCN	-0.1408546	0.4825262	1.39718804
ATP6V0A1	-0.1757019	0.4824965	1.39715928
PHC1	0.11513416	0.48212184	1.39679649
GSK3A	-0.1962269	0.48189389	1.39657581
TRAPPC9	0.00443283	0.48003436	1.39477689
CABLES2	-0.2571972	0.47937134	1.39413604

IL21R	-0.2147398	0.47909135	1.3938655
AC132008.2	-0.2238712	0.47851933	1.39331294
CD82	-0.1779405	0.47760695	1.39243207
BMX	-0.0289746	0.47637353	1.39124214
SLC38A5	-0.1811634	0.4754105	1.39031376
HNRNPAB	-0.1096536	0.47511875	1.39003263
EEF1DP7	-0.2218548	0.47487196	1.38979487
IFRD2	-0.4114312	0.47458403	1.38951753
NTNG2	-0.2807018	0.47420376	1.38915132
GPR68	-0.2247503	0.47372432	1.38868975
FBXO25	-0.1921096	0.4734976	1.38847153
PMEPA1	-0.3472359	0.47323352	1.38821741
KPNA1	-0.1520799	0.4721168	1.38714326
PRR5	-0.3205043	0.47181225	1.38685047
ZNF585A	-0.2527989	0.47162179	1.3866674
BEX4	-0.2424373	0.47131623	1.38637374
CUEDC1	0.02948843	0.47118408	1.38624675
TMEM186	-0.5360925	0.47075986	1.38583919
ANKRD9	-0.0198612	0.47054878	1.38563644
LONRF1	-0.2163587	0.47014477	1.38524847
GHRLOS	-0.3892258	0.47011801	1.38522277
MSANTD2	-0.4785298	0.4686362	1.38380073
MOSPD1	-0.2132502	0.46830622	1.38348425
RBM38	-0.2544374	0.46750068	1.38271199
TOP2A	-0.0373594	0.46741854	1.38263327
TRPT1	-0.2924127	0.46447052	1.37981086
ABAT	-0.2883687	0.46288555	1.37829581
MBOAT7	-0.1966464	0.46241724	1.37784848
PRDX2	-0.3478633	0.46239217	1.37782453
AL353625.1	-0.3614803	0.46214629	1.37758973
NBPF12	-0.089666	0.45952885	1.37509267
YARS	-0.1730098	0.45902501	1.37461252
RN7SL130P	-0.0271253	0.45889858	1.37449206
CAMKK1	-0.370001	0.45880781	1.37440559
AC024075.2	-0.3693556	0.45876863	1.37436827
DGAT2	-0.0830078	0.45862504	1.37423148
SOWAHD	-0.3168653	0.45831912	1.37394012
JUN	-0.1116049	0.45805131	1.37368509
TSPAN17	-0.1328349	0.45744195	1.373105
P2RX5	-0.1109969	0.45692097	1.37260924

AP000919.1	0.1505438	0.45647667	1.37218659
TAF12	-0.1191498	0.45452372	1.37033034
MAP1LC3B2	-0.259206	0.45420839	1.37003086
MAN1B1	-0.2013445	0.45305375	1.36893482
NIPSNAP1	-0.0921137	0.45268809	1.3685879
NKAPP1	-0.3594402	0.45246307	1.36837445
CLN8	-0.4665033	0.45212342	1.36805233
CPEB3	-0.1146493	0.45150529	1.36746631
EPHB1	-0.0828387	0.45024485	1.36627212
HPGD	-0.228964	0.44967158	1.36572932
RCC1	-0.3098555	0.44956347	1.36562698
SPSB2	0.14370278	0.44853312	1.36465202
SENP3	-0.1538807	0.44837826	1.36450554
SPACA6	0.22774673	0.44798515	1.3641338
MEMO1	-0.2066501	0.44765464	1.36382132
IGHGP	0.02551773	0.44677492	1.36298995
A2M-AS1	-0.3802431	0.44631815	1.36255848
GAB1	-0.4423975	0.44631704	1.36255744
PTOV1	-0.1514213	0.44596372	1.36222378
TAGLN	-0.3893765	0.44523638	1.36153718
PCNX3	-0.3306968	0.44492871	1.36124685
BOP1	0.04417632	0.4446433	1.36097758
GRK3	-0.1023915	0.44408634	1.36045227
ALG6	-0.227763	0.44370986	1.36009729
AL162578.1	-0.2598738	0.44251453	1.35897087
IFT122	-0.4883499	0.44175572	1.35825629
LINC00174	-0.3508658	0.44149608	1.35801186
COPG1	0.03646722	0.43950329	1.35613734
DGAT1	-0.1366957	0.43929915	1.35594546
SPTAN1	-0.3278315	0.43851773	1.35521123
MEGF6	-0.3007511	0.43841662	1.35511625
ETV3	-0.5106206	0.43779727	1.35453463
LINC00649	-0.1398142	0.43769692	1.3544404
GEMIN8	-0.5218342	0.43687985	1.35367354
SIRT7	-0.2666454	0.43672136	1.35352483
AMT	-0.3838838	0.43661135	1.35342163
NAB2	-0.0796287	0.43644874	1.35326909
P2RX1	-0.2071179	0.43636963	1.35319488
APEH	-0.0977164	0.43633416	1.35316162
PLEKHM1	-0.2907388	0.43549706	1.3523767

RN7SL368P	-0.1262462	0.43547659	1.3523575
GAS2L1	-0.2637717	0.43400713	1.35098076
HDAC8	-0.0741331	0.43388649	1.3508678
RAP1GAP2	-0.1866019	0.43349058	1.35049713
AKIRIN2	-0.1080695	0.43280411	1.34985469
TMEM40	-0.117485	0.43276362	1.34981681
ACOT11	-0.0608947	0.43182095	1.34893511
GTF2H2B	-0.0929866	0.4317098	1.34883119
E2F5	-0.2430937	0.43170803	1.34882953
SFI1	-0.3192002	0.43084812	1.34802581
AC099811.5	-0.1168342	0.43032094	1.34753332
GGCX	-0.4969922	0.4303059	1.34751926
C8orf58	0.08370768	0.4302883	1.34750283
RNF5	-0.1441914	0.43004229	1.34727307
NUBP1	-0.035427	0.429934	1.34717194
SNRNP40	-0.3504302	0.42992206	1.3471608
Z99129.4	-0.3344965	0.4292774	1.34655896
AC003072.1	-0.3352077	0.42884183	1.34615248
TCIRG1	-0.0642302	0.4281949	1.34554897
FLNB	-0.3492828	0.42812348	1.34548237
KIF3C	-0.3230062	0.42784945	1.34522682
COX10-AS1	-0.2789203	0.42753199	1.34493084
ARL13B	-0.1146617	0.42739219	1.34480052
NECTIN1	-0.1075764	0.42724789	1.34466602
UBR5-AS1	0.0999111	0.42672161	1.34417559
ERVK13-1	-0.2165189	0.42625026	1.3437365
ATRN	-0.1435705	0.42575785	1.34327794
CCM2	-0.2290329	0.42562194	1.34315141
ARAP3	-0.2830255	0.42561085	1.34314108
SCAMP3	-0.1023459	0.42557279	1.34310565
KIF27	0.13453808	0.42277333	1.34050196
GTPBP1	-0.0262024	0.42248349	1.34023268
ZNF362	-0.0313056	0.42247543	1.34022519
SH3GL1	-0.0626953	0.42215311	1.3399258
MRPL2	-0.397059	0.42211802	1.33989321
ACP1	-0.0921607	0.42198409	1.33976883
AC079331.2	0.00387469	0.42192171	1.3397109
TLE3	-0.196971	0.42139558	1.33922241
PANX2	-0.0986921	0.42069678	1.33857389
TFRC	-0.190036	0.4203619	1.33826321

TRIB1	-0.482512	0.42016769	1.33808308
GSKIP	-0.2332573	0.42012382	1.33804239
ATG9B	-0.2008824	0.42012331	1.33804191
RN7SL600P	-0.1542351	0.41950536	1.33746891
GOLGA2P5	-0.1245028	0.41934277	1.33731819
ZNF230	0.00410286	0.41902239	1.33702124
AC119428.2	-0.0115124	0.41893714	1.33694224
USP36	-0.3533773	0.41891543	1.33692213
VNN1	-0.4433843	0.41885153	1.33686291
NSUN5P1	-0.0155447	0.41779035	1.33587993
AATF	-0.1552241	0.41745385	1.33556839
SNHG15	-0.3664954	0.41742161	1.33553854
AC009404.1	-0.0083607	0.41625987	1.33446353
AF131215.4	-0.0919612	0.4161656	1.33437632
MPIG6B	-0.2921812	0.41606634	1.33428453
PLEK2	-0.1803954	0.41435279	1.33270068
F5	-0.1728106	0.41396811	1.33234538
ZDHHC14	-0.021213	0.41354824	1.33195768
KCNH2	-0.2532273	0.41348993	1.33190385
RNF169	-0.2810418	0.41314835	1.33158853
DGCR6L	-0.1759298	0.4131157	1.33155839
CLDN5	-0.4214938	0.41284426	1.33130789
NPRL2	-0.0714837	0.41161084	1.33017018
STAM	0.03744119	0.41107462	1.32967588
UBA1	0.01328011	0.41071883	1.32934801
MTMR4	-0.3166795	0.41031603	1.3289769
RECQL5	-0.1175817	0.41028307	1.32894654
PPP5C	-0.2060544	0.4100413	1.32872385
PDE6B	-0.19342	0.40995218	1.32864178
DEF8	-0.2503439	0.40980459	1.32850586
RAB4A	-0.154305	0.40910255	1.32785954
ST20-AS1	-0.1357741	0.40868748	1.32747757
POFUT1	-0.2827934	0.40863571	1.32742993
ZFYVE16	-0.2324554	0.40833703	1.32715514
SMUG1	-0.0029297	0.40798151	1.32682813
RHOB	-0.1486932	0.40752624	1.3264095
NRM	-0.2198614	0.40733246	1.32623134
AC008850.1	-0.4328104	0.4073214	1.32622118
ATP6V1E2	-0.3530385	0.40712443	1.32604012
CBR3-AS1	-0.1458184	0.40700287	1.3259284

NUP37	-0.3089221	0.4069239	1.32585582
AC135050.6	-0.334056	0.40659384	1.32555252
AC103703.1	-0.2508415	0.40623439	1.3252223
BATF	0.00446394	0.40587711	1.32489416
ZNF568	-0.1159454	0.40532226	1.32438471
DMAP1	-0.4210306	0.40528373	1.32434934
ADHFE1	-0.2562397	0.40482288	1.32392636
RASGRP1	-0.1835697	0.40455708	1.32368246
TM2D2	0.19580425	0.40420713	1.32336143
MRM3	-0.2809332	0.40412192	1.32328326
SNORA81	-0.1010323	0.40350221	1.32271497
OAT	-0.2180063	0.40301014	1.3222639
TNNT1	-0.3182025	0.40299394	1.32224905
NF1	-0.1331046	0.40293887	1.32219858
ZCWPW1	-0.1291002	0.40204687	1.32138134
HADHB	-0.1756553	0.40129253	1.32069061
KRT23	-0.1062494	0.40124104	1.32064347
IRS1	-0.0653654	0.40035121	1.31982917
GYPB	-0.1731154	0.40011663	1.31961459
SH2B1	0.03058466	0.40001086	1.31951785
NQO2	-0.1007105	0.39960337	1.3191452
SH2D1B	-0.3825377	0.39857813	1.31820809
PDCD6IPP2	-0.1401386	0.39822719	1.31788748
TGS1	-0.0218344	0.39822294	1.31788359
LSP1	-0.2148102	0.39722981	1.31697669
DUSP16	-0.344975	0.39704258	1.31680579
UBE2M	-0.0236636	0.39673603	1.31652601
DEFA3	-0.4843099	0.3965464	1.31635298
SLC9B2	-0.2060556	0.39643524	1.31625156
Y_RNA	-0.1546488	0.39603163	1.31588338
MTCO1P11	-0.2490509	0.39593286	1.31579329
CRADD	-0.2666571	0.39565628	1.31554106
AL162274.2	-0.3678429	0.39547715	1.31537773
MAP3K6	-0.1368724	0.39513536	1.31506614
KPNA5	0.04957496	0.39497866	1.31492331
CYB5R1	-0.0261975	0.39474512	1.31471047
TBL3	-0.0175065	0.39426763	1.31427542
AL135999.1	-0.1581626	0.39420075	1.31421448
AC092620.2	-0.2730135	0.39357875	1.313648
PTCD1	-0.4666319	0.39357555	1.31364508

KIAA1324	-0.115381	0.39352383	1.313598
GP6	-0.3413907	0.39324056	1.3133401
SOCS4	0.17807252	0.3930848	1.31319831
CUEDC2	-0.0168815	0.39278227	1.31292297
GCNT1P3	-0.0618248	0.39217885	1.31237394
DRAM1	-0.3322266	0.39171332	1.31195053
CHI3L2	-0.2694522	0.39162479	1.31187002
POLD2	-0.6063309	0.391504	1.31176019
SAC3D1	-0.1186426	0.39142442	1.31168784
TRPM6	-0.0385792	0.39127864	1.3115553
MIS12	-0.1580441	0.39127826	1.31155495
TMEM45B	-0.3211783	0.39110701	1.31139928
NRGN	-0.2929701	0.3907631	1.31108671
TEX2	-0.269787	0.39037677	1.31073567
PHB	-0.2742423	0.39015115	1.3105307
UNC45A	-0.1069037	0.39004892	1.31043784
FAM45A	-0.2949867	0.38996464	1.31036129
CTDP1	-0.1357414	0.38972825	1.3101466
ZNF573	-0.2927845	0.38946218	1.30990499
HIST2H2BE	-0.1524721	0.38923497	1.30969871
AL450384.2	-0.3930081	0.38880193	1.30930566
LINC00173	0.0755757	0.38870323	1.30921608
AIM2	-0.0901725	0.38863344	1.30915275
AVEN	-0.1518255	0.3884988	1.30903058
DNAJA4	-0.0476329	0.38848298	1.30901623
BRF2	-0.1187187	0.38770422	1.30830982
SLC16A10	-0.0609458	0.38613693	1.30688929
HIST1H3H	-0.3501192	0.38574643	1.3065356
BLOC1S3	-0.3423568	0.38448355	1.30539241
RHBDD3	-0.0683995	0.38387115	1.3048384
AC132938.5	-0.1306595	0.38358678	1.30458124
AC093010.2	-0.0997504	0.38344867	1.30445635
ARID5A	-0.4668407	0.38295062	1.3040061
GEMIN7	0.11219303	0.38291079	1.3039701
NOL10	0.18742876	0.38282172	1.30388959
RBM47	-0.1714522	0.3824509	1.3035545
TUBGCP6	-0.2708615	0.38231107	1.30342816
NT5M	-0.4010784	0.38203407	1.30317793
LINC01506	0.08258465	0.38181691	1.30298178
FER	-0.2987946	0.38161693	1.30280118

KCNE1	0.12806852	0.38143265	1.30263478
GAL3ST4	-0.2804141	0.38105708	1.30229571
FAM173A	-0.0895083	0.38102031	1.30226252
FAM50A	-0.256601	0.38094476	1.30219432
NEMP2	-0.2226338	0.38082985	1.30209061
SCAF1	-0.2999622	0.38067499	1.30195085
RAB11FIP4	-0.1860819	0.38032124	1.30163166
AC010894.5	-0.1023152	0.38021874	1.30153918
LRRC61	-0.0883192	0.37886425	1.30031778
GAMT	-0.016461	0.37878902	1.30024998
TOX4P1	0.04710268	0.37863191	1.30010839
TRMT61A	0.01055551	0.37849884	1.29998848
RABGEF1	-0.1764644	0.37841624	1.29991405
NUP133	-0.2315316	0.37731891	1.2989257
IL2RA	-0.1610351	0.37721016	1.29882779
ALOX5	-0.1150462	0.37658682	1.29826673
TIMM50	-0.1399033	0.37658378	1.298264
ZFYVE1	-0.1736327	0.37651868	1.29820542
LUCAT1	-0.2386506	0.37626211	1.29797456
PCK2	-0.1444592	0.37620306	1.29792143
AC242376.2	-0.0294897	0.3757574	1.29752056
ANAPC7	-0.037771	0.37447155	1.29636461
AP2A1	-0.327667	0.37356591	1.29555109
NCAM1	-0.1767601	0.37292372	1.29497453
GTPBP2	-0.1488745	0.37230629	1.29442044
ZER1	-0.2004651	0.37209425	1.29423021
TPM2	0.09615399	0.37173228	1.29390553
AC007038.2	-0.1767713	0.37163163	1.29381526
CACNB3	-0.1343614	0.3714787	1.29367812
ABHD5	-0.1891572	0.37136211	1.29357357
NR1D2	-0.1528977	0.3712742	1.29349475
TMEM69	-0.0751871	0.37110839	1.2933461
LINC00959	-0.2013845	0.37076281	1.29303633
IP6K1	-0.1362551	0.36958297	1.29197931
WASH2P	-0.2417434	0.3693385	1.2917604
EFTUD2	-0.1088806	0.36900176	1.29145893
DUSP10	-0.2364224	0.36850897	1.29101787
HAPLN3	0.07273678	0.36812054	1.29067033
SRPK1	-0.0051964	0.36753651	1.29014794
HIST1H2AE	-0.2554516	0.36713528	1.28978919

HGSNAT	-0.1074215	0.36628993	1.28903366
SYNGR1	-0.1489139	0.36510134	1.2879721
MRM1	-0.1978006	0.36504826	1.28792471
RAB11FIP2	-0.1072883	0.3637445	1.28676135
CDC14B	-0.1863541	0.36368706	1.28671011
TRMT2A	0.02654285	0.36360388	1.28663593
AL139246.5	0.10072249	0.36319737	1.28627344
SLC25A11	-0.0892464	0.36316118	1.28624118
ICAM4	-0.0960881	0.36291273	1.28601969
CLU	-0.1869963	0.36288364	1.28599376
FKBP14	-0.3347579	0.36246299	1.28561885
STK39	-0.0303229	0.36185544	1.28507756
MASTL	-0.1825676	0.3617723	1.28500351
LMNA	-0.1437981	0.3617544	1.28498756
MTHFSD	0.12732865	0.36172047	1.28495735
AP000350.6	-0.1011546	0.36170209	1.28494098
CAMK2D	-0.2782453	0.36152056	1.2847793
C3AR1	0.01173705	0.36125465	1.28454253
PDZD4	-0.2187484	0.3611508	1.28445006
CD27-AS1	-0.1493033	0.36086491	1.28419555
MMP9	-0.2474186	0.36050062	1.28387133
ABCG1	-0.2410365	0.35975338	1.28320653
NLRP12	-0.0387351	0.35962308	1.28309064
ARL2	-0.3653601	0.35960446	1.28307407
C22orf39	-0.3427197	0.35955845	1.28303316
MAF	-0.2196775	0.35949691	1.28297843
SIAH1	-0.0067269	0.35926317	1.28277058
TSPAN18	0.05109312	0.35885408	1.28240689
NOA1	-0.0220366	0.35884758	1.28240111
PXK	-0.2074391	0.35874814	1.28231272
PPP1R12C	-0.0761258	0.35862815	1.28220607
SCAMP4	-0.2049999	0.35799909	1.28164712
SCN1B	-0.4334039	0.35785494	1.28151907
SMOX	-0.2203589	0.35762634	1.28131602
UBIAD1	-0.2607539	0.35757871	1.28127372
FCHO1	-0.1166249	0.35718705	1.28092592
KCTD9	-0.3796829	0.3571709	1.28091159
KIAA0232	-0.2020164	0.35685597	1.280632
CST7	-0.2958905	0.35644731	1.2802693
PAXBP1-AS1	-0.12634	0.356427	1.28025128

XPR1	-0.5246787	0.35631359	1.28015065
SLC37A3	0.00688956	0.35529016	1.27924284
DENND5A	-0.2532989	0.35493384	1.27892693
DHX35	-0.325838	0.35431297	1.27837666
GCN1	-0.4649605	0.35428893	1.27835535
MRPS30	-0.356943	0.35370745	1.27784022
NBPF11	-0.0219041	0.35360322	1.2777479
UQCC3	-0.2688658	0.35298749	1.27720268
LZTR1	-0.2687327	0.35290428	1.27712902
USPL1	0.00720297	0.35276192	1.277003
PPP1R21	0.1162695	0.35260056	1.27686019
OGFOD1	-0.0854064	0.35242412	1.27670404
DPY19L4	-0.2303069	0.35209864	1.27641603
PTGIR	-0.0823818	0.35175539	1.27611239
PITRM1	-0.2694549	0.35174768	1.27610556
UBE2Q2P1	-0.2642683	0.35163267	1.27600384
NTAN1	0.01519603	0.35155881	1.27593852
NDUFV1	-0.0528541	0.35145746	1.27584889
TPM1	-0.1961086	0.35142394	1.27581924
MAST3	-0.0838027	0.35119823	1.27561966
SLC25A43	-0.4066433	0.35116123	1.27558694
COMTD1	-0.4304424	0.35092927	1.27538187
USP46	0.02646187	0.35088545	1.27534313
RNU6-892P	-0.0096946	0.35086646	1.27532634
NCOR2	-0.0730915	0.3506475	1.2751328
PIGP	-0.5030071	0.35037043	1.27488793
JAKMIP2	-0.4884988	0.35000576	1.27456572
TSPAN33	-0.2383935	0.34979065	1.27437569
CTDSPL2	-0.2507573	0.3497751	1.27436196
GOLGA2	-0.2303052	0.34964867	1.27425028
MCEE	-0.0514035	0.34923539	1.2738853
RNU6-611P	-0.1827913	0.34855826	1.27328755
AC026401.2	-0.1581531	0.34808769	1.2728723
DDHD2	-0.2179965	0.34798809	1.27278442
LINC02397	0.07282417	0.34770621	1.27253577
RHOT1	-0.1144671	0.34726817	1.27214945
ZMIZ2	0.00330417	0.3472367	1.2721217
FAAP100	-0.341996	0.34689901	1.27182397
TMED5	-0.2729483	0.34658986	1.27155147
PYURF	-0.2860079	0.34589043	1.27093516

NGLY1	0.00386638	0.34578178	1.27083945
HRK	-0.1158205	0.34570173	1.27076894
ABCA2	-0.5626393	0.3454925	1.27058466
MCM7	0.0713182	0.34544437	1.27054227
ASRGL1	-0.1085534	0.34519991	1.270327
PNKP	-0.2141952	0.344968	1.27012281
FAM160B1	6.28E-04	0.34480149	1.26997623
THEMIS	-0.1925606	0.34438417	1.26960892
MIATNB	-0.2633099	0.3442277	1.26947123
TTI2	-0.0515892	0.34421123	1.26945674
TSR3	-0.1793451	0.34378497	1.26908172
FAM89B	-0.2375985	0.34318913	1.26855769
HM13-IT1	-0.137176	0.34315049	1.26852371
AC008610.1	-0.1850678	0.34314449	1.26851844
ADSL	0.0672639	0.34313773	1.2685125
AP2A2	-0.1321578	0.34309572	1.26847556
NDUFA8	0.00699929	0.3430715	1.26845426
AQP10	-0.2356023	0.34266739	1.26809901
ZNF692	-0.1787109	0.34237781	1.2678445
LRRC47	-0.0536163	0.34228893	1.26776639
DNAJC11	-0.1280771	0.34215285	1.26764682
TNFRSF18	-0.1902915	0.34208725	1.26758918
FOXP1-IT1	-0.1424313	0.3420111	1.26752228
ZNF581	-0.1364686	0.34197331	1.26748907
RFX1	-0.1308228	0.34190961	1.26743311
PPP2R2D	-0.0268387	0.34183493	1.26736751
CREBBP	-0.0726447	0.34139672	1.26698261
CHST13	-0.0085111	0.34109649	1.26671898
COQ8B	-0.2033539	0.34065633	1.26633256
FCER2	-0.4883237	0.34058055	1.26626605
POLDIP3	-0.1251261	0.34054115	1.26623146
FAM174B	-0.0420986	0.3395786	1.26538693
NEURL1	-0.240091	0.33938682	1.26521873
CCS	-0.1666029	0.33909618	1.26496387
C5orf63	-0.2815439	0.33907111	1.26494189
OXSRI	0.07981769	0.33901395	1.26489178
CCDC170	0.22752851	0.33876502	1.26467354
ATAD3A	-0.2874766	0.33841721	1.26436869
TRAV17	-0.0362644	0.33812417	1.2641119
HAL	-0.2610438	0.33802306	1.2640233

XK	-0.1231095	0.33769934	1.26373971
GOLIM4	-0.2023103	0.3375674	1.26362414
GPHN	-0.1609478	0.33746355	1.26353318
TOR2A	-0.2046227	0.33722853	1.26332736
TSTA3	-0.0929294	0.33694281	1.2630772
MTIF2	0.03131453	0.33691832	1.26305575
PACS2	-0.3720201	0.33677725	1.26293225
PAXIP1-AS1	-0.1086272	0.33651203	1.2627001
TCAF2	0.0053998	0.33627418	1.26249195
LRRC8A	-0.1031996	0.33616142	1.26239327
IGLC2	-0.1016147	0.33606158	1.26230591
GPS1	0.04423065	0.33573965	1.26202427
H6PD	0.07798604	0.33573644	1.26202146
CERS5	0.07758708	0.33546026	1.26177989
SETD6	-0.1961313	0.3352273	1.26157616
AC012368.1	-0.0099041	0.33508482	1.26145157
PEX16	-0.2317357	0.33462377	1.26104851
MTMR11	-0.1773196	0.33459387	1.26102237
ITSN1	-0.317525	0.33445269	1.26089897
QSOX2	-0.068606	0.33418009	1.26066075
CCDC191	-0.096852	0.33389974	1.2604158
B3GALT4	-0.2987378	0.33361922	1.26017074
BSG	-0.2499639	0.33314362	1.25975538
DAPK2	-0.1263049	0.33281908	1.25947203
LINC02035	-0.1341412	0.33270825	1.25937528
AC013264.1	-3.10E-04	0.33259344	1.25927506
THAP7	-0.5411695	0.33255296	1.25923972
DSTYK	-0.0746474	0.33253574	1.25922469
PTPN11	-0.147956	0.33225247	1.25897748
EXO5	-0.0155847	0.33204793	1.258799
FAAP20	0.08962832	0.33201255	1.25876812
SRM	-0.0564346	0.33186163	1.25863645
LYRM9	-0.1570537	0.33161539	1.25842164
RN7SL200P	-0.2883969	0.33160813	1.25841531
JPT2	-0.2128382	0.33127703	1.25812653
GGACTION	-0.2723953	0.33124098	1.2580951
IGHMBP2	-0.5074483	0.33093447	1.25782784
EPS15L1	-0.0512358	0.33062853	1.25756113
CIPC	-0.0556217	0.33027345	1.25725166
FRMD4A	-0.3380957	0.32996374	1.25698179

SLC10A7	-0.2092143	0.32993282	1.25695485
EIF5A2	-0.0715938	0.32989818	1.25692466
LSM10	-0.1298749	0.32919218	1.25630973
CDC42EP4	-0.208618	0.3289538	1.25610216
PI3	-0.2027383	0.32840811	1.25562713
PSMA6	-0.0613662	0.32816573	1.2554162
LINC01252	-0.1798688	0.32794604	1.25522504
DBR1	-0.3186823	0.3278146	1.25511069
NCAPH2	0.05184511	0.32774383	1.25504912
ISOC1	-0.0603541	0.3277371	1.25504326
AC125437.2	0.0070033	0.32726001	1.2546283
PLCB1	-0.0591847	0.32713681	1.25452116
RAB33B	-0.0548638	0.32699806	1.25440052
FANCE	0.00841767	0.32682409	1.25424926
DLGAP4	-0.1698516	0.32678016	1.25421107
TRPS1	-0.0097543	0.32659014	1.25404589
EMC8	-0.1626601	0.32559596	1.25318201
CRISPLD2	-0.1246986	0.32547116	1.25307361
CORO1A	-0.2407758	0.32495604	1.25262627
MAN1A1	-0.1448974	0.32478246	1.25247556
FAF1	-0.1774553	0.32447912	1.25221225
BCL2L1	-0.1199657	0.32439646	1.25214051
MESDC1	-0.2209351	0.32425018	1.25201356
AC012645.1	-0.1056793	0.32413532	1.25191387
DLG1	-0.1207002	0.32395702	1.25175917
GCDH	-0.0749604	0.32373717	1.25156842
DNAJB2	-0.1670054	0.32365591	1.25149793
MED8	-0.2580009	0.32333196	1.25121695
PDXK	-0.2839079	0.32327255	1.25116542
Y_RNA	-0.1721769	0.32302868	1.25095395
POP7	-0.2160421	0.32294642	1.25088263
KIFAP3	-0.1295218	0.32290394	1.25084579
C14orf80	-0.3196419	0.32288641	1.25083059
ATP6AP1	-0.0871403	0.32285501	1.25080337
FECH	-0.1933723	0.32281496	1.25076865
GALNS	-0.023196	0.32248106	1.2504792
CCDC94	-0.2674219	0.32240327	1.25041178
SDSL	-0.2058582	0.32239122	1.25040133
ATXN10	-0.0255319	0.32187789	1.24995651
AC022098.1	0.00246826	0.32187218	1.24995156

AC104695.2	-0.0085975	0.32143926	1.24957653
VAMP2	-0.0680806	0.32126975	1.24942972
RHOBTB3	-0.1377878	0.32063752	1.2488823
AP001189.1	-0.1274492	0.32053619	1.24879459
ENO2	-0.0189556	0.32041354	1.24868843
ZFH2-AS1	-0.3346091	0.3203486	1.24863222
ALKBH2	-0.2222829	0.32012754	1.24844091
RASGEF1A	-0.3578324	0.3200886	1.24840721
C3orf18	-0.1801665	0.31999881	1.24832952
LAMTOR2	-0.4770045	0.31939951	1.24781107
UTP14A	-0.0015565	0.31933727	1.24775723
ZNF620	-0.0295085	0.31918014	1.24762135
IRF2BP1	-0.1088627	0.31860943	1.2471279
TJP2	-0.1354053	0.31832774	1.24688442
AC231981.1	-0.0682355	0.31792076	1.24653273
FUK	-0.4821387	0.31786431	1.24648395
SMC2	-0.1235512	0.31774133	1.24637771
GTF2A1	0.03247355	0.31762405	1.24627638
GID4	-0.1143876	0.31744449	1.24612128
PHF2	-0.136402	0.31724343	1.24594763
GBF1	-0.0567193	0.31722389	1.24593076
UPF3A	-0.2229811	0.31707988	1.24580639
AC114490.1	0.26428801	0.31704938	1.24578006
AC134407.3	-0.2833853	0.31704755	1.24577847
ZNF576	-0.296571	0.31687306	1.24562781
AC027279.1	-0.330735	0.31684237	1.24560131
AAAS	-0.2441698	0.31665982	1.24544372
TNIP2	-0.1147821	0.31657814	1.2453732
C3orf62	-0.1763407	0.31644914	1.24526185
BLOC1S5	-0.3545319	0.31635164	1.2451777
CASK	-0.0034511	0.31626245	1.24510072
SMAD1	-0.1199228	0.3160432	1.24491152
DPP9	-0.2351157	0.3160175	1.24488933
TNFAIP1	-0.3301743	0.31589708	1.24478543
SVIL	-0.241206	0.31586393	1.24475683
CD5	-0.1247826	0.31535981	1.24432195
SHKBP1	-0.0834903	0.31500699	1.24401768
ABHD2	-0.1337339	0.31499717	1.24400922
EFNB1	-0.0490435	0.31484019	1.24387386
STYXL1	-0.0235376	0.31477783	1.2438201

ADGRG3	-0.2023849	0.31449242	1.24357405
LRRC45	-0.0546942	0.31439427	1.24348945
WVOX	-0.0079266	0.31423863	1.24335531
AC009831.1	-0.1243312	0.31407964	1.24321829
CSPP1	-0.1134872	0.3139432	1.24310072
AL031666.3	-0.1185152	0.31389307	1.24305753
USP31	-0.1599853	0.3137621	1.24294469
CCDC102A	-0.0468556	0.31372419	1.24291203
TIMM9	-0.0130791	0.31369419	1.24288619
GMPPA	-0.2414461	0.31368402	1.24287743
SMG1P1	-0.1196365	0.31333213	1.24257431
AMMECR1L	-0.4198981	0.31314331	1.24241169
YIPF2	-0.430961	0.31311609	1.24238825
OBSCN	-0.1188819	0.31290618	1.24220749
TMEM131	-0.1233567	0.31280585	1.24212111
PLOD3	-0.0464291	0.31261615	1.24195779
ORAOV1	-0.2176838	0.31260809	1.24195086
AC020659.1	-0.3697486	0.31240549	1.24177646
SLC22A15	-0.4798423	0.31226121	1.24165228
RFK	-0.0989338	0.31189117	1.24133385
LRRC14	0.1485859	0.31168863	1.24115959
WDR76	-0.0488663	0.31154991	1.24104025
SBF2-AS1	-0.32114	0.31152289	1.24101701
ZNF778	-0.1413268	0.31147971	1.24097987
UQCRC1	-0.0011126	0.3112434	1.24077662
HEMGN	-0.1823566	0.31124224	1.24077561
EEDP1	0.08458237	0.31107012	1.2406276
MITD1	-0.0239727	0.31076231	1.24036293
ACSS3	-0.3015988	0.3107094	1.24031744
ABCC3	-0.3766045	0.31059827	1.2402219
HES1	-0.2215449	0.31056722	1.24019521
CLSPN	-0.1095735	0.31052448	1.24015847
KIAA1586	-0.1739905	0.31019036	1.23987128
PRNP	0.13227145	0.31017634	1.23985924
ALG1	-0.4465646	0.31016978	1.2398536
G6PC3	-0.0638363	0.3101556	1.23984141
IL1R1	-0.2751903	0.30992441	1.23964274
AC010997.6	-0.2328812	0.30992411	1.23964249
TMEM62	-0.2190609	0.30987587	1.23960104
KIF16B	0.09705766	0.30969678	1.23944717

IRF3	-0.26382	0.30941486	1.23920499
RCBTB1	-0.19339	0.30940522	1.23919671
CYB561D2	-0.1800421	0.30933745	1.2391385
ENTPD5	-0.3289712	0.30928045	1.23908954
NDUFV3	-0.1845102	0.30927282	1.23908299
PBRM1	-0.1335047	0.30915932	1.23898552
AMIGO1	-0.1936934	0.30884878	1.23871885
CEACAM3	-0.0826436	0.30878252	1.23866196
SORD	-0.2161243	0.30823915	1.23819552
COQ6	-0.1143769	0.30794154	1.23794012
CDADC1	-0.3158219	0.30788561	1.23789214
IGHG1	0.1067466	0.30783808	1.23785135
ZNF598	-0.2698129	0.30768519	1.23772018
TBXA2R	0.05778465	0.30767267	1.23770944
NSUN3	-0.150405	0.30735746	1.23743904
TMEM144	-0.1589699	0.30722428	1.23732482
ROGDI	-0.2198375	0.30707528	1.23719704
CHMP6	-0.0238969	0.30703503	1.23716252
PEX10	0.06060047	0.30689801	1.23704503
RIN3	-0.043614	0.30681053	1.23697002
P3H1	0.12771283	0.3066742	1.23685314
TRG-AS1	-0.1451012	0.30662658	1.2368123
CLYBL	-0.0385257	0.30660141	1.23679073
AC011374.2	-0.2288685	0.30625369	1.23649267
AP3B1	0.00956355	0.30612114	1.23637907
GLT1D1	-0.2100043	0.30602398	1.23629581
RABEPK	-0.0802895	0.30587689	1.23616977
PBXIP1	-0.1037769	0.305641	1.23596767
RNU4-78P	-0.0293195	0.30559031	1.23592424
ZNF25	-0.021469	0.30557442	1.23591063
PARP10	-0.1794139	0.30544374	1.23579868
FARS2	-0.0755768	0.30526278	1.23564369
AC104451.1	-0.3547065	0.30498962	1.23540975
CR1	-0.198326	0.30484424	1.23528526
MINCR	-0.1819399	0.3046943	1.23515689
PAWR	0.03208121	0.30464304	1.235113
MED25	-0.0518403	0.30448583	1.23497842
PRRC2A	-0.1860768	0.30434466	1.23485758
AC116366.2	-0.2331478	0.30426917	1.23479297
KATNAL1	-0.0682081	0.30406514	1.23461835

AP000936.3	-0.1743906	0.30386975	1.23445115
CCDC9	-0.1229655	0.30372904	1.23433076
XAB2	-0.3362505	0.3036111	1.23422986
LTF	-0.1503608	0.30341683	1.23406367
CLPP	-0.0944364	0.30301077	1.23371638
AC022211.3	-0.1308846	0.30260652	1.23337073
MYOF	-0.1872366	0.30248789	1.23326932
CITED4	-0.1018454	0.3023773	1.23317479
E4F1	-0.181966	0.30227547	1.23308775
HUWE1	-0.2573305	0.30223689	1.23305478
FP565260.1	-0.0834707	0.30209297	1.23293177
AC243829.1	-0.1061701	0.3018919	1.23275995
TNIP1	-0.172943	0.30179284	1.23267531
RABAC1	0.05018446	0.30150038	1.23242545
HEIH	-0.1015615	0.3013312	1.23228094
MROH6	0.10041826	0.30132476	1.23227544
PPIL2	-0.1538654	0.30112829	1.23210763
ARHGEF10	0.08924792	0.30110816	1.23209044
ANKRD39	-0.3552087	0.30101242	1.23200868
PYCR2	-0.2399175	0.30098171	1.23198245
RASGRP4	-0.130983	0.3008168	1.23184164
PAQR3	-0.2954338	0.30080485	1.23183144
PRRC2B	-0.0674767	0.30080063	1.23182784
HPCAL4	-0.1476291	0.3006408	1.23169137
CDKAL1	-0.2946752	0.30063667	1.23168784
FNBP1L	-0.0578526	0.3005919	1.23164962
BRD4	-0.1756417	0.30036673	1.23145741
ZNF143	0.0125878	0.30016629	1.23128633
CENPV	-0.1809626	0.30011491	1.23124248
MCF2L	2.49E-04	0.30010412	1.23123327
PPIF	-0.2697225	0.29995384	1.23110502
PRKCQ-AS1	-0.2620158	0.29993337	1.23108756
ZNF593	-0.2204915	0.29947887	1.23069978
DENND6B	-0.1828593	0.29873197	1.2300628
ZFP90	-0.2688965	0.29827562	1.22967377
CYP1B1-AS1	-0.0599493	0.29811459	1.22953652
AC007278.1	-0.1978952	0.29799237	1.22943237
GPR107	-0.1765708	0.29786792	1.22932631
OGFR	-0.1524395	0.29783453	1.22929786
POLD3	0.27485539	0.29760016	1.22909817

ETFB	-0.0684461	0.29756233	1.22906595
NDUFAF5	-0.1163495	0.29751729	1.22902758
ERMN	-0.1975764	0.29737208	1.22890388
FAM50B	-0.052984	0.2971466	1.22871183
PUSL1	-0.1951457	0.29701464	1.22859945
C15orf39	-0.0379976	0.2966775	1.22831238
ZFP41	-0.1650942	0.29632283	1.22801044
ATP6V1A	-0.1063724	0.29611929	1.22783721
UBALD1	-0.1706281	0.29597374	1.22771334
RIC1	-0.4554856	0.29582154	1.22758383
KIAA1147	-0.2080568	0.29570293	1.22748291
ARHGAP35	-0.1010804	0.29564793	1.22743611
SIRT6	-0.0815158	0.29545097	1.22726855
UNC93B1	-0.1282129	0.29538806	1.22721503
RPL17P50	-0.1160814	0.29530032	1.2271404
PEX6	-3.63E-04	0.29489209	1.22679321
AC024293.1	-0.1899447	0.29476936	1.22668885
HDDC3	-0.2725958	0.29461963	1.22656155
BFSP1	-0.2916882	0.29432163	1.22630822
TAF9	-0.2460298	0.29415159	1.22616369
AC026401.3	-0.2107954	0.29400835	1.22604196
CCP110	-0.2506538	0.29381881	1.22588089
RNF168	-0.0400451	0.29363407	1.22572392
ANAPC16	-0.0561136	0.29340872	1.22553248
CHMP7	-0.1375007	0.29332155	1.22545843
CMTM5	-0.0767719	0.29286614	1.22507166
AL731557.1	-0.2808527	0.29218746	1.22449549
ARHGAP10	-0.1682932	0.29205427	1.22438245
TMOD3	-0.0966115	0.29193703	1.22428295
SSNA1	-0.2444664	0.29189211	1.22424484
ENOSF1	0.04316675	0.29115555	1.22361997
ATP5L2	0.12067538	0.2907911	1.22331089
WDTC1	-0.1086326	0.29053427	1.22309314
YY1AP1	-0.1545972	0.29032373	1.22291466
SLC6A16	-0.2798684	0.29013368	1.22275357
NPLOC4	-0.1942359	0.28946671	1.22218842
BIN1	-0.0714214	0.2894265	1.22215435
CDK11B	-0.0927066	0.28942576	1.22215372
KLHL12	-0.1118309	0.28922463	1.22198335
AC144521.1	-0.2082674	0.28922434	1.22198311

CIDECP	0.02207779	0.28855626	1.22141736
ABTB1	-0.1442131	0.28838268	1.22127041
CEP85	-0.1439211	0.28825937	1.22116604
FAM153B	-0.0740223	0.28825715	1.22116416
GTF2E1	-0.0509024	0.28819371	1.22111046
AC092135.3	0.02491255	0.2881558	1.22107837
GFM2	-0.0262481	0.28811258	1.22104179
PEAK1	-0.0382046	0.2880114	1.22095616
DDX27	-0.1258226	0.28796938	1.2209206
CYB5R3	-0.0843729	0.28791854	1.22087758
CEP44	-0.1665431	0.28768336	1.22067857
TCN2	-0.0299435	0.28764196	1.22064355
FAM58A	-0.0076644	0.28752165	1.22054176
HACD2	-0.1144913	0.28719739	1.22026746
ZNF385D	-0.0677462	0.28699312	1.2200947
CLK3	-0.1820735	0.28668389	1.2198332
KDELC2	-0.0672473	0.28634067	1.21954304
MNAT1	0.00605085	0.28632206	1.2195273
METTL8	-0.3259143	0.28626284	1.21947725
RPH3AL	-0.1098528	0.28610286	1.21934202
ACAD9	-0.0115425	0.28578908	1.21907685
LINC01002	-0.0133677	0.28570222	1.21900346
PAK5	-0.0641384	0.28539657	1.21874523
PNRC2	-0.0925548	0.2852793	1.21864616
ZNF48	-0.3978339	0.28519482	1.2185748
VILL	-0.2180168	0.28517723	1.21855995
SH2D2A	-0.1920163	0.28486159	1.21829338
PRKACA	-0.112184	0.28471033	1.21816565
AC245884.12	-0.2540466	0.28468449	1.21814384
DIXDC1	-0.1050375	0.28445066	1.21794641
NBPF20	-0.1725419	0.28433056	1.21784502
MGST3	-0.2450324	0.28397886	1.21754818
USP11	-0.2644864	0.2839705	1.21754112
CPA3	-0.2076044	0.28337044	1.21703481
SULT1A1	-0.1834582	0.28290744	1.2166443
TIMM10B	0.08889535	0.28274116	1.21650408
GIMAP5	-0.0020207	0.28273238	1.21649667
RNU7-181P	0.02187704	0.28270822	1.21647631
MSS51	-0.0882911	0.28254669	1.21634011
AC036108.4	-0.0827879	0.28245874	1.21626596

NEGR1	-0.1202978	0.28244118	1.21625116
AC008741.2	-0.0840276	0.28183108	1.21573693
HOMEZ	0.19146851	0.2817814	1.21569506
TP53	-0.1408048	0.28166901	1.21560036
GIGYF2	-0.0712334	0.28160974	1.21555043
DAP	-0.1607768	0.2815139	1.21546968
CHST7	-0.3446244	0.28146749	1.21543057
NDE1	-0.144085	0.28127763	1.21527063
IFT27	-0.1073646	0.28124371	1.21524207
SMPD4	0.12892783	0.28119568	1.21520161
IL1R2	-0.2066585	0.28117524	1.21518439
PARD6B	0.11057666	0.28106498	1.21509152
AC090152.1	-0.1599694	0.28078763	1.21485795
ZNF318	-0.2079336	0.28064937	1.21474153
AL355488.2	-0.2545342	0.28045319	1.21457636
C19orf47	-0.0175657	0.28020892	1.21437073
MOB2	-0.0309548	0.27982955	1.21405144
SNX19	-0.0026173	0.27974889	1.21398356
MPST	-0.1900128	0.27959891	1.21385737
C14orf132	-0.1198597	0.27953825	1.21380633
LIPE-AS1	-0.213937	0.27953104	1.21380026
SMAGP	0.06816113	0.27941384	1.21370167
TUBA4A	-0.0745764	0.27938566	1.21367795
ARHGEF7	0.0162537	0.27900687	1.21335934
SUCLG1	-0.1180027	0.27851633	1.21294685
ZNF512	-0.3006785	0.27843106	1.21287515
S1PR3	-0.0925765	0.27838013	1.21283234
IFT172	-0.2085263	0.27823942	1.21271406
Y_RNA	-0.0316106	0.27795937	1.21247867
R3HDM4	-0.0604069	0.27772315	1.21228016
TPST1	-0.0182053	0.27694335	1.21162508
ENO3	-3.48E-04	0.27690354	1.21159165
GMDS-AS1	-0.1160702	0.27682585	1.21152641
GUF1	-0.0702768	0.27671434	1.21143277
SNX9	-0.2775561	0.27636292	1.21113771
SEC14L1	-0.1126659	0.27630363	1.21108795
EDEM3	-0.0609334	0.27628749	1.2110744
DHRS3	-0.0465334	0.27599949	1.21083266
GMIP	-0.0283299	0.27586655	1.21072109
AC097376.1	-0.3416858	0.27571577	1.21059456

NUDT19P5	-0.1526922	0.27570245	1.21058338
CFAP45	0.04295757	0.27569533	1.2105774
CECR6	0.11733248	0.27552967	1.21043841
IGHG3	-0.0391016	0.2744724	1.20955167
MAP4K2	-0.0784941	0.27422414	1.20934355
MMP25	-0.0996872	0.27408964	1.2092308
EIF4G1	-0.1707392	0.27394663	1.20911094
SRRD	-0.2513172	0.27362199	1.2088389
SETD1A	-0.2692021	0.27346571	1.20870796
TRMT2B	-0.2994028	0.27337215	1.20862958
AC103691.1	-0.0201649	0.27336395	1.20862271
NCR3	-0.0901079	0.27332127	1.20858695
ZFP64	-0.0270375	0.27307105	1.20837735
SAMD3	-0.221599	0.27302761	1.20834097
LINC01637	-0.12243	0.27293105	1.2082601
HCAR2	-0.2677148	0.27290488	1.20823818
SLC16A3	-0.0727072	0.27276107	1.20811775
WRNIP1	-0.0360616	0.27250046	1.20789953
TBC1D25	0.16446628	0.27236453	1.20778573
DTX4	0.0282441	0.27229832	1.2077303
AP000866.5	0.11797035	0.27196698	1.20745296
RNF20	0.05482927	0.27196	1.20744711
THOP1	0.06114692	0.2719262	1.20741882
HTT	0.00156489	0.27137548	1.20695801
AC147651.3	-0.2117295	0.2713434	1.20693117
SUMF1	-0.3409979	0.27120502	1.2068154
SMIM5	-0.145286	0.27119798	1.20680952
MLST8	-0.0799666	0.27029882	1.20605761
NUMBL	-0.0447285	0.27022444	1.20599543
AC109454.2	-0.0554589	0.27014162	1.2059262
LYNX1	-0.2161286	0.27002992	1.20583283
DBN1	0.11960091	0.27002025	1.20582475
AC015883.1	-0.0284182	0.26934093	1.2052571
PIAS4	0.06556956	0.26926474	1.20519345
RAB34	-0.113142	0.26901977	1.20498883
TSGA10	-0.1264672	0.26892025	1.20490571
ZNF394	-0.1131722	0.26868489	1.20470915
SETD3	-0.0422596	0.26863148	1.20466456
C11orf49	-0.2086395	0.26862329	1.20465772
ZMPSTE24	-0.2015615	0.2681158	1.20423404

SAR1B	0.1504018	0.26782921	1.20399484
PRSS21	-0.2145917	0.26782875	1.20399446
EXOSC5	-0.2253994	0.26777054	1.20394588
SLC24A3	-0.1723996	0.26752774	1.20374328
AC114495.2	-0.01768	0.2675168	1.20373415
HPS6	-0.0201259	0.26734738	1.2035928
MAP1LC3A	0.09439463	0.26718358	1.20345615
EXOC6B	0.0053399	0.26718292	1.2034556
LINC00694	-0.0031125	0.26695929	1.20326907
ABCG2	-0.2173632	0.26666931	1.20302724
FRG1BP	0.0152745	0.26639878	1.20280167
KIFC2	-0.222687	0.26587301	1.20236341
ZNF211	0.04948567	0.26571076	1.20222819
ZNF467	-0.0639577	0.26561663	1.20214976
RDH11	-0.0998039	0.26546082	1.20201994
JDP2	-0.2031044	0.26540689	1.201975
SLC25A1	-0.0990668	0.26539541	1.20196543
SIGIRR	-0.1040322	0.265364	1.20193927
AP003733.4	-0.2531794	0.26511943	1.20173553
MARK4	-0.1308958	0.26506214	1.20168781
ASCL2	-0.4033947	0.26493681	1.20158342
AC007382.1	-0.079032	0.26460105	1.20130381
BCL7A	-0.0340896	0.26440139	1.20113756
BAK1	-0.202741	0.26435479	1.20109877
GID8	-0.1499683	0.26424957	1.20101117
SLC35A4	-0.1837232	0.26417537	1.2009494
PCYT2	-0.2329255	0.26399867	1.20080232
AC009061.2	0.05985855	0.26390521	1.20072453
SESTD1	-0.1242792	0.26387361	1.20069824
CLDN15	-0.356609	0.26368044	1.20053747
QPRT	-0.251585	0.26363469	1.20049941
SLC12A9	0.05406507	0.26358412	1.20045733
NETO2	-0.1412634	0.26355548	1.2004335
CLN3	0.06458063	0.26354591	1.20042554
SMIM3	-0.310394	0.26347828	1.20036926
PDZD11	0.03139022	0.26346584	1.20035891
ELP6	-0.2293136	0.26344129	1.20033848
GSEC	-0.0148911	0.26338243	1.20028952
GTF2E2	0.22027403	-0.322143	0.79988082
NAE1	-0.0382278	-0.3222062	0.79984581

MRPL18	0.04549837	-0.3222329	0.79983099
SERTAD3	0.20161596	-0.322533	0.79966462
ZMAT1	0.04189816	-0.3226247	0.79961382
RAP2C	-0.0297137	-0.3231668	0.79931339
ANKRD13C	-0.1309529	-0.3232337	0.79927637
MGAT2	-0.0503842	-0.323272	0.79925513
TBC1D4	0.23361093	-0.3232788	0.79925139
RPL23AP2	0.09715618	-0.3233098	0.79923421
LDLR	0.12535631	-0.3233906	0.79918944
ARHGAP6	0.07650212	-0.3236782	0.79903012
ERCC6	-0.1703002	-0.3240019	0.79885087
NFYA	0.40394864	-0.3240454	0.79882678
UBE2E3	0.40182102	-0.3242197	0.79873028
ZNF703	0.33447169	-0.3244286	0.79861464
KANSL2	-0.0627506	-0.3244809	0.79858567
AC005261.2	0.21352484	-0.3245275	0.79855986
KANSL1	0.19401216	-0.3245589	0.7985425
ANKHD1-EIF4EBP3	0.27420265	-0.3248218	0.79839701
ERO1A	0.22386928	-0.3248329	0.79839084
BPHL	0.15908703	-0.3248464	0.7983834
RIMKLB	0.25038115	-0.324961	0.79831996
CEP120	0.30838914	-0.3252014	0.79818694
SMYD4	0.25161499	-0.32524	0.7981656
TTC28-AS1	0.06488395	-0.3252541	0.79815778
SSB	0.17569162	-0.3255755	0.79797998
NDC1	0.10530092	-0.3256378	0.79794556
VPS16	0.30597685	-0.3256981	0.79791218
METTL15	0.18231217	-0.3258669	0.79781883
GPRIN3	0.40378515	-0.3259727	0.79776034
MRPS15	0.38019845	-0.3260518	0.79771662
MBD2	0.20248531	-0.3260558	0.79771437
ARF6	0.08687857	-0.3261848	0.79764305
GIMAP6	0.24130203	-0.3262425	0.79761118
DYNLL1	0.11550213	-0.3263343	0.79756044
CALU	0.04675371	-0.3263446	0.79755471
PBX3	0.23983811	-0.3263967	0.79752594
DIS3	0.23478684	-0.3264877	0.79747562
PITPNM1	0.09313406	-0.3267334	0.79733981
RGS9	-0.0164896	-0.3268777	0.79726003
AKAP7	-0.0643048	-0.3269052	0.79724484

MBD1	0.26835355	-0.3269683	0.79720997
ZNF550	0.21506313	-0.3270245	0.79717892
LCLAT1	0.10164742	-0.3271042	0.79713493
OTUD7A	0.17516423	-0.3271316	0.79711978
AC131212.2	0.15349684	-0.3271382	0.7971161
DHX32	0.15281711	-0.3272838	0.79703566
AC135983.2	0.1178253	-0.3272894	0.7970326
DERL2	0.04263901	-0.3272933	0.79703041
SPG21	0.3096931	-0.3273019	0.79702569
YKT6	0.246283	-0.3273872	0.79697853
LYRM1	0.31176847	-0.3274104	0.79696574
DDX1	0.21797367	-0.3276816	0.79681594
TTC27	0.16633805	-0.3277963	0.79675257
SUGP1	0.20474142	-0.3278434	0.79672656
H3F3AP4	-0.0960724	-0.3278925	0.79669947
ATF7	0.17391452	-0.3279315	0.79667793
CYB5A	0.49197169	-0.3279733	0.79665487
VPREB3	0.30574567	-0.3280062	0.79663667
ZNF540	0.26986567	-0.3283027	0.79647294
TRNAU1AP	0.04368695	-0.328382	0.79642918
ZNF141	0.34845044	-0.3283984	0.79642014
LRBA	0.33691423	-0.3284	0.79641923
PDLIM5	-0.0286238	-0.3284277	0.79640396
RNF157	0.30463632	-0.328604	0.79630662
SPPL2A	0.32538195	-0.3287847	0.79620689
PPP2R2B	0.21078105	-0.328855	0.79616814
AP001157.1	0.50836693	-0.3288707	0.79615943
FAM69A	0.06477302	-0.3289919	0.79609255
PTPRA	0.13453631	-0.3289952	0.79609076
ZSWIM3	0.3702373	-0.3293938	0.79587082
TGFA	-0.1842213	-0.329408	0.79586299
KPNA2	0.02621205	-0.3296273	0.79574204
TRIM62	0.09297827	-0.3298564	0.79561568
MAP3K1	0.30740989	-0.329857	0.79561537
EBPL	0.34351738	-0.3304035	0.79531404
TP53RK	0.16605829	-0.3304067	0.79531227
TNRC18	0.389333	-0.3305564	0.79522973
UAP1	0.18026986	-0.3306464	0.79518012
TAF6	0.39275531	-0.3306833	0.79515981
PCNT	0.29993868	-0.330712	0.79514396

DNAJB11	0.36102459	-0.3307534	0.79512117
SERTAD1	0.51672999	-0.3308629	0.79506078
WDR54	0.31719132	-0.3309435	0.79501638
HCP5	0.03248543	-0.3309779	0.79499745
GMEB1	0.45772494	-0.3310549	0.79495499
MCM6	0.42245704	-0.3311944	0.79487813
FBXO11	-0.0226408	-0.3313519	0.79479136
SCAF8	0.23840273	-0.3313902	0.79477027
SNU13	0.21400475	-0.3315605	0.79467645
MCFD2	0.17406334	-0.3316513	0.79462645
MYD88	0.24314285	-0.3318262	0.79453009
VAMP8	0.17741463	-0.331878	0.7945016
AC008026.3	0.07076387	-0.3318879	0.79449613
TMPO	0.21496175	-0.3319755	0.79444789
LARP4B	0.32225543	-0.3320271	0.79441945
JCHAIN	0.21532751	-0.3320459	0.79440911
ZNF514	0.33614657	-0.3321902	0.79432966
FBXO22	0.11618301	-0.3322586	0.794292
ALKBH8	0.13807688	-0.3322623	0.79428995
C1GALT1	5.97E-04	-0.3322805	0.79427995
SIPA1L2	0.38228146	-0.3323443	0.79424483
SLAIN1	0.18221473	-0.3324629	0.79417956
RNU6-672P	0.07476057	-0.3324663	0.79417767
FGFBP2	0.13198082	-0.3325216	0.79414722
ZNF19	0.10645101	-0.3325756	0.79411751
KCNK6	0.26300608	-0.3328526	0.79396505
GNL2	0.1634124	-0.3330919	0.79383334
VAMP1	0.11373208	-0.3332041	0.79377161
HLA-DRB6	0.30790647	-0.3332271	0.79375899
ZNF502	0.30467322	-0.3332458	0.79374869
EXD2	0.03459901	-0.3333966	0.7936657
SCARB2	0.23273354	-0.3334601	0.79363079
NTPCR	0.27189192	-0.3335303	0.79359218
KIZ	0.35779426	-0.3336275	0.79353871
CNOT8	0.2589306	-0.3336591	0.79352134
FADS3	0.40742886	-0.3337615	0.79346499
AC055839.1	0.09011165	-0.3339979	0.79333501
SRPRB	0.16985055	-0.3344401	0.79309189
ZNF419	0.11130248	-0.3344708	0.79307501
AC008969.1	0.17447487	-0.3344904	0.7930642

DENND4B	0.18820223	-0.3345028	0.79305743
AHSA2	0.22976181	-0.3347199	0.79293806
ZNF22	0.19215955	-0.3347979	0.79289521
MRPL58	-0.1311963	-0.3348266	0.79287944
TPCN1	-0.0438985	-0.3349261	0.79282476
NOD1	0.0472078	-0.3349618	0.79280511
ATP11C	0.32240851	-0.3351484	0.79270259
UQCRB	0.1120165	-0.3351577	0.79269749
TMEM245	0.19854747	-0.3352406	0.79265193
SRP14	0.28922339	-0.335361	0.79258581
FBXL3	0.2800616	-0.3353835	0.79257341
CNOT9	0.15350348	-0.3354758	0.79252272
ZNF644	0.4677847	-0.3354814	0.79251967
ANKDD1A	0.37457391	-0.3358153	0.79233624
CTBP2	0.23486141	-0.3358232	0.79233188
IDI1	0.09859391	-0.3360254	0.79222086
CUL1	0.26628938	-0.3360993	0.79218031
RRM1	0.36321264	-0.3362264	0.79211051
RRAS2	0.19986013	-0.3362279	0.7921097
SPRYD3	0.32616843	-0.3363488	0.79204329
MYBL1	-0.0732788	-0.3363941	0.79201843
BIRC2	0.29303274	-0.3368346	0.79177663
LAP3	0.21544205	-0.3368954	0.79174327
RIC8A	0.0670294	-0.3370916	0.79163561
RPL6	0.25722601	-0.3372437	0.79155214
ARHGAP27P1-BPTFP1-			
KPNA2P3	0.19077341	-0.3372466	0.79155053
BLOC1S6	0.13640719	-0.3372956	0.79152367
CEP68	0.2451738	-0.3373225	0.79150893
HGF	0.15747801	-0.3376827	0.79131134
KLHL22	0.1107453	-0.337832	0.79122942
PKD2	0.19081644	-0.3378922	0.79119644
MRPL57	0.09322167	-0.3379866	0.79114467
ATAD2	0.04807364	-0.3380586	0.79110519
ATP5J	0.33324261	-0.3381592	0.79105002
GABPB1	0.19115167	-0.3381926	0.7910317
ZNF330	0.32882987	-0.338394	0.79092126
LRRC57	-0.1400543	-0.3384212	0.79090634
ZNF283	0.23653668	-0.3384344	0.79089913
CNOT10	0.07135508	-0.33856	0.79083029

P2RX4	0.64711725	-0.3386162	0.79079949
AF131215.6	-0.018947	-0.3386481	0.79078196
RPS3A	0.161853	-0.3386983	0.79075449
CASC4	0.27465634	-0.3387913	0.7907035
RALA	0.25909037	-0.3388494	0.79067163
DCAF16	0.17580578	-0.3388671	0.79066197
BCCIP	0.25428047	-0.3389731	0.79060384
CACTIN	0.39395018	-0.338982	0.79059896
ANKRD6	0.22600088	-0.3390648	0.79055363
MRPL3	0.06137767	-0.3390785	0.79054609
ATG4D	0.38433812	-0.3391741	0.79049373
SGSM2	0.07366506	-0.3392651	0.79044387
IKZF2	0.28188731	-0.3392775	0.79043707
FLJ20021	0.14823332	-0.3392846	0.79043317
CCDC58	0.20960872	-0.3397623	0.79017148
TMEM116	0.04296602	-0.3398464	0.79012545
THBD	0.19178426	-0.339853	0.79012182
MED9	0.05007031	-0.3398768	0.79010879
UBL3	0.18591446	-0.3400681	0.79000404
EMG1	0.2474304	-0.3400727	0.79000152
C19orf25	0.12002893	-0.3401074	0.78998251
C11orf71	0.3128076	-0.3401903	0.78993713
NEK6	0.3443029	-0.340424	0.78980913
ARL16	0.08510724	-0.340466	0.78978615
SEC11C	0.4375899	-0.3406361	0.78969305
RGS6	0.05940188	-0.3406595	0.78968025
MBOAT2	0.12936018	-0.3406923	0.78966231
HSDL1	0.130519	-0.3407676	0.78962107
ABLIM1	0.24584768	-0.3411697	0.78940102
PRKACB	0.04512056	-0.3412047	0.7893819
ANKRD42	0.25770408	-0.3415625	0.78918615
SQLE	0.16603118	-0.3416902	0.7891163
GRAP2	0.09978591	-0.3416985	0.78911175
WDR12	-0.0034199	-0.3417385	0.78908985
ILF3-AS1	0.29146344	-0.3418205	0.789045
HIC2	0.31187496	-0.341829	0.78904037
ESF1	0.24308535	-0.3418872	0.78900851
RCOR3	0.18281238	-0.3418955	0.78900399
ATP5A1	0.22881056	-0.3419864	0.7889543
U62317.5	0.13563566	-0.342124	0.78887903

SNORA72	0.33181607	-0.3421459	0.78886708
DRAXIN	0.21699161	-0.3421856	0.78884534
CCDC12	0.15255939	-0.3422119	0.788831
MTX3	0.20133268	-0.3423188	0.78877252
TBC1D14	0.14822455	-0.3424298	0.78871183
ARF4	0.21436754	-0.3424596	0.78869556
TM2D1	0.26786627	-0.3424681	0.78869089
ZC2HC1A	0.1373946	-0.3426807	0.78857467
DNAJB9	0.22146497	-0.3429553	0.7884246
ZBTB11	0.37468125	-0.3430393	0.7883787
UHRF2	0.16748439	-0.343212	0.78828435
PKIA	0.27067202	-0.3432382	0.78827001
RBP7	0.19489769	-0.3432856	0.78824411
SLC12A7	0.28856959	-0.3433317	0.78821892
TMEM18	-0.0250585	-0.3433358	0.78821667
ANAPC13	0.15621233	-0.3435301	0.78811053
MAT2A	-0.1636468	-0.3436715	0.78803332
UBLCP1	0.22940748	-0.3440038	0.78785181
ABHD14A	0.10538232	-0.3442262	0.78773038
UTP3	0.17587103	-0.3443497	0.78766294
FAM89A	0.2526876	-0.3444027	0.78763398
SRSF6	0.15583454	-0.3444281	0.78762015
RBMXL1	0.22426433	-0.3445978	0.78752749
RAN	0.12689725	-0.3447059	0.78746847
SIGLEC1	0.29886606	-0.3448486	0.78739063
COMMD6	0.22824912	-0.3449305	0.7873459
MEI1	0.29069755	-0.3452949	0.78714705
BCL9	0.16241868	-0.3453584	0.78711242
TPCN2	0.30511293	-0.3454645	0.78705455
CD86	0.19676128	-0.3455323	0.78701756
AP1AR	0.02095163	-0.3455988	0.78698126
INPP5B	-0.0761182	-0.3457121	0.78691948
GBA2	0.30020832	-0.3457425	0.78690287
MYO18A	0.19214318	-0.3458389	0.78685032
AL683813.1	-0.0288312	-0.3458554	0.78684132
TMEM39B	0.56109051	-0.3461418	0.7866851
LPIN1	0.23679811	-0.3461798	0.7866644
PIK3C3	0.06271795	-0.3462589	0.78662129
SMAD5	0.16655368	-0.3462717	0.7866143
TMEM176A	0.16768004	-0.3464453	0.78651963

ZNF346	0.29797981	-0.346733	0.7863628
EXOSC9	0.09949655	-0.3468469	0.78630076
AP5M1	-0.0214985	-0.3468992	0.78627225
MIR1254-1	0.08830005	-0.3469381	0.78625104
RPS27	0.08468337	-0.3469389	0.78625057
ITLN1	0.19673662	-0.3470167	0.78620818
JTB	0.32258833	-0.3471014	0.78616202
ZBED6	0.44516815	-0.3471237	0.78614991
ZFAT	0.16855287	-0.3472581	0.78607667
MOSPD3	0.01220792	-0.3472935	0.78605738
CRTAP	0.11844523	-0.3474475	0.78597343
ANAPC15	0.2738532	-0.3475475	0.78591898
ITM2A	0.20304673	-0.3475883	0.78589673
GOT1	0.08073668	-0.3476028	0.78588886
MRFAP1	0.20795586	-0.3477813	0.78579164
CEP41	0.23935096	-0.3478321	0.78576394
NUP43	0.39286003	-0.3485426	0.78537708
INSL3	0.17436459	-0.3485526	0.78537165
EFCAB2	0.19792913	-0.34869	0.78529684
WBP1L	0.2166233	-0.3487369	0.78527133
IFITM3	0.31683204	-0.3488063	0.78523355
LINC01772	0.06292051	-0.3489089	0.78517769
SETDB1	0.31992443	-0.3489331	0.78516454
NEMP1	0.3515557	-0.3489664	0.78514639
ANKHD1	0.22564425	-0.3490065	0.78512457
LGALS12	-0.0786191	-0.349044	0.78510418
BX284668.5	0.1109656	-0.3491542	0.78504421
CRLF3	0.31952317	-0.3494017	0.78490956
GANAB	0.16823523	-0.3494278	0.78489531
C1orf43	0.15484822	-0.3495157	0.7848475
TRAF3IP2	0.33366514	-0.3495436	0.78483235
CLINT1	0.37383665	-0.3495821	0.78481138
AC006033.2	0.09393082	-0.3500973	0.78453116
MBTD1	0.07897398	-0.3501033	0.78452794
LRPPRC	0.07468417	-0.3504032	0.78436483
RNU6-890P	0.23771297	-0.3505301	0.78429588
HIST1H2BJ	0.06607229	-0.3506787	0.78421508
Metazoa_SRP	0.14519216	-0.3507517	0.78417538
WHAMMP2	0.15526622	-0.3508839	0.78410353
FUT8	0.07056013	-0.3508975	0.78409618

HPS4	0.28285787	-0.351063	0.78400622
NCOA2	0.37932495	-0.3513244	0.78386418
SLC40A1	0.21341577	-0.3514216	0.78381135
SGMS2	0.06447379	-0.3514896	0.78377444
RPS15A	0.08424962	-0.3515874	0.78372129
USP33	0.20421221	-0.3516283	0.78369907
SCO1	0.31558897	-0.3518066	0.7836022
ZNF845	0.32094454	-0.3518552	0.78357582
ZNF696	0.2346698	-0.3518901	0.7835569
GOT2	0.47765492	-0.3521293	0.78342699
STAT1	0.30346463	-0.3521399	0.78342124
AC008622.2	0.26669339	-0.3522585	0.78335683
HSF2	0.1761189	-0.3525152	0.78321744
DNAJC5	0.15737471	-0.3526945	0.78312012
SLC35B3	0.23390269	-0.3527534	0.78308814
CCDC115	0.23643034	-0.3532608	0.78281279
HNRNPA1	0.2791291	-0.3533259	0.78277743
TCEAL4	0.3218512	-0.3533292	0.78277566
TOGARAM2	0.13594563	-0.3533662	0.78275556
B9D2	0.31726447	-0.3534007	0.78273686
ZNF780A	0.26297856	-0.3538201	0.78250933
MS4A2	0.28715035	-0.3538365	0.78250043
ZNF331	0.46951747	-0.353955	0.78243617
BPI	-0.0452562	-0.3541384	0.78233675
ACAA2	0.28573873	-0.3541748	0.78231702
AC112496.1	0.06978677	-0.3542011	0.78230273
SUSD3	0.19799015	-0.3542471	0.78227781
CXorf38	0.25670439	-0.3542738	0.7822633
UGT8	0.16599427	-0.3543174	0.78223964
YIPF1	0.29873291	-0.3543791	0.78220623
ZNF219	0.21032255	-0.3545326	0.78212302
GOLGA5P1	0.0200973	-0.3546661	0.78205062
ASTE1	0.04839941	-0.3546848	0.78204048
RAD51C	0.3097138	-0.3549568	0.78189308
NUDT19	0.1900916	-0.3549733	0.7818841
STXBP3	0.08189229	-0.3550209	0.78185834
MAN2B2	0.27436936	-0.3550388	0.78184861
LINC01184	0.14644136	-0.3550536	0.7818406
PARN	0.14435266	-0.355118	0.78180571
AC105749.1	0.24233441	-0.3551463	0.78179034

DDHD1	0.18360797	-0.3551965	0.78176315
TCEA2	-0.071576	-0.3552157	0.78175275
CHAMP1	0.07666938	-0.3552491	0.78173463
B2M	0.24283509	-0.3553212	0.78169556
CEP85L	0.34068159	-0.3559306	0.78136545
DUSP12	0.08443966	-0.3559779	0.78133982
TNFRSF4	0.02651499	-0.3560562	0.78129745
ALG11	0.34708389	-0.3560578	0.78129659
AC127024.4	0.26899288	-0.3563392	0.78114419
IGFLR1	0.35364341	-0.3564293	0.78109541
TTC14	0.12925805	-0.3564755	0.78107039
AL118508.4	0.21170828	-0.3565001	0.78105706
ZNF518B	0.26063199	-0.3566025	0.78100164
RPS24	0.28047436	-0.3567899	0.78090022
AKAP8	0.07967071	-0.356827	0.78088013
KIFC3	0.25059992	-0.3570027	0.78078505
TMEM94	0.17338219	-0.357081	0.78074263
ZNF3	0.17625633	-0.3572596	0.78064603
AMMECR1	0.19085355	-0.3572817	0.78063407
MRPL20	0.09627774	-0.3572817	0.78063407
TMEM128	0.19710477	-0.3573144	0.78061637
CDK5R1	0.16406309	-0.3573809	0.78058037
GSTO1	0.23653791	-0.3573996	0.78057024
EPG5	0.28203035	-0.357458	0.78053866
IPCEF1	0.37221077	-0.3576454	0.78043729
Y_RNA	0.48285972	-0.3576684	0.78042485
RPS27A	0.20396224	-0.3577273	0.780393
ANO6	0.2525435	-0.3578845	0.78030797
COA4	0.15192994	-0.3579193	0.78028915
TASP1	0.33201937	-0.3580918	0.78019586
RPL26	0.18485621	-0.3581579	0.78016007
TRIM69	0.17075319	-0.3583635	0.78004892
RANGRF	0.22781872	-0.3583703	0.78004522
C1RL-AS1	0.39722371	-0.3587334	0.77984895
C11orf24	0.20725993	-0.3588363	0.77979329
SENP5	0.29367164	-0.3588436	0.77978936
IMPA1	0.25680316	-0.358949	0.77973242
CCR2	0.1786691	-0.3590256	0.779691
CTPS1	0.19711413	-0.3590468	0.77967953
SUMO2	0.33507518	-0.359374	0.77950275

TRAF4	0.12377104	-0.3594353	0.77946963
SEC61B	0.27879823	-0.3595064	0.77943122
MRPS35	0.33529188	-0.3595481	0.77940867
UQCRFS1	0.03832607	-0.359681	0.77933691
AC016394.1	0.22616761	-0.359704	0.77932445
TIGD3	0.1874398	-0.3597373	0.77930648
PEA15	0.27462489	-0.3598348	0.77925379
TMEM177	0.21092983	-0.3599055	0.77921561
AGFG2	0.11547653	-0.3599452	0.7791942
MATK	0.37057914	-0.3599616	0.77918535
SNHG14	0.33804621	-0.3603009	0.7790021
ALDH3A2	0.24479884	-0.3603115	0.77899636
BTN3A1	0.25326898	-0.360439	0.77892753
ALAS1	-0.040511	-0.3605458	0.77886984
PMM1	0.24972333	-0.3607533	0.77875787
ICOS	0.06209093	-0.3608495	0.77870595
PLAG1	0.1739656	-0.3610231	0.77861225
LMTK2	0.1317528	-0.3611049	0.77856807
PRKAG2-AS1	0.14213001	-0.3612353	0.77849771
KNTC1	0.34088483	-0.361245	0.77849249
TMEM147	0.09371171	-0.361347	0.77843744
SNRNP35	0.00385525	-0.361624	0.77828801
MADD	0.03040979	-0.3616767	0.77825956
GNGT2	0.23367046	-0.3617667	0.77821102
RAB18	0.37132919	-0.3618342	0.77817462
NDUFA4	0.00655677	-0.3619941	0.77808835
NSUN2	0.25936451	-0.3620872	0.77803816
TC2N	0.19308176	-0.3622092	0.77797239
PEX2	0.10564746	-0.3622809	0.77793369
SGPL1	0.25475036	-0.3623809	0.77787979
ZBTB37	0.28083824	-0.3624419	0.7778469
C14orf93	0.15848974	-0.362609	0.77775678
TTYH3	0.29284325	-0.3626166	0.77775271
ZNF101	0.20007002	-0.3626448	0.77773752
WDSUB1	0.18646914	-0.3628719	0.77761507
CSGALNACT2	0.27669604	-0.3629353	0.77758093
FKBP2	0.21490206	-0.3631173	0.77748284
METTL2B	0.31426504	-0.3633108	0.77737856
FMC1	0.01881289	-0.3633961	0.77733257
NBEAL1	0.36281524	-0.3634217	0.77731879

U2AF2	0.28973181	-0.3634455	0.77730597
PWWP2B	0.32778419	-0.3635605	0.77724402
RGL4	0.1213842	-0.3637108	0.77716303
SDHAF2	0.14257224	-0.3637149	0.77716082
HAUS2	0.19600157	-0.3638237	0.77710225
CISD2	0.57310361	-0.3638988	0.77706178
CWC27	0.05099297	-0.3639596	0.77702905
MTCO1P40	0.23101034	-0.3646491	0.77665776
EPB41L4A-AS1	0.03039151	-0.3648024	0.77657521
SRBD1	0.19142894	-0.3649508	0.77649534
SUZ12	0.19289769	-0.3651957	0.77636358
RBM3	0.25526552	-0.3656103	0.77614049
TNFRSF10D	0.23181046	-0.3656182	0.77613622
AC108673.3	0.35931742	-0.3656369	0.77612619
AC018445.4	0.22574922	-0.3656476	0.7761204
ZNF268	0.18699976	-0.365652	0.77611805
HSP90B1	0.15558753	-0.3656588	0.7761144
NUP88	0.41143505	-0.3660041	0.77592862
TMEM230	0.04557965	-0.3660356	0.77591169
AC116618.1	0.07710664	-0.3660964	0.77587903
TMEM251	0.25407271	-0.3663228	0.77575728
IER5L	0.21248014	-0.3663913	0.77572041
PRPF4B	0.15920808	-0.3665707	0.77562397
SUGP2	0.35419056	-0.3667191	0.77554419
RAB27B	-0.1241248	-0.3670836	0.77534828
STXBP5	0.23611277	-0.3671758	0.77529875
VAMP4	0.1035674	-0.3672211	0.7752744
MTG2	0.13036388	-0.3673125	0.77522529
KCNG1	0.15835503	-0.3673343	0.77521357
CD72	0.37735005	-0.3673731	0.77519273
KLHL3	0.05257509	-0.3674124	0.77517156
IFIT2	0.41964664	-0.3675434	0.77510119
ATP6V1H	0.55722064	-0.3675465	0.77509952
TMX3	0.04957039	-0.367705	0.77501441
NPTN	0.06747596	-0.3679804	0.77486648
TP53I11	0.31173995	-0.368457	0.77461052
UBL4A	0.03657624	-0.3685588	0.77455586
FBXO34	0.29862151	-0.3685723	0.77454863
MRPL40	0.30097862	-0.3686055	0.77453077
SLC25A20	0.33459783	-0.368623	0.77452142

NAGPA	0.26470952	-0.3688693	0.7743892
SLC11A2	0.31915056	-0.3691464	0.77424048
FHIT	0.20926688	-0.3693415	0.77413576
UHRF1BP1L	0.24193558	-0.3693563	0.77412782
PRR14L	0.28345209	-0.3693868	0.77411148
C14orf166	0.31071837	-0.3695619	0.77401752
YWHAG	0.25689305	-0.3695773	0.77400926
CD302	0.1546113	-0.3695885	0.77400324
TIMM23	-0.1390269	-0.3696717	0.77395863
UBASH3B	0.16873042	-0.3697153	0.77393522
F2RL1	0.33152819	-0.3699814	0.77379248
SECISBP2L	0.21635876	-0.3702227	0.77366307
IPMK	0.50238458	-0.3702753	0.77363486
ALDH1A1	0.25894966	-0.3704562	0.77353784
SLC39A9	0.14699644	-0.3705819	0.77347048
AC245060.5	0.27059852	-0.3706156	0.77345239
SEL1L3	0.18643982	-0.3706818	0.7734169
UFSP2	0.32740106	-0.3707355	0.77338812
ZNF687	0.18479799	-0.3714757	0.7729914
RAP1GDS1	0.25230534	-0.3714843	0.7729868
MMACHC	0.22626568	-0.3715749	0.77293826
SUMO3	0.1673368	-0.3717329	0.77285363
SPAG7	0.18643311	-0.3718376	0.77279755
THAP3	0.42630923	-0.3718476	0.77279216
AC009831.4	0.14801335	-0.3719223	0.77275215
TM9SF3	0.35726705	-0.3720308	0.77269405
TXN2	0.38272549	-0.3721406	0.77263527
ATAD5	0.43200651	-0.3723068	0.77254622
BISPR	0.40897945	-0.3724882	0.77244912
RIN2	0.2624528	-0.3725411	0.77242081
ZBTB18	0.24943242	-0.3726428	0.77236635
CEP97	0.1684057	-0.3727056	0.77233273
MYDGF	0.33535087	-0.3727863	0.77228954
RRP15	0.36232107	-0.3729154	0.7722204
ZMYND8	0.29215271	-0.3729909	0.77218003
LANCL1	-0.0132804	-0.3729976	0.77217641
PSEN2	0.19186163	-0.3730388	0.77215437
XRN1	0.22607126	-0.3732238	0.77205536
R3HDM1	0.31846457	-0.3734858	0.77191516
RDX	0.15504065	-0.3734871	0.77191447

KYNU	0.2306765	-0.373542	0.77188508
ZNF542P	-0.0026661	-0.3736064	0.77185064
CBX3	0.27513251	-0.3737059	0.7717974
AC027449.1	-0.0122331	-0.3737194	0.7717902
ADK	0.16212584	-0.3740119	0.77163371
TNFSF13B	0.16395077	-0.3743881	0.77143254
CKAP5	0.1890668	-0.3745987	0.77131992
RBFA	0.19835255	-0.3747029	0.77126423
ZNF75D	0.07818992	-0.3747495	0.77123931
TUBA1C	0.25509451	-0.3747711	0.77122776
BORCS6	0.49202717	-0.374781	0.77122248
ZNF439	0.40690535	-0.3748618	0.77117929
PIGH	0.42722404	-0.3748693	0.77117525
ICE2	0.16803989	-0.3749244	0.77114584
ADAT2	0.2621788	-0.3750152	0.77109731
PLAGL2	0.13010596	-0.3752149	0.77099058
TRAPPC2	0.33854239	-0.3752967	0.77094687
SLC35A3	0.30091072	-0.3754075	0.77088764
TTC1	0.20582806	-0.3754202	0.77088084
ZNF710	0.11249121	-0.3754616	0.77085874
CNTNAP2	0.38067704	-0.3758033	0.77067617
CSTB	0.21246466	-0.3758639	0.7706438
ECD	0.23113912	-0.3759693	0.77058753
MIOS	0.34706277	-0.3759696	0.77058735
GMPS	0.4350639	-0.3760503	0.77054425
TCF12	0.06156862	-0.37624	0.77044294
NAXD	0.07597032	-0.376278	0.77042266
AC055822.1	0.09677902	-0.3763259	0.77039709
C16orf74	0.21852659	-0.3764913	0.77030876
MRPS33	0.33592233	-0.3764991	0.77030457
DIMT1	0.08167075	-0.3768372	0.77012405
NRIP1	-0.0015505	-0.3769066	0.77008706
BACH1	0.14814687	-0.3769524	0.7700626
EXOC5	0.19084302	-0.3770677	0.77000104
GALNT3	0.28579555	-0.3771937	0.76993379
FAM175B	0.19106468	-0.3772661	0.76989518
CSTA	0.21755087	-0.3773387	0.76985641
CYTH3	0.39212707	-0.377509	0.76976552
ZNF808	0.42174627	-0.3778537	0.76958164
RBM45	-0.0043867	-0.3778865	0.76956416

SSFA2	0.47821528	-0.3780177	0.76949414
STT3B	0.41663988	-0.3780327	0.76948616
SARAF	0.3294216	-0.3781546	0.76942114
CPEB2	0.14845697	-0.3782306	0.76938061
NHLRC2	0.17810215	-0.37846	0.76925832
CAPZA1	0.20897707	-0.3784614	0.76925754
NUDT14	0.04164228	-0.3788322	0.76905987
TCF7L2	0.3115611	-0.3789754	0.76898354
ARPIN	0.12918804	-0.3792261	0.76884992
NAA35	0.08568969	-0.3792293	0.7688482
KCNJ2	0.22999587	-0.3793649	0.76877595
FAM118B	0.33576172	-0.3794458	0.76873282
TBC1D32	0.34386317	-0.3795211	0.76869273
ASF1B	0.05229844	-0.3795695	0.76866693
SLC25A40	0.26302047	-0.3795753	0.76866383
ZNF764	0.16250258	-0.3796435	0.76862748
FBRSL1	0.30920773	-0.3797863	0.7685514
GOLGA8B	0.29508894	-0.3798704	0.7685066
CMTR1	0.27402145	-0.3801356	0.76836537
SLC22A18	0.1806257	-0.3803802	0.76823512
KLHL42	0.20018282	-0.3806741	0.76807861
PPP2R5E	0.18744897	-0.3810553	0.7678757
EIF4A2	0.16373094	-0.3810573	0.76787461
FARSB	0.33838914	-0.3811493	0.76782567
MRPL36	0.56019545	-0.3812218	0.76778711
DDB2	0.15460964	-0.3812695	0.76776172
SSR3	0.16357874	-0.3814435	0.76766914
C4orf32	0.10789216	-0.3814528	0.76766414
ATXN7L1	0.18452198	-0.3815873	0.76759261
ECHDC2	-0.018716	-0.3816481	0.76756023
NDOR1	0.15338649	-0.3817269	0.76751832
ARRB1	0.17139912	-0.3818347	0.76746097
FAM114A2	0.14284246	-0.3824315	0.76714356
SLFN11	0.44191482	-0.3826509	0.76702693
NDUFC1	0.05972144	-0.3827184	0.76699105
CCDC186	0.12023483	-0.3827881	0.76695399
GIMAP7	0.15010394	-0.3828559	0.76691791
SMIM14	0.17031615	-0.3828951	0.76689707
MAGED1	0.27947802	-0.3829574	0.766864
ZNF45	0.14529005	-0.3831067	0.76678463

RPS6KB1	0.24918526	-0.3831899	0.76674041
RFX3-AS1	0.19957708	-0.3834353	0.76661001
IFFO1	0.15107686	-0.3836371	0.76650277
CCR5	-0.0432772	-0.3838949	0.76636583
PHKA2	0.21448712	-0.3840346	0.76629159
C8orf33	0.31570037	-0.3842957	0.76615294
DR1	0.23859858	-0.3844465	0.76607287
MOAP1	0.27265185	-0.3845132	0.76603746
AC007406.5	0.11977853	-0.3845706	0.76600694
MTMR12	0.15655132	-0.3846599	0.76595954
SLC46A3	0.19486932	-0.3850108	0.76577329
SLC43A1	0.26700724	-0.3851127	0.76571919
ENTPD4	0.38318509	-0.3852181	0.76566324
MR1	0.21635649	-0.3852203	0.76566209
DIAPH2	0.28748375	-0.3853011	0.76561918
GALC	0.33104042	-0.3853481	0.76559428
FAM208A	0.36932095	-0.3858294	0.76533888
CHCHD3	0.22443872	-0.3858841	0.76530988
SNPH	0.17256036	-0.3861422	0.76517298
EEF1B2	0.28795192	-0.3862943	0.76509231
PRR7-AS1	0.09817894	-0.3865074	0.76497928
GZMA	0.26015356	-0.3867605	0.76484512
PARP15	0.05749631	-0.3868087	0.76481953
RNMT	0.2122768	-0.3869423	0.76474871
SENP1	0.33777729	-0.3869696	0.76473428
NEK1	-0.1245734	-0.3873097	0.764554
ASPM	0.19118562	-0.3874955	0.76445551
TMEM192	-0.0018952	-0.3875059	0.76445001
TMEM135	0.19509636	-0.3876254	0.76438672
SLU7	0.25920361	-0.3877127	0.76434046
LTBP4	0.33634275	-0.3877694	0.76431042
DNAJB14	0.20810597	-0.3878259	0.76428048
WARS	0.241373	-0.3878437	0.76427107
EMSY	0.21912785	-0.3880242	0.76417545
FOXN2	0.15105246	-0.388101	0.76413474
RSBN1L	0.39752655	-0.3887591	0.76378628
SUGT1	0.09821055	-0.3888603	0.76373271
AL080317.3	0.2977868	-0.3889365	0.76369235
ZNRD1ASP	0.19072256	-0.389275	0.76351322
SS18L2	0.16741315	-0.3895852	0.76334905

CREG1	0.02078636	-0.3898247	0.76322233
CARHSP1	0.29899599	-0.390169	0.76304019
SFT2D1	0.47750488	-0.3903182	0.76296131
ZBTB40	0.11675432	-0.3905857	0.76281983
DCK	0.21677982	-0.3906398	0.76279125
ZNF326	0.23972104	-0.390813	0.76269968
DPM1	0.00229164	-0.3908457	0.76268238
SLF2	0.32225787	-0.3910216	0.76258941
FXYD6	0.35514966	-0.3912051	0.76249241
FOCAD	0.1954297	-0.3912078	0.76249102
TCN1	0.1253512	-0.3913035	0.76244042
CD244	-0.048677	-0.3913374	0.76242251
TMX2	0.42033235	-0.391598	0.7622848
OTUD1	0.27871256	-0.3917509	0.76220401
ACOT7	0.31459864	-0.3918035	0.76217623
CD47	0.2533716	-0.392038	0.76205237
SCAMP1-AS1	0.25680113	-0.392147	0.76199479
STRAP	0.11477929	-0.3922956	0.76191631
NBPF15	0.14149157	-0.3924124	0.76185463
LEO1	-0.0273387	-0.392691	0.76170748
FCER1A	0.41614968	-0.3927755	0.7616629
SAMD9	0.3168457	-0.3928907	0.76160205
SLC24A1	0.16285132	-0.392898	0.76159822
CDK17	0.17567493	-0.3931717	0.76145372
PIK3R6	-0.073684	-0.3932976	0.76138727
AC023157.3	0.0533058	-0.3935068	0.76127691
GPBP1	0.33679552	-0.393548	0.76125516
MCTP1	0.36428536	-0.3940564	0.76098695
CRYZL1	0.13274865	-0.3946177	0.76069091
EBAG9	0.25407071	-0.3950426	0.76046693
AMN1	0.23468878	-0.3952998	0.76033135
ZFAND6	0.29759687	-0.395572	0.76018791
RIN1	0.05292968	-0.3957499	0.76009418
CAPN7	0.23267734	-0.3962979	0.75980554
TTC12	0.19067404	-0.3963752	0.75976483
C6orf136	0.26050276	-0.3964023	0.75975054
EDRF1	0.28159298	-0.3964458	0.75972762
CNPY4	0.02872064	-0.3965003	0.75969892
POLI	-0.0617254	-0.3965687	0.75966292
FXN	0.16994334	-0.3966824	0.75960303

DUSP5	-0.0661783	-0.3967259	0.75958013
LRRFIP2	0.34966577	-0.3968296	0.75952556
ZSWIM8	0.15342764	-0.3970452	0.75941204
MAP4K5	0.1154905	-0.3970669	0.75940062
ZNF84	0.4904437	-0.39721	0.75932531
ANGPT1	0.23613438	-0.3972575	0.75930031
NDUFAF4	0.05931289	-0.3975871	0.75912686
PRPF38A	0.13955452	-0.3978252	0.75900161
SGF29	0.26131454	-0.3979748	0.7589229
TTC39C	0.45618577	-0.3980319	0.75889284
PCCB	-0.1401332	-0.398043	0.758887
TIMM8B	0.35751931	-0.3983637	0.75871834
ENSG00000188206	0.29010127	-0.3986082	0.75858976
ARL10	0.22942126	-0.3986148	0.7585863
RN7SL589P	0.32760807	-0.398672	0.75855623
GRWD1	-0.2449651	-0.3987572	0.75851142
SLC41A1	0.12143629	-0.3988106	0.75848335
ENSG00000283013	0.27610327	-0.3988108	0.75848324
CYCS	0.06089674	-0.3989379	0.75841643
ALG5	0.11347468	-0.3989381	0.75841633
GNS	0.22990055	-0.3989566	0.75840657
PRPF39	0.3184793	-0.3992472	0.75825385
ZNF275	0.12498478	-0.3993636	0.75819264
FPGS	0.33346528	-0.3994619	0.75814098
MAPK8IP3	0.30460806	-0.3996677	0.75803287
OSTM1	0.31658507	-0.4001449	0.75778216
TMEM216	0.39482416	-0.4002258	0.75773969
COPS6	0.39592955	-0.4003976	0.75764945
RAB3GAP2	0.22709905	-0.4006369	0.75752381
TRMT61B	0.32532561	-0.4006462	0.75751889
CD164	0.28163667	-0.4007145	0.75748305
NCBP2-AS2	0.13419628	-0.4008964	0.75738753
ZNF675	-0.0151319	-0.4010243	0.75732039
CFAP97	0.12571809	-0.4014757	0.75708347
SNX16	0.24281927	-0.4018126	0.75690669
MGST2	0.09577909	-0.4020832	0.75676478
ZNF280D	0.36163729	-0.4025758	0.75650643
ZC3H8	0.24615256	-0.4025862	0.75650095
CEP290	0.42427052	-0.40291	0.75633118
ITPR3	0.32560516	-0.4031042	0.75622936

ERCC3	0.25691381	-0.4032179	0.75616979
KBTBD11	0.2188689	-0.4032981	0.75612773
ZNF566	0.37150474	-0.4037155	0.75590903
ZKSCAN4	0.07429404	-0.4037629	0.7558842
SLC17A5	0.30329088	-0.4040614	0.75572778
CXCR3	0.27844845	-0.4043842	0.75555874
PTAR1	0.37051376	-0.4046519	0.75541854
PPARGC1B	0.35330915	-0.4050585	0.75520568
RTN1	0.31609141	-0.4051595	0.75515281
SNX4	0.20340114	-0.4052729	0.75509344
LINC02019	0.40405366	-0.4053747	0.75504018
RECQL	0.21628019	-0.4054602	0.75499542
MICB	0.16333539	-0.4055577	0.75494441
BCAS3	0.57341153	-0.4056842	0.75487822
MAP9	0.29919633	-0.4057127	0.75486331
RRP9	0.19577245	-0.4057215	0.75485871
MAP3K13	0.13390884	-0.4057791	0.75482857
TMIGD2	0.25164412	-0.4061425	0.75463842
SLC25A19	0.21434746	-0.4063195	0.75454586
AC006141.1	0.44487304	-0.4063441	0.75453302
VBP1	0.13475456	-0.406351	0.75452938
CD3G	0.28662588	-0.4066159	0.75439086
NUP155	0.40716217	-0.4066218	0.75438777
LILRA5	-0.0130547	-0.4066828	0.7543559
CCDC43	0.43184613	-0.4071074	0.75413392
TIA1	0.32010901	-0.40732	0.75402279
PSME2	0.22902838	-0.4074023	0.75397975
FAM105A	0.26224378	-0.4076184	0.75386686
GIN1	0.18101578	-0.4077573	0.75379425
ZBTB21	0.16075035	-0.4078235	0.75375965
HAT1	0.31318941	-0.4079052	0.75371697
TCEANC2	0.30567881	-0.407912	0.75371343
CHORDC1	0.10135283	-0.408098	0.75361625
SLC20A2	0.1820282	-0.4086017	0.75335317
AKAP11	0.05770778	-0.4087426	0.75327962
TRAF6	-0.1168812	-0.4089192	0.75318743
TMEM87B	0.13209469	-0.4090198	0.75313487
PAM	0.37196029	-0.4090777	0.75310467
SLC25A30	0.18650516	-0.4091601	0.75306165
UGDH	0.0870543	-0.4094965	0.7528861

Z93930.2	0.14955409	-0.4095447	0.75286096
RPL31	0.17842717	-0.4096568	0.75280245
KDM1B	0.26989667	-0.4098351	0.75270942
NFE2L3	0.18050246	-0.4099432	0.752653
CISD3	0.16794142	-0.4101512	0.75254452
ADO	0.32399677	-0.4101552	0.75254243
SLC33A1	0.17302929	-0.4104212	0.75240369
MIER3	0.23098812	-0.4105896	0.75231588
AC083798.2	0.27974385	-0.410624	0.75229789
PPIL3	0.05722602	-0.4106327	0.75229338
RAB29	0.34745807	-0.4106634	0.7522774
NELFA	0.23288667	-0.4107692	0.75222222
TPD52	9.37E-04	-0.410911	0.75214825
COQ2	0.13474723	-0.4115988	0.75178976
LGALS9	0.18158074	-0.4117638	0.7517038
CPD	0.27377987	-0.4118402	0.75166401
SNORD89	0.16309728	-0.412059	0.75154999
CROCC	0.18117268	-0.4121361	0.75150984
AC004865.2	0.13076091	-0.4121721	0.75149107
PARP9	0.28673085	-0.4123943	0.75137534
PYROXD1	0.22688599	-0.4125808	0.75127825
AC012467.2	0.0799176	-0.4127325	0.75119926
FBXO4	0.41620951	-0.4128739	0.7511256
RB1CC1	0.31678953	-0.4129236	0.75109972
MRPS18C	0.33746252	-0.4129441	0.75108906
STARD4	0.08570406	-0.4129729	0.75107409
PTCD2	0.4326092	-0.4131216	0.75099668
HEG1	0.27452881	-0.4132721	0.75091832
MRPL51	0.10879071	-0.4136915	0.75070007
RXRB	0.25196223	-0.4137827	0.7506526
YIPF3	0.38215303	-0.4138668	0.75060884
ECT2	0.26183833	-0.4138967	0.75059331
BRCA1	0.21593629	-0.4139453	0.75056798
MCRS1	0.22888646	-0.4142357	0.75041693
SNRPG	0.01337633	-0.4144217	0.7503202
ZNF420	0.25466641	-0.4147662	0.75014104
44621	0.31391588	-0.4147687	0.75013973
CLDND1	0.2277806	-0.4150225	0.75000781
C1orf27	0.25399461	-0.4150434	0.74999693
NHS	0.29062678	-0.4150703	0.74998297

METTL26	0.59075883	-0.4151774	0.74992729
AC006504.1	0.1642084	-0.4153345	0.74984562
AC009120.1	0.51942661	-0.4153357	0.74984498
TSEN2	0.03677919	-0.4154116	0.74980555
XPO4	0.40107135	-0.4155591	0.74972891
TOR1B	0.07007701	-0.4156092	0.74970284
CNOT7	0.12797425	-0.4158455	0.74958009
GBP3	0.26507309	-0.4162193	0.74938586
KDM6A	-0.1633649	-0.4163112	0.74933813
ARHGAP5	0.20260714	-0.4165837	0.74919663
PRSS23	0.2222114	-0.4165951	0.74919069
RAB10	0.28203701	-0.4166645	0.74915465
NUP85	0.27630214	-0.4168596	0.74905334
VMA21	0.21587751	-0.4170131	0.74897365
HLA-DRA	0.25492902	-0.4170293	0.74896528
TMEM9B	0.13318147	-0.4173422	0.74880285
ARID1B	0.15160799	-0.4176077	0.74866505
ADAM28	0.1238952	-0.4179669	0.74847866
EPSTI1	0.24034791	-0.4180326	0.74844457
CGGBP1	0.1782828	-0.4181423	0.74838765
MRI1	0.20180063	-0.4181632	0.74837684
ESCO1	-0.0420416	-0.4182607	0.74832627
MRPL9	0.35886445	-0.4183654	0.74827193
AP1G1	0.4390786	-0.4183862	0.74826118
SNRPB2	0.20546381	-0.4185722	0.74816468
PRICKLE1	0.3752908	-0.4189554	0.747966
PLEKHG2	0.43209607	-0.4192265	0.74782546
VPS50	0.00393719	-0.419258	0.74780914
FAM96A	0.22185901	-0.419291	0.74779203
AC007191.1	0.16991324	-0.4194373	0.74771619
SASS6	0.16634699	-0.4206721	0.74707649
UBOX5	0.19126772	-0.420759	0.74703149
METTL2A	0.35794958	-0.4208641	0.74697709
GMPR2	0.30652242	-0.4212703	0.74676682
LTN1	0.30501585	-0.4213254	0.74673826
ADH5	0.19788041	-0.4213999	0.74669971
COMMD4	0.18795807	-0.4219215	0.74642982
CSNK1E	0.51992924	-0.4222302	0.74627013
IPO8	0.23109686	-0.4223223	0.74622248
TRGC1	0.37782228	-0.4223926	0.7461861

AHCY	0.36993154	-0.4228304	0.74595969
GPR27	0.55133497	-0.4228727	0.74593785
SPATS2L	0.18228943	-0.4228982	0.74592465
AL021368.3	0.18835012	-0.4232716	0.74573159
SRD5A3	0.27179054	-0.4233158	0.74570877
PDCL	0.09729367	-0.4233553	0.74568837
TRIM68	0.11056464	-0.4235782	0.74557317
Y_RNA	0.50036187	-0.4236585	0.74553162
XRCC4	0.24544024	-0.4238145	0.74545102
SNRPD1	-0.0479431	-0.4242304	0.74523619
KCTD12	0.24237909	-0.4249836	0.74484719
CSAD	0.21694497	-0.4250373	0.74481945
NLRX1	0.34699673	-0.4251221	0.74477567
PRPF19	0.19343354	-0.4251265	0.74477344
CHP1	0.31822927	-0.4251387	0.74476713
CCDC112	0.44795104	-0.4252457	0.74471189
ELMO2	0.33281769	-0.4254218	0.744621
FXR1	0.31181003	-0.4254663	0.74459803
ZNF526	0.34776416	-0.425728	0.74446295
ZBTB41	0.19349992	-0.4259295	0.74435899
ZNF480	0.10210759	-0.4259423	0.74435242
SERPING1	0.31923605	-0.4259448	0.7443511
TRIM4	0.0265374	-0.4267119	0.74395544
RBM4B	0.45286121	-0.4267872	0.74391659
ACSM3	0.17752795	-0.4269034	0.74385668
ZCCHC4	0.24502761	-0.4273735	0.74361434
GRB10	0.21039725	-0.4274393	0.74358041
ZNF831	0.45961044	-0.4276371	0.74347847
LNPK	0.34571853	-0.4280745	0.74325312
HMGXB3	-0.0711334	-0.4282249	0.74317563
TUBG1	-0.0063638	-0.4283915	0.74308983
E2F6	0.22682402	-0.428527	0.74302004
NOP9	0.18599215	-0.4286797	0.74294139
DTD1	0.20525932	-0.4290347	0.74275858
NEK9	0.41583896	-0.429211	0.74266782
HIBADH	0.15495998	-0.4293517	0.74259541
NOLC1	0.38070191	-0.4296898	0.74242138
NINJ2	0.24688947	-0.4298022	0.74236357
AP4E1	0.00856148	-0.4298235	0.7423526
CCAR2	0.46521707	-0.4299398	0.74229274

AC004893.2	0.58733054	-0.4302345	0.74214114
HKR1	0.62043131	-0.4303722	0.74207033
RALGPS1	0.2048356	-0.4304375	0.74203675
MALSU1	0.188717	-0.4308694	0.74181462
ZNF600	0.41588882	-0.4312205	0.74163411
C5orf22	0.30159026	-0.431667	0.7414046
PPP4R3B	0.04345268	-0.4317898	0.74134154
XPA	0.01399719	-0.4318958	0.74128706
OARD1	0.49363257	-0.4319107	0.74127937
MT-TV	-0.1093021	-0.4321037	0.74118022
NAA15	0.326826	-0.432592	0.74092939
UGGT2	0.23249959	-0.4329227	0.74075961
IFT88	0.0945475	-0.4330395	0.74069962
TOMM20	0.27131291	-0.4331008	0.74066813
DDX59	0.15170751	-0.4331856	0.74062463
C11orf1	0.12909392	-0.4333006	0.74056557
AP003168.2	0.27281797	-0.4334212	0.74050369
NUP50-AS1	0.24355164	-0.4334433	0.74049235
UTP6	0.27272944	-0.4339307	0.74024223
RN7SL32P	0.42106699	-0.4339812	0.74021628
ATG101	0.20306544	-0.4343571	0.74002347
CNEP1R1	0.25517036	-0.4343875	0.74000784
NFKBIB	-0.016409	-0.4344336	0.73998422
NUPL2	0.3097442	-0.4350042	0.73969162
ANXA1	0.27748853	-0.435042	0.73967221
PAAF1	0.44784441	-0.4351394	0.73962227
WDFY1	0.43337119	-0.4352115	0.73958533
LRRC42	0.18191664	-0.4352925	0.73954378
GRAP	0.18290231	-0.4355745	0.73939926
SNX2	0.22626842	-0.4356013	0.73938554
SLC41A3	0.49204927	-0.4358389	0.73926377
ZNF140	0.18128831	-0.4359289	0.73921763
DUS4L	0.2971357	-0.4363025	0.73902623
CENPBD1	0.3671078	-0.4364493	0.73895104
MYL5	0.11325799	-0.4368445	0.73874865
AL390728.4	0.38733843	-0.4374057	0.73846132
UBA3	0.29451685	-0.4375989	0.73836243
EIF2D	0.16076385	-0.4376937	0.73831395
NABP2	-0.1343687	-0.4377296	0.73829558
ITPR1	0.36786296	-0.4377432	0.73828861

SLC39A3	-0.1465408	-0.4378631	0.73822727
SSX2IP	0.1057979	-0.4384573	0.73792324
EMC4	0.35783248	-0.4387226	0.73778758
HMGB2	0.19085077	-0.4393146	0.73748491
SRP9	0.27841821	-0.4393523	0.73746561
CRELD1	0.17473338	-0.4393575	0.73746298
APOL6	0.31455745	-0.4394865	0.73739703
SLC25A17	0.19387159	-0.4395122	0.73738387
DCPS	0.30333337	-0.4396539	0.73731149
UTP23	0.0600036	-0.4399	0.73718573
MIR320D1	0.23752292	-0.4399344	0.73716812
LMO7	0.18835961	-0.4399375	0.73716656
AL035071.1	0.20115654	-0.4399912	0.73713913
ZNF638	0.41240655	-0.4399961	0.73713663
SAMSN1	0.25981004	-0.4400297	0.73711944
FAM109A	0.18408959	-0.4401797	0.73704281
CCL4	0.3083286	-0.4402747	0.73699426
STXBP4	0.02260167	-0.4404769	0.73689099
SP4	0.21549562	-0.4407453	0.73675389
METAP1	0.31934219	-0.4408156	0.73671799
ZNF623	0.54348167	-0.4410159	0.73661573
NAXE	0.53534733	-0.4410442	0.73660125
CKB	0.19880999	-0.4415167	0.73636007
ZNF519	0.09954123	-0.441984	0.73612158
STAG3L5P-PVRIG2P-PILRB	0.27210251	-0.4419935	0.73611677
NDUFB1	0.27676247	-0.4423233	0.73594849
KRIT1	0.55897706	-0.4426638	0.73577483
OSTC	0.23200566	-0.442873	0.73566811
C5orf56	0.23761366	-0.4429748	0.73561623
C1orf109	0.19573949	-0.4429854	0.73561084
AC073869.1	0.30605084	-0.4430163	0.73559506
BEX3	0.38046128	-0.4431687	0.73551736
RPL41	0.17697356	-0.4433129	0.73544385
DEGS1	0.09026962	-0.4433884	0.73540538
TMEM150A	-0.1782082	-0.4435525	0.73532174
C18orf32	0.10810211	-0.443709	0.73524197
ISCA2	-0.0213302	-0.4437629	0.73521448
CWF19L1	0.50739179	-0.4438627	0.73516365
ARFGAP3	0.26489159	-0.444092	0.73504679
AC018628.1	0.12981299	-0.4447969	0.73468774

SGK494	0.14489019	-0.4448556	0.73465784
UNKL	0.12316868	-0.4450564	0.73455558
SMARCD3	0.03503493	-0.4456162	0.73427063
FMN1	0.11283446	-0.4457279	0.7342138
DTWD1	0.03992111	-0.4459457	0.73410297
PPCS	0.28358499	-0.4461176	0.73401549
GPR18	0.22329951	-0.4461849	0.73398126
PRIMPOL	0.23156364	-0.4465028	0.73381952
BNIP3	0.09377927	-0.4470149	0.73355909
RRNAD1	0.01955797	-0.4470973	0.7335172
ENSG00000271997	0.43259582	-0.4472585	0.73343526
AL158212.3	0.24029918	-0.4472747	0.73342701
FAM111A	0.26217516	-0.4473727	0.73337719
NDUFAF8	0.29683144	-0.4476759	0.73322309
FAM129B	0.20873869	-0.4477951	0.73316248
RTL8A	0.19340302	-0.4478917	0.73311343
COQ10B	0.02369316	-0.4486657	0.73272021
CD300C	0.20312285	-0.4488393	0.73263202
TMEM50B	0.14696442	-0.4489432	0.7325793
SEC11A	0.43106266	-0.4489562	0.7325727
SLF1	0.26366636	-0.4490608	0.73251957
KIAA1143	0.18843309	-0.4495188	0.73228706
ZC3HC1	0.25584326	-0.4496897	0.73220034
PTP4A1	0.1801324	-0.4497046	0.73219277
IQCG	0.04163051	-0.4497136	0.73218818
C11orf58	0.27333244	-0.4498179	0.73213524
AC027020.2	-0.0449452	-0.450485	0.7317968
ZNF200	0.0800228	-0.4508051	0.73163447
FASTKD2	0.50899709	-0.4512053	0.73143154
LCORL	0.17976349	-0.4514409	0.73131208
KIF5C	0.13685791	-0.4515327	0.73126555
TEX10	0.27634735	-0.4517569	0.73115194
PPP3CC	0.21150238	-0.4522874	0.73088313
RAB11B-AS1	0.04335586	-0.4528691	0.73058849
RNF8	0.26694583	-0.4529962	0.73052412
SMC4	0.26300106	-0.4535327	0.73025248
SUMF2	0.24382745	-0.4535947	0.73022111
MED10	0.56822121	-0.4537608	0.73013706
CMC2	0.16900824	-0.4540412	0.72999517
CTDSPL	0.12182942	-0.4544983	0.72976389

CASP3	0.22693385	-0.4545758	0.72972468
ATP5O	0.12880127	-0.4551771	0.72942062
TMEM238	0.2063181	-0.4552297	0.72939405
AC008764.10	0.25288026	-0.4557252	0.72914358
FCRL3	0.31975892	-0.4557737	0.72911906
KCTD5	0.21972804	-0.4561928	0.72890728
TENM1	0.16404083	-0.456234	0.72888645
TMEM56	0.06756473	-0.4563213	0.72884236
MED19	0.35773654	-0.4567013	0.72865039
SLC25A32	0.46852885	-0.456785	0.72860815
POM121	0.34640899	-0.4568426	0.72857904
RCHY1	0.22151803	-0.4569866	0.72850632
SLC39A13	0.41997941	-0.4575264	0.72823378
ATL3	-0.0609238	-0.4576764	0.7281581
MFSD5	0.16394523	-0.4579781	0.72800584
MAD2L2	0.27400055	-0.45806	0.72796451
PDCD10	0.27019693	-0.4583291	0.72782872
RAP2B	0.05089878	-0.4584118	0.72778703
PATL2	0.26502384	-0.4587677	0.7276075
CCND2	0.24992529	-0.459431	0.72727305
LRRC75A	0.33576194	-0.4595243	0.72722601
B3GNTL1	0.13108871	-0.4606069	0.72668048
ERO1B	0.25703133	-0.4611209	0.72642166
RNF6	0.31373685	-0.4612796	0.72634174
AC136475.9	0.19821774	-0.4613368	0.72631296
KATNB1	0.07132421	-0.4615146	0.72622343
MANBAL	-0.006695	-0.4616249	0.72616794
NFX1	0.49576308	-0.4617582	0.72610084
DCP2	0.32196695	-0.4618118	0.72607384
CD59	0.25031023	-0.4618211	0.72606919
BLOC1S2	-0.1176534	-0.461869	0.72604506
NDUFS5	0.47686557	-0.4619293	0.7260147
DDOST	0.25515345	-0.4620169	0.72597062
ZNF384	0.24700896	-0.4621055	0.72592603
ALDH6A1	0.2707458	-0.4622033	0.72587684
MPP5	0.2849041	-0.4625	0.72572757
FAM169A	0.27717948	-0.4625493	0.72570277
PQLC3	0.22793868	-0.4629194	0.72551664
HKDC1	0.26918577	-0.4629792	0.72548657
KAT14	0.25931343	-0.46299	0.72548116

NFKBIL1	0.32847483	-0.4630631	0.72544438
RANBP9	0.30224636	-0.4632123	0.72536934
NAA20	0.1197608	-0.4632621	0.72534432
PDE4DIP	0.3061694	-0.4634365	0.72525662
TAF1C	0.18191752	-0.4641628	0.72489163
PTPN2	0.21660584	-0.4643749	0.72478507
AC073957.3	0.30504112	-0.4644444	0.72475014
REEP4	0.29770531	-0.4646143	0.72466481
ACAD8	0.04132302	-0.4656184	0.72416059
FAM162A	0.25074311	-0.465944	0.72399719
FGD2	0.38051654	-0.4659999	0.72396911
IFT80	0.36854821	-0.4660309	0.72395357
AK3	0.4136225	-0.4660686	0.72393466
AC117382.1	0.13625774	-0.4662058	0.7238658
OGFOD3	0.41211923	-0.4667281	0.7236038
RAD1	0.18416123	-0.4667806	0.72357747
NDUFA5	0.13541567	-0.4669498	0.72349262
FUOM	0.1744848	-0.4669815	0.72347675
TRIM22	0.23634823	-0.4669963	0.7234693
PTRHD1	-0.1020098	-0.4671548	0.7233898
NR6A1	0.22443343	-0.4672616	0.72333627
GPR65	0.38199208	-0.4675632	0.72318506
RHOU	0.13730135	-0.467631	0.7231511
VRK2	0.34419709	-0.467648	0.72314257
LNX2	0.36849159	-0.4677757	0.72307856
SLC27A1	0.52843506	-0.4681421	0.72289494
MAP3K7	0.27050636	-0.4682585	0.72283663
NIPSNAP2	0.30905982	-0.4682881	0.72282179
WDR18	0.46922596	-0.4687105	0.72261019
SCRN1	0.10799368	-0.4687677	0.72258154
CIAPIN1	0.41326626	-0.4690493	0.72244049
SUFU	0.45216825	-0.469531	0.72219933
SLC25A25-AS1	0.2314522	-0.4695686	0.72218053
SKA2	0.31728169	-0.469692	0.72211872
SCIMP	0.28824579	-0.4698532	0.72203808
BEX2	0.23572195	-0.4701538	0.72188762
AC138409.2	0.04623071	-0.4702741	0.72182742
REV1	0.47364026	-0.4705202	0.72170432
COMMD9	0.13116832	-0.470944	0.72149237
CNIH1	0.33133924	-0.4711421	0.72139329

ZNF761	0.3103	-0.471305	0.72131182
KBTBD3	0.26234166	-0.471309	0.72130984
PAICS	0.23635216	-0.4714046	0.72126204
PFDN5	0.12517472	-0.4721652	0.72088189
FAM210A	0.10713171	-0.4722964	0.72081632
MYCL	0.27250248	-0.4723415	0.72079378
IKZF4	0.47752663	-0.472739	0.72059523
FAM3C	0.12003152	-0.4728465	0.72054154
CYP4V2	0.22632343	-0.4731256	0.72040216
MRPL22	0.18217746	-0.4736961	0.72011731
MIER2	0.30737344	-0.4737035	0.72011363
DCAF4	0.16693087	-0.4738207	0.72005513
LATS2	0.36569634	-0.4744224	0.71975491
ZNF706	0.21468989	-0.4749776	0.71947796
SRC	0.0048908	-0.4751136	0.71941014
ANAPC4	0.16327228	-0.4754366	0.71924912
USP30	0.21205578	-0.4756491	0.71914318
CLK2	0.31339442	-0.4758283	0.71905384
CTSH	0.39811845	-0.4761006	0.71891816
CROCCP3	0.23195301	-0.476332	0.71880285
TRMT10C	-0.0203989	-0.4770425	0.71844891
PLCB3	-0.0576885	-0.4773856	0.7182781
AC131009.4	-0.0705998	-0.4775222	0.71821006
ZNF720	0.28154491	-0.4779691	0.71798762
CUTC	0.13059801	-0.4780476	0.71794856
CCNK	0.24372544	-0.4781045	0.71792025
MIF4GD	0.25326895	-0.4788174	0.71756558
PGAM5	0.25457317	-0.4791732	0.71738866
KLRC1	0.27337779	-0.4791904	0.7173801
ZNF252P	0.09192304	-0.4796734	0.71713997
TMEM106C	0.27085045	-0.4797207	0.71711645
IKBIP	0.11849893	-0.4800045	0.71697537
ZNF264	0.16510241	-0.4801746	0.71689084
MAP3K12	0.33796796	-0.4804243	0.71676679
ZXDC	0.33692633	-0.4804926	0.71673288
DNAAF5	0.15664465	-0.4815823	0.71619171
CXorf21	0.311953	-0.4824997	0.71573643
EZH2	0.19274783	-0.4825188	0.71572694
AC079630.1	0.1655604	-0.4834496	0.71526535
AC090948.1	0.27414189	-0.4834812	0.71524964

FAM76A	0.30287668	-0.4836453	0.7151683
FANCD2	0.17463318	-0.4836891	0.71514659
RPL23	0.27927256	-0.4838331	0.7150752
PLA2G6	0.12365616	-0.4838658	0.71505901
PKD1	0.30379667	-0.4843178	0.71483502
ATP1B1	0.35920712	-0.4845066	0.71474147
LINC00869	0.40592628	-0.4857498	0.71412583
FLAD1	0.11928346	-0.485839	0.71408169
DCTPP1	0.22681231	-0.4862594	0.71387361
IFI44	0.2956611	-0.4865564	0.71372666
EPHA4	0.43000921	-0.4867794	0.71361635
HIST1H2BC	0.0729906	-0.4869475	0.71353324
YAF2	0.30069476	-0.4870087	0.71350295
SCLT1	0.22832532	-0.48702	0.71349736
NIPA2	0.2073633	-0.4871887	0.71341391
EXOSC3	0.27083485	-0.4872318	0.71339262
MRPL34	-0.0933727	-0.4874162	0.71330145
NKAP	0.32026515	-0.4882709	0.71287899
AP003486.2	0.0113402	-0.4885484	0.71274189
SMCO4	0.37916519	-0.4886427	0.7126953
UBE2D4	0.41286655	-0.4887843	0.71262535
DCUN1D1	0.10940058	-0.4894481	0.71229755
PARP8	0.26255714	-0.4896751	0.71218547
MAPK8	0.35212246	-0.4899512	0.71204919
RAD18	0.03198495	-0.4900762	0.71198748
MARCO	0.10504734	-0.4901777	0.71193743
HEXDC	0.36913225	-0.4905125	0.71177222
SMYD2	0.3615202	-0.4906529	0.71170296
API5	0.24898672	-0.4910914	0.71148665
FBXO46	0.30380171	-0.4913743	0.71134715
UBFD1	-0.0746536	-0.4914606	0.71130462
POLA2	0.36737666	-0.4915931	0.71123926
SF3B6	0.47690701	-0.4921732	0.71095334
STAT2	0.32716329	-0.492216	0.71093227
SRP54	0.11376053	-0.492256	0.71091257
ANXA3	0.341318	-0.4922797	0.71090087
ACVR1B	0.71308821	-0.4928369	0.71062638
COPS7A	0.25201662	-0.4931016	0.71049597
ZNRF2	0.2419997	-0.4931401	0.71047701
ILF2	0.31197691	-0.4932648	0.71041564

LRRK1	0.37801502	-0.4934014	0.71034837
PABPC1P3	0.28370802	-0.4934929	0.7103033
KCMF1	0.26328608	-0.4936122	0.71024455
NCDN	0.2376791	-0.4938482	0.71012839
REEP3	0.41503554	-0.4939274	0.71008941
INSIG2	-0.0120828	-0.4939571	0.71007481
YIF1A	0.38738079	-0.4939875	0.71005984
MUS81	0.26083188	-0.4940477	0.7100302
AC027097.1	0.25178175	-0.4941163	0.70999645
APOL1	0.27831503	-0.4947905	0.70966475
SUN1	0.23358508	-0.4950832	0.70952075
SZT2	0.24907752	-0.4952915	0.70941834
PMVK	0.33688849	-0.4953404	0.70939428
HPF1	-0.0020332	-0.4953467	0.70939119
RNF4	0.20485729	-0.4955043	0.70931371
RBM19	0.07477179	-0.4957539	0.709191
CLCN7	0.08822398	-0.4957605	0.70918772
BRIX1	0.29748582	-0.4963421	0.70890191
ANKZF1	0.15321837	-0.4964162	0.70886548
PGM1	0.29725544	-0.4964969	0.70882586
ZC3H10	0.41685889	-0.4965859	0.7087821
PAOX	0.3239905	-0.4966577	0.70874685
YPEL2	0.14498665	-0.496688	0.70873194
HIST1H2BD	0.22034284	-0.4970684	0.70854508
PDCL3	0.27816175	-0.4973424	0.70841056
DUSP23	0.14490495	-0.4981307	0.70802356
AL079342.1	0.31453782	-0.4981753	0.70800167
AC064805.1	0.15679553	-0.4981803	0.70799924
RRAS	0.48527442	-0.4982466	0.70796667
TUBB6	0.30704152	-0.4986678	0.70776001
FAM189B	0.36598804	-0.4988264	0.70768224
GBP1	0.30909687	-0.4991747	0.70751141
POLR3C	0.1106285	-0.4993937	0.707404
APEX1	0.32948442	-0.499537	0.70733377
NOM1	0.26496549	-0.4996772	0.70726503
FAM13B	0.20143445	-0.4997242	0.70724196
AGK	0.30168435	-0.5003358	0.70694224
FBXO3	0.33787454	-0.500526	0.70684903
SERINC1	0.36484354	-0.5009466	0.70664298
PCSK5	0.23227621	-0.5012839	0.70647779

HLA-F-AS1	0.34185198	-0.5016486	0.70629921
ERH	0.41244631	-0.5024452	0.70590933
C21orf58	0.1269842	-0.5024553	0.70590439
EIF4E	0.47047711	-0.5026444	0.70581188
IL2RB	0.44940525	-0.5028177	0.70572708
EIF3E	0.35616985	-0.5029492	0.70566277
RABL2B	0.14263806	-0.5029674	0.70565386
NXT1	0.44047595	-0.5038898	0.70520283
HCAR3	0.13164043	-0.5039464	0.70517519
ATP1B3	0.18424155	-0.503949	0.70517391
AC048341.2	0.47958877	-0.5046069	0.70485241
CCDC174	0.32934011	-0.5047704	0.70477255
C15orf57	0.39921614	-0.5048233	0.70474671
MED30	0.11054003	-0.5049237	0.70469767
NAA16	-0.0846635	-0.5051541	0.70458513
ZNF783	0.22619824	-0.5053471	0.70449085
HEXB	0.40601618	-0.5053889	0.70447047
RFXAP	0.29067375	-0.5059656	0.70418889
C12orf43	0.26719763	-0.5063232	0.70401437
ATG12	0.34052801	-0.5064251	0.70396463
RASGRF2	0.30966822	-0.5066458	0.70385696
HTATSF1	0.23085639	-0.5067321	0.70381488
ZFP62	0.49788731	-0.5070671	0.70365147
LPCAT2	0.34154865	-0.5071837	0.70359457
ZMYM6	0.40241705	-0.5072634	0.70355573
TNNI2	0.33172981	-0.5074403	0.70346946
ZNF224	0.29183639	-0.5076231	0.70338035
BNC2	0.24130693	-0.5076282	0.70337785
HAUS6	0.31635775	-0.5076861	0.70334963
CEP95	0.32950289	-0.5081772	0.70311023
DBI	0.21302719	-0.5081947	0.70310169
HLA-DQA2	0.05635635	-0.5083914	0.70300583
HSPE1	0.40537714	-0.5086151	0.70289683
GYPA	0.3377087	-0.5087627	0.70282496
C1orf162	0.27971326	-0.5091203	0.70265075
PPP1R16A	0.29681282	-0.5096313	0.70240191
KIAA1191	0.26270855	-0.509666	0.70238501
GFPT1	0.00748512	-0.5096874	0.7023746
VASH1	0.18340474	-0.509916	0.70226331
ATP10A	0.18044634	-0.5099359	0.70225365

OSGIN2	0.54988399	-0.5106142	0.70192355
ZZZ3	0.49943319	-0.5122195	0.70114296
SNHG7	0.38830795	-0.5126505	0.70093353
TIMM17A	0.3170955	-0.5128059	0.70085802
RAB20	0.16903857	-0.5130011	0.70076317
ZNF776	0.39376122	-0.5134185	0.70056049
RIT1	-0.034273	-0.5134348	0.70055254
CPM	0.23089745	-0.5140542	0.70025185
IFIT5	0.53575819	-0.5141225	0.7002187
CCDC28B	0.20934838	-0.514145	0.70020777
AC147067.1	-0.109573	-0.5151593	0.69971565
MAPK9	0.50514331	-0.515432	0.6995834
MRE11	0.30737145	-0.5156901	0.69945826
AP003068.2	0.13129916	-0.515988	0.69931385
ERMP1	0.07746774	-0.5168524	0.69889497
IFIT3	0.436477	-0.516883	0.69888014
DVL2	0.30552842	-0.517131	0.69876003
CTNS	0.05529016	-0.5174707	0.69859552
FBXO21	0.21172247	-0.5177332	0.69846841
WDR47	0.36810201	-0.5177891	0.69844138
DDX10	0.42993599	-0.5180798	0.69830063
CAPN10	0.55950292	-0.5183174	0.69818565
NOMO1	0.42057602	-0.5185701	0.69806338
ADCY7	0.49993947	-0.5187271	0.69798742
CEBPE	0.08096707	-0.5190073	0.69785186
CDPF1	0.22732031	-0.5193292	0.69769616
GTPBP10	0.37859277	-0.5197326	0.69750109
TP53I13	0.2012278	-0.5197895	0.69747362
ANXA2R	0.23062341	-0.5198595	0.69743975
DCUN1D5	0.26416487	-0.5203682	0.69719388
ZCCHC9	0.25631649	-0.5205113	0.69712474
TRAV6	0.07456909	-0.5205785	0.69709225
ELOC	0.01068259	-0.5208313	0.69697013
SEPSECS	0.42445587	-0.5208623	0.69695515
POLG2	0.23865392	-0.5214257	0.69668304
C18orf21	0.37346303	-0.5217497	0.6965266
SCOC	0.2851498	-0.5222429	0.6962885
MRPL35	0.07323783	-0.5229521	0.69594629
AC004846.2	0.25432959	-0.5230104	0.6959182
MED11	0.21790482	-0.5231475	0.69585206

SLC43A3	0.28413997	-0.5232598	0.69579787
SEC24A	0.12330836	-0.5240715	0.69540653
AC008467.1	0.45064391	-0.5240811	0.69540187
ZNF768	0.45959204	-0.5240858	0.69539961
UBE4A	0.20385608	-0.5244791	0.69521006
BZW2	0.4167312	-0.5247019	0.69510272
COPRS	0.24848193	-0.5253737	0.6947791
JAK2	0.19148597	-0.5256863	0.69462859
SH3BGR2	0.10601825	-0.5259398	0.69450656
OAS1	0.25195281	-0.5261317	0.69441416
HAVCR2	0.15161684	-0.5263368	0.69431544
APTX	0.28579738	-0.5269076	0.69404083
CKS1B	0.31153139	-0.5269275	0.69403123
ANKRD36BP2	0.33972347	-0.5275204	0.69374608
UMPS	0.42620504	-0.5275753	0.69371965
POMGNT2	0.25723241	-0.5281726	0.69343253
VDAC3	0.31721547	-0.5285101	0.6932703
ELL2	0.39913096	-0.5285943	0.69322984
SORT1	0.25987241	-0.5302382	0.69244039
STK35	0.54447833	-0.5313634	0.69190058
OTUD6B	0.35243726	-0.5313833	0.69189101
NEIL2	0.64008911	-0.5314798	0.69184471
FEM1B	0.44811698	-0.5320253	0.69158319
GTPBP3	0.18855608	-0.5323475	0.69142877
NMD3	0.3581546	-0.5323656	0.6914201
PLCH2	-0.0767174	-0.5325064	0.6913526
SLC25A28	0.34963505	-0.532909	0.69115971
RCAN1	0.35323076	-0.5334845	0.69088405
KNOP1	0.44920653	-0.5336726	0.69079397
KCNQ5-IT1	0.3407492	-0.5337566	0.69075374
N4BP2L1	0.32054967	-0.5341157	0.69058183
SLC15A2	0.45689141	-0.5345424	0.69037761
BTBD10	0.56972175	-0.5350401	0.69013951
CEP162	0.22844998	-0.5351226	0.69010002
APOBEC3D	0.36980302	-0.5354596	0.68993886
CDC42-IT1	0.30039937	-0.5354721	0.68993286
GBP5	0.26612713	-0.5369115	0.68924484
SUB1	0.20049282	-0.5376172	0.68890779
CYB561	0.19739173	-0.5379575	0.68874533
IDH3A	0.20020652	-0.5381749	0.68864151

AP000560.1	0.28537449	-0.5383831	0.68854216
POLR2M	0.16744376	-0.5384033	0.68853254
COG7	0.04535491	-0.539178	0.68816287
COMMD5	0.06117082	-0.5402475	0.68765291
DHRS9	0.17530463	-0.5410519	0.68726961
C16orf87	0.09649566	-0.5411181	0.68723807
VAV2	0.32573069	-0.5412898	0.68715628
CSE1L	0.24749541	-0.5414454	0.6870822
RPP14	0.10927296	-0.5416943	0.68696367
NAGA	0.41346988	-0.5421406	0.68675118
PPP1CC	0.24197462	-0.5424926	0.68658364
PRDX1	0.24382701	-0.54253	0.68656584
HINFP	0.30688752	-0.5432049	0.68624474
RFC5	0.4419482	-0.5438292	0.68594786
TYW5	0.25459406	-0.5439608	0.68588528
CYBRD1	0.26132325	-0.544596	0.68558337
SNAPIN	0.29904276	-0.5449396	0.68542011
LRRC37B	0.38325704	-0.5452157	0.68528892
LINC00476	0.07716242	-0.5455432	0.6851334
ETNK1	0.34864189	-0.545949	0.6849407
MRPS6	0.22798522	-0.5460868	0.68487526
TOR1AIP1	0.32401109	-0.5461546	0.68484309
TGFBR1	0.18428456	-0.5466845	0.68459162
VRK1	0.40306034	-0.5471227	0.68438368
BNIP2	0.23894521	-0.5471616	0.68436526
EHBP1	0.63211649	-0.547391	0.68425644
VAV3	0.55517554	-0.5475957	0.68415935
TOR3A	0.58607304	-0.5476338	0.68414131
C21orf91	0.34339147	-0.547988	0.68397333
FAM168B	0.41552142	-0.5482539	0.68384727
RNF121	0.25943759	-0.548557	0.68370363
REPS2	0.28640374	-0.5488917	0.68354505
SIGLEC7	0.24267091	-0.5493071	0.68334824
CEACAM1	0.18078107	-0.5497726	0.68312779
STK36	0.21077662	-0.5498844	0.68307486
SACS	0.38387805	-0.5501722	0.6829386
DUSP7	0.53712116	-0.5507946	0.68264404
ZNF175	0.39572242	-0.550998	0.68254782
BTRC	0.10124267	-0.5511888	0.68245755
CASP8AP2	0.35242655	-0.5512179	0.68244379

SS18	0.2175692	-0.5512249	0.68244045
MT1E	0.24183071	-0.551371	0.68237138
CSTF3	-0.0760332	-0.5513927	0.6823611
POLR2H	0.4828162	-0.55166	0.68223469
RPL9	0.30479109	-0.5519788	0.68208392
R3HCC1L	0.28212255	-0.5527678	0.681711
UBE2E1	0.14449946	-0.5533878	0.6814181
ZNF555	0.2976875	-0.5538038	0.68122166
LRRC37A4P	0.50284259	-0.5541064	0.6810788
GINM1	0.39037238	-0.5542179	0.68102617
FKBP3	0.34616079	-0.554346	0.68096569
LRSAM1	0.49683188	-0.5543784	0.68095041
CTSL	0.14332503	-0.5550357	0.68064022
SH2B3	0.35622885	-0.5558327	0.68026433
LILRB1	0.45425952	-0.5560084	0.68018145
ATG3	0.46718784	-0.5564985	0.67995042
AC069366.2	0.36330965	-0.556568	0.67991767
NAPG	0.38020846	-0.5567444	0.67983456
SYNJ2BP	0.24951434	-0.5570892	0.67967208
SRSF7	0.3944804	-0.5572211	0.67960994
MRPL46	0.22636181	-0.5574802	0.67948794
INTS6L	0.25636243	-0.5578826	0.67929841
SP3	0.24780015	-0.5579806	0.67925229
WDR36	0.19772271	-0.5583479	0.67907935
AC007292.2	0.15442147	-0.5585167	0.67899991
DNASE1L1	0.25193462	-0.5586309	0.67894615
ZC3H12D	0.47418919	-0.559438	0.67856647
KLF4	0.47882113	-0.5594624	0.67855499
TMED4	0.4528178	-0.5601307	0.67824072
PIGB	0.38031806	-0.5606026	0.67801891
ZBP1	0.4209725	-0.5607245	0.6779616
AC004918.1	0.32030017	-0.5613332	0.67767564
ZNF506	0.41668561	-0.5614565	0.67761771
IL18RAP	0.24487164	-0.5617942	0.67745914
REXO2	0.3745028	-0.5623667	0.67719033
PHLDB2	0.38392746	-0.562687	0.67704002
ACOX3	0.62060697	-0.5628414	0.67696756
ARRDC4	0.40098764	-0.5628862	0.67694655
DERA	0.4376798	-0.5629106	0.67693507
ZNF587B	0.3288217	-0.5632363	0.67678229

ITGAE	0.18221559	-0.5633471	0.6767303
AKR7A2	0.22677002	-0.5635193	0.67664954
MFSD8	0.22520456	-0.5635951	0.67661397
SLC25A24	0.34197327	-0.5636636	0.67658185
AC024075.1	0.3610122	-0.5640617	0.6763952
PPARD	0.51203405	-0.5655798	0.67568382
RPAIN	0.26239334	-0.5661443	0.67541948
ZNF426	0.4375588	-0.5663532	0.67532171
NSMCE3	0.48689987	-0.5664338	0.67528398
ANKRD52	0.63633168	-0.5664402	0.67528098
ETHE1	0.2726024	-0.5664459	0.6752783
ST3GAL5	0.30762644	-0.5665751	0.67521784
TSNAX	0.34318213	-0.5672945	0.6748812
BUB3	0.1498339	-0.5674447	0.67481094
TAPT1	0.3938171	-0.5677979	0.67464578
CDCA4	0.32089026	-0.56782	0.67463544
RNF125	0.31819361	-0.5683152	0.67440392
AL121839.2	0.29895045	-0.5685526	0.67429292
LRIG1	0.3075266	-0.5688711	0.67414408
SMIM24	0.20784533	-0.5699294	0.67364973
FUCA1	0.40335879	-0.5704828	0.67339139
TTC37	0.36006279	-0.5710417	0.67313057
TRIB2	0.42610764	-0.5712906	0.67301447
MCUB	0.34885098	-0.5714659	0.67293267
MOV10	0.37625687	-0.5718121	0.67277121
RCC1L	0.15339665	-0.5718284	0.67276363
MPHOSPH10	0.67739412	-0.572187	0.67259642
C21orf62-AS1	0.0807822	-0.572512	0.6724449
ZBED5-AS1	0.42952121	-0.5730451	0.6721965
TMEM14C	0.31255082	-0.5731243	0.67215957
TIMM21	0.28477728	-0.5735288	0.67197115
SNRPA1	0.13467213	-0.5737524	0.67186703
C2orf49	0.39973113	-0.5740071	0.67174842
MIA3	0.49068961	-0.5740204	0.67174223
CWC15	0.37130509	-0.574085	0.67171213
LACTB	0.24465619	-0.5745456	0.67149773
SDF2L1	0.375582	-0.5745632	0.67148954
TRMT12	0.25683595	-0.5747168	0.67141806
SLC25A46	0.37603537	-0.5751936	0.67119616
MRPS7	0.31776684	-0.5763622	0.67065272

EXOSC2	0.43416838	-0.5765167	0.67058088
MEAF6	0.22524402	-0.5765454	0.67056758
DNAJC27	0.36274287	-0.5765611	0.67056025
HS2ST1	0.12717139	-0.5774231	0.67015974
TM9SF2	0.27108696	-0.5778195	0.6699756
GM2A	0.25527905	-0.5783423	0.66973286
GCLM	0.19351929	-0.5784328	0.66969087
HS6ST1	0.48572125	-0.578759	0.66953949
IGFBP7	0.57502794	-0.5791244	0.66936991
STAMBP	0.24647058	-0.5793082	0.66928464
RAB9A	0.25769777	-0.5796769	0.66911363
CD28	0.1197685	-0.5802018	0.6688702
HENMT1	0.0305696	-0.5806168	0.66867781
ADAP2	0.08271462	-0.580942	0.6685271
ATRAID	0.37988799	-0.5811475	0.66843192
CPOX	0.17844495	-0.5811868	0.66841369
ADGRL1	0.42911323	-0.5813731	0.66832738
CTBP1-AS2	0.50787123	-0.581535	0.6682524
ALG2	0.310622	-0.5818883	0.66808877
SLC35A1	0.34660475	-0.5823312	0.6678837
POP4	0.35712816	-0.5824886	0.66781082
TRIT1	0.22496698	-0.5825759	0.66777043
EIF4ENIF1	0.54972147	-0.5832766	0.66744619
DIS3L2	0.32244481	-0.5832959	0.66743723
ZNF92	0.37700274	-0.5837533	0.66722565
EYA3	0.20230016	-0.5842243	0.66700786
SRFBP1	0.18657489	-0.5847715	0.66675495
ZNF780B	0.28411456	-0.5848826	0.66670361
LMAN2L	0.21597964	-0.5859553	0.66620803
DHX40	0.36822548	-0.586004	0.66618559
AC007342.2	0.4764585	-0.5863035	0.6660473
ITGB3	0.26258765	-0.5867549	0.66583893
TNFAIP6	0.24465924	-0.5868261	0.66580604
CCDC117	0.16055438	-0.587052	0.6657018
DHRS4-AS1	0.28993711	-0.5870939	0.66568248
CLTA	0.19619904	-0.5874209	0.66553163
DNAJC19	0.3263287	-0.5879153	0.66530356
ABCC13	0.74951404	-0.5892952	0.66466753
LINC00937	0.49068181	-0.5894321	0.66460446
G3BP2	0.22767234	-0.5897318	0.66446642

PYM1	0.29528397	-0.5902329	0.66423569
RSPH3	0.47104657	-0.5903633	0.66417561
AC093726.1	0.41747707	-0.5912356	0.66377419
PRELID3B	0.32457978	-0.5922033	0.66332908
AC125257.1	0.21582165	-0.5930497	0.66294002
TMEM170B	0.18066244	-0.5932044	0.66286895
RABGGTA	0.48538053	-0.5939876	0.6625092
ASH2L	0.35573953	-0.5942729	0.66237819
ARL1	0.34996559	-0.5945762	0.66223898
COASY	0.51457313	-0.5947763	0.66214711
PAPD7	0.4658788	-0.594828	0.66212339
CEBPG	0.38872228	-0.5950129	0.66203854
AL355816.2	0.19397258	-0.595394	0.66186368
LIG1	0.36352806	-0.5954996	0.66181522
ARMC1	0.37989193	-0.5955223	0.66180482
YARS2	0.63072166	-0.596498	0.6613574
ACTR5	0.28077353	-0.5967832	0.66122667
LPAR6	0.39009009	-0.5970064	0.66112438
SLA2	0.62283007	-0.5971227	0.66107106
NPEPL1	0.38180197	-0.597783	0.66076858
METTL17	0.49275936	-0.5981831	0.66058534
OTUD6B-AS1	0.09935679	-0.59832	0.66052267
AC096733.2	0.24256687	-0.5985983	0.66039527
BDH1	0.23875439	-0.5991338	0.66015018
ZSCAN30	0.22994223	-0.5992306	0.66010588
FAM157A	0.28820034	-0.5995536	0.65995812
DDX19A	0.3746681	-0.6003431	0.65959706
EXOSC7	0.56727384	-0.6006299	0.65946594
NFU1	0.32001014	-0.602152	0.65877059
CLPX	0.45802972	-0.6022572	0.65872252
COPS8	0.45213509	-0.6024318	0.6586428
SUCO	0.34925665	-0.6030708	0.65835117
ZNF589	0.22873686	-0.6031025	0.65833668
HIGD1A	0.27038195	-0.6032688	0.6582608
CCDC82	0.31581846	-0.6033537	0.65822205
SLC25A12	0.36639639	-0.6034197	0.65819196
TPT1-AS1	0.38372687	-0.6044603	0.65771737
DLD	0.38666015	-0.6048756	0.65752805
TOB1	0.19771933	-0.6060954	0.65697236
WWP1	0.29364808	-0.6070459	0.65653966

RYK	0.38120918	-0.6076026	0.65628636
LDAH	0.65253797	-0.6080247	0.65609441
TUBE1	0.19029744	-0.6082422	0.6559955
MRPL33	0.28415064	-0.6087801	0.65575094
CLEC2B	0.6054436	-0.6100798	0.65516045
AUTS2	0.16268594	-0.6103144	0.65505393
EED	0.41348899	-0.6114876	0.65452145
PSMA4	0.53271951	-0.6121488	0.65422154
PPID	0.53771149	-0.6122513	0.65417508
AIG1	0.23451166	-0.6130079	0.65383209
TULP4	0.33087381	-0.6132468	0.65372385
USP44	0.37205584	-0.6135845	0.65357084
MGLL	0.33993067	-0.6137911	0.65347726
AC098679.1	0.46761006	-0.6139001	0.65342788
TBC1D2	0.41945465	-0.6149463	0.65295422
NDUFB3	0.29421763	-0.6152436	0.65281965
AC007066.2	0.13767262	-0.6152559	0.65281409
CCDC127	0.28436167	-0.6170503	0.65200264
LINC01215	0.28921013	-0.617446	0.65182384
PHTF2	0.54408768	-0.6178684	0.651633
MICA	-0.0452541	-0.6179363	0.65160236
REPS1	0.41772596	-0.6181979	0.65148421
AC093323.1	0.2848851	-0.618253	0.65145932
ELAVL1	0.19125857	-0.6183643	0.65140906
ATP6V1G1	0.29985219	-0.6185096	0.65134345
GPRASP1	0.23249846	-0.618861	0.65118482
MGMT	0.00873528	-0.6193016	0.65098599
HMG3	0.52925394	-0.6193366	0.65097018
IGIP	0.26443859	-0.6193516	0.65096341
RNU7-41P	0.30117361	-0.6197624	0.65077809
DDX51	0.25840853	-0.6205085	0.65044165
TIMM44	0.32465391	-0.6215507	0.64997194
CLASP2	0.07883851	-0.6220518	0.64974621
MORC2	0.5205878	-0.622603	0.649498
TSTD2	0.21397427	-0.6231728	0.64924155
AACS	0.2139599	-0.6235623	0.64906628
PHF10	0.27319912	-0.6235683	0.64906358
GTPBP8	0.37035892	-0.6236931	0.64900744
OPN3	0.43734987	-0.6239718	0.64888207
TRIAP1	0.46229163	-0.6245284	0.64863177

CAMKMT	0.33865432	-0.6248707	0.64847788
GMPPB	0.32514183	-0.6256407	0.64813189
UTP4	0.65612392	-0.625646	0.64812951
MTA2	0.43248222	-0.6264714	0.64775881
HDHD5	0.27319034	-0.6268372	0.64759457
STX6	0.26606473	-0.6274502	0.64731946
TERF2	0.46721027	-0.6279452	0.64709739
PGGT1B	0.36659484	-0.6280465	0.64705199
ANKRD10	0.44307329	-0.6281094	0.64702377
SERGEF	0.25169874	-0.6284942	0.6468512
WDR89	0.57231473	-0.6285056	0.64684608
AC007342.4	0.24889933	-0.6286221	0.64679388
ZDHHC20	0.44549818	-0.6294618	0.6464175
TSPOAP1	0.35037685	-0.629755	0.64628615
METTL12	0.55457331	-0.6298757	0.64623208
PTER	0.17467689	-0.6300902	0.64613603
PDP2	0.62445806	-0.6303698	0.6460108
NAA30	0.27862553	-0.6308753	0.64578451
EID2	0.4021904	-0.6314439	0.64553004
DRG1	0.18807819	-0.6325726	0.64502519
C18orf25	0.12302748	-0.6343495	0.64423124
ACTA2	0.56850337	-0.6355724	0.64368536
POLR3E	0.30159791	-0.6372841	0.64292212
DRAM2	0.50671939	-0.6377389	0.64271946
TOGARAM1	0.34197438	-0.6378807	0.64265631
ASF1A	0.34405122	-0.6379259	0.64263619
EHD4	0.19381227	-0.6388315	0.64223289
TTC26	0.37904948	-0.6401126	0.64166285
MCM2	0.34358344	-0.6411976	0.64118046
CHIC1	0.4226668	-0.641294	0.64113765
FBXO45	0.07576634	-0.6420157	0.64081699
NLRP3	0.26792019	-0.6420501	0.64080173
ASNSD1	0.51455094	-0.6427813	0.64047702
SPATA5	0.40580301	-0.6432652	0.64026224
MICU2	0.60510523	-0.6449818	0.63950084
RIPK2	0.57915099	-0.6453327	0.63934532
RIOK1	0.57192841	-0.6453472	0.63933892
DOHH	0.2863982	-0.6456693	0.63919616
ISY1	0.71138492	-0.6457006	0.63918232
FCGR1A	0.1511084	-0.646132	0.63899121

VIM-AS1	0.24381816	-0.6466187	0.63877569
THAP5	0.30779649	-0.6475021	0.63838466
MAN1C1	0.52603156	-0.6479659	0.63817949
CYSLTR2	0.05174081	-0.6483334	0.63801693
ALG10B	0.45745988	-0.6487929	0.63781377
AC110769.2	0.14147817	-0.6490654	0.63769328
CSTF2T	0.35272811	-0.6496537	0.63743329
SEC24D	0.54023754	-0.6516363	0.63655794
NEPRO	0.23385526	-0.6521151	0.6363467
PRKCI	0.20532297	-0.6523502	0.63624301
HNMT	0.30698192	-0.6524503	0.63619888
SETDB2	0.23044233	-0.6525192	0.63616847
FBXO8	0.18758995	-0.6528041	0.63604286
GTF2H5	0.30271918	-0.6539692	0.63552941
SEC23IP	0.16832564	-0.654319	0.63537536
EMC2	0.47420209	-0.6552245	0.63497669
TMEM42	0.42576945	-0.6558248	0.63471251
MTHFD2	0.16831495	-0.6558259	0.63471204
AC004951.1	0.47310857	-0.6565383	0.63439871
TANGO6	0.32122883	-0.6575326	0.63396164
TMEM123	0.26874455	-0.6592102	0.63322488
IMPAD1	0.33491893	-0.6597623	0.63298257
ARHGAP19	0.23056323	-0.6626502	0.63171677
TRIM5	0.33060853	-0.6643601	0.63096849
ZNHIT3	0.6880678	-0.6650312	0.63067505
UBE2N	0.43013319	-0.6651349	0.63062973
CEBPZ	0.40137135	-0.6660423	0.63023323
TSHZ1	0.46105552	-0.666637	0.62997346
C3orf38	0.45501645	-0.6677288	0.62949691
TOP1MT	0.16423452	-0.668235	0.62927607
IFI44L	0.53753961	-0.6715076	0.62785025
COPS3	0.24259899	-0.6722308	0.62753561
COA3	0.26433507	-0.6740733	0.62673468
CAND1	0.40615412	-0.6759598	0.62591565
XPNPEP3	0.2904909	-0.6761266	0.6258433
ACADS	0.33206502	-0.6766329	0.62562372
RPL22L1	0.36279309	-0.6774987	0.62524836
CHUK	0.47131066	-0.6779616	0.62504777
RTL6	0.56652108	-0.6781334	0.62497334
AL021707.6	0.40480124	-0.6785982	0.62477206

HACL1	0.60067252	-0.6796417	0.62432032
UBP1	0.23681497	-0.6800293	0.62415261
KIAA0100	0.21452431	-0.6803577	0.62401053
EME2	0.29307962	-0.681758	0.62340517
STX11	0.37389423	-0.6818086	0.62338328
TBK1	0.51396741	-0.6820271	0.6232889
XAF1	0.35868211	-0.6823789	0.62313691
HOPX	0.36278675	-0.6832517	0.62276006
HEATR1	0.27469993	-0.6836659	0.62258126
SPG20	0.38327512	-0.6838657	0.62249507
ZNF337	0.55347425	-0.6839658	0.62245187
ZDHHC12	0.26629529	-0.6846674	0.62214925
LINC00909	0.38872564	-0.6847554	0.62211128
NDUFB5	0.11559163	-0.6856903	0.62170827
BCOR	0.40614023	-0.6866822	0.62128099
TFPT	0.2487434	-0.6874322	0.62095811
METTL25	0.17997373	-0.6885275	0.62048685
RPARP-AS1	0.21111883	-0.6886346	0.62044077
GCFC2	0.06193899	-0.6897091	0.61997887
RBM27	0.41196276	-0.6898268	0.61992826
ZNF551	0.34446227	-0.6898568	0.61991536
WDR5	0.43223076	-0.6902369	0.61975207
MUT	0.56098705	-0.6919383	0.61902164
RSAD2	0.47718184	-0.6922944	0.61886886
GPALPP1	0.48770144	-0.6947095	0.61783373
SOCS2	0.44645497	-0.6969387	0.61687981
NSUN5P2	0.3085176	-0.6971769	0.61677795
DNAJA3	0.42033062	-0.6972964	0.61672688
ZNF12	0.29130002	-0.6979019	0.61646808
TRIM52-AS1	0.33719391	-0.6981069	0.61638051
KLRF1	0.53565664	-0.7013684	0.61498863
ANKRD36B	0.26271798	-0.7017282	0.61483525
LSM6	0.20827894	-0.7019493	0.61474104
TAMM41	0.1249127	-0.7027764	0.61438869
PCNP	0.36543286	-0.703237	0.61419258
SLC38A6	0.50117759	-0.7057952	0.61310444
PURB	0.33864419	-0.7060952	0.612977
RNF185	0.69285692	-0.7063878	0.61285266
PIGK	0.53186248	-0.7085614	0.61193004
PNOC	0.27340947	-0.7089064	0.6117837

TRIM37	0.72484646	-0.7098384	0.61138863
ABHD15	0.22967023	-0.7108756	0.61094923
MYO19	0.39473693	-0.710911	0.61093423
LINC00847	0.62901603	-0.711478	0.61069416
PHAX	0.51029318	-0.7122145	0.61038249
AC005674.2	0.32085342	-0.7125435	0.61024331
PRR4	0.44347322	-0.7126001	0.61021939
MRPS21	0.51273489	-0.7141537	0.6095626
HMG2	0.38895856	-0.7146105	0.60936965
PMS1	0.30176727	-0.7150763	0.6091729
IFIH1	0.47350336	-0.7158202	0.60885889
GLMP	0.41847798	-0.7160721	0.60875258
PCYOX1	0.38849522	-0.7175359	0.60813523
LINC00342	0.08875924	-0.7179473	0.60796183
ECI2	0.1704326	-0.7184963	0.60773056
COQ5	0.45994799	-0.7187226	0.6076352
TSEN15	0.61608425	-0.7198774	0.60714903
LINC00106	0.50766377	-0.720425	0.60691864
RAPGEF6	0.26144382	-0.7214468	0.60648892
HERC5	0.5500807	-0.7216829	0.60638966
SNAPC2	0.32452912	-0.7222438	0.60615397
HNRNPH2	0.38027	-0.7224319	0.60607495
EIF4B	0.25691819	-0.7237282	0.6055306
ARAP2	0.54018184	-0.7241376	0.60535882
SAP30	0.35553362	-0.7247085	0.60511929
SLC30A6	0.31407636	-0.7267344	0.60427016
NPHP3	0.30207004	-0.7290153	0.60331557
ZDHHC8	0.48980464	-0.7294129	0.6031493
SLC39A8	0.33971355	-0.7300894	0.60286654
MRPS9	0.18463673	-0.7306279	0.60264157
FARP2	0.6075814	-0.7340335	0.60122067
RABEP2	0.41991911	-0.7346168	0.60097762
FUNDC1	0.37749198	-0.7360859	0.60036597
STT3A	0.38084183	-0.7367379	0.60009472
ALKBH3	0.32381501	-0.7368252	0.60005839
TATDN1	0.36058326	-0.7371272	0.59993278
TWINK	0.15090349	-0.737303	0.59985968
AC126474.2	0.4237729	-0.7377252	0.59968418
FOPNL	0.46180653	-0.7378365	0.59963791
PRKAG2	0.65511854	-0.7390349	0.59914002

ACSL3	0.6138204	-0.7405506	0.59851088
TMEM261	0.6660953	-0.7405737	0.5985013
TTC21B	0.16607896	-0.7416772	0.5980437
SACM1L	0.3547082	-0.7419484	0.59793129
FAM160B2	0.27791081	-0.7430068	0.59749279
MTM1	0.38854459	-0.7457783	0.59634607
PAXIP1-AS2	0.15559803	-0.7465902	0.59601057
HINT2	0.17641131	-0.746926	0.59587187
STK26	0.39671861	-0.7513877	0.5940319
BORCS7	0.38584505	-0.752541	0.59355722
CDC37L1	0.61299382	-0.7529727	0.59337964
TERF1	0.4295469	-0.7562717	0.59202429
NXPE3	0.38821601	-0.757872	0.59136796
ICMT	0.18717468	-0.7589029	0.59094556
DPH3	0.48299479	-0.7606723	0.59022121
ZHX2	0.41692908	-0.7608314	0.59015614
NMRK1	0.57558821	-0.7613364	0.58994959
DENND1B	0.31978163	-0.7643329	0.58872552
LINC-PINT	0.56614117	-0.7662082	0.58796076
TGFBR3	0.34016682	-0.7665316	0.587829
AL139317.3	0.3773741	-0.7671616	0.58757236
BAG4	0.21456842	-0.7673217	0.58750715
ABHD13	0.44501871	-0.7766461	0.58372224
TBC1D7	0.38698684	-0.7781668	0.58310727
ACLY	0.32686842	-0.7789768	0.58277997
SMPD1	0.64551982	-0.7800691	0.58233891
TNF	0.62814665	-0.7802054	0.5822839
CCNG1	0.27419765	-0.7820665	0.58153321
TTBK2	0.59190952	-0.7821702	0.58149143
CHMP5	0.4192272	-0.7850124	0.58034695
RABGGTB	0.33448594	-0.7864085	0.57978563
BCL2A1	0.51791453	-0.7866522	0.5796877
DCAF1	0.4067458	-0.7896976	0.57846533
SASH3	0.37410722	-0.7939937	0.57674533
CASZ1	0.57519267	-0.7977674	0.5752387
GABPA	0.52776665	-0.7992251	0.57465776
CAAP1	0.37959998	-0.7993815	0.57459546
AP002807.1	0.46042755	-0.8003675	0.57420289
LAMTOR3	0.2110276	-0.8062366	0.5718717
FBXW4P1	0.51459154	-0.814339	0.56866897

TBC1D8	0.46314392	-0.8149069	0.56844515
FAM228B	0.69770894	-0.8162421	0.56791932
ASCC3	0.32792581	-0.8164842	0.56782401
ZCCHC3	0.35090018	-0.8174676	0.56743712
AUH	0.6748279	-0.8282834	0.56319896
INPP1	0.47272785	-0.8318421	0.56181143
SPCS2	0.43581477	-0.8326532	0.56149568
LARP4	0.614324	-0.8374876	0.55961726
RBM48	0.50431628	-0.8405551	0.55842868
EXOSC8	0.40959721	-0.841446	0.55808392
ITPRIPL2	0.35932106	-0.8423234	0.55774461
SPRTN	0.63937445	-0.8429861	0.55748848
ANXA4	0.4040994	-0.8478668	0.55560566
HIST1H1D	0.49308917	-0.8521192	0.55397039
PRDX3	0.50816714	-0.8540047	0.55324686
S1PR1	0.34904898	-0.8590901	0.55130013
MIB2	0.54967584	-0.8596429	0.55108896
TIFA	0.39029922	-0.8629608	0.54982301
NEDD1	0.77937265	-0.8652615	0.54894689
C2orf69	0.55594837	-0.8758478	0.54493356
ZNF721	0.44979948	-0.8816068	0.54276261
LINC00467	0.37088467	-0.8891567	0.53992963
PDSS2	0.42236348	-0.8892627	0.53988997
WDR92	0.4803565	-0.8895374	0.53978716
VEZT	0.46325508	-0.8913678	0.53910274
MLH1	0.59378846	-0.8961707	0.537311
COA5	0.57012382	-0.9050896	0.53399953
GTF2B	0.41302292	-0.9054514	0.53386563
NCAPG2	0.51953865	-0.9080439	0.53290715
PRR11	0.64098019	-0.9099551	0.53220166
ALAD	0.68081784	-0.9109087	0.53185
MPP6	0.8280456	-0.9189691	0.5288868
MPC1	0.58578116	-0.9199784	0.52851693
NOL6	0.66332978	-0.92354	0.5272138
PPA2	0.46133653	-0.9321429	0.52407934
POLE	1.00898157	-0.9365726	0.52247263
SLC35D2	0.33614511	-0.9415693	0.52066623
STYX	0.56882509	-0.9463232	0.51895336
VPS26A	0.69096991	-0.9469412	0.51873111
MRPL14	0.64881938	-0.9574389	0.5149703

ABL2	0.60588384	-0.9700431	0.51049082
SNHG8	0.53611476	-0.9760422	0.50837248
MOB4	0.7955774	-0.9913664	0.50300116
OAF	0.76143337	-0.99139	0.50299292
VWA8	0.59256699	-0.9969772	0.50104871
MED27	0.57234929	-1.0031718	0.49890195
ZNF136	0.48531187	-1.0129802	0.49552159
RNGTT	0.38236088	-1.0264231	0.49092579
DNAJC15	0.67101698	-1.0292873	0.48995211
NOG	0.67577579	-1.0547855	0.48136877
POFUT2	0.57708345	-1.090505	0.46959696
GIMAP2	0.46251612	-1.0967864	0.46755682
TMX1	0.44286519	-1.1166881	0.46115125
XPOT	0.65340427	-1.1358213	0.45507579
DESI2	0.61411435	-1.1417261	0.453217
POLE4	0.39893314	-1.1544675	0.44923198
PGRMC1	0.4348273	-1.1721843	0.44374896

## Appendix C



<b>Title:</b>	The Effects of High Intensity Interval Training on Gene Expression
<b>Description:</b>	Effects of a 3 times per week, 4-week, 10X1 HIIT protocol on gene expression. Functional Enrichment analysis cutoff threshold >1.2 or <.8
<b>Organism:</b>	Homo sapiens (9606)
<b>Contrast</b>	Condition vs. Control - mRNA (RNA-seq)
<b>Creation time:</b>	10-23-2022 06:42 PM

## 1. Introduction

In this experiment, **2,653** differentially expressed (DE) genes were identified out of a total of **54,683** genes in Advaita Knowledge Base (AKB). These data were analyzed in the context of pathways obtained from the Kyoto Encyclopedia of Genes and Genomes (KEGG) database (Release 100.0+/11-12, Nov 21) (Kanehisa et al., 2000; Kanehisa et al., 2002), gene ontologies from the Gene Ontology Consortium database (2021-Nov4) (Ashburner et al., 2000; Gene Ontology Consortium, 2001), miRNAs from the miRBase (MIRBASE Version:Version22.1,10/18) and TARGETSCAN (Targetscan version: Mouse:8.0, Human:8.0) databases (Agarwal et al., 2015; Nam et al., 2014; Griffiths-Jones et al., 2008; Kozomara and Griffiths-Jones, 2014; Friedman et al., 2009; Grimson et al., 2007), network of regulatory relations from BioGRID: Biological General Repository for Interaction Datasets v4.4.203. Oct. 25th, 2021 (Szkklarczyk et al., 2017), chemicals/drugs/toxicants from the Comparative Toxicogenomics Database Nov 2021 (Davis et al., 2019), and diseases from the KEGG database (Release 100.0+/11-12, Nov 21) (Kanehisa et al., 2000; Kanehisa et al., 2002). In summary, **229** pathways were found to be significantly impacted. In addition, **1,365** Gene Ontology (GO) terms, **0** miRNAs, **477** gene upstream regulators, **231** chemical upstream regulators and **259** diseases were found to be significantly enriched before the correction for multiple comparisons.

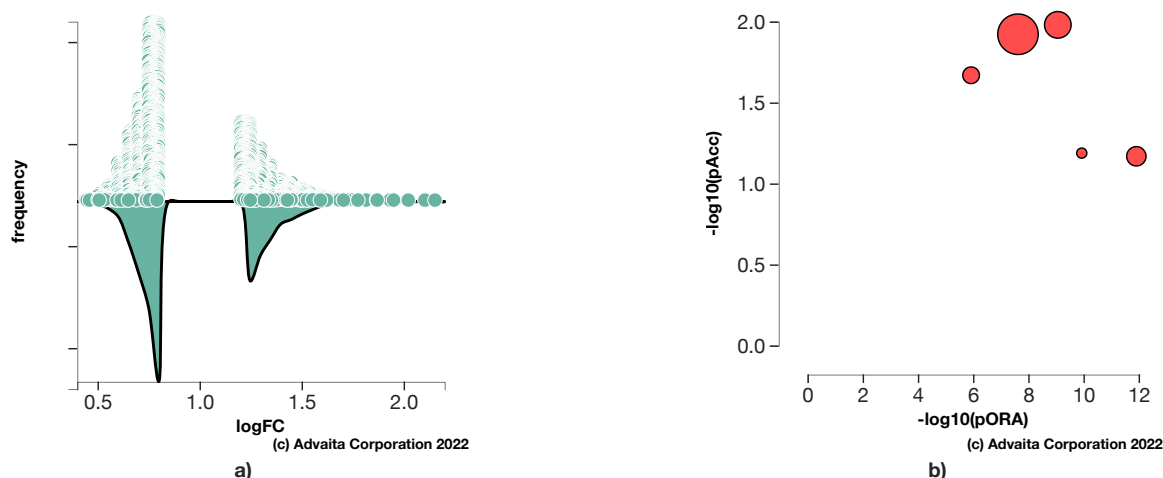


**Fig. 1.1:** a) **Violin plot:** All **2653** significantly differentially expressed (DE) genes are represented in terms of their measured expression change (x-axis) and frequency of genes measured at a given expression change (y-axis) b) **Pathways perturbation vs over-representation:** The top 5 pathways are plotted in terms of the two types of evidence computed by iPathwayGuide: over-representation on the x-axis (pORA) and the total pathway accumulation on the y-axis (pAcc). Each pathway is represented by a single dot, with significant pathways shown in red, non-significant in black, and the size of each dot is proportional to the size of the pathway it represents. Both p-values are shown in terms of their negative log (base 10) values.

## 2. Pathway Analysis

### 2.1. Methods

iPathwayGuide scores pathways using the Impact Analysis method (Draghici et al., 2007; Tarca et al., 2009; Khatri et al., 2007). Impact analysis uses two types of evidence: i) the over-representation of differentially expressed (DE) genes in a given pathway and ii) the perturbation of that pathway computed by propagating the measured expression changes across the pathway topology. These aspects are captured by two independent probability values, pORA and pAcc, that are then combined in a unique pathway-specific p-value. The underlying pathway topologies, comprised of genes and their directional interactions, are obtained from the KEGG database (Kanehisa et al., 2000; Kanehisa et al., 2010; Kanehisa et al., 2012; Kanehisa et al., 2014).

The first probability, pORA, expresses the probability of observing the number of DE genes in a given pathway that is greater than or equal to the number observed, by random chance (Draghici et al., 2003; Draghici 2011). Let us consider there are  $N$  genes measured in the experiment, with  $M$  of these on the given pathway. Based on the user-defined a priori selection of DE genes,  $K$  out of  $M$  genes were found to be differentially expressed. The probability of observing exactly  $x$  differentially expressed genes on the given pathway is computed based on the hypergeometric distribution:

$$(1) \quad P(X=x|N,M,K) = \frac{\binom{M}{x} \binom{N-M}{K-x}}{\binom{N}{K}}$$

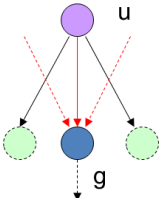
Because the hypergeometric distribution is discrete, the probability of observing fewer than  $x$  genes on the given pathway just by chance can be calculated by summing the probabilities of randomly observing 0, 1, 2, ..., up to  $x-1$  DE genes on the pathway:

$$(2) \quad p_u(x-1) = P(X=1)+P(X=2)+\dots+P(X=x-1) = \sum_{i=0}^{x-1} \frac{\binom{M}{i} \binom{N-M}{K-i}}{\binom{N}{K}}$$

iPathwayGuide calculates the probability of randomly observing a number of DE genes on the given pathway that is greater than or equal to the number of DE genes obtained from data, by computing the over-representation p-value:  $pORA = p_o(x) = 1 - p_u(x-1)$ :

$$(3) \quad p_o(x) = 1 - \sum_{i=0}^{x-1} \frac{\binom{M}{i} \binom{N-M}{K-i}}{\binom{N}{K}}$$

The second probability, pAcc, is calculated based on the amount of total accumulation measured in each pathway. A perturbation factor is computed for each gene on the pathway using:

$$(4) \quad PF(g) = \alpha(g) \cdot \Delta E(g) + \sum_{u \in US_g} \beta_{ug} \frac{PF(u)}{N_{ds}(u)}$$


In Equation 4,  $PF(g)$  is the perturbation factor for gene  $g$ , the term  $\Delta E(g)$  represents the signed normalized measured expression change of gene  $g$ , and  $\alpha(g)$  is a priori weight based on the type of the gene. The last term is the sum of the perturbation factors of all genes  $u$ , directly upstream of the target gene  $g$ , normalized by the number of downstream genes of each such gene  $N_{ds}(u)$ . The value of  $\beta_{ug}$  quantifies the strength of the interaction between genes  $g$  and  $u$ . The sign of  $\beta$  represents the type of interaction: positive for activation-like signals, and negative for inhibition-like signals. Subsequently, iPathwayGuide calculates the accumulation at the level of each gene,  $Acc(g)$ , as the difference between the perturbation factor  $PF(g)$  and the observed log fold-change:

$$(5) \quad Acc(g_i) = PF(g_i) - \Delta E(g_i)$$

All perturbation accumulations are computed at the same time by solving the system of linear equations resulting from combining Equation 4 for all genes on a given pathway. Once all gene perturbation accumulations are computed, iPathwayGuide computes the total accumulation of the pathway as the sum of all absolute accumulations of the genes in a given pathway. The significance of obtaining a total accumulation (pAcc) at least as large as observed, just by chance, is assessed through bootstrap analysis.

The two types of evidence, pORA and pAcc, are combined into an overall pathway score by calculating a p-value using Fisher's method. This p-value is then corrected for multiple comparisons using false discovery rate (FDR) and Bonferroni corrections. Bonferroni is simpler and more conservative of the two (Bonferroni, 1935; Bonferroni, 1936). It reduces the false discovery rate by imposing a stringent threshold on each comparison adjusted for the total

number of comparisons. The FDR correction has more power, but only controls the family-wise false positives rate (Benjamini and Hochberg, 1995; Benjamini and Yekutieli, 2001).

## 2.2. Results

Table 2.2.1: Top pathways and their associated p-values

Pathway name	Pathway Id	p-value	p-value (FDR)	p-value (Bonferroni)
Human T-cell leukemia virus 1 infection	05166	2.033e-7	3.888e-5	6.851e-5
Pathways in cancer	05200	2.308e-7	3.888e-5	7.776e-5
Neurotrophin signaling pathway	04722	4.670e-7	5.246e-5	1.574e-4
RNA degradation	03018	1.140e-6	5.939e-5	3.842e-4
Autophagy - animal	04140	1.190e-6	5.939e-5	4.009e-4

\* the p-value corresponding to the pathway was computed using only over-representation analysis.

### Human T-cell leukemia virus 1 infection (KEGG: 05166)

Human T-cell leukemia virus type 1 (HTLV-1) is a pathogenic retrovirus that is associated with adult T-cell leukemia/lymphoma (ATL). It is also strongly implicated in non-neoplastic chronic inflammatory diseases such as HTLV-1-associated myelopathy/tropical spastic paraparesis (HAM/TSP). Expression of Tax, a viral regulatory protein is critical to the pathogenesis. Tax is a transcriptional co-factor that interfere several signaling pathways related to anti-apoptosis or cell proliferation. The modulation of the signaling by Tax involve its binding to transcription factors like CREB/ATF, NF-kappa B, and SRF.

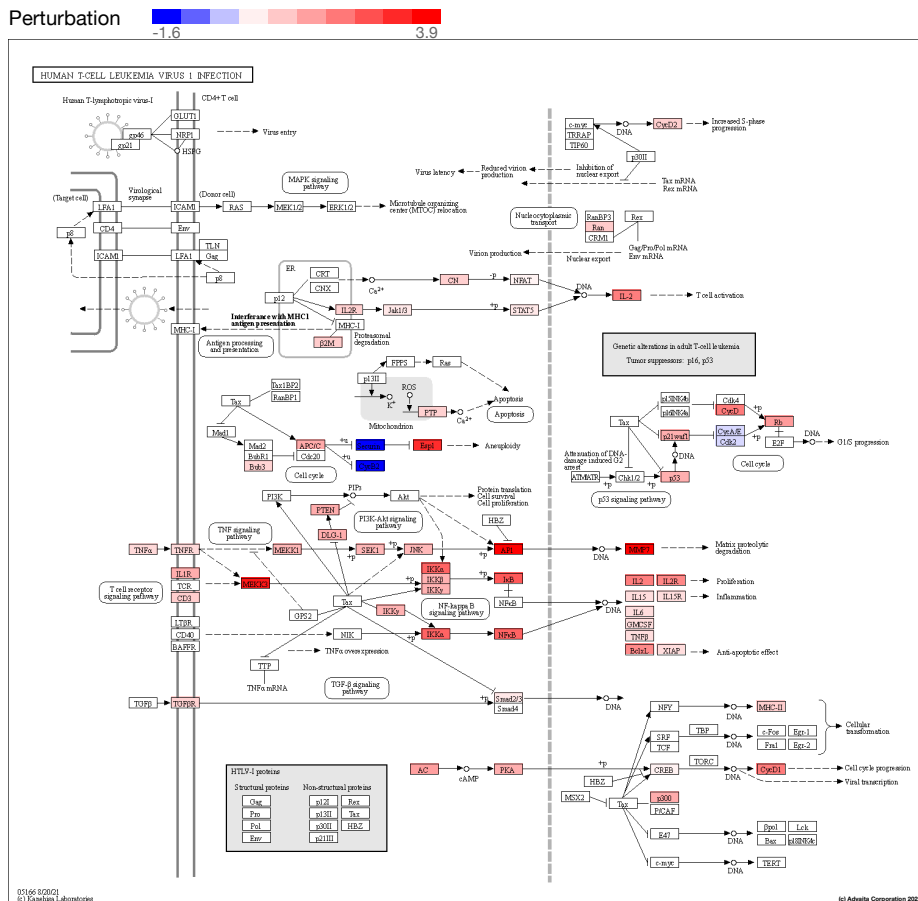
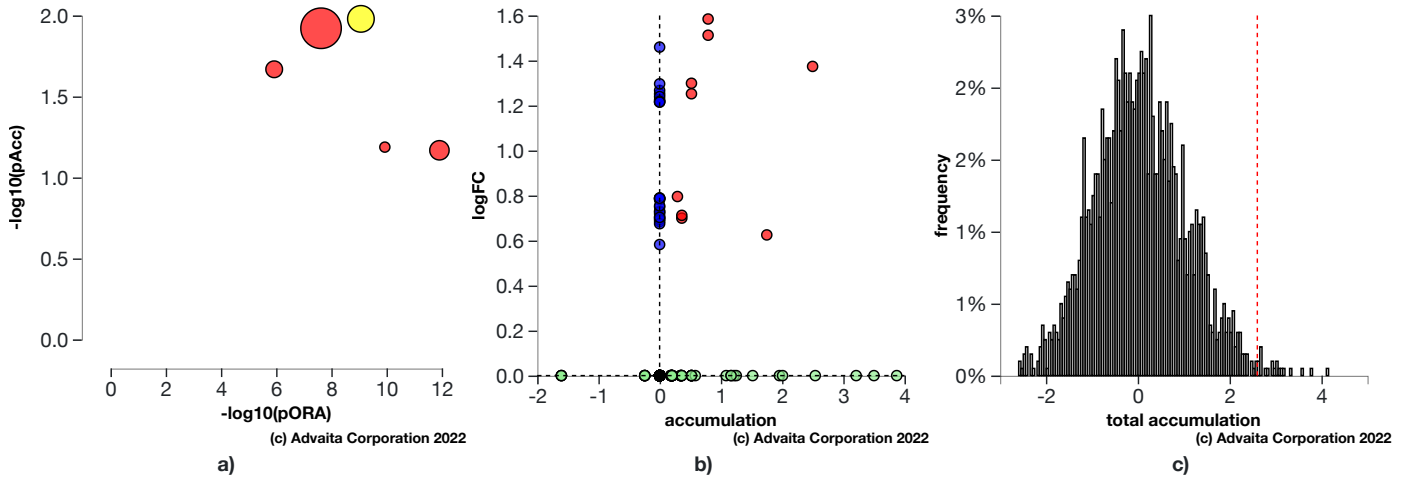


Fig. 2.2.1: Human T-cell leukemia virus 1 infection (KEGG: 05166): The pathway diagram is overlaid with the computed perturbation of each gene. The perturbation accounts both for the gene's measured fold change and for the accumulated perturbation propagated from any upstream genes (accumulation). The highest negative perturbation is shown in dark blue, while the highest positive perturbation in dark red. The legend describes the values on the gradient. Note: For legibility, one gene may be represented in multiple places in the diagram and one box may represent multiple genes in the same gene family. A gene is highlighted in all locations it occurs in the diagram. For each gene family, the color corresponding to the gene with the highest absolute perturbation is displayed.



(c) Advaita Corporation 2022

**Fig. 2.2.2: Gene measured expression bar plot:** All the differentially expressed genes in Human T-cell leukemia virus 1 infection (KEGG: 05166) are ranked based on their absolute value of log fold change. The plot is limited to the top 20 genes out of a total of 35 differentially expressed genes. Upregulated genes are shown in red, downregulated genes are shown in blue. The box and whisker plot on the left summarizes the distribution of all the differentially expressed genes in this pathway. The box represents the 1st quartile, the median and the 3rd quartile, while the outliers are represented by circles.



**Fig. 2.2.3: a) Perturbation vs over-representation:** Human T-cell leukemia virus 1 infection (KEGG: 05166) (yellow) is shown, using negative log of the accumulation and over-representation p-values, along with the other most significant pathways. Pathways in red are significant based on the combined uncorrected p-values, whereas the ones in black are non-significant (where applicable). **b) Gene measured expression vs accumulation:** All the genes from this pathway are represented in terms of their measured fold change (y-axis) and accumulation (x-axis). Accumulation is the perturbation received by the gene from any upstream genes. Genes displayed in red had both accumulation and measured fold change. Genes in blue had only measured fold change. Genes in green had only accumulation. The remaining genes that were not measured and had no accumulation are shown in black. **c) Bootstrap diagram:** The perturbation p-value is computed using bootstrap analysis. Bootstrapping assesses the probability of observing a sum of all absolute gene accumulation total accumulation at least as extreme as the computed one just by chance. A null distribution (gray bars) is computed through an iterative process that is repeated 2000 times. At each iteration, a number of genes equal to the number of differentially expressed genes in this pathway is randomly assigned anywhere in the pathway and the total accumulation is recomputed. The red line indicates the observed total accumulation of genes in the given pathway in relation to the distribution of expected values. The perturbation p-value is more significant the further away from the mean it is.

### Pathways in cancer (KEGG: 05200)

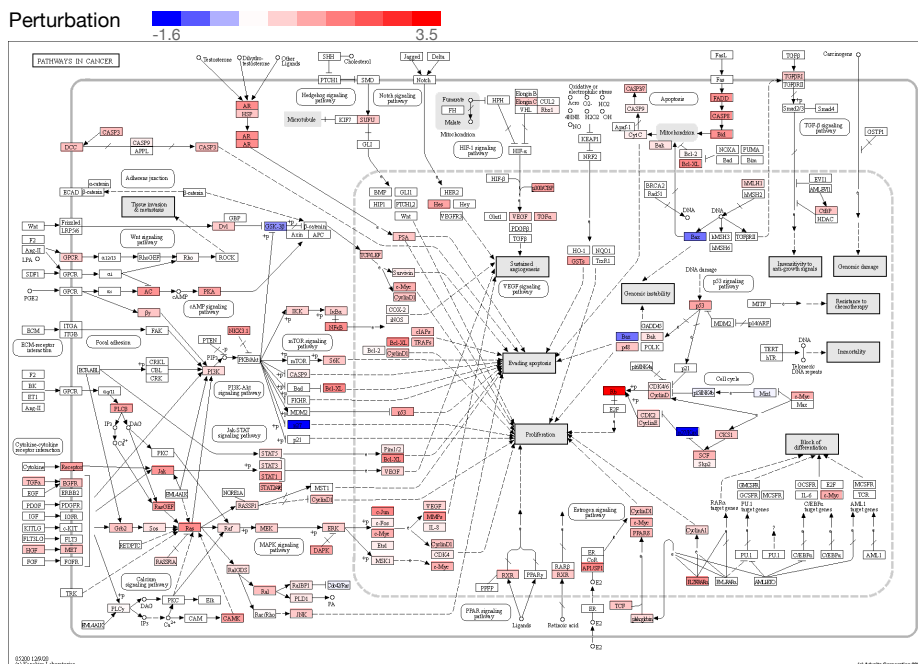
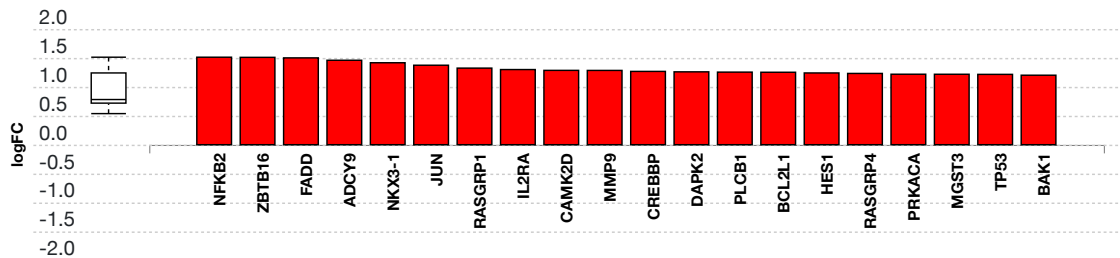


**Fig. 2.2.4: Pathways in cancer (KEGG: 05200):** The pathway diagram is overlaid with the computed perturbation of each gene. The perturbation accounts both for the gene's measured fold change and for the accumulated perturbation propagated from any upstream genes (accumulation). The highest negative perturbation is shown in dark blue, while the highest positive perturbation in dark red. The legend describes the values on the gradient. Note: For legibility, one gene may be represented in multiple places in the diagram and one box may represent multiple genes in the same gene family. A gene is highlighted in all locations it occurs in the diagram. For each gene family, the color corresponding to the gene with the highest absolute perturbation is displayed.



(c) Advaita Corporation 2022

**Fig. 2.2.5: Gene measured expression bar plot:** All the differentially expressed genes in Pathways in cancer (KEGG: 05200) are ranked based on their absolute value of log fold change. The plot is limited to the top 20 genes out of a total of 57 differentially expressed genes. Upregulated genes are shown in red, downregulated genes are shown in blue. The box and whisker plot on the left summarizes the distribution of all the differentially expressed genes in this pathway. The box represents the 1st quartile, the median and the 3rd quartile, while the outliers are represented by circles.

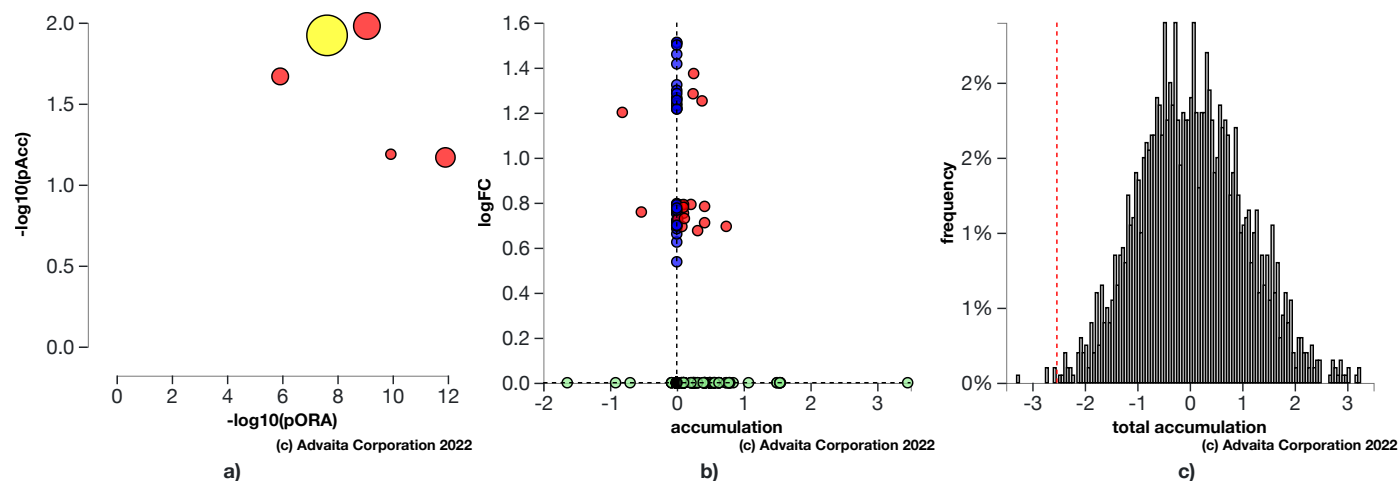


**Fig. 2.2.6: a) Perturbation vs over-representation:** Pathways in cancer (KEGG: 05200) (yellow) is shown, using negative log of the accumulation and over-representation  $p$ -values, along with the other most significant pathways. Pathways in red are significant based on the combined uncorrected  $p$ -values, whereas the ones in black are non-significant (where applicable). **b) Gene measured expression vs accumulation:** All the genes from this pathway are represented in terms of their measured fold change ( $y$ -axis) and accumulation ( $x$ -axis). Accumulation is the perturbation received by the gene from any upstream genes. Genes displayed in red had both accumulation and measured fold change. Genes in blue had only measured fold change. Genes in green had only accumulation. The remaining genes that were not measured and had no accumulation are shown in black. **c) Bootstrap diagram:** The perturbation  $p$ -value is computed using bootstrap analysis. Bootstrapping assesses the probability of observing a sum of all absolute gene accumulation total accumulation at least as extreme as the computed one just by chance. A null distribution (gray bars) is computed through an iterative process that is repeated 2000 times. At each iteration, a number of genes equal to the number of differentially expressed genes in this pathway is randomly assigned anywhere in the pathway and the total accumulation is recomputed. The red line indicates the observed total accumulation of genes in the given pathway in relation to the distribution of expected values. The perturbation  $p$ -value is more significant the further away from the mean it is.

## Neurotrophin signaling pathway (KEGG: 04722)

Neurotrophins are a family of trophic factors involved in differentiation and survival of neural cells. The neurotrophin family consists of nerve growth factor (NGF), brain derived neurotrophic factor (BDNF), neurotrophin 3 (NT-3), and neurotrophin 4 (NT-4). Neurotrophins exert their functions through engagement of Trk tyrosine kinase receptors or p75 neurotrophin receptor (p75NTR). Neurotrophin/Trk signaling is regulated by connecting a variety of intracellular signaling cascades, which include MAPK pathway, PI-3 kinase pathway, and PLC pathway, transmitting positive signals like enhanced survival and growth. On the other hand, p75NTR transmits both positive and negative signals. These signals play an important role for neural development and additional higher-order activities such as learning and memory.

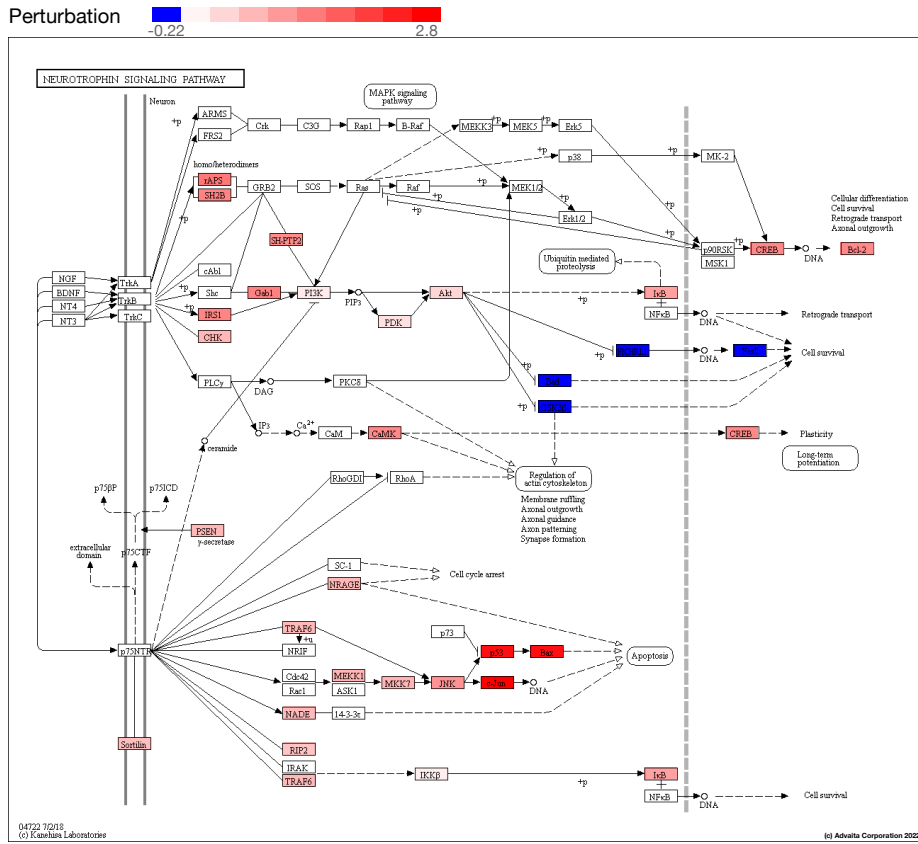
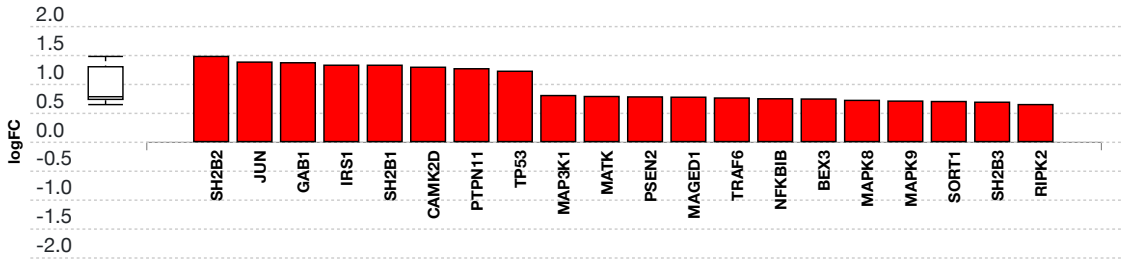


**Fig. 2.2.7: Neurotrophin signaling pathway (KEGG: 04722):** The pathway diagram is overlaid with the computed perturbation of each gene. The perturbation accounts both for the gene's measured fold change and for the accumulated perturbation propagated from any upstream genes (accumulation). The highest negative perturbation is shown in dark blue, while the highest positive perturbation in dark red. The legend describes the values on the gradient. Note: For legibility, one gene may be represented in multiple places in the diagram and one box may represent multiple genes in the same gene family. A gene is highlighted in all locations it occurs in the diagram. For each gene family, the color corresponding to the gene with the highest absolute perturbation is displayed.



(c) Advaita Corporation 2022

**Fig. 2.2.8: Gene measured expression bar plot:** All the differentially expressed genes in Neurotrophin signaling pathway (KEGG: 04722) are ranked based on their absolute value of log fold change. Upregulated genes are shown in red, downregulated genes are shown in blue. The box and whisker plot on the left summarizes the distribution of all the differentially expressed genes in this pathway. The box represents the 1st quartile, the median and the 3rd quartile, while the outliers are represented by circles.

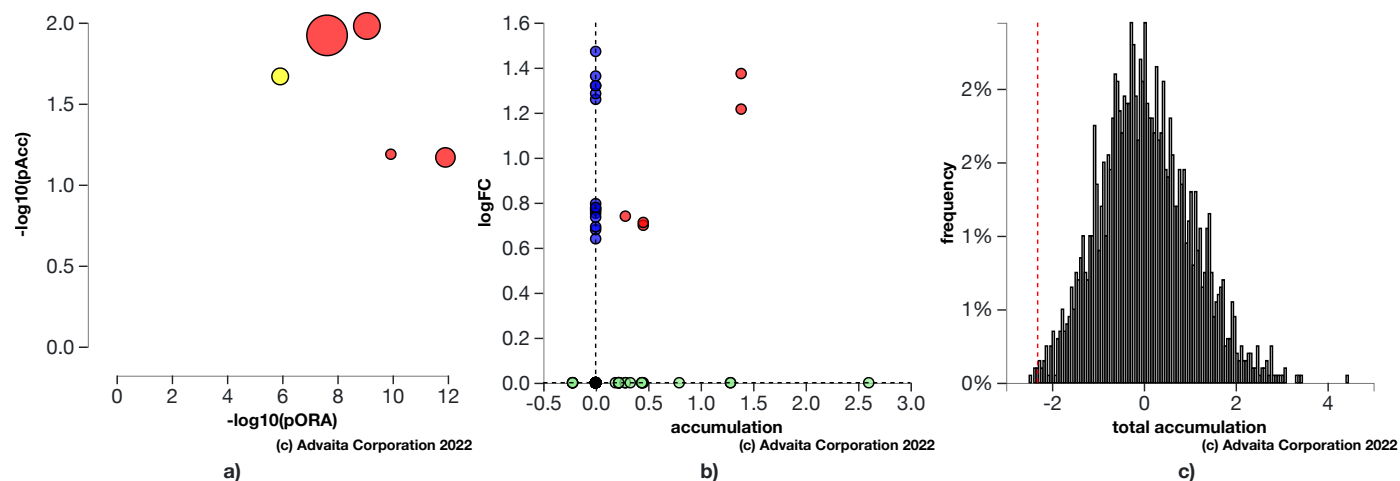


**Fig. 2.2.9: a) Perturbation vs over-representation:** Neurotrophin signaling pathway (KEGG: 04722) (yellow) is shown, using negative log of the accumulation and over-representation  $p$ -values, along with the other most significant pathways. Pathways in red are significant based on the combined uncorrected  $p$ -values, whereas the ones in black are non-significant (where applicable). **b) Gene measured expression vs accumulation:** All the genes from this pathway are represented in terms of their measured fold change ( $y$ -axis) and accumulation ( $x$ -axis). Accumulation is the perturbation received by the gene from any upstream genes. Genes displayed in red had both accumulation and measured fold change. Genes in blue had only measured fold change. Genes in green had only accumulation. The remaining genes that were not measured and had no accumulation are shown in black. **c) Bootstrap diagram:** The perturbation  $p$ -value is computed using bootstrap analysis. Bootstrapping assesses the probability of observing a sum of all absolute gene accumulation total accumulation at least as extreme as the computed one just by chance. A null distribution (gray bars) is computed through an iterative process that is repeated 2000 times. At each iteration, a number of genes equal to the number of differentially expressed genes in this pathway is randomly assigned anywhere in the pathway and the total accumulation is recomputed. The red line indicates the observed total accumulation of genes in the given pathway in relation to the distribution of expected values. The perturbation  $p$ -value is more significant the further away from the mean it is.

## RNA degradation (KEGG: 03018)

The correct processing, quality control and turnover of cellular RNA molecules are critical to many aspects in the expression of genetic information. In eukaryotes, two major pathways of mRNA decay exist and both pathways are initiated by poly(A) shortening of the mRNA. In the 5' to 3' pathway, this is followed by decapping which then permits the 5' to 3' exonucleolytic degradation of transcripts. In the 3' to 5' pathway, the exosome, a large multisubunit complex, plays a key role. The exosome exists in archaeal cells, too. In bacteria, endoribonuclease E, a key enzyme involved in RNA decay and processing, organizes a protein complex called degradosome. RNase E or R interacts with the phosphate-dependent exoribonuclease polynucleotide phosphorylase, DEAD-box helicases, and additional factors in the RNA-degrading complex.

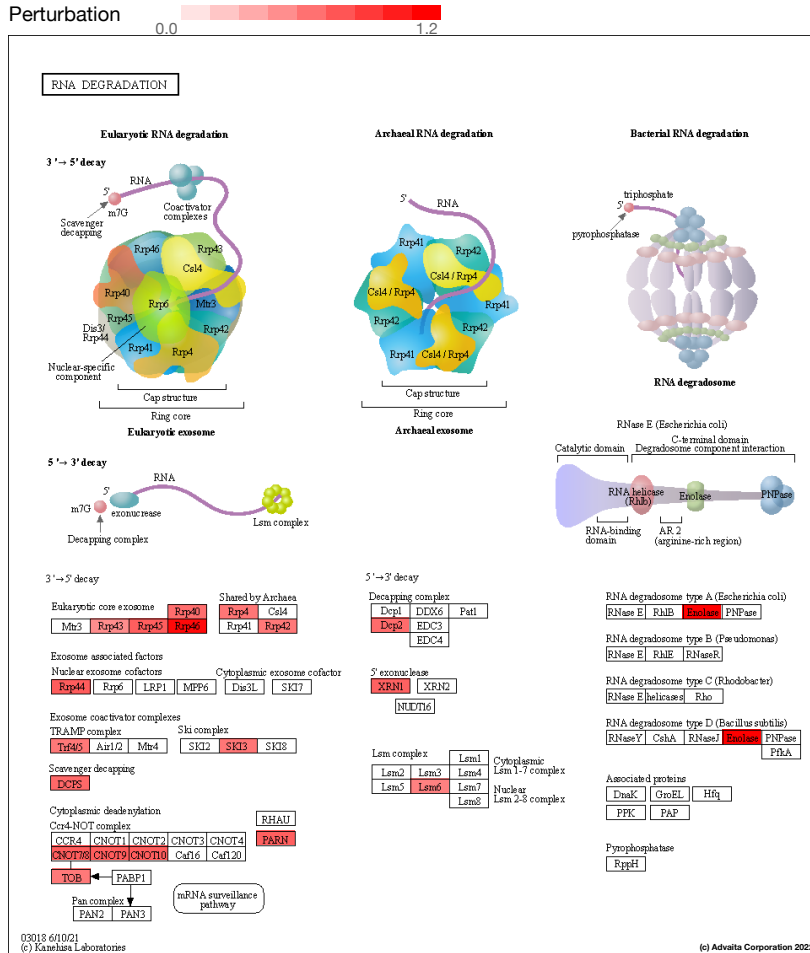


**Fig. 2.2.10: RNA degradation (KEGG: 03018):** The pathway diagram is overlaid with the computed perturbation of each gene. The perturbation accounts both for the gene's measured fold change and for the accumulated perturbation propagated from any upstream genes (accumulation). The highest negative perturbation is shown in dark blue, while the highest positive perturbation in dark red. The legend describes the values on the gradient. Note: For legibility, one gene may be represented in multiple places in the diagram and one box may represent multiple genes in the same gene family. A gene is highlighted in all locations it occurs in the diagram. For each gene family, the color corresponding to the gene with the highest absolute perturbation is displayed.



**Fig. 2.2.11: Gene measured expression bar plot:** All the differentially expressed genes in RNA degradation (KEGG: 03018) are ranked based on their absolute value of log fold change. The plot is limited to the top 20 genes out of a total of 21 differentially expressed genes. Upregulated genes are shown in red, downregulated genes are shown in blue. The box and whisker plot on the left summarizes the distribution of all the differentially expressed genes in this pathway. The box represents the 1st quartile, the median and the 3rd quartile, while the outliers are represented by circles.

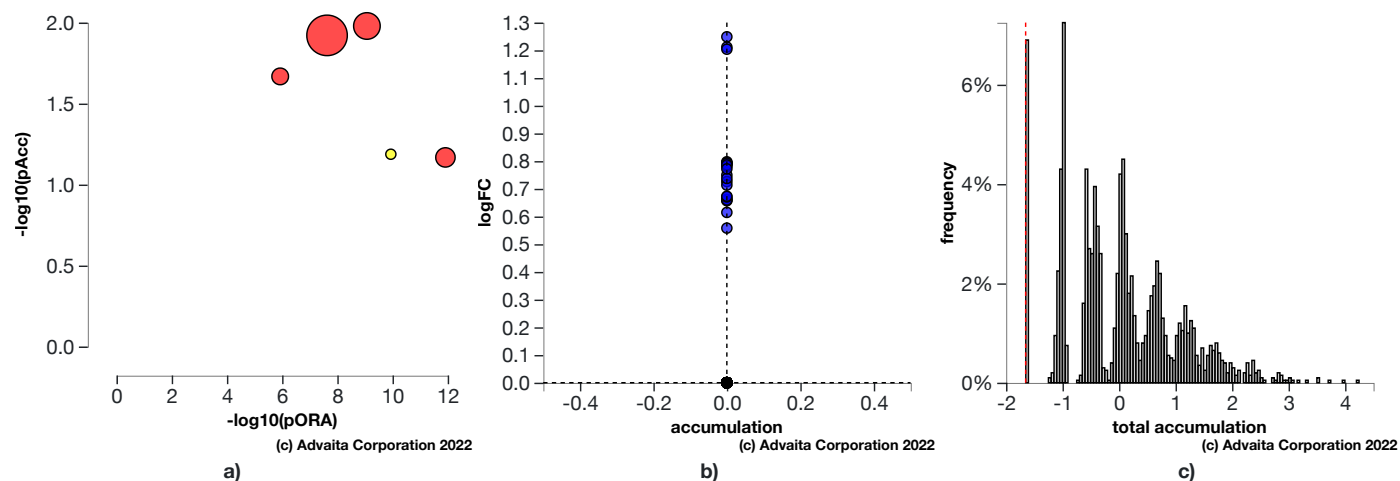


**Fig. 2.2.12: a) Perturbation vs over-representation:** RNA degradation (KEGG: 03018) (yellow) is shown, using negative log of the accumulation and over-representation  $p$ -values, along with the other most significant pathways. Pathways in red are significant based on the combined uncorrected  $p$ -values, whereas the ones in black are non-significant (where applicable). **b) Gene measured expression vs accumulation:** All the genes from this pathway are represented in terms of their measured fold change ( $y$ -axis) and accumulation ( $x$ -axis). Accumulation is the perturbation received by the gene from any upstream genes. Genes in blue had only measured fold change. The remaining genes that were not measured and had no accumulation are shown in black. **c) Bootstrap diagram:** The perturbation  $p$ -value is computed using bootstrap analysis. Bootstrapping assesses the probability of observing a sum of all absolute gene accumulation total accumulation at least as extreme as the computed one just by chance. A null distribution (gray bars) is computed through an iterative process that is repeated 2000 times. At each iteration, a number of genes equal to the number of differentially expressed genes in this pathway is randomly assigned anywhere in the pathway and the total accumulation is recomputed. The red line indicates the observed total accumulation of genes in the given pathway in relation to the distribution of expected values. The perturbation  $p$ -value is more significant the further away from the mean it is.

## Autophagy - animal (KEGG: 04140)

Autophagy (or macroautophagy) is a cellular catabolic pathway involving in protein degradation, organelle turnover, and non-selective breakdown of cytoplasmic components, which is evolutionarily conserved among eukaryotes and exquisitely regulated. This process initiates with production of the autophagosome, a double-membrane intracellular structure of reticular origin that engulfs cytoplasmic contents and ultimately fuses with lysosomes for cargo degradation. Autophagy is regulated in response to extra- or intracellular stress and signals such as starvation, growth factor deprivation and ER stress. Constitutive level of autophagy plays an important role in cellular homeostasis and maintains quality control of essential cellular components.

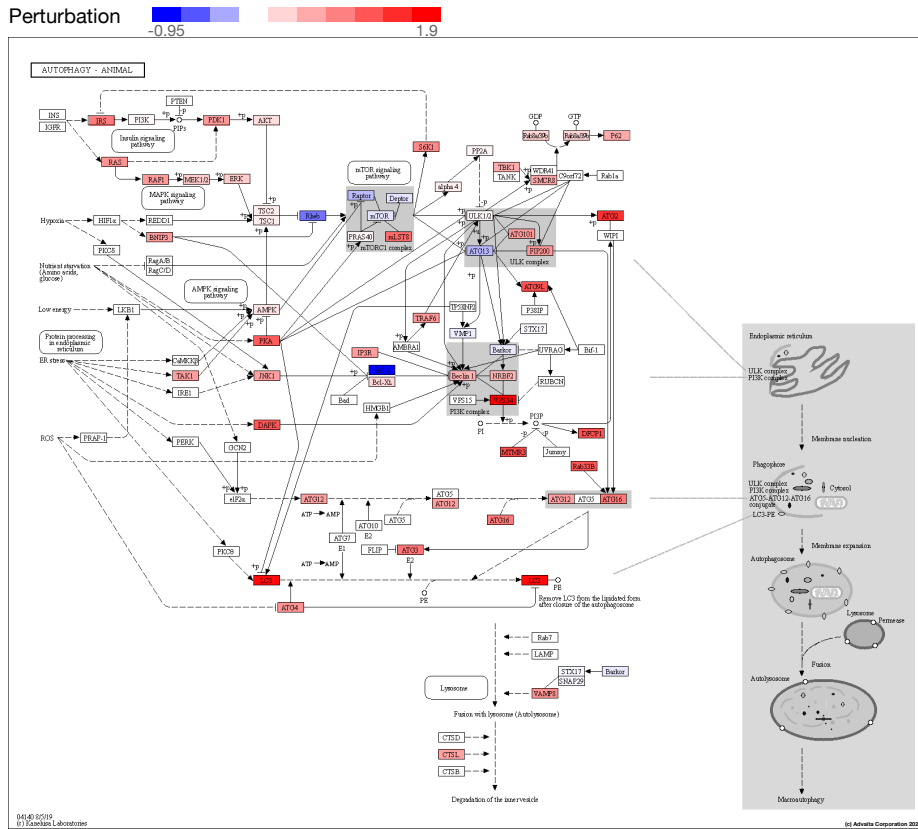
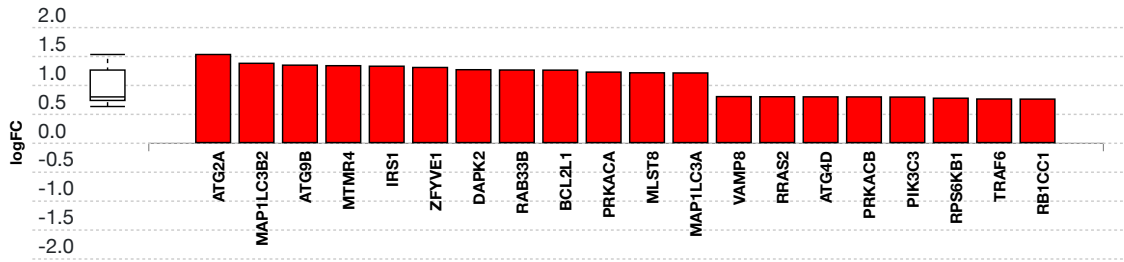


**Fig. 2.2.13: Autophagy - animal (KEGG: 04140):** The pathway diagram is overlaid with the computed perturbation of each gene. The perturbation accounts both for the gene's measured fold change and for the accumulated perturbation propagated from any upstream genes (accumulation). The highest negative perturbation is shown in dark blue, while the highest positive perturbation in dark red. The legend describes the values on the gradient. Note: For legibility, one gene may be represented in multiple places in the diagram and one box may represent multiple genes in the same gene family. A gene is highlighted in all locations it occurs in the diagram. For each gene family, the color corresponding to the gene with the highest absolute perturbation is displayed.



(c) Advaita Corporation 2022

**Fig. 2.2.14: Gene measured expression bar plot:** All the differentially expressed genes in Autophagy - animal (KEGG: 04140) are ranked based on their absolute value of log fold change. The plot is limited to the top 20 genes out of a total of 31 differentially expressed genes. Upregulated genes are shown in red, downregulated genes are shown in blue. The box and whisker plot on the left summarizes the distribution of all the differentially expressed genes in this pathway. The box represents the 1st quartile, the median and the 3rd quartile, while the outliers are represented by circles.

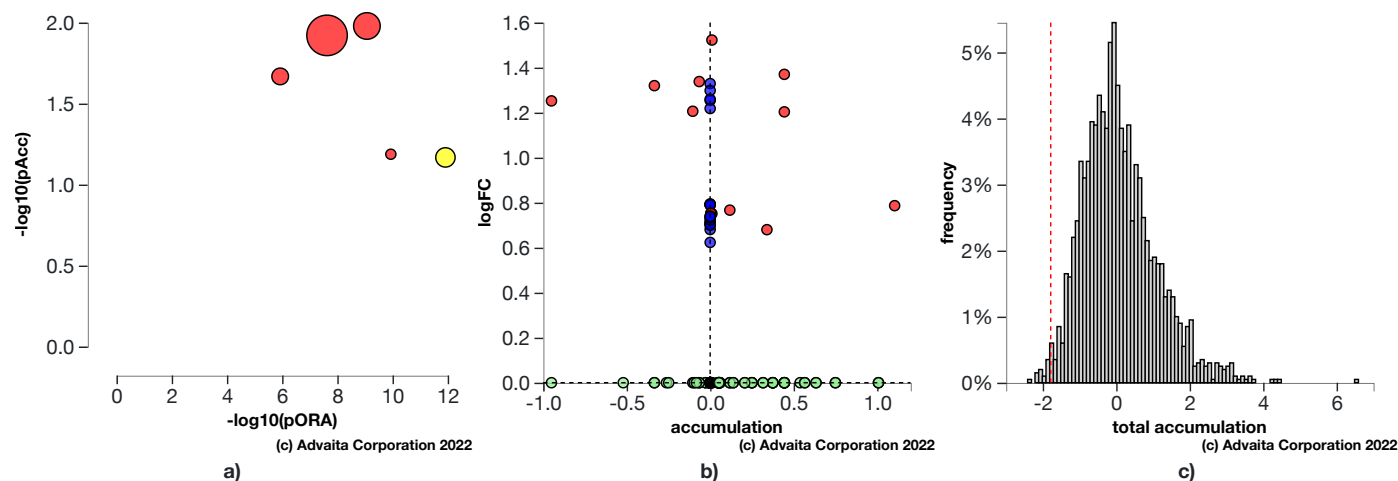


**Fig. 2.2.15: a) Perturbation vs over-representation:** *Autophagy - animal* (KEGG: 04140) (yellow) is shown, using negative log of the accumulation and over-representation  $p$ -values, along with the other most significant pathways. Pathways in red are significant based on the combined uncorrected  $p$ -values, whereas the ones in black are non-significant (where applicable). **b) Gene measured expression vs accumulation:** All the genes from this pathway are represented in terms of their measured fold change ( $y$ -axis) and accumulation ( $x$ -axis). Accumulation is the perturbation received by the gene from any upstream genes. Genes displayed in red had both accumulation and measured fold change. Genes in blue had only measured fold change. Genes in green had only accumulation. The remaining genes that were not measured and had no accumulation are shown in black. **c) Bootstrap diagram:** The perturbation  $p$ -value is computed using bootstrap analysis. Bootstrapping assesses the probability of observing a sum of all absolute gene accumulation total accumulation at least as extreme as the computed one just by chance. A null distribution (gray bars) is computed through an iterative process that is repeated 2000 times. At each iteration, a number of genes equal to the number of differentially expressed genes in this pathway is randomly assigned anywhere in the pathway and the total accumulation is recomputed. The red line indicates the observed total accumulation of genes in the given pathway in relation to the distribution of expected values. The perturbation  $p$ -value is more significant the further away from the mean it is.

## 3. Gene Ontology Analysis

### 3.1. Methods

For each Gene Ontology (GO) term (Ashburner et al., 2002; Gene Ontology Consortium, 2004), the number of differentially expressed (DE) genes annotated to the term is compared to the number of DE genes expected just by chance. iPathwayGuide uses an over-representation approach to compute the statistical significance of observing at least the given number of DE genes. The  $p$ -value is computed using the hypergeometric distribution as described for pORA in the Pathway Analysis section. This  $p$ -value is corrected for multiple comparisons using FDR and Bonferroni.

The classical enrichment method used above considers all GO terms to be independent. By definition, all genes annotated to a GO term are also annotated to its ancestors. Because of this, the enrichment approach counts each gene multiple times by propagating it through the GO hierarchy from the most specific term the gene is associated with, all the way to the root of the ontology. This introduces redundancy in the analysis and reports many general and non-informative terms as significant. To overcome this limitation, iPathwayGuide allows users to use two more sophisticated pruning methods: *high-specificity pruning* and *smallest common denominator pruning*. The **high-specificity** pruning method *identifies the most specific GO terms* that are significantly associated with the set of DE genes. Let us consider, BP1 = “induction of apoptosis by intracellular signals” and BP2 = “induction of apoptosis by extracellular signals,” which are two of the children of BP3 = “induction of apoptosis.” If enough DE genes are associated with BP1 and BP2, the high-specificity pruning will report them as significant. The **smallest common denominator** pruning method *identifies the GO terms that best encapsulate the set of DE genes*, at times consolidating significance of two or more specific terms into their common parent. In the example above, this pruning method might report BP3 as significant because it is the most specific biological term that would include all DE genes that make both BP1 and BP2 significant.

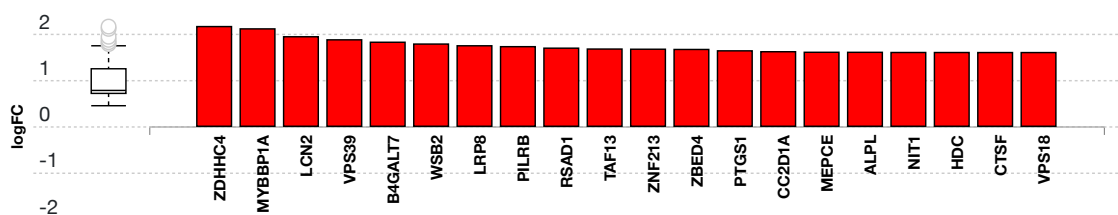
## 3.2. Biological Processes results

Table 3.2.1: Top identified biological processes. Only the top scoring biological process for each pruning type is described below the table.

Pruning Type: None				Pruning Type: High-specificity		Pruning Type: Smallest Common Denominator	
GO Term	p-value	p-value (FDR)	p-value (Bonferroni)	GO Term	p-value	GO Term	p-value
cellular metabolic process	4.100e-19	3.769e-15	3.769e-15	exonucleolytic catabolism of deadenylated mRNA	5.883e-5	exonucleolytic catabolism of deadenylated mRNA	5.883e-5
organonitrogen compound metabolic process	3.600e-15	1.655e-11	3.309e-11	nuclear-transcribed mRNA catabolic process, exonucleolytic, 3'-5'	0.029	tRNA processing	0.004
nitrogen compound metabolic process	1.400e-14	4.290e-11	1.287e-10	U4 snRNA 3'-end processing	0.248	RNA methylation	0.006
cellular macromolecule metabolic process	2.100e-14	4.826e-11	1.930e-10	nuclear polyadenylation-dependent rRNA catabolic process	0.294	nuclear-transcribed mRNA catabolic process, exonucleolytic, 3'-5'	0.015
macromolecule modification	2.300e-13	3.677e-10	2.114e-9	nuclear polyadenylation-dependent tRNA catabolic process	0.294	ribosome biogenesis	0.034

### cellular metabolic process (GO:0044237)

The chemical reactions and pathways by which individual cells transform chemical substances. In this experiment, the algorithm identified 1,540 differentially expressed gene(s) out of ALL 10,861 gene(s).

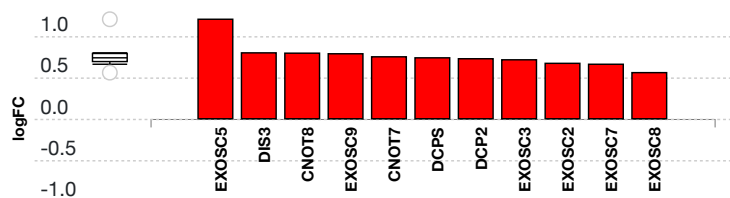


(c) Advaita Corporation 2022

Fig. 3.2.1: Gene measured expression bar plot: All the differentially expressed genes that are annotated to cellular metabolic process are ranked based on their absolute value of log fold change. The plot is limited to the top 20 genes out of a total of 1540 differentially expressed genes. Upregulated genes are shown in red, downregulated genes are shown in blue. The box and whisker plot on the left summarizes the distribution of all the differentially expressed genes that are annotated to this GO term. The box represents the 1st quartile, the median and the 3rd quartile, while the outliers are represented by circles.

### exonucleolytic catabolism of deadenylated mRNA (GO:0043928)

The chemical reactions and pathways resulting in the breakdown of the transcript body of a nuclear-transcribed mRNA that occurs when the ends are not protected by the 3'-poly(A) tail. In this experiment, the algorithm identified 11 differentially expressed gene(s) out of ALL 13 gene(s).



(c) Advaita Corporation 2022

**Fig. 3.2.2: Gene measured expression bar plot:** All the differentially expressed genes that are annotated to exonucleolytic catabolism of deadenylated mRNA are ranked based on their absolute value of log fold change. Upregulated genes are shown in red, downregulated genes are shown in blue. The box and whisker plot on the left summarizes the distribution of all the differentially expressed genes that are annotated to this GO term. The box represents the 1st quartile, the median and the 3rd quartile, while the outliers are represented by circles.

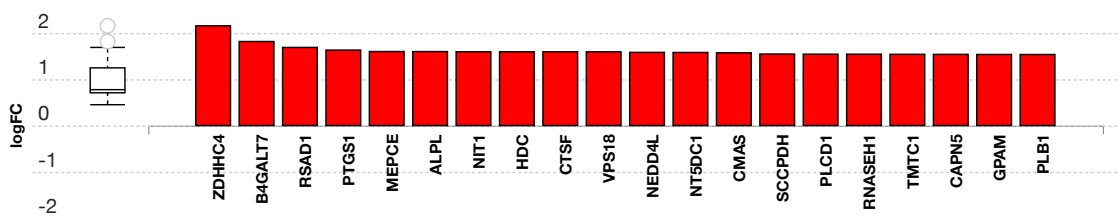
### 3.3. Molecular Functions results

**Table 3.3.1: Top identified molecular functions.** Only the top scoring molecular function for each pruning type is described below the table.

Pruning Type: None				Pruning Type: High-specificity		Pruning Type: Smallest Common Denominator	
GO Term	p-value	p-value (FDR)	p-value (Bonferroni)	GO Term	p-value	GO Term	p-value
catalytic activity	1.500e-18	2.183e-15	3.447e-15	protein binding	1.907e-9	protein binding	1.769e-12
protein binding	1.900e-18	2.183e-15	4.366e-15	guanyl-nucleotide exchange factor activity	0.010	3'-5' exonuclease activity	0.003
catalytic activity, acting on a nucleic acid	3.100e-10	2.375e-7	7.124e-7	RNA binding	0.041	guanyl-nucleotide exchange factor activity	0.007
transferase activity	2.700e-9	1.551e-6	6.205e-6	3'-5'-exoribonuclease activity	0.155	exoribonuclease activity	0.007
catalytic activity, acting on RNA	1.900e-8	8.732e-6	4.366e-5	GTP binding	0.234	RNA binding	0.011

#### catalytic activity (GO:0003824)

Catalysis of a biochemical reaction at physiological temperatures. In biologically catalyzed reactions, the reactants are known as substrates, and the catalysts are naturally occurring macromolecular substances known as enzymes. Enzymes possess specific binding sites for substrates, and are usually composed wholly or largely of protein, but RNA that has catalytic activity (ribozyme) is often also regarded as enzymatic. In this experiment, the algorithm identified **911** differentially expressed gene(s) out of ALL **5,574** gene(s).

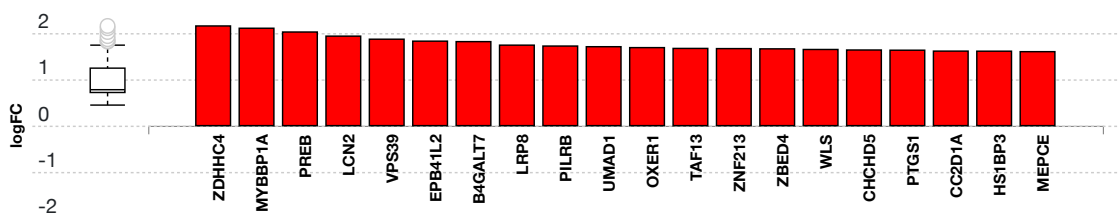


(c) Advaita Corporation 2022

**Fig. 3.3.3: Gene measured expression bar plot:** All the differentially expressed genes that are annotated to catalytic activity are ranked based on their absolute value of log fold change. The plot is limited to the top 20 genes out of a total of 911 differentially expressed genes. Upregulated genes are shown in red, downregulated genes are shown in blue. The box and whisker plot on the left summarizes the distribution of all the differentially expressed genes that are annotated to this GO term. The box represents the 1st quartile, the median and the 3rd quartile, while the outliers are represented by circles.

#### protein binding (GO:0005515)

Binding to a protein. In this experiment, the algorithm identified **1,963** differentially expressed gene(s) out of ALL **13,830** gene(s).



(c) Advaita Corporation 2022

**Fig. 3.3.4: Gene measured expression bar plot:** All the differentially expressed genes that are annotated to protein binding are ranked based on their absolute value of log fold change. The plot is limited to the top 20 genes out of a total of 1963 differentially expressed genes. Upregulated genes are shown in red, downregulated genes are shown in blue. The box and whisker plot on the left summarizes the distribution of all the differentially expressed genes that are annotated to this GO term. The box represents the 1st quartile, the median and the 3rd quartile, while the outliers are represented by circles.

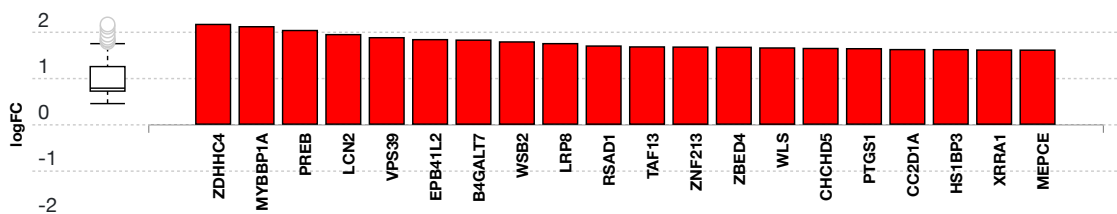
### 3.4. Cellular Components results

**Table 3.4.1: Top identified cellular components.** Only the top scoring cellular component for each pruning type is described below the table.

Pruning Type: None				Pruning Type: High-specificity		Pruning Type: Smallest Common Denominator	
GO Term	p-value	p-value (FDR)	p-value (Bonferroni)	GO Term	p-value	GO Term	p-value
intracellular anatomical structure	1.000e-24	1.000e-24	1.000e-24	nucleoplasm	4.388e-21	cytoplasm	1.000e-24
intracellular membrane-bounded organelle	1.000e-24	1.000e-24	1.000e-24	cytosol	5.546e-20	nucleoplasm	7.314e-23
cytoplasm	1.000e-24	1.000e-24	1.000e-24	mitochondrion	3.169e-6	organelle envelope	6.095e-12
intracellular organelle	1.000e-24	1.000e-24	1.000e-24	mitochondrial matrix	1.219e-5	intracellular membrane-bounded organelle	6.400e-6
membrane-bounded organelle	1.000e-24	1.000e-24	1.000e-24	cytoplasm	1.463e-5	transferase complex	4.876e-4

#### intracellular anatomical structure (GO:0005622)

A component of a cell contained within (but not including) the plasma membrane. In eukaryotes it includes the nucleus and cytoplasm. In this experiment, the algorithm identified **2,189** differentially expressed gene(s) out of ALL **15,336** gene(s).

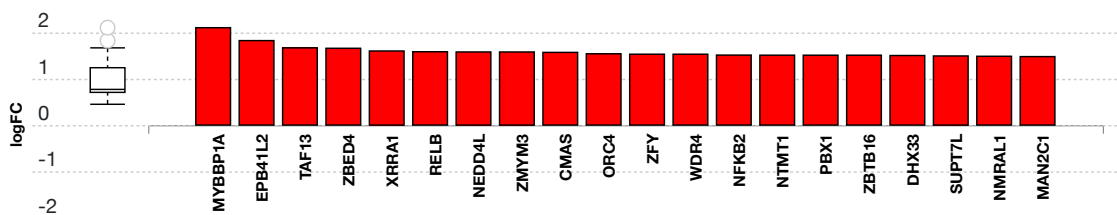


(c) Advaita Corporation 2022

**Fig. 3.4.5: Gene measured expression bar plot:** All the differentially expressed genes that are annotated to intracellular anatomical structure are ranked based on their absolute value of log fold change. The plot is limited to the top 20 genes out of a total of 2189 differentially expressed genes. Upregulated genes are shown in red, downregulated genes are shown in blue. The box and whisker plot on the left summarizes the distribution of all the differentially expressed genes that are annotated to this GO term. The box represents the 1st quartile, the median and the 3rd quartile, while the outliers are represented by circles.

#### nucleoplasm (GO:0005654)

That part of the nuclear content other than the chromosomes or the nucleolus. In this experiment, the algorithm identified **720** differentially expressed gene(s) out of ALL **4,085** gene(s).

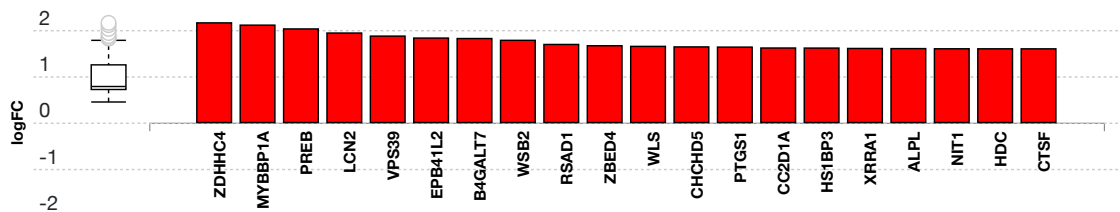


(c) Advaita Corporation 2022

**Fig. 3.4.6: Gene measured expression bar plot:** All the differentially expressed genes that are annotated to nucleoplasm are ranked based on their absolute value of log fold change. The plot is limited to the top 20 genes out of a total of 720 differentially expressed genes. Upregulated genes are shown in red, downregulated genes are shown in blue. The box and whisker plot on the left summarizes the distribution of all the differentially expressed genes that are annotated to this GO term. The box represents the 1st quartile, the median and the 3rd quartile, while the outliers are represented by circles.

### cytoplasm (GO:0005737)

The contents of a cell excluding the plasma membrane and nucleus, but including other subcellular structures. In this experiment, the algorithm identified **1,814** differentially expressed gene(s) out of ALL **11,909** gene(s).



(c) Advaita Corporation 2022

**Fig. 3.4.7: Gene measured expression bar plot:** All the differentially expressed genes that are annotated to cytoplasm are ranked based on their absolute value of log fold change. The plot is limited to the top 20 genes out of a total of 1814 differentially expressed genes. Upregulated genes are shown in red, downregulated genes are shown in blue. The box and whisker plot on the left summarizes the distribution of all the differentially expressed genes that are annotated to this GO term. The box represents the 1st quartile, the median and the 3rd quartile, while the outliers are represented by circles.

## 4. Predicted Upstream Regulator Analysis - miRNAs

### 4.1. Methods

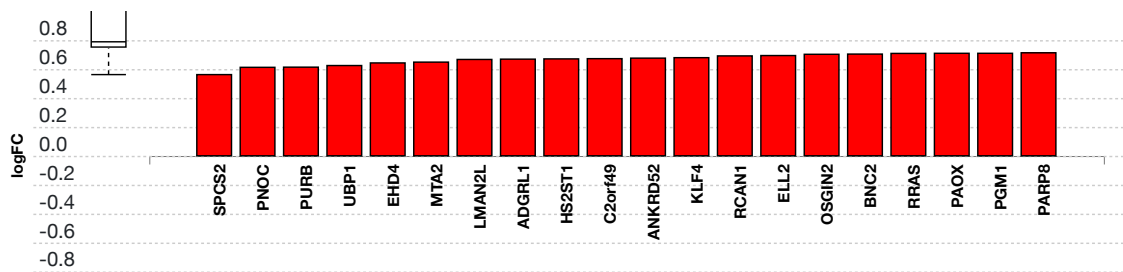
The prediction of active miRNAs (Friedman et al., 2009; Lewis et al., 2005) is based on enrichment of differentially downregulated target genes of the miRNAs. In general, miRNAs have an inhibitory effect on their targets. Therefore, for any given miRNA the method computes the ratio between the number of differentially downregulated targets and all differentially expressed targets, and compares it to the ratio of all downwardly expressed targets to all targets. Overall, iPathwayGuide calculates the probability of observing at least the number of differentially downregulated target genes for a given miRNA just by chance. This p-value is computed using the hypergeometric distribution as described for pORA in the Pathway Analysis section.

### 4.2. Results

Table 4.2.1: Top identified miRNAs

miRNA Name	p-value	p-value (FDR)	p-value (Bonferroni)
hsa-miR-34c-5p	1.000	1.000	1.000
hsa-miR-892c-3p	1.000	1.000	1.000
hsa-miR-330-3p	1.000	1.000	1.000
hsa-let-7g-5p	1.000	1.000	1.000
hsa-miR-299-3p	1.000	1.000	1.000

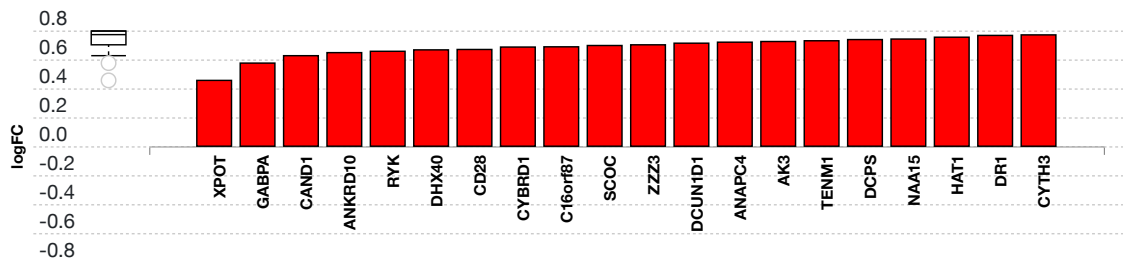
## hsa-miR-34c-5p (MIMAT0000686)



(c) Advaita Corporation 2022

**Fig. 4.2.1: Gene measured expression bar plot:** All the differentially expressed genes that are targeted by hsa-miR-34c-5p are ranked based on their measured expression change (most downregulated to upregulated). The downregulated genes are shown in blue, and the upregulated ones are shown in red (where applicable). The plot is limited to the top 20 genes out of a total of 103 differentially expressed target genes. Out of all the differentially expressed target genes, 0 were found to be downregulated. The box and whisker plot on the left summarizes the distribution of all the differentially expressed genes targeted by this miRNA. The box represents the 1st quartile, the median and the 3rd quartile, while the outliers are represented by circles.

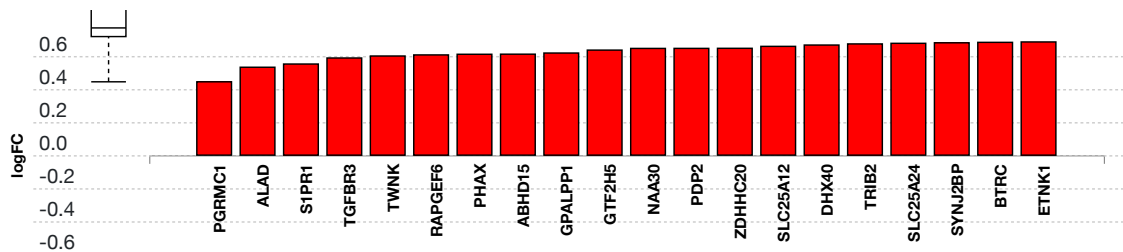
## hsa-miR-892c-3p (MIMAT0025858)



(c) Advaita Corporation 2022

**Fig. 4.2.2: Gene measured expression bar plot:** All the differentially expressed genes that are targeted by hsa-miR-892c-3p are ranked based on their measured expression change (most downregulated to upregulated). The downregulated genes are shown in blue, and the upregulated ones are shown in red (where applicable). The plot is limited to the top 20 genes out of a total of 41 differentially expressed target genes. Out of all the differentially expressed target genes, 0 were found to be downregulated. The box and whisker plot on the left summarizes the distribution of all the differentially expressed genes targeted by this miRNA. The box represents the 1st quartile, the median and the 3rd quartile, while the outliers are represented by circles.

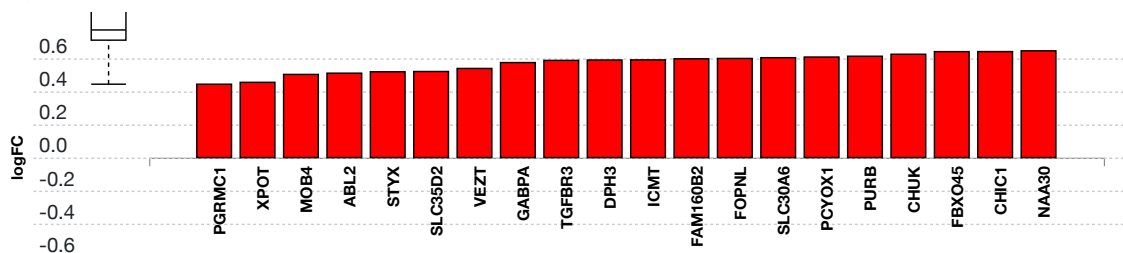
## hsa-miR-330-3p (MIMAT0000751)



(c) Advaita Corporation 2022

**Fig. 4.2.3: Gene measured expression bar plot:** All the differentially expressed genes that are targeted by hsa-miR-330-3p are ranked based on their measured expression change (most downregulated to upregulated). The downregulated genes are shown in blue, and the upregulated ones are shown in red (where applicable). The plot is limited to the top 20 genes out of a total of 153 differentially expressed target genes. Out of all the differentially expressed target genes, 0 were found to be downregulated. The box and whisker plot on the left summarizes the distribution of all the differentially expressed genes targeted by this miRNA. The box represents the 1st quartile, the median and the 3rd quartile, while the outliers are represented by circles.

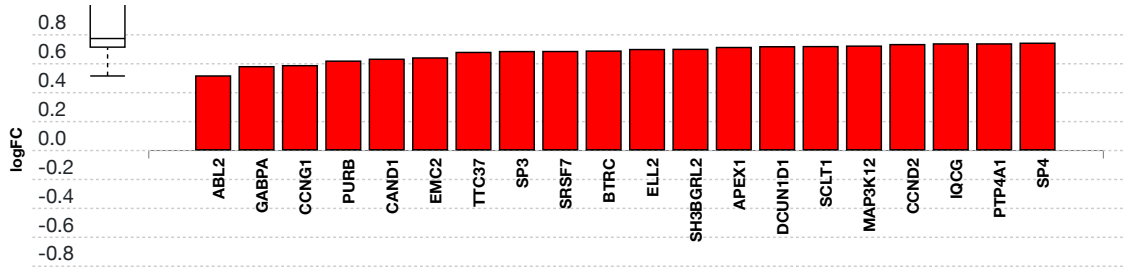
## hsa-let-7g-5p (MIMAT0000414)



(c) Advaita Corporation 2022

**Fig. 4.2.4: Gene measured expression bar plot:** All the differentially expressed genes that are targeted by hsa-let-7g-5p are ranked based on their measured expression change (most downregulated to upregulated). The downregulated genes are shown in blue, and the upregulated ones are shown in red (where applicable). The plot is limited to the top 20 genes out of a total of 193 differentially expressed target genes. Out of all the differentially expressed target genes, 0 were found to be downregulated. The box and whisker plot on the left summarizes the distribution of all the differentially expressed genes targeted by this miRNA. The box represents the 1st quartile, the median and the 3rd quartile, while the outliers are represented by circles.

# hsa-miR-299-3p (MIMAT0000687)



(c) Advaita Corporation 2022

**Fig. 4.2.5: Gene measured expression bar plot:** All the differentially expressed genes that are targeted by hsa-miR-299-3p are ranked based on their measured expression change (most downregulated to upregulated). The downregulated genes are shown in blue, and the upregulated ones are shown in red (where applicable). The plot is limited to the top 20 genes out of a total of 51 differentially expressed target genes. Out of all the differentially expressed target genes, 0 were found to be downregulated. The box and whisker plot on the left summarizes the distribution of all the differentially expressed genes targeted by this miRNA. The box represents the 1st quartile, the median and the 3rd quartile, while the outliers are represented by circles.

## 5. Predicted Upstream Regulator Analysis - Genes

### 5.1. Methods

The prediction of upstream regulators is based on two types of information: i) the enrichment of differentially expressed genes from the experiment and ii) a network of regulatory interactions from our proprietary knowledge base (see the report information for details). The network is a directed graph in which the nodes represent genes, and the edges represent regulatory interactions between two genes. A signed edge in this graph consists of a source gene, a target gene, and a sign to indicate the type of signal: activation (+) or inhibition (-). To create the network, the analysis selects only those edges observed in the literature with at least a medium confidence (evidence score greater than or equal to 400). The analysis considers two hypotheses:

- HA. The upstream regulator is **activated** in the condition studied.
- HI. The upstream regulator is **inhibited** in the condition studied.

The analysis divides the set of all the genes obtained from NCBI Gene database into several subsets based on the measurements in the experiment and the definitions shown in Figure 5.1.1 and Figure 5.1.2. Let the sign of a measured DE gene be the sign of the log fold change value: (+) for up-regulated genes and (-) for down-regulated genes. A gene is a target gene if it corresponds to a node in the network that has at least one incoming edge. We define a *consistent gene* as a target DE gene such that the sign of the gene is consistent both with the type of the signal **and** with the hypothesis considered. Formally, by definition, a target DE gene  $g$  is consistent with Hypothesis HA if and only if an incoming edge  $e$  exists such that  $sign(g) = sign(e)$ . In other words, this describes the situation when the upstream regulator is predicted as activated, the signal is activation and the target DE gene is up-regulated, or the signal is inhibition and the target DE gene is down-regulated (see panel A in Figure 5.1.1). A target DE gene  $g$  is consistent with Hypothesis HI if and only if an incoming edge  $e$  exists such that  $sign(g) \neq sign(e)$ . This second case captures the situation in which the upstream regulator is inhibited, the signal is inhibition and the target DE gene is up-regulated, or the signal is activation and the target DE gene is down-regulated (see panel B in Figure 5.1.1).

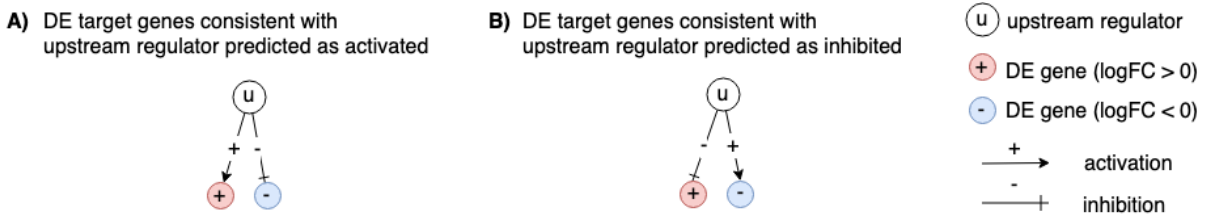


**Fig. 5.1.1: Target genes consistent with the hypothesis considered:** In panel A, the signs of the DE genes match the signs of their respective incoming edges, increasing the likelihood that the upstream regulator  $u$  is activated. In panel B, the signs of the DE genes are opposite to the signs of their edges, increasing the likelihood that the upstream regulator  $u$  is inhibited.

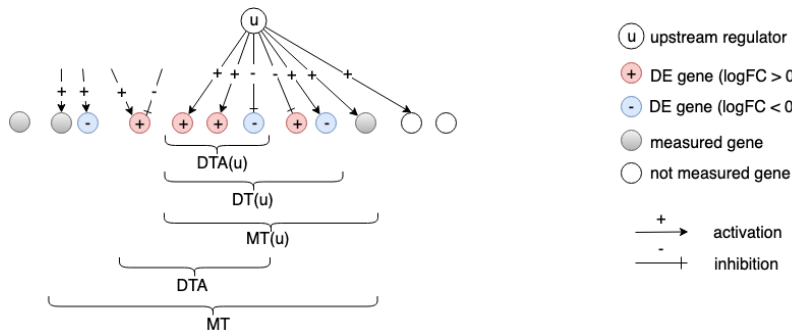


**Fig. 5.1.2:** The set of all genes includes the set of measured genes that are also targets in the network, or *Measured Targets (MT)*. We define the subset of "DE Targets consistent with the first hypothesis that the upstream regulators are Activated", *DTA*. For a selected upstream regulator  $u$ , we have the set of "Measured Targets of  $u$ "  $MT(u)$ , "Differentially expressed Targets downstream of  $u$ "  $DT(u)$ , and the set of "DE targets consistent with the hypothesis HA that  $u$  is Activated"  $DTA(u)$ . The equivalent graphic for the hypothesis HI associated with  $DTI$  and  $DTI(u)$  is

not shown.

## Upstream regulators Z-score

For both research hypotheses, the analysis computes a Z-score for each upstream regulator  $z(u)$  by iterating over the genes in  $DT(u)$  and their incoming edges  $in(g)$ . We can then compute the p-value corresponding to the z-score  $P_z$  as the one-tailed area under the probability density function for a normal distribution,  $N(0,1)$ .

## Upstream regulators predicted as activated

Here, the research hypothesis considers the upstream regulator as activated. For each upstream regulator  $u$ , the number of consistent DE genes downstream of  $u$ ,  $DTA(u)$  is compared to the number of measured target genes expected to be both consistent and DE just by chance. iPathwayGuide uses an over-representation approach to compute the statistical significance of observing at least the given number of consistent DE genes. The p-value  $P_{act}$  is computed using the hypergeometric distribution (Draghici et al., 2003, Draghici 2011).

After computing a p-value for both types of evidence,  $P_z$  and  $P_{act}$ , we need to combine these two probabilities into one global probability value,  $P_G$  that is used to rank the upstream regulators and test the research hypothesis that the upstream regulators are predicted as activated in the condition studied. Since only a positive z-score indicates that the upstream regulator is predicted as activated, we only combine p-values for a positive z-score. Moreover, to avoid introducing false positives, only  $P_z$  for significant z-scores ( $z \geq 2$ ) are combined. The analysis uses the standard Fisher's method to combine p-values into one test statistic (Fisher 1925).

## Upstream regulators predicted as inhibited

In parallel with upstream regulators predicted as activated, we use  $P_{inh}$  and  $P_z$  to predict upstream regulators that are inhibited. Here, the research hypothesis states that the upstream regulators are inhibited in the conditions studied. For each upstream regulator  $u$ , the number of consistent DE genes downstream of  $u$ ,  $DTI(u)$  is compared to the number of measured target genes expected to be both consistent and DE just by chance. Using the Fisher's method as above, the analysis combines  $P_{inh}$  and  $P_z$ , where  $P_z$  is considered only for significant negative z-scores ( $z \leq -2$ ).

## 5.2. Results: upstream regulators predicted as activated

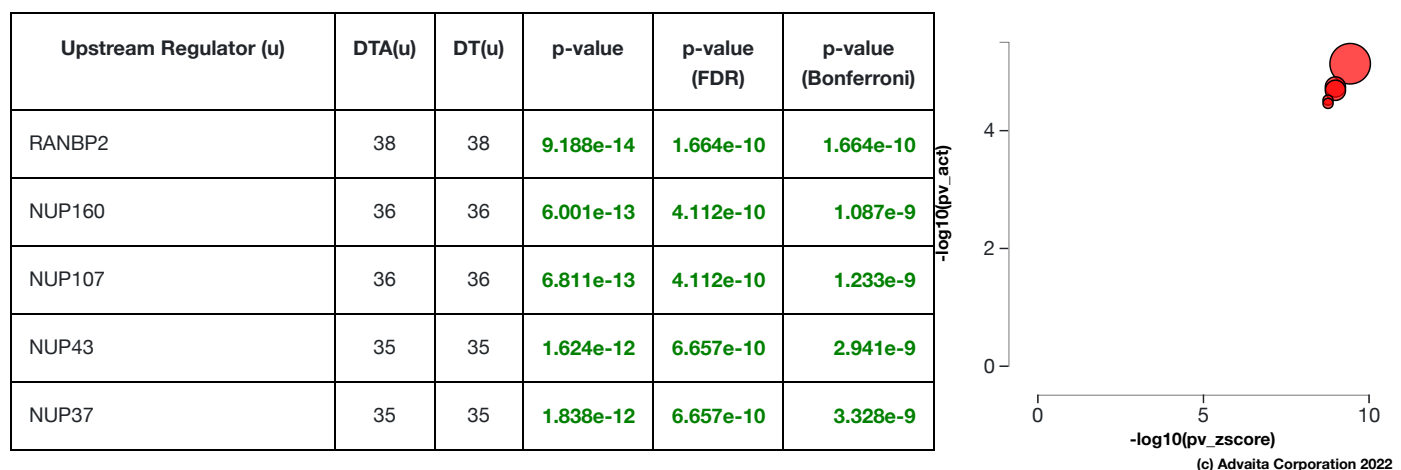


**Table 5.2.1: Top upstream regulators predicted as activated.** For each upstream regulator  $u$ , the table shows the number of DE targets supporting the hypothesis that the regulator is activated  $DTA(u)$  the total number of DE genes downstream of  $u$   $DT(u)$ , the combined raw p-value, and the p-value corrected for multiple comparisons. **Fig. 5.2.1: A two-way plot showing the top five upstream regulators predicted as activated.** Dots representing upstream regulators are positioned using  $P_{zscore}$  on the horizontal axis, and using  $P_{act}$  on the vertical axis.  $P_{act}$  is the p-value based on the number of DE targets consistent with the type of the incoming signal and with the selected hypothesis type. Upstream regulators with a significant combined p-value are shown in red. The size of each dot represents the number of consistent DE genes for that regulator.

## RANBP2 (RAN binding protein 2)

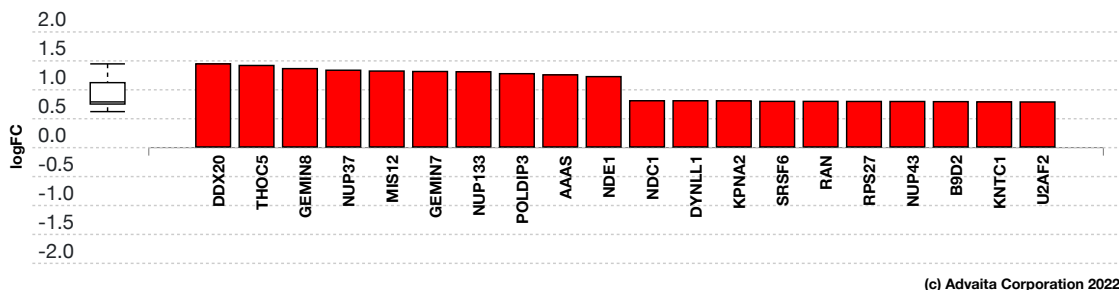


**Fig. 5.2.3: Gene measured expression bar plot:** All the consistent differentially expressed genes that are targeted by RANBP2 are ranked based on their absolute value of log fold change. The plot is limited to the top 20 genes out of a total of 38 consistent differentially expressed target genes. Upregulated genes are shown in red, downregulated genes are shown in blue. The box and whisker plot on the left summarizes the distribution of all the consistent differentially expressed genes targeted by this upstream regulator. The box shows the 1st quartile, the median and the 3rd quartile, while the outliers are represented by circles.

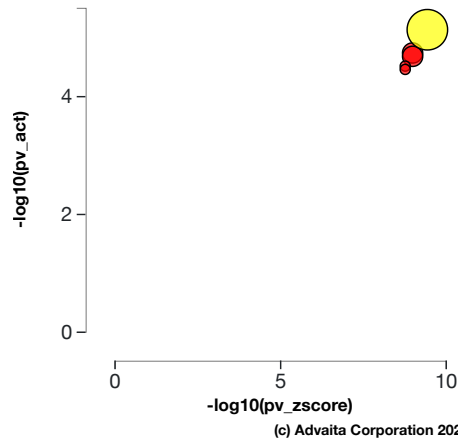


**Fig. 5.2.4: Activation p-value vs zscore p-value:** *RANBP2*, *RAN* binding protein 2, (yellow) is shown, using negative log of the activation and zscore p-values, along with the other most significant upstream regulators. The size of the dot represents the relative number of consistent DE genes, which for selected upstream regulator is 38.

### NUP160 (nucleoporin 160)

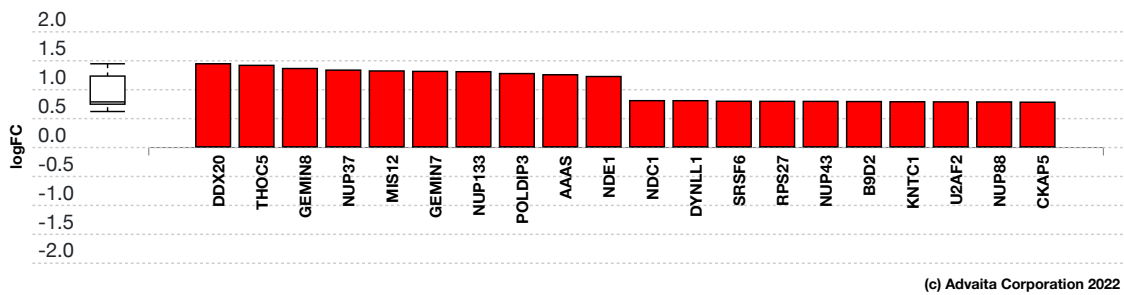


**Fig. 5.2.5: Gene measured expression bar plot:** All the consistent differentially expressed genes that are targeted by *NUP160* are ranked based on their absolute value of log fold change. The plot is limited to the top 20 genes out of a total of 36 consistent differentially expressed target genes. Upregulated genes are shown in red, downregulated genes are shown in blue. The box and whisker plot on the left summarizes the distribution of all the consistent differentially expressed genes targeted by this upstream regulator. The box shows the 1st quartile, the median and the 3rd quartile, while the outliers are represented by circles.

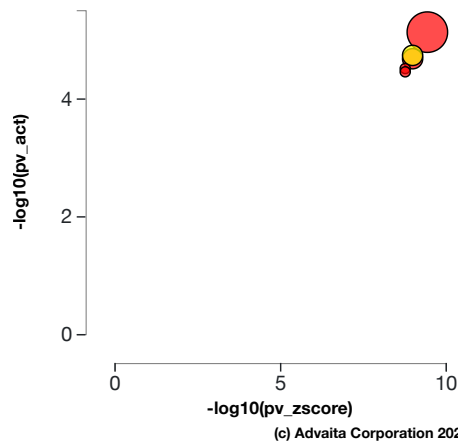
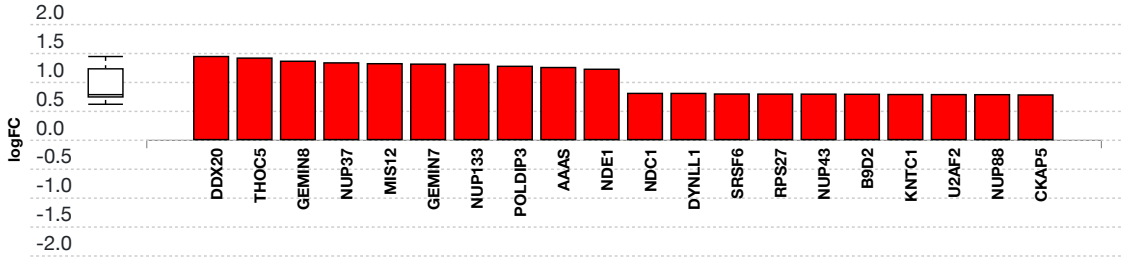


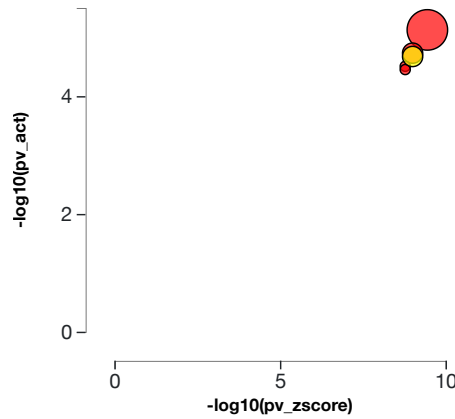
**Fig. 5.2.6: Activation p-value vs zscore p-value:** *NUP160*, nucleoporin 160, (yellow) is shown, using negative log of the activation and zscore p-values, along with the other most significant upstream regulators. The size of the dot represents the relative number of consistent DE genes, which for selected upstream regulator is 36.

### NUP107 (nucleoporin 107)



(c) Advaita Corporation 2022

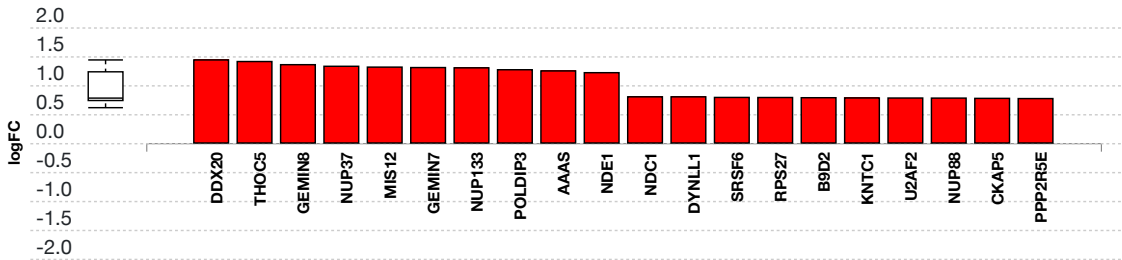
**Fig. 5.2.7: Gene measured expression bar plot:** All the consistent differentially expressed genes that are targeted by NUP107 are ranked based on their absolute value of log fold change. The plot is limited to the top 20 genes out of a total of 36 consistent differentially expressed target genes. Upregulated genes are shown in red, downregulated genes are shown in blue. The box and whisker plot on the left summarizes the distribution of all the consistent differentially expressed genes targeted by this upstream regulator. The box shows the 1st quartile, the median and the 3rd quartile, while the outliers are represented by circles.



(c) Advaita Corporation 2022

**Fig. 5.2.8: Activation p-value vs zscore p-value:** NUP107, nucleoporin 107, (yellow) is shown, using negative log of the activation and zscore p-values, along with the other most significant upstream regulators. The size of the dot represents the relative number of consistent DE genes, which for selected upstream regulator is 36.

### NUP43 (nucleoporin 43)



(c) Advaita Corporation 2022

**Fig. 5.2.9: Gene measured expression bar plot:** All the consistent differentially expressed genes that are targeted by NUP43 are ranked based on their absolute value of log fold change. The plot is limited to the top 20 genes out of a total of 35 consistent differentially expressed target genes. Upregulated genes are shown in red, downregulated genes are shown in blue. The box and whisker plot on the left summarizes the distribution of all the consistent differentially expressed genes targeted by this upstream regulator. The box shows the 1st quartile, the median and the 3rd quartile, while the outliers are represented by circles.

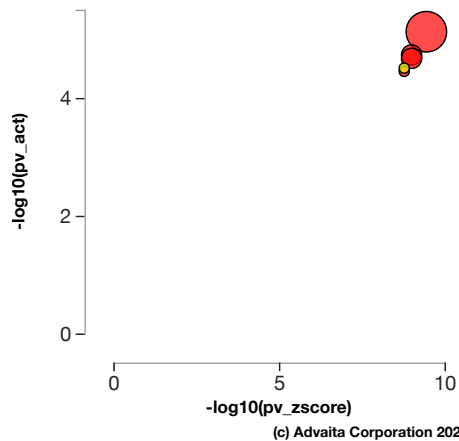


Fig. 5.2.10: Activation p-value vs zscore p-value: NUP43, nucleoporin 43, (yellow) is shown, using negative log of the activation and zscore p-values, along with the other most significant upstream regulators. The size of the dot represents the relative number of consistent DE genes, which for selected upstream regulator is 35.

### NUP37 (nucleoporin 37)

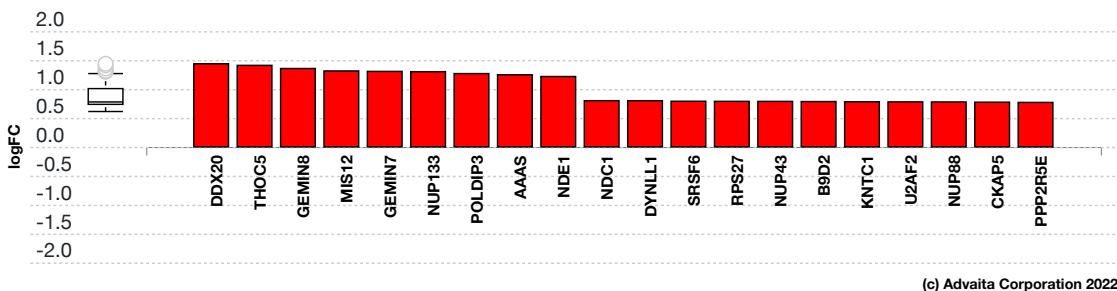


Fig. 5.2.11: Gene measured expression bar plot: All the consistent differentially expressed genes that are targeted by NUP37 are ranked based on their absolute value of log fold change. The plot is limited to the top 20 genes out of a total of 35 consistent differentially expressed target genes. Upregulated genes are shown in red, downregulated genes are shown in blue. The box and whisker plot on the left summarizes the distribution of all the consistent differentially expressed genes targeted by this upstream regulator. The box shows the 1st quartile, the median and the 3rd quartile, while the outliers are represented by circles.

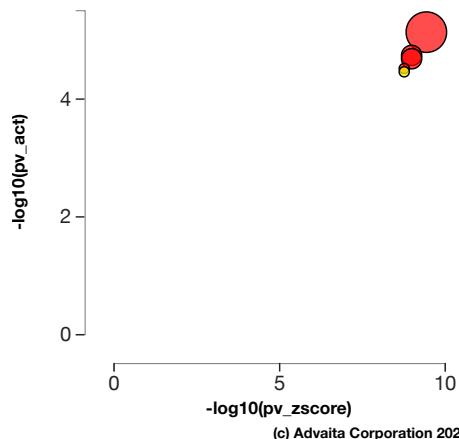
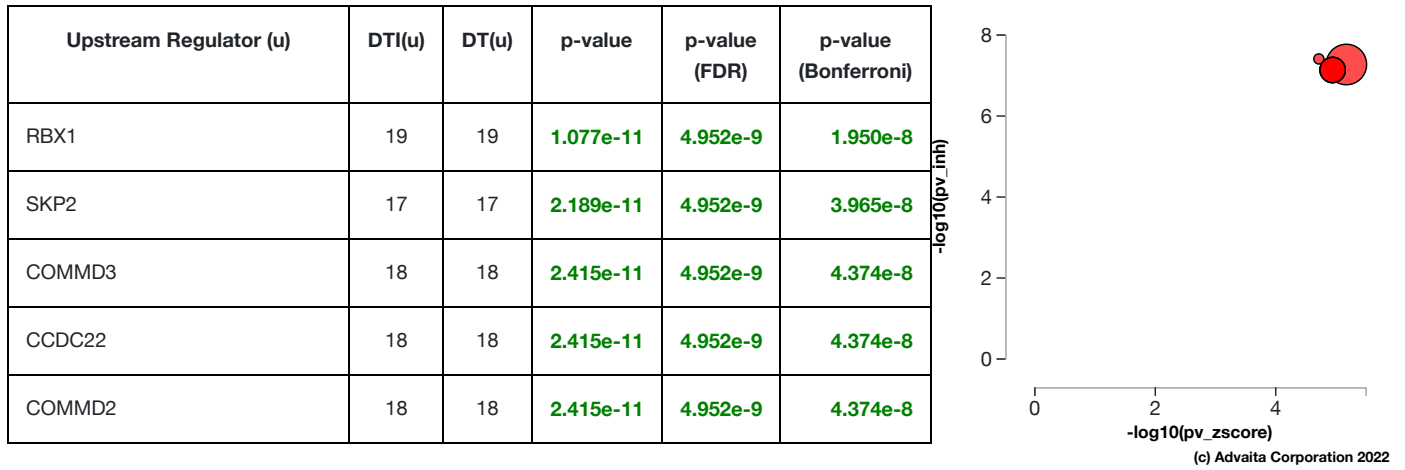


Fig. 5.2.12: Activation p-value vs zscore p-value: NUP37, nucleoporin 37, (yellow) is shown, using negative log of the activation and zscore p-values, along with the other most significant upstream regulators. The size of the dot represents the relative number of consistent DE genes, which for selected upstream regulator is 35.

### 5.3. Results: upstream regulators predicted as inhibited



**Table 5.3.1: Top upstream regulators predicted as inhibited.** For each upstream regulator *u*, the table shows the number of DE targets supporting the hypothesis that the regulator is inhibited DTI(*u*) the total number of DE genes downstream of *u* DT(*u*), the combined raw *p*-value, and the *p*-value corrected for multiple comparisons. **Fig. 5.3.1: A two-way plot showing the top five upstream regulators predicted as inhibited.** Dots representing upstream regulators are positioned using  $P_{zscore}$  on the horizontal axis, and using  $P_{inh}$  on the vertical axis.  $P_{inh}$  is the *p*-value based on the number of DE targets consistent with the type of the incoming signal and with the selected hypothesis type. Upstream regulators with a significant combined *p*-value are shown in red. The size of each dot represents the number of consistent DE genes for that regulator.

#### RBX1 (ring-box 1)

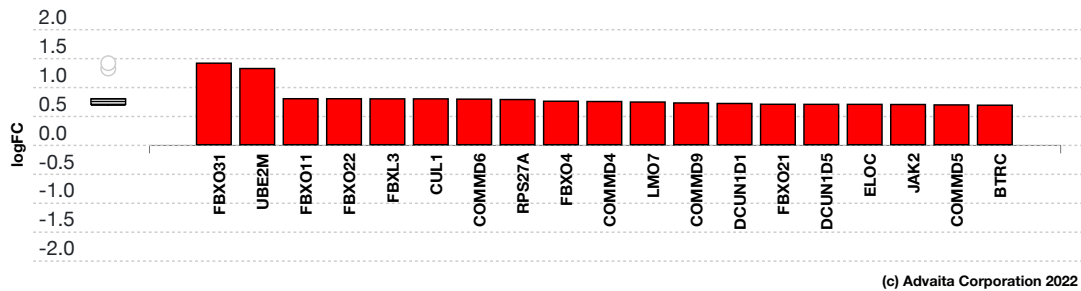


**Fig. 5.3.13: Gene measured expression bar plot:** All the consistent differentially expressed genes that are targeted by RBX1 are ranked based on their absolute value of log fold change. Upregulated genes are shown in red, downregulated genes are shown in blue. The box and whisker plot on the left summarizes the distribution of all the consistent differentially expressed genes targeted by this upstream regulator. The box shows the 1st quartile, the median and the 3rd quartile, while the outliers are represented by circles.

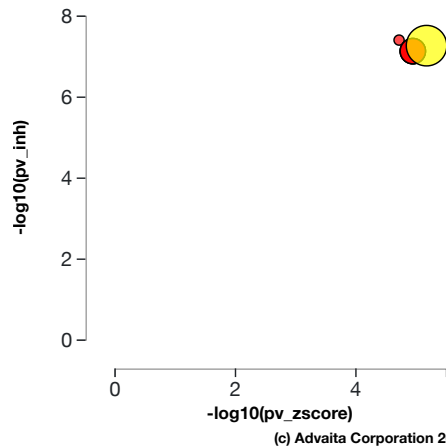


**Fig. 5.3.14: Inhibition *p*-value vs zscore *p*-value:** RBX1, ring-box 1, (yellow) is shown, using negative log of the inhibition and zscore *p*-values, along with the other most significant upstream regulators. The size of the dot represents the relative number of consistent DE genes, which for selected upstream regulator is 19.

### SKP2 (S-phase kinase associated protein 2)

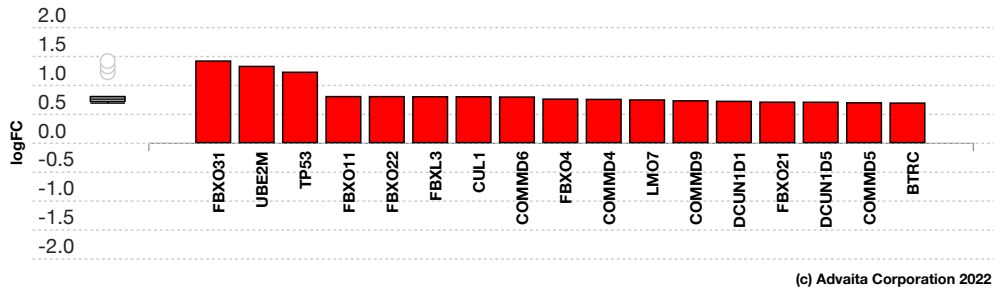


**Fig. 5.3.15: Gene measured expression bar plot:** All the consistent differentially expressed genes that are targeted by SKP2 are ranked based on their absolute value of log fold change. Upregulated genes are shown in red, downregulated genes are shown in blue. The box and whisker plot on the left summarizes the distribution of all the consistent differentially expressed genes targeted by this upstream regulator. The box shows the 1st quartile, the median and the 3rd quartile, while the outliers are represented by circles.

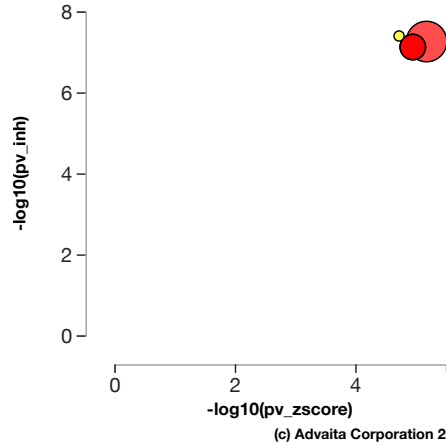


**Fig. 5.3.16: Inhibition p-value vs zscore p-value:** SKP2, S-phase kinase associated protein 2, (yellow) is shown, using negative log of the inhibition and zscore p-values, along with the other most significant upstream regulators. The size of the dot represents the relative number of consistent DE genes, which for selected upstream regulator is 17.

### COMMD3 (COMM domain containing 3)

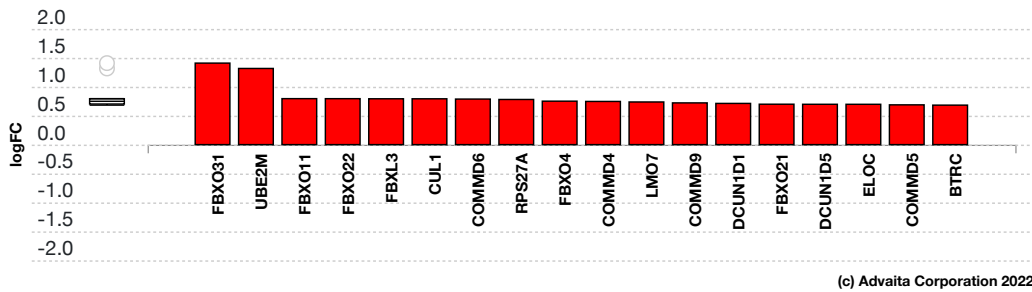
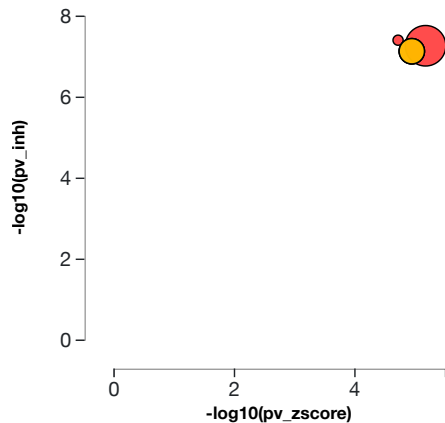


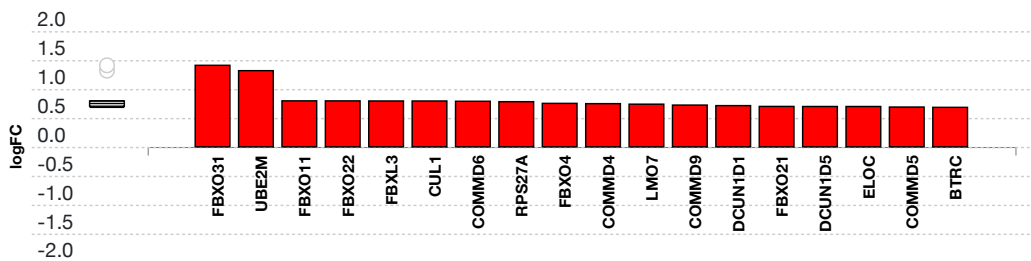
**Fig. 5.3.17: Gene measured expression bar plot:** All the consistent differentially expressed genes that are targeted by COMMD3 are ranked based on their absolute value of log fold change. Upregulated genes are shown in red, downregulated genes are shown in blue. The box and whisker plot on the left summarizes the distribution of all the consistent differentially expressed genes targeted by this upstream regulator. The box shows the 1st quartile, the median and the 3rd quartile, while the outliers are represented by circles.



(c) Advaita Corporation 2022

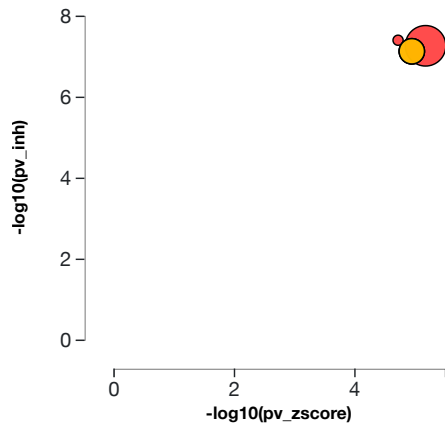
Fig. 5.3.18: Inhibition p-value vs zscore p-value: COMMD3, COMM domain containing 3, (yellow) is shown, using negative log of the inhibition and zscore p-values, along with the other most significant upstream regulators. The size of the dot represents the relative number of consistent DE genes, which for selected upstream regulator is 18.

### CCDC22 (coiled-coil domain containing 22)



(c) Advaita Corporation 2022

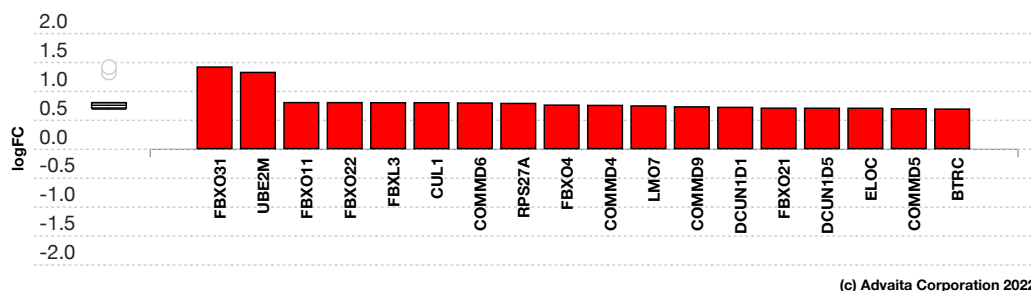
Fig. 5.3.19: Gene measured expression bar plot: All the consistent differentially expressed genes that are targeted by CCDC22 are ranked based on their absolute value of log fold change. Upregulated genes are shown in red, downregulated genes are shown in blue. The box and whisker plot on the left summarizes the distribution of all the consistent differentially expressed genes targeted by this upstream regulator. The box shows the 1st quartile, the median and the 3rd quartile, while the outliers are represented by circles.



(c) Advaita Corporation 2022

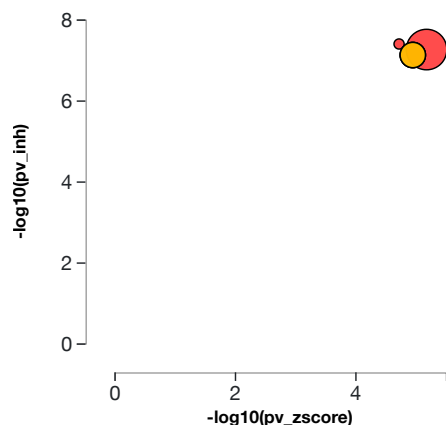
Fig. 5.3.20: Inhibition p-value vs zscore p-value: CCDC22, coiled-coil domain containing 22, (yellow) is shown, using negative log of the inhibition and zscore p-values, along with the other most significant upstream regulators. The size of the dot represents the relative number of consistent DE genes, which for selected upstream regulator is 18.

## COMMD2 (COMM domain containing 2)



(c) Advaita Corporation 2022

**Fig. 5.3.21: Gene measured expression bar plot:** All the consistent differentially expressed genes that are targeted by COMMD2 are ranked based on their absolute value of log fold change. Upregulated genes are shown in red, downregulated genes are shown in blue. The box and whisker plot on the left summarizes the distribution of all the consistent differentially expressed genes targeted by this upstream regulator. The box shows the 1st quartile, the median and the 3rd quartile, while the outliers are represented by circles.



(c) Advaita Corporation 2022

**Fig. 5.3.22: Inhibition p-value vs zscore p-value:** COMMD2, COMM domain containing 2, (yellow) is shown, using negative log of the inhibition and zscore p-values, along with the other most significant upstream regulators. The size of the dot represents the relative number of consistent DE genes, which for selected upstream regulator is 18.

## 6. Predicted Upstream Regulator Analysis – Chemicals, Drugs, Toxicants (CDTs)

### 6.1. Methods

The prediction of upstream Chemicals, Drugs, Toxicants (CDTs) is based on two types of information: i) the enrichment of differentially expressed genes from the experiment and ii) a network of interactions from the Advaita Knowledge Base (AKB v2201). The network is a directed graph in which the source node represents either a chemical substance or compound (e.g. zinc), a drug (e.g. aspirin), or a toxicant (e.g. tobacco smoke). The generic abbreviation CDT will be used henceforth to designate any of these. The edges represent known effects that these CDTs have on various genes. A signed edge in this graph consists of a source CDT, a target gene, and a sign to indicate the type of effect: activation (+) or inhibition (-). The analysis considers two hypotheses:

HP. The upstream chemical, drug or toxicant is **present (or overly abundant)** in the condition studied.

HA. The upstream chemical, drug or toxicant is **absent (or insufficient)** in the condition studied.

The analysis divides the set of all the genes from AKB into several subsets based on the measurements in the experiment and the definitions shown in **Figure 6.1.1** and **Figure 6.1.2**. Let the sign of a measured DE gene be the sign of the log fold change value: (+) for up-regulated genes and (-) for down-regulated genes. A gene is a target gene if it corresponds to a node in the network that has at least one incoming edge. We define a *consistent gene* as a target DE gene such that the sign of the gene is consistent both with the type of the signal **and** with the hypothesis considered. Formally, by definition, a target DE gene  $g$  is consistent with Hypothesis HP if and only if an incoming edge  $e$  exists such that  $sign(g) = sign(e)$ . In other words, this describes the situation when the CDT is predicted as present, the signal is activation and the target DE gene is up-regulated, or the signal is inhibition and the target DE gene is down-regulated (see panel A in **Figure 6.1.1**). A target DE gene  $g$  is consistent with Hypothesis HA if and only if an incoming edge  $e$  exists such that  $sign(g) \neq sign(e)$ . This second case captures the situation in which the CDT is absent (or insufficient), the signal is inhibition and the target DE gene is up-regulated, or the signal is activation and the target DE gene is down-regulated (see panel B in **Figure 6.1.1**).

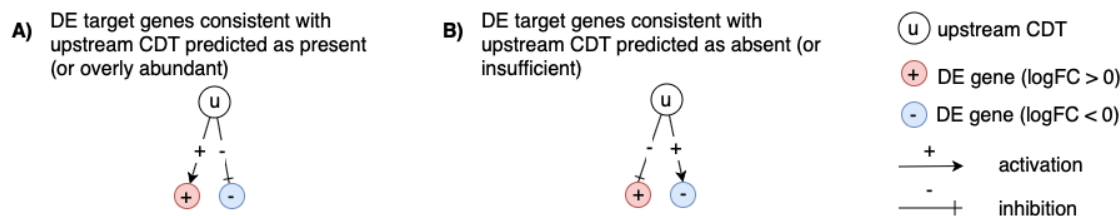


**Fig. 6.1.1: Target genes consistent with the hypothesis considered:** In panel A, the signs of the DE genes match the signs of their respective incoming edges, increasing the likelihood that the CDT  $u$  is present. In panel B, the signs of the DE genes are opposite to the signs of their edges, increasing the likelihood that the CDT  $u$  is absent.

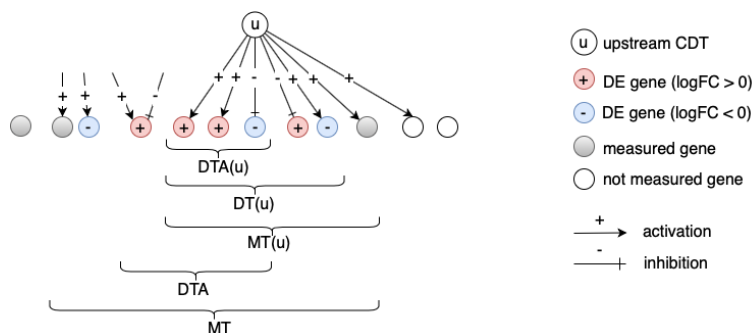


**Fig. 6.1.2:** The set of all genes includes the set of measured genes that are also targets in the network, or Measured Targets (MT). We define the subset of "DE Targets consistent with the first hypothesis that the CDTs are Present (or overly abundant)", DTA. For a selected upstream CDT  $u$ , we have the set of "Measured Targets of  $u$ "  $MT(u)$ , "Differentially expressed Targets downstream of  $u$ "  $DT(u)$ , and the set of "DE targets consistent with the hypothesis HP that  $u$  is Present"  $DTA(u)$ . The equivalent graphic for the hypothesis  $H_A$  associated with  $DTI$  and  $DTI(u)$  is not shown.

## Z-score

For both research hypotheses, the analysis computes a Z-score for each CDT  $z(u)$  by iterating over the genes in  $DT(u)$  and their incoming edges  $in(g)$ . We can then compute the p-value corresponding to the z-score  $P_z$  as the one-tailed area under the probability density function for a normal distribution,  $N(0,1)$ .

## Upstream CDTs predicted as present (or overly abundant)

Here, the research hypothesis considers presence of the CDT. This hypothesis is useful when investigating whether the given phenotype has been impacted by the presence of a given chemical, drug or toxicant (e.g. tobacco smoke, dioxin, etc.). For each CDT  $u$ , the number of consistent DE genes downstream of  $u$ ,  $DTA(u)$  is compared to the number of measured target genes expected to be both consistent and DE just by chance. iPathwayGuide uses an over-representation approach to compute the statistical significance of observing at least the given number of consistent DE genes. The p-value  $P_{pres}$  is computed using the hypergeometric distribution (Draghici et al., 2003, Draghici 2011).

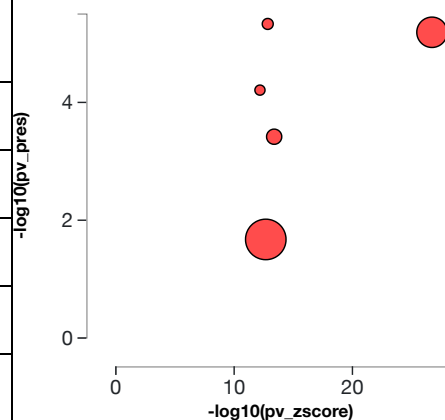
After computing a p-value for both types of evidence,  $P_z$  and  $P_{pres}$ , we combine these two probabilities into one global probability value,  $P_G$  that is used to rank the upstream regulators and test the research hypothesis that the upstream CDTs are predicted as present in the condition studied. The analysis uses the standard Fisher's method to combine p-values into one test statistic (Fisher 1925).

## Upstream CDTs predicted as absent (or insufficient)

In parallel with upstream CDTs predicted as present, we use  $P_{abs}$  and  $P_z$  to predict upstream CDTs that are absent. This hypothesis is relevant when investigating whether the given phenotype has been impacted by the lack of a given chemical that is necessary for the well-functioning of the organism or cell (e.g. a vitamin deficiency, iron deficiency, etc.). Here, the research hypothesis states that the upstream CDT are insufficient in the condition studied. For each upstream CDT  $u$ , the number of consistent DE genes downstream of  $u$ ,  $DTI(u)$  is compared to the number of measured target genes expected to be both consistent and DE just by chance. Using the Fisher's method as above, the analysis combines  $P_{abs}$  and  $P_z$ , where  $P_z$  is considered only for significant negative z-scores ( $z \leq -2$ ).

## 6.2. Results: upstream CDTs predicted as present (or overly abundant)

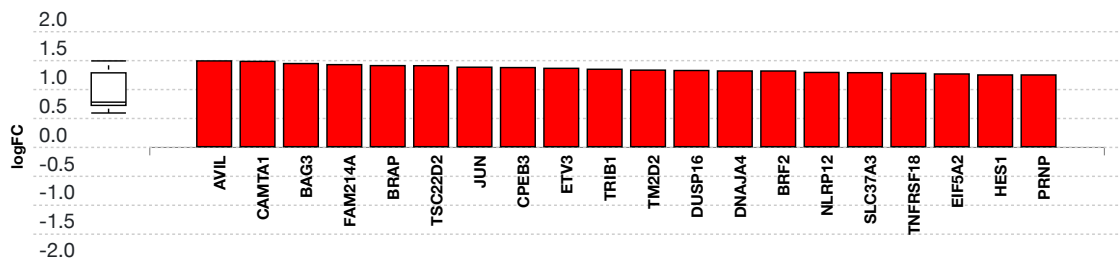
CDT (u)	DTA(u)	DT(u)	p-value	p-value (FDR)	p-value (Bonferroni)
Naphthoquinones	62	63	1.957e-16	2.972e-13	4.323e-13
geldanamycin	59	61	2.437e-15	1.794e-12	5.383e-12
Dihydrotestosterone	131	135	2.691e-16	2.972e-13	5.944e-13
cyllindrospermopsin	77	85	1.435e-14	7.922e-12	3.169e-11
Sodium Selenite	167	224	7.077e-13	3.127e-10	1.563e-9



(c) Advaita Corporation 2022

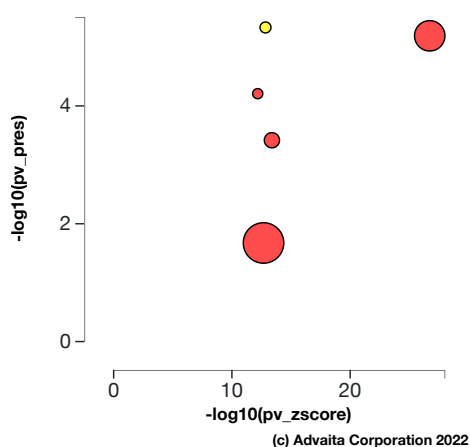
**Table 6.2.1: Top upstream CDTs predicted as present (or overly abundant).** For each upstream CDT *u*, the table shows the number of DE targets supporting the hypothesis that the CDT is present *DTA(u)* the total number of DE genes downstream of *u* *DT(u)*, the combined raw *p*-value, and the *p*-value corrected for multiple comparisons. **Fig. 6.2.1: A two-way plot showing the top five upstream CDTs predicted as present (or overly abundant).** Dots representing upstream CDTs are positioned using  $P_{zscore}$  on the horizontal axis, and using  $P_{pres}$  on the vertical axis.  $P_{pres}$  is the *p*-value based on the number of DE targets consistent with the type of the incoming signal and with the selected hypothesis type. Upstream CDTs with a significant combined *p*-value are shown in red. The size of each dot represents the relative number of consistent DE genes for that CDT.

### Naphthoquinones

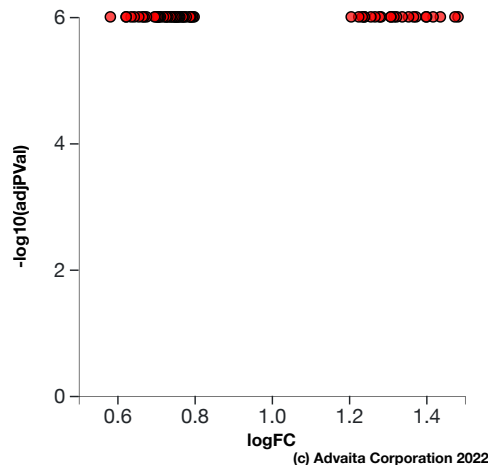


(c) Advaita Corporation 2022

**Fig. 6.2.3: Consistent DE target genes measured expression bar plot:** All the consistent differentially expressed genes that are targeted by Naphthoquinones are ranked based on their absolute value of log fold change. The plot is limited to the top 20 genes out of a total of 62 consistent differentially expressed target genes. Upregulated genes are shown in red, downregulated genes are shown in blue. The box and whisker plot on the left summarizes the distribution of all the consistent differentially expressed genes targeted by this upstream regulator. The box shows the 1st quartile, the median and the 3rd quartile, while any outliers are represented by circles.



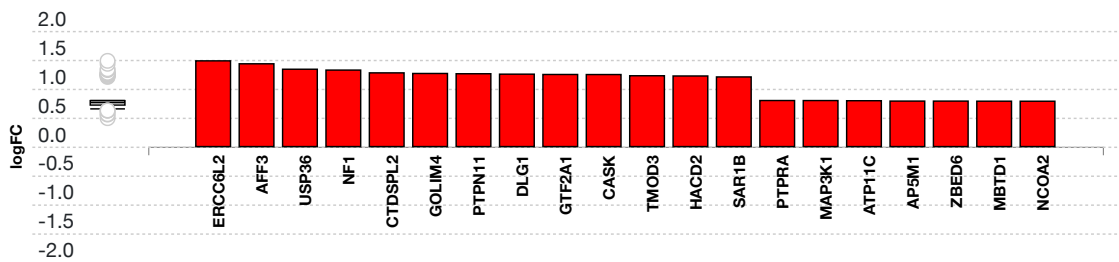
a)



b)

**Fig. 6.2.4: a) Present (overly abundant) p-value vs zscore p-value:** The significance of Naphthoquinones is plotted on two axes, with negative log of  $P_z$  on x-axis and negative log of  $P_{pres}$  on y-axis. The size of the dot represents the relative number of consistent DE genes, which for selected upstream regulator is 62. **b) Volcano plot:** There are 62 DE genes that are targets of Naphthoquinones consistent with the hypothesis that Naphthoquinones is present (overly abundant) The target genes are represented in terms of their measured expression change (x-axis) and the significance of the change (y-axis). The significance is represented in terms of the negative log (base 10) of the *p*-value, so that more significant genes are plotted higher on the y-axis.

### geldanamycin



(c) Advaita Corporation 2022

**Fig. 6.2.5: Consistent DE target genes measured expression bar plot:** All the consistent differentially expressed genes that are targeted by geldanamycin are ranked based on their absolute value of log fold change. The plot is limited to the top 20 genes out of a total of 59 consistent differentially expressed target genes. Upregulated genes are shown in red, downregulated genes are shown in blue. The box and whisker plot on the left summarizes the distribution of all the consistent differentially expressed genes targeted by this upstream regulator. The box shows the 1st quartile, the median and the 3rd quartile, while any outliers are represented by circles.

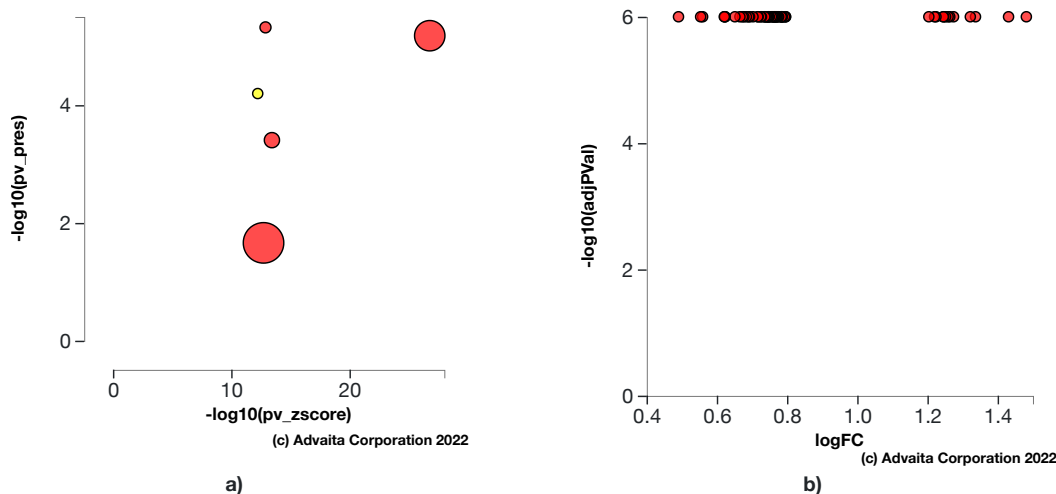
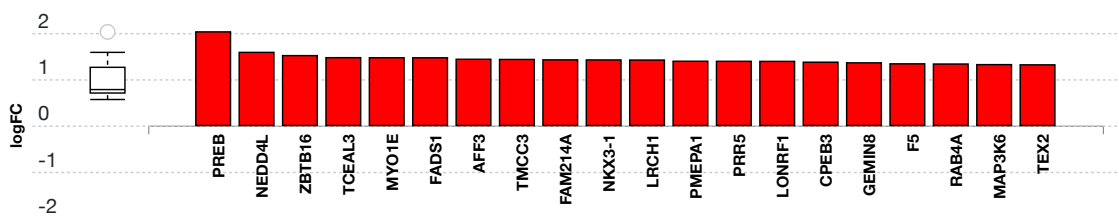


**Fig. 6.2.6: a) Present (overly abundant) p-value vs zscore p-value:** The significance of geldanamycin is plotted on two axes, with negative log of  $P_2$  on x-axis and negative log of  $P_{pres}$  on y-axis. The size of the dot represents the relative number of consistent DE genes, which for selected upstream regulator is 59. **b) Volcano plot:** There are 59 DE genes that are targets of geldanamycin consistent with the hypothesis that geldanamycin is present (overly abundant) The target genes are represented in terms of their measured expression change (x-axis) and the significance of the change (y-axis). The significance is represented in terms of the negative log (base 10) of the p-value, so that more significant genes are plotted higher on the y-axis.

### Dihydrotestosterone



(c) Advaita Corporation 2022

**Fig. 6.2.7: Consistent DE target genes measured expression bar plot:** All the consistent differentially expressed genes that are targeted by Dihydrotestosterone are ranked based on their absolute value of log fold change. The plot is limited to the top 20 genes out of a total of 131 consistent differentially expressed target genes. Upregulated genes are shown in red, downregulated genes are shown in blue. The box and whisker plot on the left summarizes the distribution of all the consistent differentially expressed genes targeted by this upstream regulator. The box shows the 1st quartile, the median and the 3rd quartile, while any outliers are represented by circles.

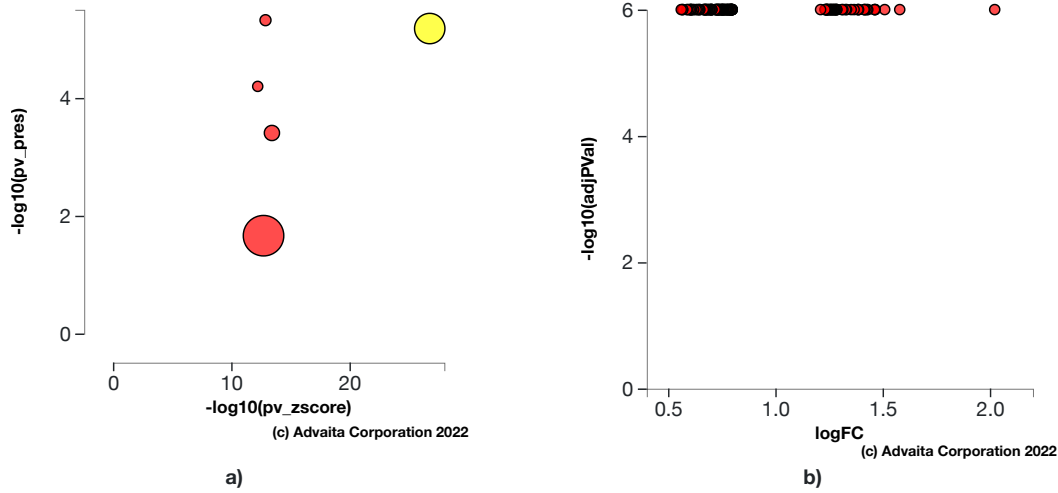


**Fig. 6.2.8: a) Present (overly abundant) p-value vs zscore p-value:** The significance of Dihydrotestosterone is plotted on two axes, with negative log of  $P_z$  on x-axis and negative log of  $P_{pres}$  on y-axis. The size of the dot represents the relative number of consistent DE genes, which for selected upstream regulator is 131. **b) Volcano plot:** There are 131 DE genes that are targets of Dihydrotestosterone consistent with the hypothesis that Dihydrotestosterone is present (overly abundant) The target genes are represented in terms of their measured expression change (x-axis) and the significance of the change (y-axis). The significance is represented in terms of the negative log (base 10) of the p-value, so that more significant genes are plotted higher on the y-axis.

**cylindrospermopsin**

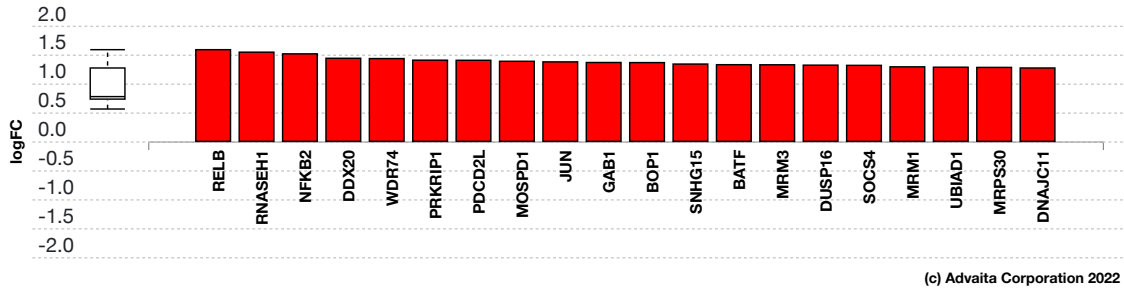


**Fig. 6.2.9: Consistent DE target genes measured expression bar plot:** All the consistent differentially expressed genes that are targeted by cylindrospermopsin are ranked based on their absolute value of log fold change. The plot is limited to the top 20 genes out of a total of 77 consistent differentially expressed target genes. Upregulated genes are shown in red, downregulated genes are shown in blue. The box and whisker plot on the left summarizes the distribution of all the consistent differentially expressed genes targeted by this upstream regulator. The box shows the 1st quartile, the median and the 3rd quartile, while any outliers are represented by circles.

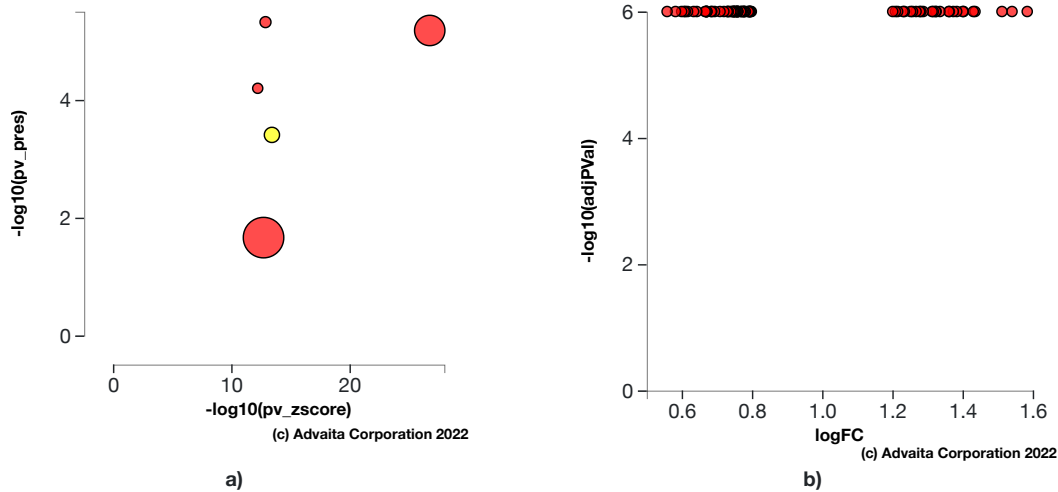
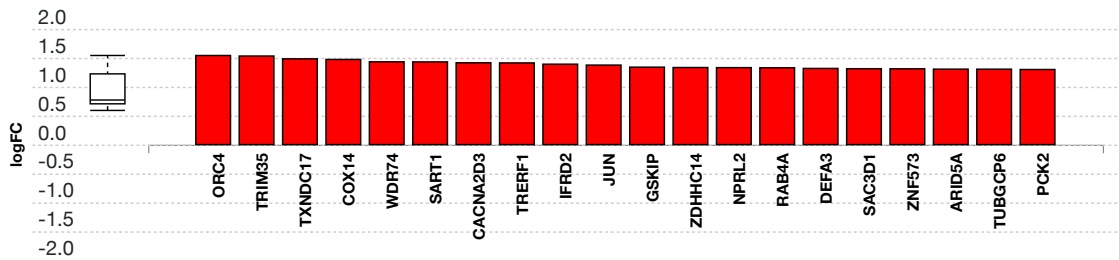


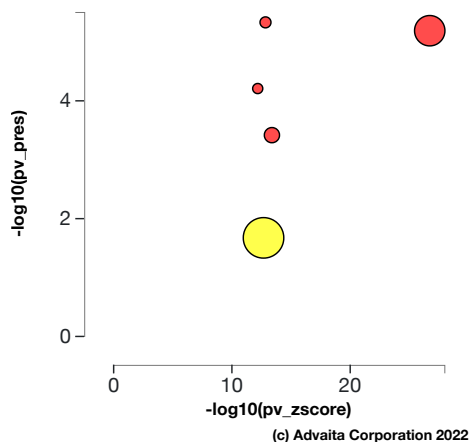
**Fig. 6.2.10: a) Present (overly abundant) p-value vs zscore p-value:** The significance of cylindrospermopsin is plotted on two axes, with negative log of  $P_z$  on x-axis and negative log of  $P_{pres}$  on y-axis. The size of the dot represents the relative number of consistent DE genes, which for selected upstream regulator is 77. **b) Volcano plot:** There are 77 DE genes that are targets of cylindrospermopsin consistent with the hypothesis that cylindrospermopsin is present (overly abundant) The target genes are represented in terms of their measured expression change (x-axis) and the significance of the change (y-axis). The significance is represented in terms of the negative log (base 10) of the p-value, so that more significant genes are plotted higher on the y-axis.

### Sodium Selenite

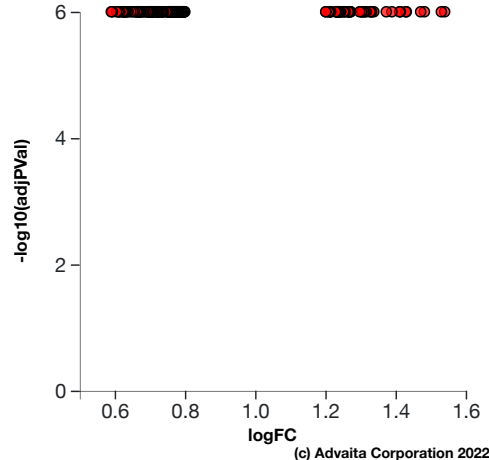


(c) Advaita Corporation 2022

**Fig. 6.2.11: Consistent DE target genes measured expression bar plot:** All the consistent differentially expressed genes that are targeted by Sodium Selenite are ranked based on their absolute value of log fold change. The plot is limited to the top 20 genes out of a total of 167 consistent differentially expressed target genes. Upregulated genes are shown in red, downregulated genes are shown in blue. The box and whisker plot on the left summarizes the distribution of all the consistent differentially expressed genes targeted by this upstream regulator. The box shows the 1st quartile, the median and the 3rd quartile, while any outliers are represented by circles.



a)



b)

**Fig. 6.2.12: a) Present (overly abundant) p-value vs zscore p-value:** The significance of Sodium Selenite is plotted on two axes, with negative log of  $P_z$  on x-axis and negative log of  $P_{pres}$  on y-axis. The size of the dot represents the relative number of consistent DE genes, which for selected upstream regulator is 167. **b) Volcano plot:** There are 167 DE genes that are targets of Sodium Selenite consistent with the hypothesis that Sodium Selenite is present (overly abundant) The target genes are represented in terms of their measured expression change (x-axis) and the significance of the change (y-axis). The significance is represented in terms of the negative log (base 10) of the p-value, so that more significant genes are plotted higher on the y-axis.

### 6.3. Results: upstream CDTs predicted as absent (or insufficient)

CDT (u)	DTI(u)	DT(u)	p-value	p-value (FDR)	p-value (Bonferroni)
Doxorubicin	932	1131	5.626e-23	3.355e-20	1.243e-19
Ivermectin	833	848	5.626e-23	3.355e-20	1.243e-19
dicrotophos	499	696	5.626e-23	3.355e-20	1.243e-19
3-((6-(2-methoxyphenyl)pyrimidin-4-yl)amino)phenyl)methane sulfonamide	162	167	6.075e-23	3.355e-20	1.342e-19
7,8-Dihydro-7,8-dihydroxybenzo(a)pyrene 9,10-oxide	440	563	7.519e-19	3.322e-16	1.661e-15

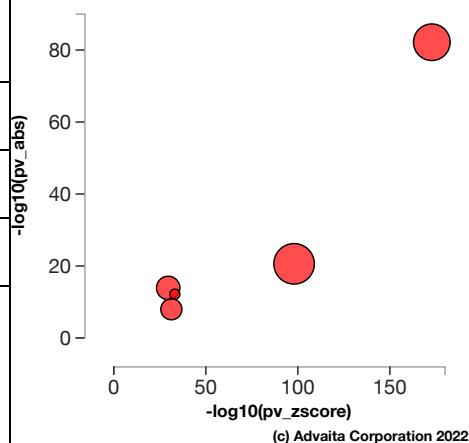


**Table 6.3.1: Top upstream CDTs predicted as absent (or insufficient).** For each upstream CDT *u*, the table shows the number of DE targets supporting the hypothesis that the CDT is absent DTI(*u*) the total number of DE genes downstream of *u* DT(*u*), the combined raw *p*-value, and the *p*-value corrected for multiple comparisons. **Fig. 6.3.1: A two-way plot showing the top five upstream CDTs predicted as absent (or insufficient).** Dots representing upstream CDTs are positioned using  $P_{zscore}$  on the horizontal axis, and using  $P_{abs}$  on the vertical axis.  $P_{abs}$  is the *p*-value based on the number of DE targets consistent with the type of the incoming signal and with the selected hypothesis type. Upstream CDTs with a significant combined *p*-value are shown in red. The size of each dot represents the relative number of consistent DE genes for that CDT.

#### Doxorubicin

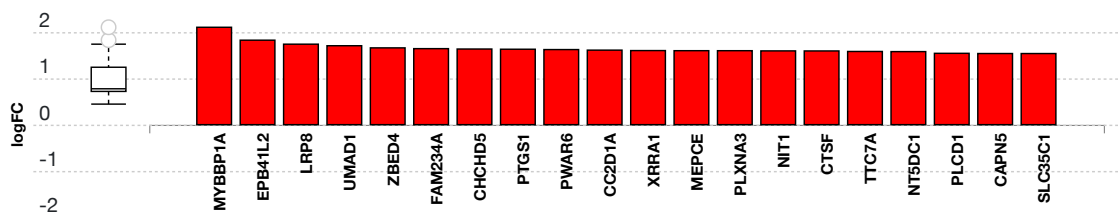


**Fig. 6.3.13: Consistent DE target genes measured expression bar plot:** All the consistent differentially expressed genes that are targeted by Doxorubicin are ranked based on their absolute value of log fold change. The plot is limited to the top 20 genes out of a total of 932 consistent differentially expressed target genes. Upregulated genes are shown in red, downregulated genes are shown in blue. The box and whisker plot on the left summarizes the distribution of all the consistent differentially expressed genes targeted by this upstream regulator. The box shows the 1st quartile, the median and the 3rd quartile, while any outliers are represented by circles.

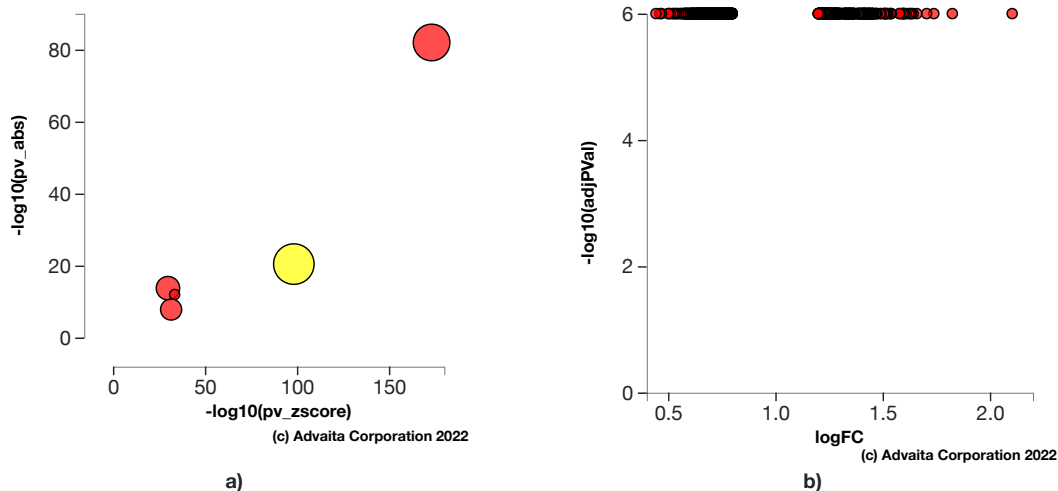


**Fig. 6.3.14: a) Absent (or insufficient) p-value vs zscore p-value:** The significance of Doxorubicin is plotted on two axes, with negative log of  $P_z$  on x-axis and negative log of  $P_{abs}$  on y-axis. The size of the dot represents the relative number of consistent DE genes, which for selected upstream regulator is 932. **b) Volcano plot:** There are 932 DE genes that are targets of Doxorubicin consistent with the hypothesis that Doxorubicin is absent (or insufficient) The target genes are represented in terms of their measured expression change (x-axis) and the significance of the change (y-axis). The significance is represented in terms of the negative log (base 10) of the p-value, so that more significant genes are plotted higher on the y-axis.

Ivermectin

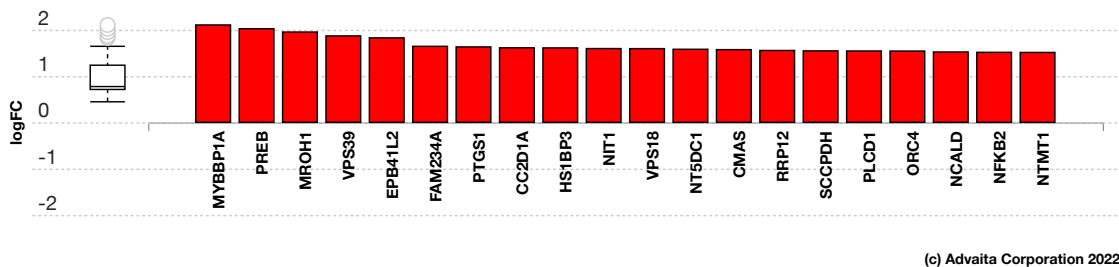


**Fig. 6.3.15: Consistent DE target genes measured expression bar plot:** All the consistent differentially expressed genes that are targeted by Ivermectin are ranked based on their absolute value of log fold change. The plot is limited to the top 20 genes out of a total of 833 consistent differentially expressed target genes. Upregulated genes are shown in red, downregulated genes are shown in blue. The box and whisker plot on the left summarizes the distribution of all the consistent differentially expressed genes targeted by this upstream regulator. The box shows the 1st quartile, the median and the 3rd quartile, while any outliers are represented by circles.

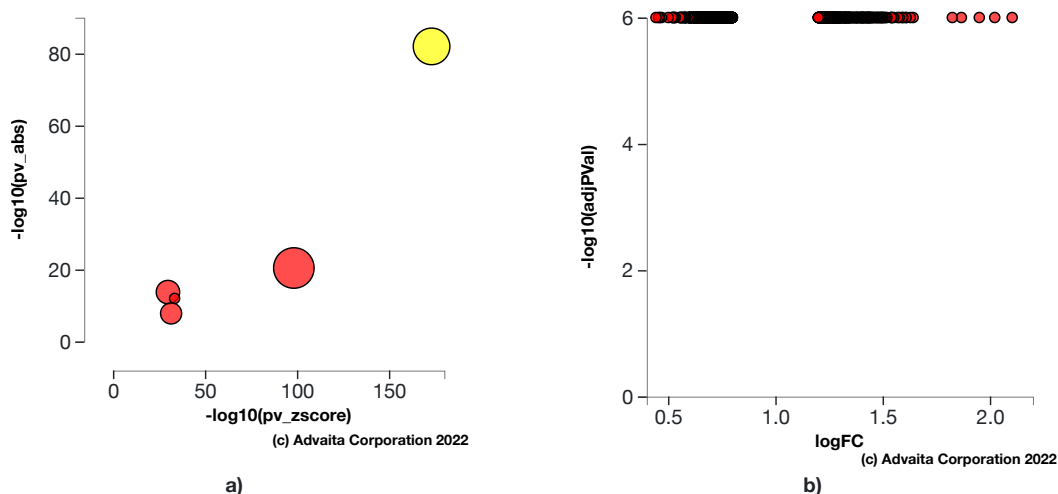
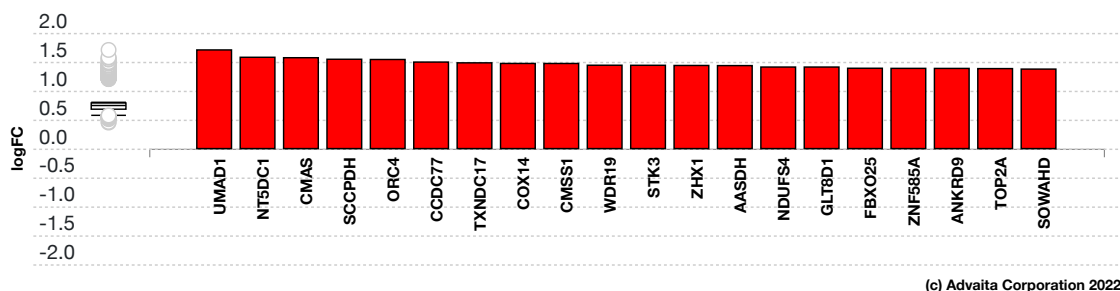


**Fig. 6.3.16: a) Absent (or insufficient) p-value vs zscore p-value:** The significance of Ivermectin is plotted on two axes, with negative log of  $P_z$  on x-axis and negative log of  $P_{abs}$  on y-axis. The size of the dot represents the relative number of consistent DE genes, which for selected upstream regulator is 833. **b) Volcano plot:** There are 833 DE genes that are targets of Ivermectin consistent with the hypothesis that Ivermectin is absent (or insufficient) The target genes are represented in terms of their measured expression change (x-axis) and the significance of the change (y-axis). The significance is represented in terms of the negative log (base 10) of the p-value, so that more significant genes are plotted higher on the y-axis.

## dicrotophos



(c) Advaita Corporation 2022

**Fig. 6.3.17: Consistent DE target genes measured expression bar plot:** All the consistent differentially expressed genes that are targeted by dicrotophos are ranked based on their absolute value of log fold change. The plot is limited to the top 20 genes out of a total of 499 consistent differentially expressed target genes. Upregulated genes are shown in red, downregulated genes are shown in blue. The box and whisker plot on the left summarizes the distribution of all the consistent differentially expressed genes targeted by this upstream regulator. The box shows the 1st quartile, the median and the 3rd quartile, while any outliers are represented by circles.

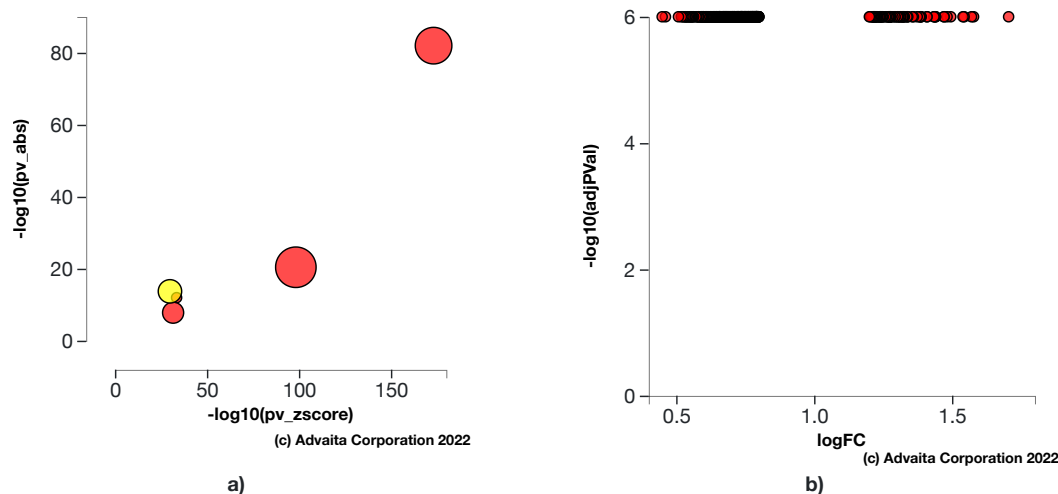
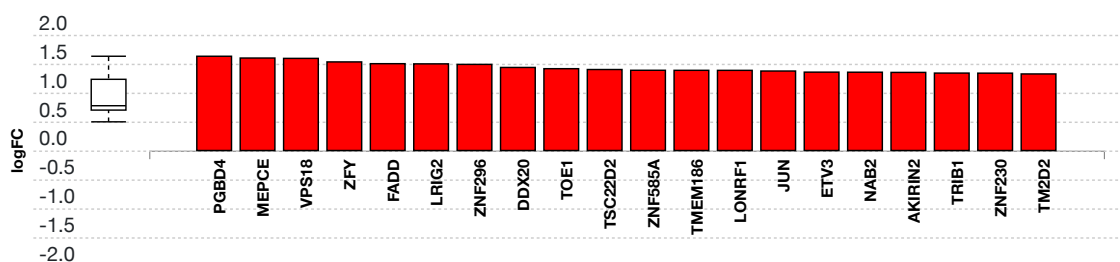


**Fig. 6.3.18: a) Absent (or insufficient) p-value vs zscore p-value:** The significance of dicrotophos is plotted on two axes, with negative log of  $P_z$  on x-axis and negative log of  $P_{abs}$  on y-axis. The size of the dot represents the relative number of consistent DE genes, which for selected upstream regulator is 499. **b) Volcano plot:** There are 499 DE genes that are targets of dicrotophos consistent with the hypothesis that dicrotophos is absent (or insufficient). The target genes are represented in terms of their measured expression change (x-axis) and the significance of the change (y-axis). The significance is represented in terms of the negative log (base 10) of the p-value, so that more significant genes are plotted higher on the y-axis.

## 3-((6-(2-methoxyphenyl)pyrimidin-4-yl)amino)phenyl)methane sulfonamide



(c) Advaita Corporation 2022

**Fig. 6.3.19: Consistent DE target genes measured expression bar plot:** All the consistent differentially expressed genes that are targeted by 3-((6-(2-methoxyphenyl)pyrimidin-4-yl)amino)phenyl)methane sulfonamide are ranked based on their absolute value of log fold change. The plot is limited to the top 20 genes out of a total of 162 consistent differentially expressed target genes. Upregulated genes are shown in red, downregulated genes are shown in blue. The box and whisker plot on the left summarizes the distribution of all the consistent differentially expressed genes targeted by this upstream regulator. The box shows the 1st quartile, the median and the 3rd quartile, while any outliers are represented by circles.

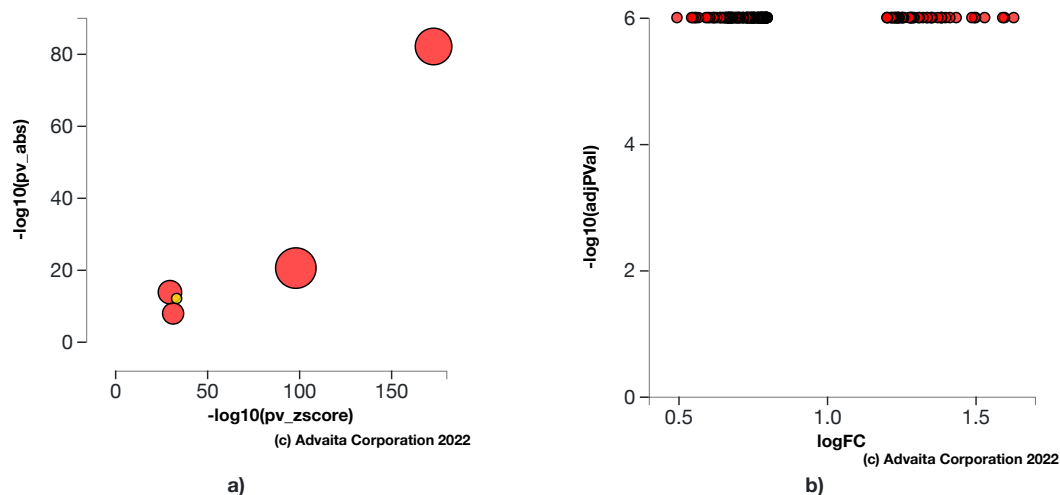


**Fig. 6.3.20: a) Absent (or insufficient) p-value vs zscore p-value:** The significance of 3-((6-(2-methoxyphenyl)pyrimidin-4-yl)amino)phenyl)methane sulfonamide is plotted on two axes, with negative log of  $P_z$  on x-axis and negative log of  $P_{abs}$  on y-axis. The size of the dot represents the relative number of consistent DE genes, which for selected upstream regulator is 162. **b) Volcano plot:** There are 162 DE genes that are targets of 3-((6-(2-methoxyphenyl)pyrimidin-4-yl)amino)phenyl)methane sulfonamide consistent with the hypothesis that 3-((6-(2-methoxyphenyl)pyrimidin-4-yl)amino)phenyl)methane sulfonamide is absent (or insufficient) The target genes are represented in terms of their measured expression change (x-axis) and the significance of the change (y-axis). The significance is represented in terms of the negative log (base 10) of the p-value, so that more significant genes are plotted higher on the y-axis.

## 7,8-Dihydro-7,8-dihydroxybenzo(a)pyrene 9,10-oxide

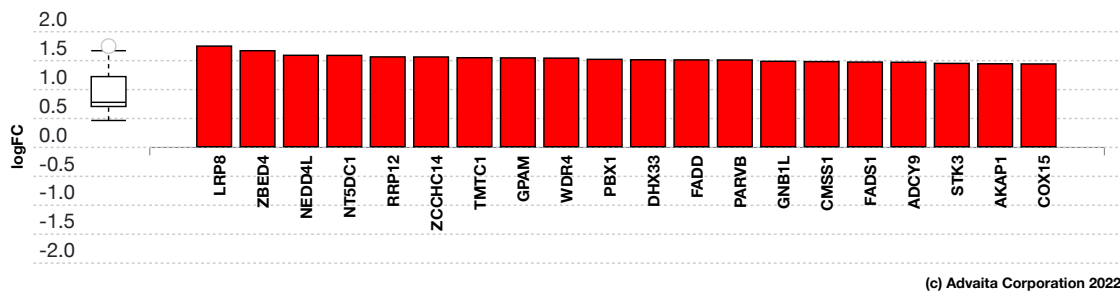


**Fig. 6.3.21: Consistent DE target genes measured expression bar plot:** All the consistent differentially expressed genes that are targeted by 7,8-Dihydro-7,8-dihydroxybenzo(a)pyrene 9,10-oxide are ranked based on their absolute value of log fold change. The plot is limited to the top 20 genes out of a total of 440 consistent differentially expressed target genes. Upregulated genes are shown in red, downregulated genes are shown in blue. The box and whisker plot on the left summarizes the distribution of all the consistent differentially expressed genes targeted by this upstream regulator. The box shows the 1st quartile, the median and the 3rd quartile, while any outliers are represented by circles.

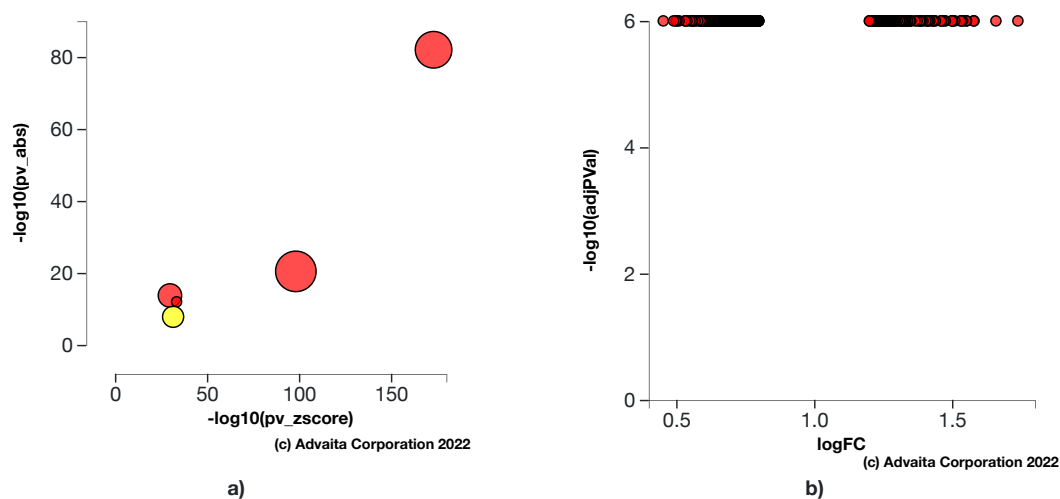


**Fig. 6.3.22: a) Absent (or insufficient) p-value vs zscore p-value:** The significance of 7,8-Dihydro-7,8-dihydroxybenzo(a)pyrene 9,10-oxide is plotted on two axes, with negative log of  $P_z$  on x-axis and negative log of  $P_{abs}$  on y-axis. The size of the dot represents the relative number of consistent DE genes, which for selected upstream regulator is 440. **b) Volcano plot:** There are 440 DE genes that are targets of 7,8-Dihydro-7,8-dihydroxybenzo(a)pyrene 9,10-oxide consistent with the hypothesis that 7,8-Dihydro-7,8-dihydroxybenzo(a)pyrene 9,10-oxide is absent (or insufficient) The target genes are represented in terms of their measured expression change (x-axis) and the significance of the change (y-axis). The significance is represented in terms of the negative log (base 10) of the p-value, so that more significant genes are plotted higher on the y-axis.

## 7. Disease Analysis

## 7.1. Methods

For each disease, the number of differentially expressed (DE) genes annotated to a disease term is compared to the number of DE genes expected just by chance. iPathwayGuide uses an over-representation approach to compute the statistical significance of observing at least the given number of DE genes. The p-value is computed using the hypergeometric distribution as described for pORA in the Pathway Analysis section. This p-value is corrected for multiple comparisons using FDR and Bonferroni.

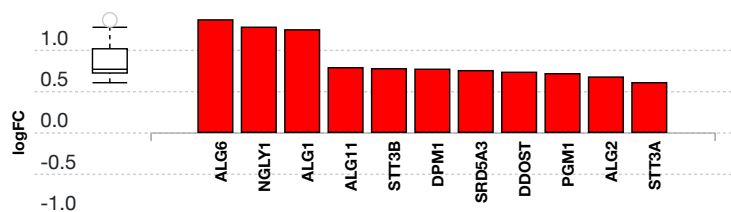
## 7.2. Results

Table 7.2.1: Top identified diseases

Disease Name	p-value	p-value (FDR)	p-value (Bonferroni)
Congenital disorders of glycosylation type I	5.272e-8	1.763e-5	2.673e-5
Autosomal recessive mental retardation	6.954e-8	1.763e-5	3.526e-5
Joubert syndrome	9.091e-7	1.536e-4	4.609e-4
Pontocerebellar hypoplasia	2.861e-6	2.901e-4	0.001
Cytochrome c oxidase (COX) deficiency; Mitochondrial complex IV deficiency (MT-C4D)	2.861e-6	2.901e-4	0.001

### Congenital disorders of glycosylation type I (H00118)

Congenital disorders of glycosylation (CDG) are a group of disorders caused by defects in various genes for N-glycan biosynthesis. CDG type I is defined by mutations in genes encoding enzymes which involves disrupted synthesis of the lipid linked oligosaccharide precursor and its transfer to polypeptide chain of protein, affecting N-glycan assembly in cytosol and endoplasmic reticulum. An increasing number of disorders have been discovered, with many subtypes identified. PMM2-CDG is the most common form, with over 800 patients diagnosed mostly in Europe. Almost all type present in infancy. These diseases demonstrate a broad range of clinical manifestation, associated with developmental delay, psychomotor retardation, hypotonia, seizures, hepatomegaly, microcephaly, and pericardial effusion. In this experiment, the algorithm identified **11** differentially expressed genes out of **29** genes associated with the disease.

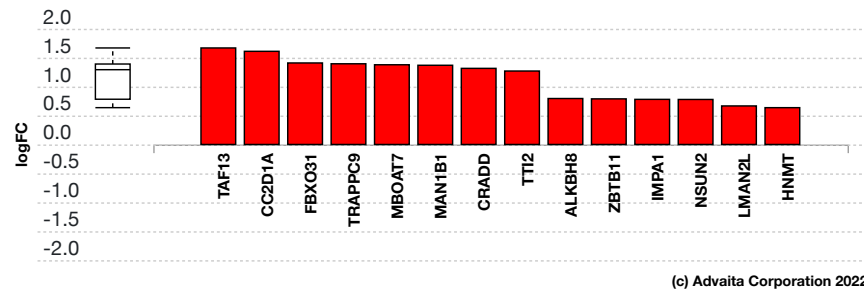


(c) Advaita Corporation 2022

**Fig. 7.2.1: Gene measured expression bar plot:** All the differentially expressed genes that are annotated to Congenital disorders of glycosylation type I are ranked based on their absolute value of log fold change. Upregulated genes are shown in red, downregulated genes are shown in blue. The box plot on the left summarizes the distribution of all the differentially expressed genes that are annotated to this disease. The box represents the 1st quartile, the median and the 3rd quartile, while the outliers are represented by circles.

## Autosomal recessive mental retardation (H00768)

Mental retardation (MR) is a neurodevelopmental disorder characterized by low intelligence quotient (IQ) and deficits in adaptive behaviors. Although X-linked MR has been extensively studied, and over 80 causal genes have been cloned, little is known about the genetic basis of autosomal recessive mental retardation (MRT). To date, several genes have been identified. These genes have a variety of functions and participate in multiple biochemical pathways. In addition, there are several known disease loci for which genes have not yet been identified. In this experiment, the algorithm identified **14** differentially expressed genes out of **50** genes associated with the disease.

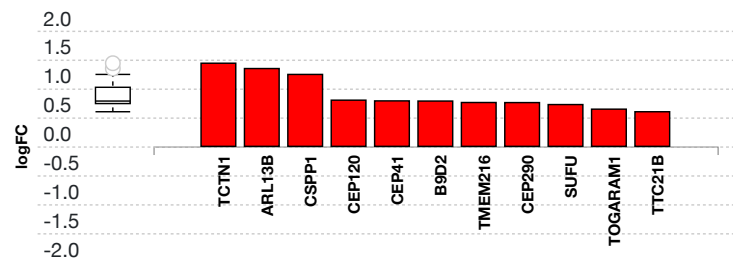


(c) Advaita Corporation 2022

**Fig. 7.2.2: Gene measured expression bar plot:** All the differentially expressed genes that are annotated to Autosomal recessive mental retardation are ranked based on their absolute value of log fold change. Upregulated genes are shown in red, downregulated genes are shown in blue. The box plot on the left summarizes the distribution of all the differentially expressed genes that are annotated to this disease. The box represents the 1st quartile, the median and the 3rd quartile, while the outliers are represented by circles.

## Joubert syndrome (H00530)

Joubert syndrome and related disorders are a group of multiple congenital anomaly syndromes characterized by 'molar tooth sign', a specific midbrain-hindbrain malformation seen in brain images. Joubert syndrome is associated with retinal dystrophy, nephronophthisis, liver fibrosis and polydactyly. Most of the causative genes encode cilium-related proteins. In this experiment, the algorithm identified **11** differentially expressed genes out of **37** genes associated with the disease.

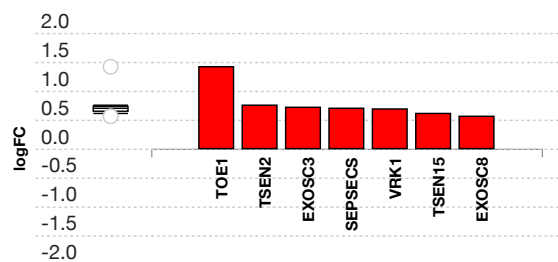


(c) Advaita Corporation 2022

**Fig. 7.2.3: Gene measured expression bar plot:** All the differentially expressed genes that are annotated to Joubert syndrome are ranked based on their absolute value of log fold change. Upregulated genes are shown in red, downregulated genes are shown in blue. The box plot on the left summarizes the distribution of all the differentially expressed genes that are annotated to this disease. The box represents the 1st quartile, the median and the 3rd quartile, while the outliers are represented by circles.

## Pontocerebellar hypoplasia (H00897)

Pontocerebellar hypoplasia (PCH) is a group of inherited progressive neurodegenerative disorders with prenatal onset. Up to now ten different subtypes have been reported. All subtypes share common characteristics, including hypoplasia/atrophy of cerebellum and pons, progressive microcephaly, and variable cerebral involvement. Mutations in three tRNA splicing endonuclease subunit genes were found to be responsible for PCH2, PCH4 and PCH5. Mutations in the nuclear encoded mitochondrial arginyl- tRNA synthetase gene underlie PCH6. PCH1 is caused by homozygous mutation in the VRK1 gene. In this experiment, the algorithm identified **7** differentially expressed genes out of **15** genes associated with the disease.

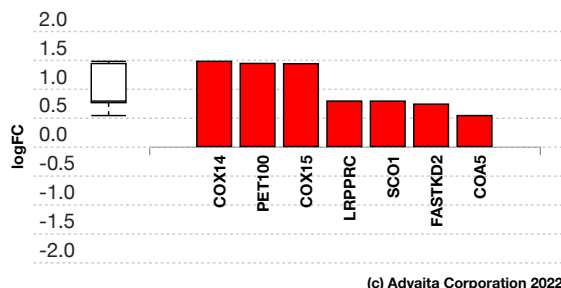


(c) Advaita Corporation 2022

**Fig. 7.2.4: Gene measured expression bar plot:** All the differentially expressed genes that are annotated to Pontocerebellar hypoplasia are ranked based on their absolute value of log fold change. Upregulated genes are shown in red, downregulated genes are shown in blue. The box plot on the left summarizes the distribution of all the differentially expressed genes that are annotated to this disease. The box represents the 1st quartile, the median and the 3rd quartile, while the outliers are represented by circles.

## Cytochrome c oxidase (COX) deficiency; Mitochondrial complex IV deficiency (MT-C4D) (H01368)

Cytochrome c oxidase (COX) deficiency is a mitochondrial disease that is caused by the lack of the COX. Cytochrome c oxidase (COX) is the terminal enzyme of the mitochondrial respiratory chain (complex IV). Since COX is encoded by nuclear and mitochondrial genes, COX deficiency can be inherited in either an autosomal recessive or a maternal pattern. Patients can present with a number of different clinical phenotypes, including Leigh syndrome, Fatal infantile cardioencephalomyopathy, and Leber hereditary optic neuropathy. In this experiment, the algorithm identified 7 differentially expressed genes out of 15 genes associated with the disease.



(c) Advaita Corporation 2022

**Fig. 7.2.5: Gene measured expression bar plot:** All the differentially expressed genes that are annotated to Cytochrome c oxidase (COX) deficiency; Mitochondrial complex IV deficiency (MT-C4D) are ranked based on their absolute value of log fold change. Upregulated genes are shown in red, downregulated genes are shown in blue. The box plot on the left summarizes the distribution of all the differentially expressed genes that are annotated to this disease. The box represents the 1st quartile, the median and the 3rd quartile, while the outliers are represented by circles.

## 8. References

- Agarwal V, Bell GW, Nam J, Bartel DP. Predicting effective microRNA target sites in mammalian mRNAs. *eLife*, 4:e05005 (2015).
- Alexa, A., Rahnenfuehrer, J., Lengauer, T.: Improved scoring of functional groups from gene expression data by decorrelating GO graph structure. *Bioinformatics* 22(13): 1600-1607 (2006).
- Ashburner, M., Ball, C.A., Blake, J.A., Botstein, D., Butler, H., Cherry, J.M., Davis, A.P., Dolinski, K., Dwight, S.S., Eppig, J.T., Harris, M.A., Hill, D.P., Issel-Tarver, L., Kasarskis, A., Lewis, S., Matese, J.C., Richardson, J.E., Ringwald, M., Rubin, G.M., Sherlock, G.: The Gene Ontology Consortium. Gene ontology: Tool for the unification of biology. *Nature Genetics* 25(1): 25-9 (2000).
- Ashburner, M., Lewis, S.: On Ontologies for Biologists: The Gene Ontology - Untangling the web: 'In Silico' simulation of biological processes: *Novartis Found Symp*, 247:66-80; discussion 80-3, 84-90: 244-52 (2002).
- Benjamini, Y. and Hochberg, Y.: Controlling the false discovery rate: A practical and powerful approach to multiple testing. *Journal of the Royal Statistical Society B*, 57(1):289-300, (1995).
- Benjamini, Y. and Yekutieli, D.: The control of the false discovery rate in multiple testing under dependency. *Annals of Statistics*, 29(4):1165-1188, (2001).
- Bonferroni, C. E.: Il calcolo delle assicurazioni su gruppi di teste, chapter "Studi in Onore del Professore Salvatore Ortu Carboni", pages 13-60, Rome, (1935).
- Bonferroni, C. E.: Teoria statistica delle classi e calcolo delle probabilita. *Pubblicazioni del Istituto Superiore di Scienze Economiche e Commerciali di Firenze*, 8:3-62, (1936).
- Camon, E., Magrane, M., Barrell, D., Lee, V., Dimmer, E., Maslen, J., Binns, D., Harte, N., Lopez, R., Apweiler, R.: The Gene Ontology Annotation (GOA) database: sharing knowledge in Uniprot with Gene Ontology. *Nucleic Acids Research*, 32(Database issue), D262-D266 (2004).
- Davis AP, Grondin CJ, Johnson RJ, Sciaky D, McMorran R, Wiegiers J, Wiegiers TC, Mattingly CJ, The Comparative Toxicogenomics Database: update 2019, *Nucleic Acids Research*, 47(D1): D948-D954 (2019).
- Draghici, S., Khatri, P., Martins, R.P., Ostermeier, G.C. and Krawetz, S.A.: Global functional profiling of gene expression. *Genomics*, 81(2), pp.98-104 (2003).
- Draghici, S., Khatri, P., Bhavsar, P., Shah, A., Krawetz, S., Tainsky, M.A.: Onto-Tools, The toolkit of the modern biologist: Onto-Express, Onto-Compare, Onto-Design and Onto-Translate. *Nucleic Acids Research*, 31(13): 3775-81 (2003).
- Draghici, S., Khatri, P., Tarca, A.L., Amin, K., Done, A., Voichita, C., Georgescu, C., Romero, R.: A systems biology approach for pathway level analysis. *Genome Research*, 17(10): 1537-45 (2007).
- Draghici, S.: *Statistics and Data Analysis for Microarrays Using R and Bioconductor*, second edition. Chapman and Hall/CRC (2011).
- Friedman, R.C., Farh, K.K., Burge, C.B., Bartel, D.P.: Most mammalian mRNAs are conserved targets of microRNAs. *Genome Research*, 19: 92-105 (2009).

- Garcia, D.M., Baek, D., Shin, C., Bell, G.W., Grimson, A., Bartel, D.P.: Weak seed-pairing stability and high target-site abundance decrease the proficiency of Isy-6 and other miRNAs. *Nature Structural & Molecular Biology*, 18: 1139-1146 (2011).
- Gene Ontology Consortium. Creating the Gene Ontology Resource: Design and Implementation. *Genome Research* 11: 1425-1433 (2001).
- Gene Ontology Consortium. The Gene Ontology (GO) database and informatics resource. *Nucleic Acids Research* 32 (suppl 1): D258-D261 (2004).
- Griffiths-Jones S.: The microRNA Registry. *Nucleic Acids Research* 32:D109-D111 (2004).
- Griffiths-Jones S., Grocock R.J., van Dongen S., Bateman A., Enright A.J.: miRBase: microRNA sequences, targets and gene nomenclature. *Nucleic Acids Research* 34:D140-D144 (2006).
- Griffiths-Jones S., Saini H.K., van Dongen S., Enright A.J.: miRBase: tools for microRNA genomics. *Nucleic Acids Research* 36:D154-D158 (2008).
- Grimson, A., Farh, K.K., Johnston, W.K., Garrett-Engele, P., Lim, L.P., Bartel, D.P.: MicroRNA targeting specificity in mammals: Determinants beyond seed pairing. *Molecular Cell*, 27: 91-105 (2007).
- Fisher R. A.: *Statistical methods for research workers*. Oliver & Boyd, Edinburgh, (1925).
- Kanehisa, M., Goto, S.: KEGG: Kyoto Encyclopedia of Genes and Genomes. *Nucleic Acids Research* 28: 27-30 (2000).
- Kanehisa, M., Goto, S., Kawashima, S., and Nakaya, A.: The KEGG databases at GenomeNet. *Nucleic Acids Research* 30: 42-46 (2002).
- Kanehisa, M., Goto, S., Kawashima, S., Okuno, Y., and Hattori, M.; The KEGG resources for deciphering the genome. *Nucleic Acids Research* 32: D277-D280 (2004).
- Kanehisa, M., Araki, M., Goto, S., Hattori, M., Hirakawa, M., Itoh, M., Katayama, T., Kawashima, S., Okuda, S., Tokimatsu, T., and Yamanishi, Y.: KEGG for linking genomes to life and the environment. *Nucleic Acids Research* 36: D480-D484 (2008).
- Kanehisa, M., Goto, S., Furumichi, M., Tanabe, M., Hirakawa, M.: KEGG for representation and analysis of molecular networks involving diseases and drugs. *Nucleic Acids Research* 38: D355-D360 (2010).
- Kanehisa, M., Goto, S., Sato, Y., Furumichi, M., Tanabe, M.: KEGG for integration and interpretation of large-scale molecular datasets. *Nucleic Acids Research* 40: D109-D114 (2012).
- Kanehisa, M., Goto, S., Sato, Y., Kawashima, M., Furumichi, M., and Tanabe, M.; Data, information, knowledge and principle: back to metabolism in KEGG. *Nucleic Acids Research* 42: D199-D205 (2014).
- Khatri, P., Draghici, S., Tarca, A.D., Hassan, S.S., Romero, R.: A system biology approach for the steady-state analysis of gene signaling networks. *Lecture Notes in Computer Science (LNCS)* 4756, pp 32-41 (2007).
- Kozomara A., Griffiths-Jones S.: miRBase: integrating microRNA annotation and deep-sequencing data. *Nucleic Acids Research* 39:D152-D157 (2011).
- Kozomara A., Griffiths-Jones S.: miRBase: annotating high confidence microRNAs using deep sequencing data. *Nucleic Acids Research* 42:D68-D73 (2014).
- Lewis, B.P., Burge, C.B., Bartel, D.P.: Conserved seed pairing, often flanked by adenosines, indicates that thousands of human genes are microRNA targets. *Cell*, 120(1):15-20 (2005).
- Nam J, Rissland OS, Koppstein D, Abreu-Goodger C, Jan CH, Agarwal V, Yildirim MA, Rodriguez A, Bartel DP. Global analyses of the effect of different cellular contexts on microRNA targeting. *Molecular Cell*, 53:1031-43 (2014).
- Rhee, S.Y., Wood, V., Dolinski, K., Draghici, S.: Use and misuse of the gene ontology annotations. *Nature Reviews Genetics* 9(4):509-515 (2008).
- Szklarczyk, D., Morris, J.H., Cook, H., et al. The STRING database in 2017: quality-controlled protein-protein association networks, made broadly accessible. *Nucleic Acids Research* 45(D1):D362-D368 (2017).
- Tarca, A.L., Draghici, S., Khatri, P., Hassan, S., Mittal, P., Kim, J.S., Kim, C.J., Kusanovic, J.P., Romero, R.: A novel Signaling Pathway Impact Analysis (SPIA). *Bioinformatics* 25(1), 75-82 (2009).

**APPROVED**

By LLUH IRB: 5210437 - 11/22/2021 at 4:13 pm, Nov 22, 2021

LOMA LINDA UNIVERSITY

School of Allied Health Professions

**INFORMED CONSENT**

**TITLE:** THE EFFECTS OF HIGH INTENSITY EXERCISE ON BIOLOGICAL AGE

**SPONSOR:** Loma Linda University Department of Physical Therapy

**PRINCIPAL INVESTIGATOR:** Gurinder Bains PhD, Associate Professor School of Allied Health Professions

**Key Information for You to Consider**

**Voluntary Consent.** You are being asked to volunteer for a research study. It is up to you whether you choose to participate or not. There will be no penalty or loss of benefits to which you are otherwise entitled if you choose not to participate or discontinue participation.

**Purpose.** The purpose of this graduate student research study is to determine if a high-intensity exercise program can slow or reverse biological aging and shed light on the underlying pathways involved.

**Duration.** It is expected that your participation will last one month. You are asked to visit the Physical Therapy laboratory a total of 14 times: twelve 1-hour exercise visits 3-times per week, and two 1-hour data collection visits.

**Procedures and Activities.** If you are eligible to participate, you will be randomized to 1 of 2 groups: Control group or Exercise group. Control group participants will make no modifications to regular diet or exercise habits. Exercise group participants will perform supervised high intensity exercise three times per week at the LLU department of physical therapy laboratory utilizing treadmills, stationary bicycles, and rowing machines. You will have your body composition and vital signs measured. You will complete 5 questionnaires (on stress, sleep, depression, activity level, and fitness) taking you approximately 25 minutes. You will provide approximately 1.5 teaspoons of blood drawn by a certified phlebotomist to measure gene expression levels on visit 1 and the final day.

**Risks.** Some of the foreseeable risks or discomforts of your participation include exercise induced fatigue, falls, and breach of confidentiality.

**Benefits.** No direct benefit to you. However, the knowledge we gain may help researchers better understand the effects of high intensity exercise on gene expression and mortality risk. This information may help pinpoint the specific mechanism behind exercise's effect on health and lifespan.

**Alternatives.** Participation is voluntary and the only alternative is to not participate.

## **WHY IS THIS STUDY BEING DONE?**

The purpose of this graduate student research study is to determine if a high-intensity exercise program can slow or reverse biological aging and shed light on the underlying pathways involved. Biological aging is a method for predicting remaining lifespan based on your health status.

You are invited to be in this study because you are a 45 to 60-year-old male or female of below average fitness and low activity levels. You will be excluded from the study if you have a prior (within the last 5 years) or current history of cardiovascular disease, stroke, unexplained weight loss, clinical depression, congestive heart failure, cancer, irregular heartbeat, respiratory disease, or other serious medical conditions that would make exercise unsafe or prevent full participation in the exercise protocol. Additional reasons for exclusion include any significant increase or decrease in activity levels within the past thirty days, or the current use of the following medications: antibiotics, glucocorticoids, anticoagulants, narcotics, antiepileptic medications, antipsychotics, antidepressants, or hypoglycemic agents.

Approximately 48 subjects (24 males and 24 females) will participate at LLU.

You will be asked to visit the Physical Therapy laboratory a total of 14 times: twelve 1-hour exercise visits 3-times per week, and two 1-hour data collection visits over the course of approximately 1 month.

## **HOW WILL I BE INVOLVED?**

Participation in this study involves the following:

On visit 1 you will:

- Complete a Covid-19 screening form
- Complete the Informed Consent Document and PHI form
- Be randomly assigned (through a random block assignment) to either a non-exercise control group or a 3-times per week, approximately 20-minute duration, high intensity exercise group for 1-month

If you are in the non-exercise control group, you will

- Avoid modification of your usual diet and activity level
- Complete a compliance log on diet and activity level changes

If you are in the exercise group, you will

- Perform high-intensity exercise including warmups and cool downs on a treadmill, stationary bike, and a rower
- Complete a compliance log on diet and activity level changes

**APPROVED**

By LLUH IRB: 5210437 - 11/22/2021 at 4:13 pm, Nov 22, 2021

On visit 1 and the final visit you will:

- Provide approximately 1.5 teaspoons of blood drawn by a certified phlebotomist in order to measure gene expression levels
- Complete five questionnaires on stress, sleep, depression, activity level, and fitness (approximately 25 minutes)
- Have your Body composition assessed utilizing the InBody 770 bioelectrical impedance machine
- Have your vital signs (heart rate, blood pressure) and waist to hip ratio assessed

### **WHAT ARE THE REASONABLY FORESEEABLE RISKS OR DISCOMFORTS I MIGHT HAVE?**

This study poses no greater risk to you than what you routinely encounter in day-to-day life. Participating in this study will involve the following risks: exercise induced fatigue, potential to fall while using a treadmill, and breach of confidentiality.

All records and research materials that identify you will be held confidential. Any published document resulting from this study will not disclose your identity without your permission. Information identifying you will only be available to the study personnel.

The use of your Protected Health Information is explained in the separate authorization form.

### **WILL THERE BE ANY BENEFIT TO ME OR OTHERS?**

Although you may not personally benefit from this study, your participation may help practitioners better identify/provide insights into the effects of high intensity exercise on gene expression and mortality risk. This information may help pinpoint the specific mechanism behind exercise's effect on health and lifespan.

### **WHAT ARE MY RIGHTS AS A SUBJECT?**

Your participation in this study is entirely voluntary. You may refuse to participate or withdraw once the study has started. Your decision whether or not to participate or terminate at any time will not affect your standing with the researchers. You do not give up any legal rights by participating in this study.

Regarding the questionnaires in this study: If at any time you feel uncomfortable, you may skip a question, stop the questionnaire, or refuse to submit the questionnaire.

### **WHAT COSTS ARE INVOLVED?**

There is no cost to you for participating in this study. Inbody 770 body composition exam and biological age predictions are provided free of charge.

**WILL I BE PAID TO PARTICIPATE IN THIS STUDY?**

Upon completion of all your responsibilities you will be paid \$100 gift card for completing this study.

In order to receive such payments, you may be asked to provide your home address and/or your Social Security number. If you receive \$600 or more from Loma Linda University for taking part in this research study or a combination of studies in one tax year, you will be sent a 1099 form as required by IRS.

**WHO DO I CALL IF I AM INJURED AS A RESULT OF BEING IN THIS STUDY?**

If you feel you have been injured by taking part in this study, consult with a physician or call 911 if the situation is a medical emergency. No funds have been set aside nor any plans made to compensate you for time lost for work, disability, pain, or other discomforts resulting from your participation in this research.

**WHO DO I CALL IF I HAVE QUESTIONS?**

Call 909-558-4647 or e-mail [patientrelations@llu.edu](mailto:patientrelations@llu.edu) for information and assistance with complaints or concerns about your rights in this study.

**SUBJECT'S STATEMENT OF CONSENT**

- I have read the contents of the consent form and have listened to the verbal explanation given by the investigator.
- My questions concerning this study have been answered to my satisfaction.
- Signing this consent document does not waive my rights nor does it release the investigators, institution or sponsors from their responsibilities.
- I may call the principal investigator Gurinder Bains PhD at 909-558-7274 during routine office hours if I have additional questions or concerns.
- I hereby give voluntary consent to participate in this study.

I understand I will be given a copy of this consent form after signing it.

\_\_\_\_\_  
Signature of Subject

\_\_\_\_\_  
Printed Name of Subject

\_\_\_\_\_  
Date



**INVESTIGATOR'S STATEMENT**

I have reviewed the contents of this consent form with the person signing above. I have explained potential risks and benefits of the study.

\_\_\_\_\_  
Signature of Investigator

\_\_\_\_\_  
Printed Name of Investigator

\_\_\_\_\_  
Date

**APPROVED**

By LLUH IRB: 5210437 - 11/22/2021 at 4:13 pm, Nov 22, 2021